OPTICAL AND ELECTRICAL PUMPING OF COLOUR-CENTRE MEDIA.

Colin I. Johnston

A Thesis Submitted for the Degree of PhD
at the
University of St Andrews

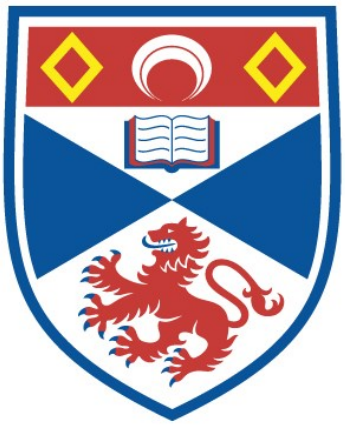

1991

Optical and Electrical Pumping of Colour-Centre Media

Thesis submitted for the degree of Doctor of Philosophy to the University of St.Andrews

by

Colin.I.Johnston, B.Sc., M.Sc.

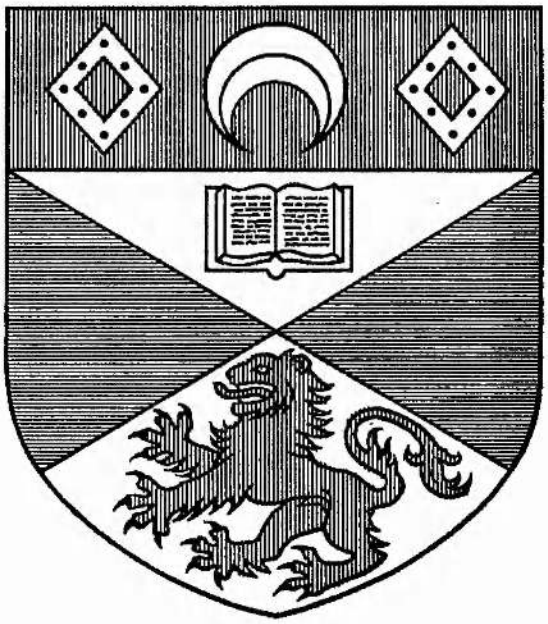

J.F.Allen Research Laboratories
Department of Physics and Astronomy
University of St.Andrews
North Haugh
St.Andrews, Fife
Scotland. KY16 9SS

ProQuest LLC.
789 East Eisenhower Parkway
P.O. Box 1346
Ann Arbor, MI 48106 – 1346

Declaration

I hereby certify that this thesis has been composed by myself, that it is a record of my own work and that it has not been accepted in partial or complete fulfilment of any other degree or professional qualification.

I was admitted to the Faculty of Science of the University of St.Andrews as a canditate for the degree of Ph.D under ordinance general no.12 on 1ST October 1986.

Signed Date 12 Feb 1991

Certificate

I hereby certify that the canditate has fulfilled the conditions of the Resolution and Regulations appropriate to the degree of Ph.D.

Signature of Supervisor Date

Copyright

Dedicated to
my
Mother and Father

Abstract

Within this thesis the exploitation of the large homogeneously broadened bandwidth of the LiF:F_2^+ colour-centre laser by production of frequency tunable ultrashort optical pulses over the 0.8-1.0μm spectral region has been presented.

A synchronously pumped LiF:F_2^+ colour-centre laser produced pulses of 700fs duration with average powers of 30mW when a colliding-pulse-modelocked travelling-wave cavity was implemented. Passive modelocking of the LiF:F_2^+ colour-centre laser was achieved over two spectral operating regions centred around 860nm and 930nm when the saturable absorber dyes IR140 and DaQTeC were employed. Pulse durations as short as 180fs and 130fs were obtained at 860nm and 930nm respectively using colliding-pulse-modelocked group-velocity-dispersion compensated resonators. The laser was pumped at a 10% duty cycle throughout. The use of coupled-cavity-modelocking techniques combined with passive modelocking was found to extend both the tuning range of the laser and useful operating lifetime of the saturable dye.

A home built NaCl:OH^- colour-centre laser which encorporates the stabilised F_2^+ colour-centre is presented. Output powers of up to 450mW were obtained for input pump powers of 4W and the laser tuned from 1.4-1.8μm.

Electroluminescence studies of NaCl, CsI, CsI:Na, CsI:Tl, and KI crystals are also presented in a study to assess the feasibility of obtaining laser action from such materials by electrical excitation. KI is shown to be the favoured laser candidate by this excitation method and evidence of temporal narrowing and signal enhancement of the electroluminescence output is presented.

Contents

Chapter 1

Introductory Overview

Colour-centres may be described as the defects within a crystal lattice which lead to optical absorption. In many cases the presence of these centres gives rise to optical absorptions such that the normally transparent or opaque host materials become coloured. The electronic structure and physical nature of many species of colour-centres enable them to be suitable for sustaining laser action when the necessary excitation of the centres is provided, and the diversity of such laser-active colour-centres provide a unique facility whereby laser action covering the extended 0.8-4.0μm spectral range may be exploited. In particular, the large homogeneously broadened bandwidths of these laser-active media enable in one operational regime, ultrashort optical pulses to be produced by a technique known as modelocking [1] and in another, laser outputs exhibiting ultrahigh spectral purity [2]. Such is the versatility of this type of laser that it has become immensely important and popular as a coherent source for applications in high resolution-spectroscopy [3], time-domain spectroscopy [4] and optical communications [5]. The mechanism by which colour-centre lasers are excited and operated is normally provided by pumping the laser active host crystal by optical means within suitable optical resonators having close similarities with dye lasers [6].

This thesis describes experimental work on the generation of frequency tuneable near infrared (NIR) ultrashort optical pulses using optically pumped LiF:F_2^+ colour-centre lasers and studies that were undertaken to determine the feasibility of producing laser action from electrically pumped alkali halides. In the initial chapters an introduction is given to the physics of colour-centres, and, in particular, to the method by which the large homogeneously broadened bandwidths of these laser types can be exploited to produce a laser output consisting of a train of ultrashort optical pulses. The techniques by which the duration of picosecond and subpicosecond laser pulses are measured are also discussed.

A novel inhouse-designed laser cryostat was initially installed which had the advantage over its commercial counterparts that all the cavity optics were located outside the cryostat and thus allowed the laser resonator configurations to be easily and readily altered when required. The performance characteristics of a LiF:F_2^+ colour-centre laser were assessed using this facility. This laser proved to be a reliable source of tunable coherent radiation in the 0.8-1.0μm near infra-red (NIR) spectral region where under chopped pumping conditions approximately 350mW output power was obtained for input powers of 2W for up to 200 hours operating time. This performance proved to be substantially better than that of dye lasers operating over this spectral range, and only since the completion of our experimental study has its performance been surpassed with the development of the Titanium-sapphire laser [7], the large homogeneously broadened operating range (0.7-1.1μm) of which encompasses that of the LiF:F_2^+ colour-centre laser.

An upgraded version of this early cryostat design was constructed which has significant advantages over that of its predecessor. These include a more efficient heat removal mechanism by means of allowing the liquid nitrogen coolant to flow directly to the crystal mounting block, and a facility to pump electrically as well as optically relevant crystals by the use of two dedicated interchangeable crystal chambers. The performance characteristics of the optically pumped LiF:F_2^+ colour-centre laser when operated within both old and new cryostats were assessed. While it was not possible to directly compare the performance of replica crystals it was concluded that the upgraded cryostat offered a much improved facility for colour-centre laser research.

The large homogeneously broadened bandwidths of the LiF:F_2^+ colour-centre laser provided favourable laser properties enabling ultrashort pulses to be produced by application of the technique of modelocking [1]. Active modelocking of the LiF:F_2^+ colour-centre laser was implemented by synchronously pumping the LiF:F_2^+ colour-centre crystal by an acousto-optically modelocked Kr-ion pump laser source. Typical output pulse durations from the Kr-ion laser were 80-120ps and, when suitable matching of the two

laser cavity lengths was carried out, optical pulses with typical durations of 1-3ps were obtained from the LiF:F_2^+ colour-centre laser configured as a standing-wave cavity. When a colliding-pulse-modelocked (CPM) cavity configuration [8] was used pulses having the somewhat shorter durations of 700fs were generated.

Passive modelocking of the LiF:F_2^+ colour-centre laser was achieved within two distinct spectral operating regimes, namely around 860nm using the saturable absorber dye IR140 and also at 930nm when the saturable absorber dye DaQTeC was used. Passive modelocking of this colour-centre laser was first demonstrated by Langford et al at 860nm [9] working within this research group and a continuation of this research was carried out within this project. Initial investigations at 860nm were carried out when a simple standing-wave cavity was employed. Typical pulse durations of 1-2ps were readily obtained and the average output power obtained was 10mW for pumping powers of ≈2W. When the cavity optics were suitably reorientated to form a CPM ring cavity a significant reduction in the modelocked pulse duration was observed. The shortest pulse durations recorded were 390fs and the average output power from each output beam was 5mW, again for input pump powers of ≈2W. The large pulse-duration-bandwidth products observed of approximately 0.4 were greatly in excess of the Fourier transform limited figure of 0.315 for assumed sech^2 pulse profiles and this suggested the presence of considerable amounts of intracavity frequency dispersion. Such dispersive effects within the passively modelocked colour-centre laser originate due to the presence of two infrasil windows, the LiF crystal itself and also due to the optical Kerr effect arising within the saturable absorber dye solvent. Consequently group velocity dispersion (GVD) compensation was implemented by the insertion of a suitable prism sequence into the laser cavity [10]. For a GVD compensated standing-wave resonator the pulse durations were dramatically reduced to 250fs, and a further improvement to 180fs was obtained when a CPM, GVD-compensated resonator was constructed.

Further passive modelocking studies of the LiF:F_2^+ colour-centre laser were carried out using the saturable absorber DaQTeC in the 930nm spectral region. Similar resonators to those described within the previous paragraph were used. Significantly, very little or no frequency chirping was observed when this saturable absorber was used and when GVD compensated resonators were constructed for investigative purposes, this only served to retain the stability of the pulse trains and no further reduction in the pulse duration was observed. For standing wave resonators, pulse durations of 170fs were obtained. Again, when a CPM ring resonator was constructed, reductions in the pulse durations to around 130fs were realised.

Passive modelocking, in general, was found to produce shorter modelocked pulses than synchronous modelocking. However the spectral operating range of a passive system was restricted, typically, to the peak of the absorption profile of the absorber. To alleviate this operational constraint the technique of coupled-cavity modelocking [11] was applied to the passively modelocked LiF:F_2^+ colour-centre laser. This technique involved allowing some of the laser output to pass through a nonlinear element located within a second optical resonator whose round-trip period was matched or made a multiple of the master cavity. The modelocking process becomes enhanced by suitable interferometric interaction between the main cavity radiation and that returning from the coupled nonlinear cavity. This "hybrid" passively modelocked technique proved to be useful in that the operating lifetime and spectral tuning of the laser was substantially increased. Operation of the modelocked laser was spectrally extended from the normally narrow (typically a few nanometers) region around 930nm to cover the 900-950nm spectral region and the practical operational lifetime of the saturable dye solution was extended to weeks rather than days.

Though versatile, the F_2^+ colour-centre is thermally quasi-degenerate and therefore it was decided that laser gain media containing stabilized F_2^+ colour-centres would be investigated. Stabilized F_2^+ colour-centres within NaCl host crystals doped with NaOH were processed "in-house" and the performance parameters of this laser gain media were subsequently

investigated and compared to those produced by other workers [12]. Production of such stabilized centres was carried out by actively colouring the NaCl crystals within suitably designed pressure chambers followed by some optical processing of the crystals. The NaCl:OH^- colour-centre laser is tuneable from 1.4-1.8μm and this together with the much higher output powers that are obtainable from such stabilized colour-centres (outputs of 3W have been observed when pumped by a 10W Nd:YAG laser [13]) make it a much more desirable NIR laser source covering this spectral region than say, for example, the KCl:Tl laser [14].

Electroluminescence studies were carried out on several alkali halide crystals, namely; KI, NaCl, CsI, CsI(Na), CsI(Tl) to assess the feasibility of obtaining laser action by a novel electrical pumping mechanism. Experimental investigations have shown that the most likely mechanism of electroluminescence within the alkali halides is that of electron injection and subsequent acceleration, within a high field region, to impact excitation energies to create self-trapped excitons and this synopsis may be compared to that of other workers [15]. The luminescence spectra obtained confirmed the creation of this species of centre within the alkali halides and typically luminescence was observed within the ultraviolet and visible regions of the spectrum. Several electrical contacting schemes onto the crystal surfaces were investigated in order to obtain the necessary current densities required to establish a population inversion by this process. It was concluded that to obtain sufficient current flow within these insulators Ohmic contacts should be constructed, but this proved to be technically difficult and the contacts assessed here were found to be of the blocking type. The build-up of considerable amounts of space charge within the crystals was observed after relatively short (minutes) excitation periods and this was indicated by a steady reduction of the output luminescence signal. Such a space charge could be released by suitably raising the crystal temperature or by means of optical excitation. KI was found to produce electroluminescence more readily than the other crystals tested and in fact it was in this crystal that optical feedback was observed. Laser action within such materials excited by electrical means is theoretically possible, but a major hurdle is the construction of

suitable current injecting electrodes and attainment of the necessary threshold current densities. One possible solution is to construct ultrathin alkali halide wafers (several microns) because it has been shown [16] that the breakdown field strength for such thin crystals is dramatically higher than for the 100μm thick crystals used here. Thus considerably higher electric fields could be applied to the crystal which may enable threshold current densities to be achieved without crystal breakdown. In our studies on the 100μm thick KI crystals evidence of stimulated emission was observed but laser action in an external cavity was unfortunately not achieved. However substantial ground work has been carried out which may prove useful for further work to be carried out in this area.

Chapter 1. References

1. G.H.C.New; Rep.Prog.Phys. **46**, 877 (1983)

2.L.F.Mollenauer; Colour Centre Lasers in Quantum Electronics; Part B (Ed.C.L.Tang)(Academic Press, NY 1979)

3. High Resolution Laser Spectroscopy; (Ed. K.Shimoda) Topics in App.Phys. **13**, Springer-Verlag (1976)

4. D.H.Austen, K.B.Eisenthal, (Eds) Ultrafast Phen.IV (Springer series in chem.Phys.38) Berlin: Springer-Verlag (1984)

5. Optical Fiber Telecomunications, (Ed.S.E.Miller, A.G.Chynoweth) Academic Press (1979)

6. N. Langford, K.Smith, W.Sibbett; Opt.Lett. **12**, 903 (1987)

7. A.Sanchez, A.J.Strauss, R.L.Aggrawal, R.E.Fahey; IEEE. Journ.Quan.Elect. **QE-24**, 995 (1988)

8. D. Kuhlke, W. Rudolph, B. Wilhelmi; IEEE. Journ.Quan.Elect. **QE-19**, 526 (1983)

9. N.Langford, K.Smith, W,Sibbett; Opt.Lett. **12**, 903 (1987)

10. R.L.Fork, O.E.Martinez, J.P.Gorden; Opt.Lett. **9**, 150 (1984)

11. L.F.Mollenauer, R.H.Stolen; Opt.Lett. **9**, 13 (1984)

12. J.F.Pinto, E.Georgiou, C.R.Pollock; Opt.Lett. **11**, 519 (1986)

13. R.Beigang, K.Klameth, B.Becker, Y.Zoon, H.Welling; Opt.Commun. **65**, 383 (1988

14. L.F.Mollenauer; Tunable Solid State Lasers, (Eds. J.C.White, L.F.Mollenauer) Springer-Verlag, Berlin (1986)

15. R.W.Boyd, M.S.Malcuit, K.J.Teegarden; IEEE. Journ.Quan.Elect. **QE-18**, 1202 (1982)

16. N.I.Lebedeva, Sov.Phys.Solid.State., **16**, 378 (1974)

Chapter 2

Introduction to the Physics of Colour-Centres

2.1 Introduction

Colour centre lasers provide tunable sources of coherent radiation operating from 0.8-4.0μm when hosted within the alkali halides. Their operating range begins where dye lasers cease to operate thus providing a complete continuation of tunable laser radiation from the visible to infrared regions of the spectrum.

Within this chapter the basic physics of colour centres will be introduced. Particular emphasis will be placed upon the F_2^+ colour centre situated within LiF and NaCl crystal lattices as it will be these two colour centre lasers that will be operated and discussed at various stages of this thesis.

2.2 Colour Centre Physics

Colour centres are essentially point defects occurring in crystalline host materials and may consist of one or more electrons trapped at lattice anion vacancies. The types of these defects are numerous and have been studied extensively by several workers [1-7]. In the context of this thesis here I will deal only with colour centres located within alkali halide crystal lattices. The term colour centre originates from the fact that these defects give rise to broad optical absorption (and emission) bands within the wide (typically 9-10 eV) bandgaps of these normally transparent or opaque insulating materials, thus "colouring them".

The most basic colour centre is the F-centre (F coming from the German word for colour - farbe) which simply consists of a single electron trapped at an anion vacancy. Though this

is not suitable for laser action it is from this centre that the more complex colour centre aggregates may be formed and some of these provide suitable laser levels. Figure 2.1 illustrates several types of colour centre, including, the F_2^+ colour centre, which consists of two F centres aligned along the [110] axis with one electron missing. When suitably pumped an F_2^+ laser is capable of power outputs ≈1-2.5 W where a high pumping efficiency is facilitated by a small Stokes shift.

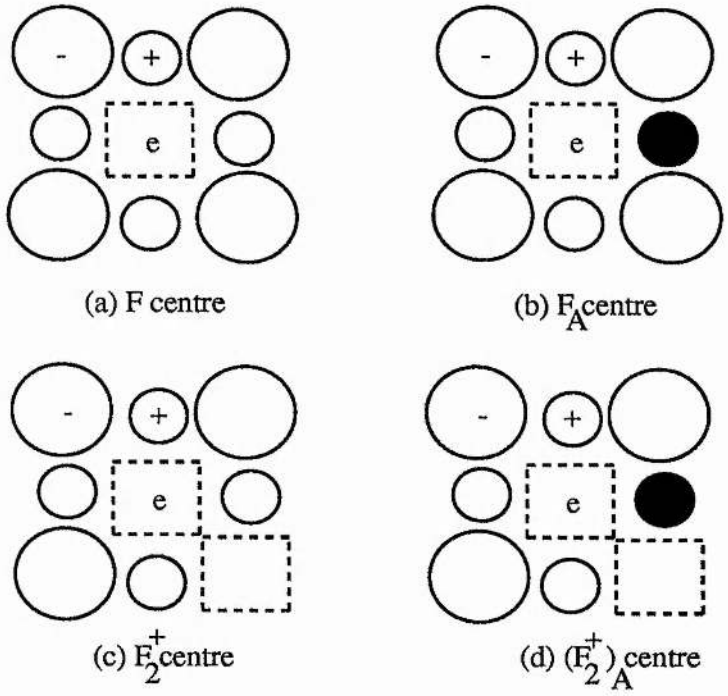

Figure 2.1 Schematic representation of some basic colour centres within an alkali halide lattice

Laser-active colour centres produced within a range of alkali halide materials cover the spectral range from 0.8 μm to 4.0 μm (fig 2.2) thereby continuing the spectral range where organic dye lasers either cease to operate [6-9] or suffer serious instability problems. The operation of colour centre lasers is very similar to dye lasers in that they have large gain cross sections ($\sigma \approx 3 \times 10^{-16} cm^2$) and thus need only be excited by modest pump powers when a tightly focused beam waist is formed in the gain medium. However, unlike

counterparts, colour centre lasers are relatively easy to operate in that the fast flowing dye jet is replaced by a thin Brewster-angled crystal with typical dimensions ≈ 2-3 mm.

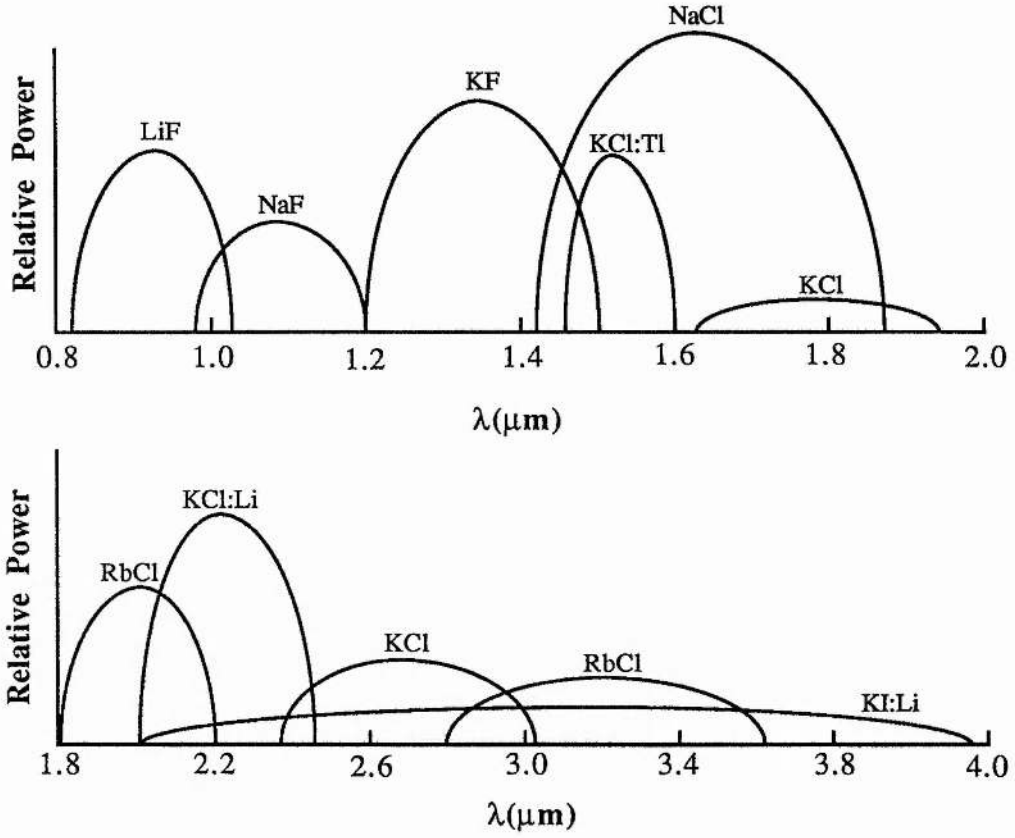

Figure 2.2 Tuning curves for several colour centre lasers. The tuning range of 0.8-2.0μm in the upper graph is provided entirely by F_2^+ colour centres. (All centres are identified in table 2.1)

Most colour centre lasers perform best at cryogenic temperatures because at room temperature thermal dissociation of the centre occurs along with the added problem that the laser active colour centres become mobile and migrate to form non-laser-active centres. Therefore, to overcome these effects the laser gain crystal is mounted onto a "cold finger" located within an evacuated chamber, as will be discussed in chapter 4.

An extremely advantageous feature of colour centre lasers is that their absorption and emission bands are homogeneously broadened [6,7], thus once excited all the centres can contribute energy to a given laser mode, and also, that all of the centres may be pumped by a narrow bandwidth laser operating within the colour centre absorption band. Therefore, as a consequence of these homogeneously broadened absorption and emission bands colour centre lasers are capable of producing very narrow linewidths (≈1 kHz or less) [10] and at the other extreme the large homogeneously broadened bandwidth may be modelocked to produce optical pulses in the femtosecond regime [6,11]. Table 2.1 gives the performance characteristics of several colour centre lasers.

Host / Centre	Pump (μm)	Tuning range (μm)	Max. P_{out} (CW) (mW)
CaO / F^+	0.351	0.36 - 0.40	20
LiF / F_2^+	0.647 / 0.676	0.82 - 1.05	1800
$NaF / (F_2^+)^*$	0.87	0.99 - 1.22	400
KF / F_2^+	1.064	1.22 - 1.50	2700
$NaCl / F_2^+ : O^{2-}$	1.064	1.40 - 1.75	3000
$KCl : Tl / Tl^0$ (1)	1.064	1.4 - 1.6	1100
$KCl : Na / (F_2^+)_A$	1.34	1.62 - 1.91	12
$KCl : Li / (F_2^+)_A$	1.34	2.0 - 2.5	10
$KCl : Na / F_B$ (ii)	0.595	2.22 - 2.74	60
$KCl : Li / F_A$ (ii)	0.647	2.3 - 3.1	280
$RbCl : Li / F_A$ (ii)	0.647 / 0.676	2.5 - 3.65	92
$KI : Li / (F_2^+)_A$	1.73	2.38 - 3.99	0.3 mj (pulsed)

Table 2.1 The performance characteristics of several selected colour centre lasers. (Ref 10)

Modelling of colour centres can be carried out to a good approximation by considering them as atoms or molecules embedded in a dielectric medium [7,10,12]. For example, the simple F centre may be treated as a hydrogen atom contained within a box shaped potential well and the F_2^+ centre may be treated as an H_2^+ ion housed within a suitable crystal lattice. In both cases these colour centres may be distinguished from their molecular counterparts by the large broadening which occurs to their absorption and emission bands and also by the Stokes shift that is evidenced in emission. Here the F centre model will be discussed.

Though not laser active, the F centre is the the simplest of all the colour centres and as already mentioned is the basic building block from which all colour centres can be constructed. It is by considering this centre, therefore, that the basic physics of colour centres may be deduced. By referring to figure 2.1 it may be seen that the F centre consists of a single electron trapped at an anion vacancy with the nearest neighbours being six positively charged alkali metal ions. This surrounding positive charge may be considered as a single point charge centred at the vacancy and we may, for simplicity, therefore consider the F centre as a hydrogen atom in order to model its optical properties.

Though effective in describing the basic physics of the colour centre this model is crude in its simplicity and therefore to understand the more complex nature of the absorption and emission bands of the F centre it is necessary to consider the harmonic vibrations within the crystal lattice as in the alkali halides there is a strong coupling between lattice distortion and transition energy [4]. These periodic vibrations alter the size of the potential well with the result of homogeneously broadening the absorption and emission bands. In this simple model it also is assumed that the energy of the potential well is affected only by the vibration of nearest neighbour ions. The potential energy of such a system can be represented by a configurational coordinate (Q) diagram as illustrated in figure 2.3 and is used to describe the principal phenomena associated with the colour centre optical transitions. The physical basis of this model is the Born-Oppenheimer approximation which is described in reference [4]. From this approximation the quantum mechanical

eigenvalues for a coupled system consisting of bound electrons and the nearest neighbour ions are given by

$$E_g = (n + \frac{1}{2})\, h\nu_g \qquad (2.1)$$

$$E_e = (m + \frac{1}{2})\, h\nu_e + E_o \qquad (2.2)$$

where ν_g and ν_e are the frequencies of the lattice vibrations (phonons) for the ground and excited state respectively; n and m are the vibrational quantum numbers and E_o is the energy separation between the two states.

For simplicity (reference figure 2.3) we have considered the allowed transitions at 0 K as then only the n = 0 vibrational level will be occupied and therefore transitions will occur from this level only. The lower curve represents the potential energy of the ground state as a function of the ionic displacement from the equilibrium position whilst the upper parabola represents the the potential energy of the excited state for the same function. The horizontal lines represent the allowed vibrational states of the system and are separated by the phonon energy. Optical transitions are represented by vertical lines as the Franck-Condon principal states that the time taken for an electronic transition is short (10^{-16} s) compared with the period of atomic vibrations ($\approx 10^{-13}$ s). It can be seen that the upper curve is displaced relative to the lower this being due to the fact that when in the excited state the wave function of the colour centre changes and this is no longer in equilibrium with the crystal lattice. A repulsive force is therefore exerted on the nearest neighbour ions forcing them to be displaced to a new equilibrium position. The consequences of this is that the absorption and emission process of the colour centre involves four steps, namely;

(a) Photon absorption

(b) Configurational relaxation to the relaxed excited state (RES)

(c) Photon emission

(d) Configurational relaxation to the ground state

This represents a four-level system which is very efficient for laser action.

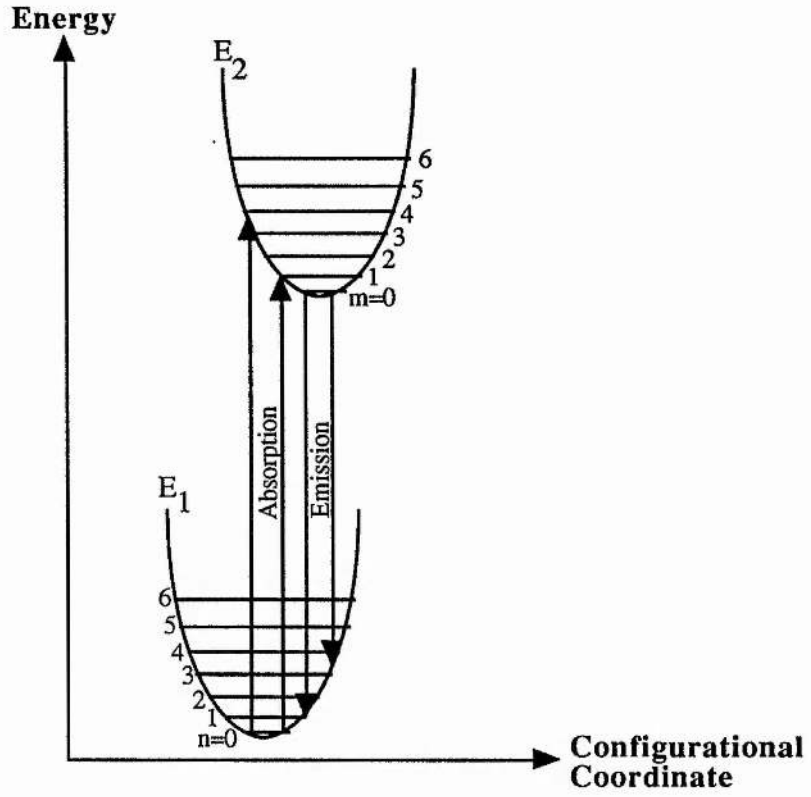

Figure 2.3 Configurational Coordinate (Q) diagram. (Adapted from ref.4)

A simplified representation of the optical pumping cycle of the colour centre is given in figure 2.4. The first process in the optical pumping cycle, ie, the absorption of photons, occurs rapidly and excites the electrons from the 1s to the 2p state of the potential well. Secondly the crystal lattice reorientates itself to a new equilibrium configuration known as the relaxed excited state (RES), with the emission of the appropriate number of phonons thus producing a Stokes shift between the emission and absorption profile. Photon emission occurs between the RES and the ground excited state in a radiative lifetime denoted τ_{rad}. The fourth process involves the electron relaxing by emission of phonons to

the lower ground state. The F centre is not suitable for laser action due to the fact that after excitation to the first state followed by subsequent lattice relaxation the F centre electrons are only weakly bound to the anion vacancy and are therefore easily ionized by phonons or low energy photons. Nevertheless, the optical properties of the F centre give an introduction into the understanding of the physics of other suitable laser active colour centres.

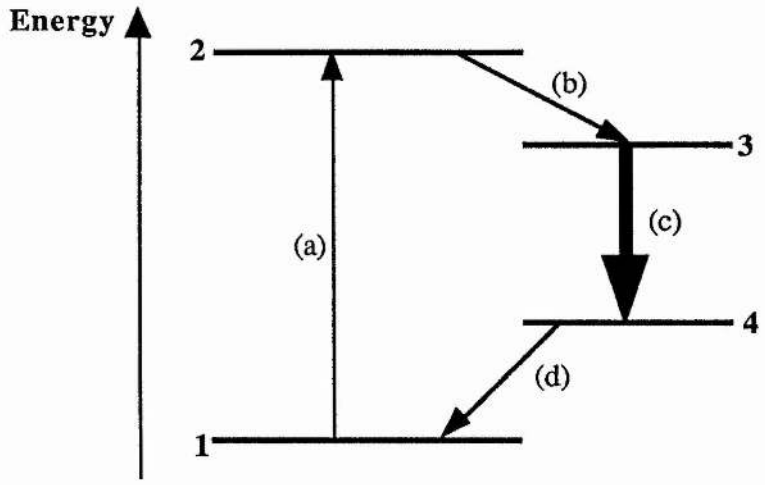

Figure 2.4 Schematic diagram of the optical pumping cycle of a colour centre medium

2.3 The F_2^+ colour centre in LiF

The F_2^+ colour centre has been briefly mentioned in the previous section, and as already stated this centre consists of a single electron trapped by a pair of adjacent anion vacancies orientated in the [110] direction. In this section the F_2^+ centre within a LiF alkali halide lattice will be described.

To model the basic physics of the F_2^+ colour centre it may be treated as an H_2^+ molecular ion embedded in a dielectric continuum of dielectric constant k_o, where the two lattice vacancies play the role of protons.This model has proved to be very useful in predicting

and interpreting phenomena relating to the behaviour of F_2^+ colour centre lasers [12]. Using this model the energy levels may be calculated as

$$E_{F_2^+} = k_0^{-2} E_{H_2^+} (r_{12}) \qquad (2.3)$$

where r_{12} is the proton separation and is given by

$$r_{12} = k_0^{-1} R_{12} \qquad (2.4)$$

and where R_{12} is the vacancy pair separation.

It may thus be deduced from equations (2.3-2.4) that a large tuning range is possible from the F_2^+ centre when it is incorporated into different alkali halide host crystals which have different dielectric constants and lattice parameters as illustrated in figure 2.2. In fact, as with the F centre, the F_2^+ centre obeys a Mollwo-type relation in that the emission bands shift towards the longer wavelengths with increasing lattice constants [7]. An energy level diagram of the F_2^+ centre with the levels named after their molecular counterparts is illustrated in figure 2.5. The left hand side of this figure shows the normal configuration whilst the relaxed excited state is shown on the right hand side. It may be seen that there is a relatively small Stokes shift suggesting that the pump-emission efficiency can be high, ie, little energy is given to the crystal lattice in the form of phonons. It may also be seen from this figure that the four-level optical pumping cycle for the F_2^+ centre takes place from the lowest energy transition, namely the $1s\sigma_g$-$2p\sigma_u$ transition. When excited to the $2p\sigma_u$ state the electron relaxes via phonon emission to the slightly lower energy configuration as indicated thereby producing a four level system which has attractive properties for laser action. These include; (i) large absorption and emission cross section $\sigma \approx 10^{-16} cm^2$, thus allowing highly efficient pumping and large single pass gains in thin 1-3 mm thick crystals with modest centre densities (10^{17}-$10^{18} cm^{-3}$) and (ii) the quantum efficiency of the pumping-emission cycle is ≈100% and is independent of temperature, (iii) self-absorption is minimal as the Stokes shift is just large enough to separate the higher excited state from

the emitting level, ie the absorption and emission bands are completely resolved, therefore the heat dissipated into the crystal lattice is minimal and (iv) losses due to singlet-to-triplet conversion do not occur as the F_2^+ colour centre only contains one trapped electron.

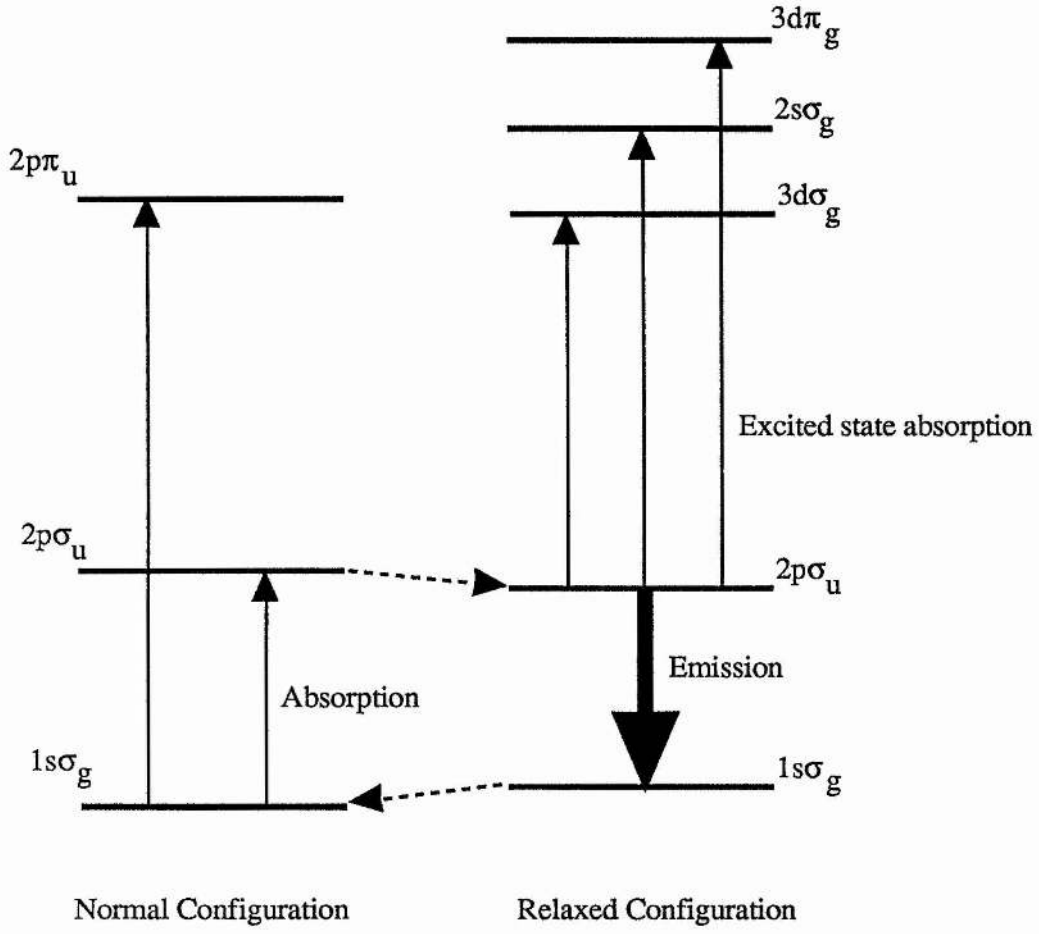

Figure 2.5 Energy level diagram for the F_2^+ colour centre. The energy bands are described according to their molecular counterparts.

The laser transition for the F_2^+ colour centre, as expected, is polarised along the [110] axis, thus efficient laser operation will occur when the polarization of the pump source is orientated along one of these axis as illustrated in figure 2.6.

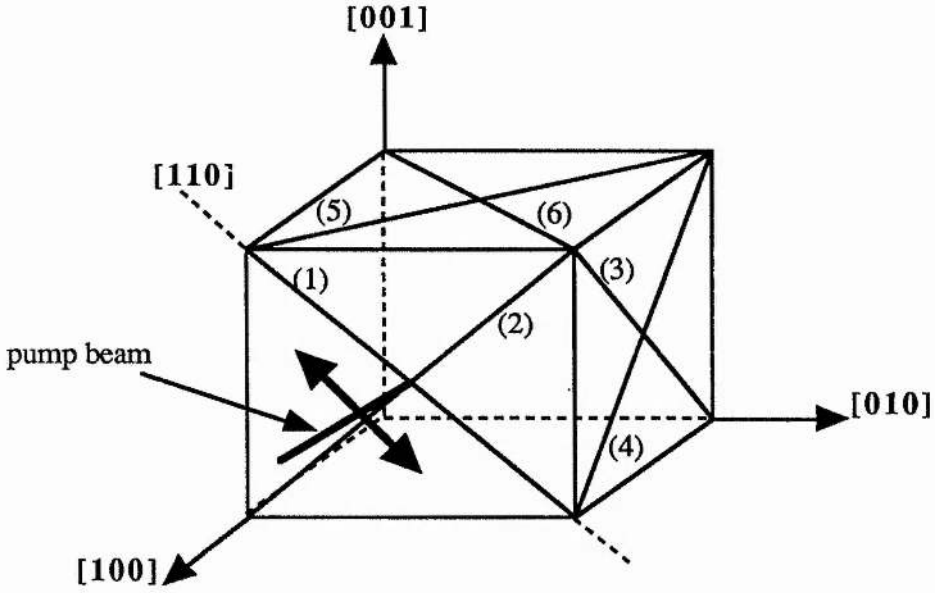

Figure 2.6 Diagram showing the six possible axis along which the pump laser polarization may be orientated for the F_2^+ colour centre.

When produced within a LiF lattice, the absorption and emission bands of the F_2^+ colour centre lie at the short wavelength end of the spectrum for the complete alkali halide F_2^+ tuning range, in fact the LiF:F_2^+ colour centre laser (CCL) operates where dye lasers cease to operate thus providing a convenient continuation for laser action from the visible to the infrared (NIR) region of the spectrum. The LiF:F_2^+ CCL may be pumped by a krypton-ion laser on the 647,676 nm lines whereupon this pump energy can be distributed to all of the homogeneously broadened modes. In this and other alkali halide hosts for the F_2^+ colour centres the long term stability of the LiF:F_2^+ CCL is poor and fading of the output power can occur during extended operational periods. This is due to several reasons. Firstly, optical pumping to levels higher than the $2p\sigma_u$ transition by way of multi-phonon absorption may occur and when this is accompanied by sufficient phonon absorption by the crystal lattice this can lead to orientational bleaching of the centres with the result of reduced performance [7]. Secondly, the F_2^+ is positively charged with respect to the crystal lattice and therefore acts as a strong electron trap and thus trapping of electrons by F_2^+ centres to produce F_2 centres, which are not suitable for laser action, reduces the efficiency of the laser. To overcome this problem it is necessary that the lattice is electronically neutral by

containing F^- and higher order similarly charged centres which are in fact produced during preparation of the colour centre crystal. Such centres are easily ionized at room temperature and by the local heating produced by the pump beam. In an attempt to overcome both these problems the LiF host crystal is maintained at the liquid nitrogen temperature (77K) by means of a suitably designed cryostat and the pump beam is chopped.

F_2^+ centres are formed in a LiF host crystal lattice by means of electron bombardment. The formation process will briefly be described here. Boules of pure LiF are annealed in a vacuum oven for 24 hours at temperatures just below their melting point (~1000K) and then allowed to cool slowly back to room temperature. This step removes any stress and strain from the lattice which if unremoved would cause the crystal to shatter when cleaving is attempted. The boule is then cleaved along a [100] axis to produce 2x10x10mm slabs of crystal and the 10x10mm surfaces are then polished to optical quality. The polished crystals are then wrapped in a protective layer of aluminium foil and irradiated for 2-3 minutes with 1.5 MeV electrons which are produced from a van de Graaff generator with current densities incident upon the crystal in the order of $0.5\mu Acm^{-2}$. This electron beam produces F centres and anion vacancies which are then immobilised within the crystal when stored at 77K.

The F_2^+ centres themselves are produced when the crystal is loaded into the laser cryostat at room temperature as it is at these temperatures that the anion vacancies become mobile and "associate" with the F centres to form F_2^+ centres. The loading process takes approximately 10 minutes and the F_2^+ centres may be seen to form as a dark blue "colouring" of the crystal is seen to occur. The density of the colouration gives some indication as to how the LiF:F_2^+ laser will perform.

A table of the basic optical properties of the F_2^+ centre in LiF is given in table 2.2.

Parameter	Value
λ_{abs}(peak)	645 nm
λ_{em}(peak)	910 nm
Emission FWHM	0.2 ev
Dipole direction	[110]
τ_{rad}	29 ns
σ	1.0×10^{-16} cm^2
n	1.39
η	~1

Table 2.2 Some of the basic optical properties of the F_2^+ centre in LiF. (σ is the gain cross section, n the refractive index and η luminescence quantum efficiency) [6]

2.4 The F_2^+ colour centre in NaCl:OH$^-$

The F_2^+ colour centre accommodated within alkali halide host materials has excellent laser properties but irreversible fading of the centres by thermal and optical bleaching reduces the operating performance and lifetime of these centres. To alleviate these effects, attempts have been made to stabilize this centre [13,14]. This may be achieved by providing both a spatial trap that anchors the position of the F_2^+ centre thus deterring migration and also an electron trap which serves to capture the extra electron freed from the initial F_2 centre when the F_2^+ is produced.

Several workers have attempted such a scheme [14] by introducing divalent metals into the crystal lattice in an effort to create strong electron traps, but, even with the electron tightly coupled to the trap site the F_2^+ centre was observed to be unstable due to centre reorientation produced by the intense pump beam. One of the first successful stabilization schemes was the formation of the $(F_2^+)_A$ centre which was previously shown in figure

2.1. Here an impurity cation is introduced to the crystal lattice with the F_2^+ centre located adjacent to the impurity which serves to provide two beneficial effects. These are (a) the F_2^+ centre is spatially trapped and (b) the impurity causes a shift in the absorption and emission bands, thereby enabling the tuning range of the centre to be broadened by suitable choice of impurity. This was demonstrated by Schneider [13] using Na^+ and Li^+ doped KCl. The normal emission band for an F_2^+ centre in KCl is centred at 1.62 μm and when Na^+(similar atomic size to K), is introduced to the lattice only a small perturbation of the KCl: F_2^+ colour centre occurs and the centre of the emission band is shifted to 1.75 μm. However, when Li^+ is introduced to the KCl lattice, (Li^+ is much smaller than K) a large perturbation occurs such that the centre of the emission is shifted to 2.3 μm [10].

More recently several workers [15] have discovered a new and much more powerful stabilized F_2^+ centre in a NaCl host lattice. When first reported this centre was thought to be a $(F_2^+)_A$ centre doped with K. This report was later corrected [16] when the important crystal melt impurity OH^- was identified. When "treated" this produces an O^{2-} perturbed F_2^+ defect labelled as the $F_2^+:O^{2-}$ centre. A schematic representation of the structure of this colour centre is shown in figure 2.7.

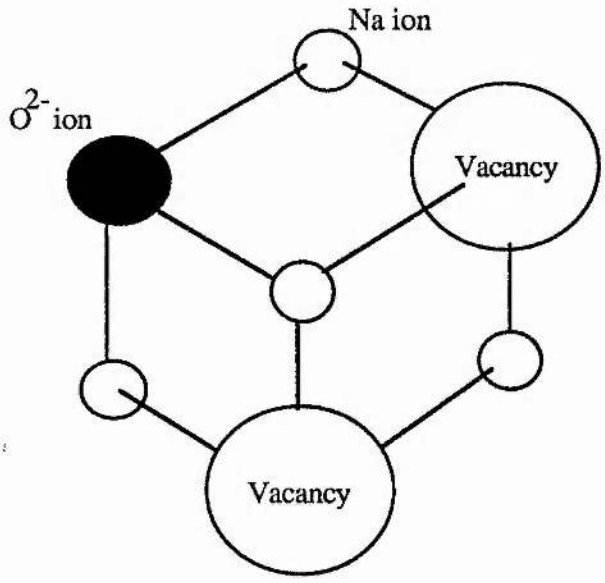

Figure 2.7 Schematic structural diagram of the $F_2^+:O^{2-}$ colour centre

This colour centre has proven to be a powerful laser active medium and it has been observed in NaCl, KCl, KBr and LiF [8], the most powerful laser action being produced from a NaCl host to give > 3 W output power when pumped by a CW 10 W Nd: YAG laser [17]. The reason for this centre's high stability and output power is that the stabilizing O^{2-} ion is extremely electronegative, therefore it can act both as an electron and spatial trap for the F_2^+ centre. As may be seen from the schematic structural diagram of the $F_2^+:O^{2-}$ colour centre it may be seen that it differs from the $(F_2^+)_A$ colour centre in that the oxygen impurity is orientated along the cubic diagonal from the F_2^+ centre as a halogen substitute, hence the F_2^+ centre is not only bound to the O^{2-} ion by lattice forces but also by Coulomb attraction. Also, an additional advantage of the centre is that it has overall charge neutrality within the ionic lattice which therefore minimises the probability of charge capture and centre transformation. The basic optical properties of the $F_2^+:O^{2-}$ colour centre are given in table 2.3

Parameter	Value
$\lambda_{abs(peak)}$	1.09 μ m
$\lambda_{em(peak)}$	1.55 μ m
Emission FWHM	0.136 ev
Stokes shift	0.34 ev
Dipole direction	[110]
τ_{rad}	150 nsec
σ	8.5×10^{-17} cm^2
n	1.53
η	~1

Table 2.3 Some of the basic optical properties of the NaCl $F_2^+:O^{2-}$ colour centre gain medium. [ref 6]

Utilizing this colour centre within a NaCl lattice, pulses of 5 ps duration have been reported when synchronously pumped by a Nd:YAG laser [6] and in single frequency operation powers of up to 460 mW with a linewidth < 2 MHz were achieved [6]. Pulsed room temperature operation has also been reported [18].

A detailed description of the experimental procedure for the $F_2^+:O^{2-}$ centre production is described by other workers [19] and therefore only a brief description will be given here. The NaCl crystals are grown with a small concentration of NaOH ($\approx 500 \times 10^{-6}$ mol%) using the Kryopoulos technique. This gives rise to an OH^- concentration in the range 5 - 50 ppm within the crystal lattice which was found to produce the optimum $F_2^+:O^{2-}$ population densities . The crystal is then additively coloured in a Na vapour heat pipe at an appropriate Na pressure which leads to the production of F_1, F_2 and F_3 centres as well as dissociating the OH^- radicals into H^-, O^{2-} and O^- ions which occupy the newly produced anion sites. The crystal is then stored at 77K until ready to use. When required for use the processed crystal is illuminated, at room temperature by F band light (452 nm) for 30 minutes, which serves to produce F_2^+ centres in the crystal. The crystal is then recooled to 77K and then reexposed to the the same F band light for 3-5 minutes. This exposure causes a long wavelength shift, along with a slight broadening, of the absorption and emission bands as the $F_2^+:O^{2-}$ centre is formed. An energy level diagram of the $F_2^+:O^{2-}$ centre is reproduced in figure 2.8

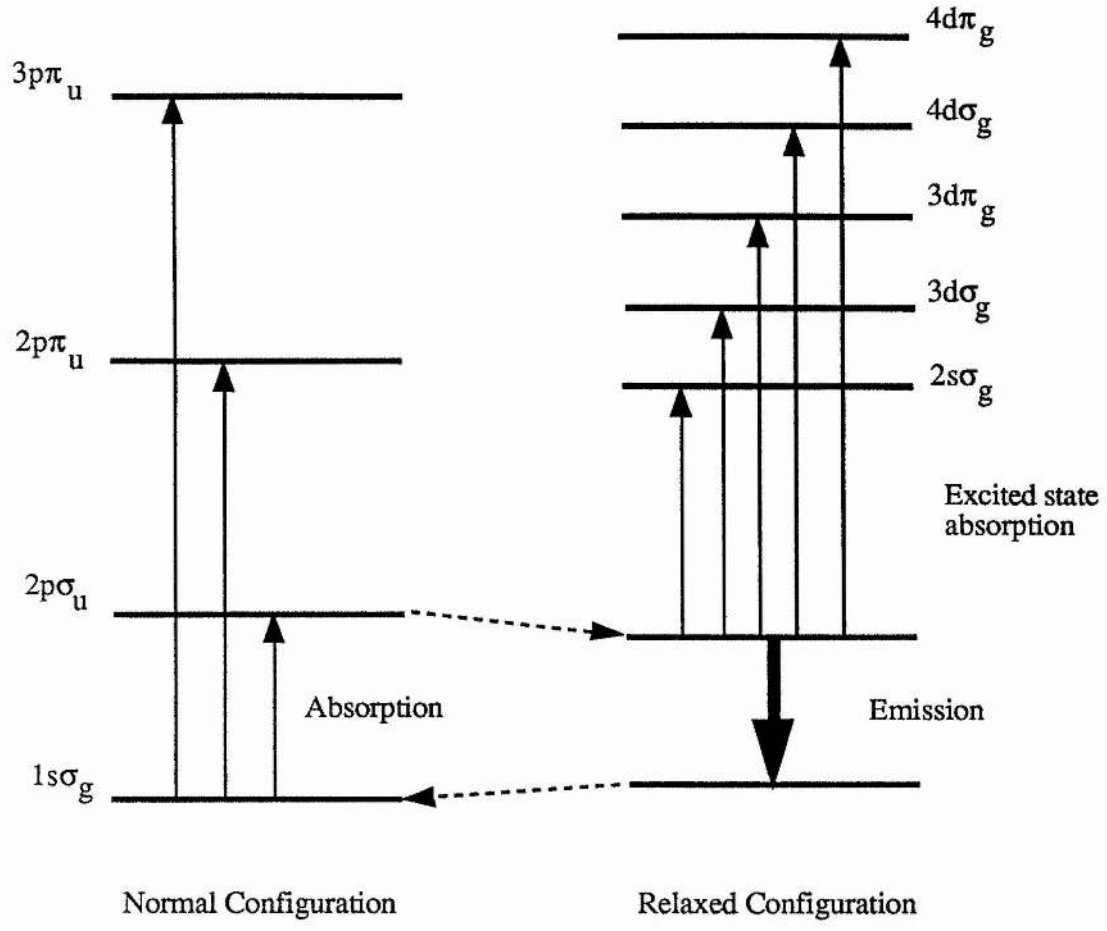

Figure (2.8) Energy level diagram for the $F_2^+:O^{2-}$ colour centre laser medium

2.5 Optical pumping of colour centres

A laser oscillator comprises an optical resonator with mirrors having reflectivities R_1 and R_2 separated by a distance L inside which the gain medium such as a laser active colour centre crystal is located as illustrated in figure 2.9. It is desirable to have a system which has a high gain profile, as with such a system cavity losses occuring due to misalignment etc can easily be overcome. For a colour centre laser the laser active cycle has already been outlined as being a four level process. For this system, which has a Lorentzian luminescence band the gain coefficient at the band peak α_0 may be calculated from;

$$\alpha_0 = \frac{N^* \lambda_0^2 \eta}{8\pi n^2 \tau_{rad}(1.07\,\delta\nu)} \qquad (2.5)$$

where N^* is the population of the RES, λ_0 the wavelength of the band peak, η the luminescence quantum efficiency, n the refractive index, $\delta\nu$ the FWHM of the luminescence band and τ_{rad} the luminescence decay time [20].

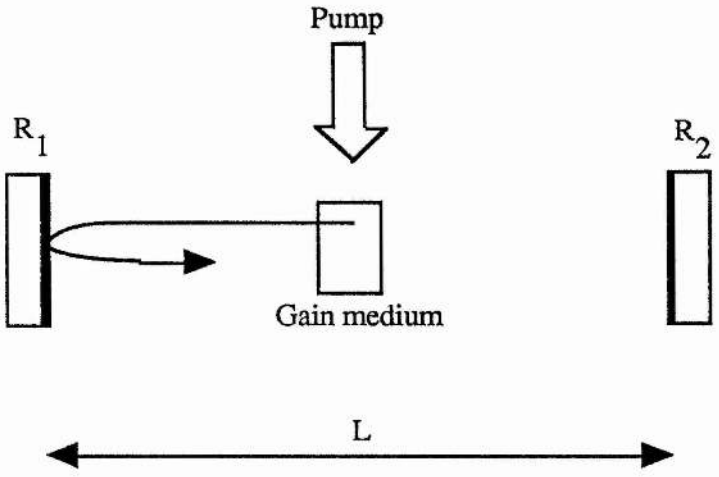

Figure 2.9 A simple optical resonator. R_1 and R_2 are the mirror reflectivities.

The net optical gain is given by ;

$$\text{Gain}_{net} = \frac{I_{out}}{I_{in}} = \exp(\alpha l) \qquad (2.6)$$

where I_{in} and I_{out} are the input and output optical intensities respectively, l is the gain path length and α the net gain coefficient given by $\alpha=\alpha_g-\alpha_l$ where α_g is the gain coefficient calculated for the inverted luminescence levels only and α_l is the coefficient of absorption losses. The population of the RES may be found from the expression;

$$N^* = \frac{\beta I}{E_p} \cdot \tau_{rad} \qquad (2.7)$$

where β is the absorption coefficient at the pump wavelength, I is the intensity of the pump wavelength and E_p the pump photon energy. Therefore the gain coefficient may be found in terms of the pump intensity by substituting (2.7) into (2.5) to give

$$\alpha_0 = \frac{\beta I}{E_p} \cdot \frac{\lambda_0^2 \eta}{8\pi n^2 (1.07\ \delta\nu)} \qquad (2.8)$$

Now for the case of a coaxially pumped gain medium the gain coefficient α may be expressed as

$$\alpha = \alpha_0 \exp (-\beta l) \qquad (2.9)$$

By substituting (2.12) into (2.9) the optical gain can then be expanded as

$$G = \exp [\alpha_0 \int_0^d \exp (-\beta l) dl] \qquad (2.10)$$

This may be further simplified if the path length through the crystal d is much greater than β^{-1}, to

$$G = \exp (\frac{\alpha_0}{\beta}) \qquad (2.11)$$

This is applicable to the case for the LiF:F_2^+ colour centre laser which will be described later in this thesis, where d = 0.2 cm and β = 10 - 100 cm^{-1}. Combining (2.11) with (2.14) the gain may be given as

$$\ln G = \frac{I}{E_p} \cdot \frac{\lambda_0^2 \eta}{8\pi n^2 (1.07\ \delta\nu)} \qquad (2.12)$$

Applying equation (2.12) for the case of the LiF:F_2^+ and the NaCl:F_2^+:O^{2-} colour centre lasers respectively using the data given in tables (2.2) and (2.3) the pump power densities for the threshold lasing conditions are obtained as $\approx$1kWcm^{-2}.

2.6 Astigmatic aberration compensation of laser cavities.

By considering equation (2.12) it may be evaluated that a pump power density of $\approx$1kWcm^{-2} is required to achieve threshold laser condition with the LiF:F_2^+ colour centre laser. It may be readily deduced, therefore, that in order to obtain pump power densities of this magnitude that some sort of intracavity focussing element is required. In addition to this operating requirement it is convenient that the laser cavity length be of the order of 2m such that mode-locking requirements, bandwidth (BW) filtering purposes may be facilitated. Clearly such a resonator that can offer these two contradictory requirements must contain appropriate internal focussing lenses, or alternatively an appropriate mirror arrangement such as two concave focussing mirrors arranged to form a small folded section off the main cavity as illustrated in figure 2.10.

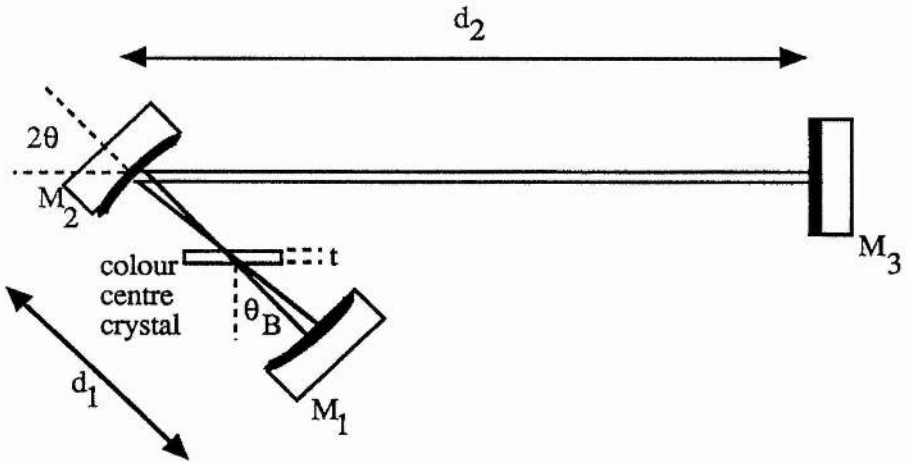

Figure 2.10 Simple three mirror folded cavity where $d_2 >> d_1$ and t is the crystal thickness.

By referring to the laser resonator (figure 2.10) it may be observed that the colour-centre crystal is placed at the common focus and centre of curvature of the concave mirrors M_1 and M_2 and is located at the Brewster angle θ_B (θ_B=54.3^0 where n=1.39) to minimise Fresnel losses. Such an alternative as this is more desirable than that of a cavity containing internal lenses because the Fresnel and bulk losses of lenses can be high whereas the reflectivity losses of the mirrors can be made relatively low. Convenient as this may be, such a folded section within the laser cavity introduces astigmatic aberrations to the beam which in turn leads to reduced laser stability [21]. To overcome these aberrations the analysis of Kogelnik et al [21] may be implemented where the cavity optics are arranged such that the astigmatism produced by the mirrors may be offset by the astigmatism incurred by the internal cell placed at the beam waist, by rotating M_2 to an angle 2θ as shown in figure 2.10.

Such cavity designs are highly efficient as the tightly focussed pump beam spot also ensures that all the incident pump power is used to pump a gain volume equal to that which is depleted by the transverse mode of the laser. The analysis and construction of the laser cavities used in this thesis have therefore been undertaken by applying Kogelnik's imaging rules. With small spot systems of this type the separation d_1 of the folded-section mirrors M_1 and M_2 is critical with the cavity being only stable over a small range of values typically in the range of a few millimetres near $d_1=R_1+f$, where R_1 is the radius of curvature of mirror M_1 and f the focal length of M_2. The mirror adjustment latitude δ may be defined by

$$d_1 = R_1 + f + \delta \qquad (2.13)$$

and it may be shown that for the cavity to be stable the following inequality must be satisfied

$$0 \leq \left(1 - \frac{d}{R_3} \right)\left(1 - \frac{d}{R_1} \right) \leq 1 \qquad (2.14)$$

$$\text{where } d = d_1 - \frac{d_2\, f}{d_2 - f} \qquad (2.15)$$

Thus the stability range of the resonator may be found by solving (2.14) to give

$$\delta_{min} = \frac{f^2}{d_2 - R_3 - f} \qquad (2.16)$$

$$\delta_{max} = \frac{f^2}{d_2 - f} \qquad (2.17)$$

For the typical resonator design used throughout this work $d_2 \gg f$ and $R_3 \approx \infty$ and so the stability region may be expressed as

$$2S = \delta_{max} - \delta_{min} \approx \frac{f^2}{d_2} \qquad (2.18)$$

The beam diameter w_0 in the beam waist region is given by

$$\left(\frac{\pi w_0^2}{\lambda}\right)^2 \approx (\delta_{max} - \delta)(\delta - \delta_{min}) \qquad (2.19)$$

If $R_1 \gg S$ then $w_0 \rightarrow 0$ at the limits of the stability regions. As d_1 is moved away from these limits towards the centre of the stability range then

$$S = \frac{\delta_{max} - \delta_{min}}{2} \qquad (2.20)$$

$$\text{ie } S \approx \frac{\pi w_0^2}{\lambda} \qquad (2.21)$$

In a cavity of this design the centre mirror M_2 and the internal Brewster-angled cell introduce astigmatism in the beam such that the effective focal lengths f_x and f_y for the sagital (xz) and tangential (yz) rays are given by

$$f_x = \frac{f}{\cos\theta} \qquad (2.22)$$

$$f_y = f\cos\theta \qquad (2.23)$$

The effective path lengths for the sagittal and tangential rays are

$$d_x = t\frac{(n^2 + 1)^{1/2}}{n^2} \qquad (2.24)$$

$$\text{and } d_y = t\frac{(n^2 + 1)^{1/2}}{n^4} \qquad (2.25)$$

n and t are the refractive index and thickness of the Brewster-angled cell. Thus the sagittal and tangential ray stability region positions $P_{(x)}$, $P_{(y)}$ are

$$P_{(x)} = d_x + R_3 + f_x + \delta_x \qquad (2.26)$$

$$P_{(y)} = d_y + R_3 + f_y + \delta_y \qquad (2.27)$$

A stability region of ≈500μm was calculated to be the case here for typical beam waists within the colour centre crystal of 20μm.. By careful selection of the angle 2θ the astigmatic aberration produced by the angled mirror M_2 may be offset against that produced by the Brewster angled cell to produce a region of maximum overlap of the stability regions when the following condition is satisfied:

$$Nt = f\sin\theta\tan\theta \qquad (2.28)$$

$$\text{where } N = \frac{(n^2 - 1)(n^2 + 1)^{1/2}}{n^5} \qquad (2.29)$$

It should be mentioned that astigmatic compensation is not completely obtained within the crystal due to the asymmetric arrangement of mirrors M_1 and M_2 and consequently the

waist is slightly elliptical [21]. Thus the cavity can be astigmatically compensated with respect to stability but not with respect to focussing within the crystal. For a crystal thickness of 2mm and refractive index 1.39 and windows of thickness 2mm with refractive index 1.52 a folding angle of 22^0 was calculated for the cavities constructed throughout this work.

2.7 Summary

The pertinent physics of the colour centre has been introduced. In particular the F_2^+ colour centre has been discussed when incorporated within LiF and NaCl host crystals. In general the long term stability of the F_2^+ colour centre is poor and fading of the output power with time is observed. However when formed within a NaCl host, which has incorporated within its lattice suitable dopants, a highly stabilized F_2^+ colour centre may be formed. The performance characteristics of such a non stabilized F_2^+ colour centre will be described within this thesis.

Chapter 2 References

1. J.H. Schulman, W.D. Compton; Colour Centres in Solids, Pergamon Press, Oxford (1963)

2. W.B.Fowler; Physics of Colour Centres, Academic Press, NY (1968)

3. J.J.Markman; F-Centres in Alkali Halides, Solid State Physics, Supplement 8, Academic Press NY (1966)

4. B.Henderson; Defects in Crystalline Solids, Edward Arnold, London (1972)

5. V.A.Arkhangel'skaya, P.P. Feofilov; Sov.J.Quan.Electron.**10**, 6 (1980)

6. L.F.Mollenauer; Tunable Solid State Lasers, (Eds. J.C.White, L.F.Mollenauer) Springer-Verlag, Berlin (1986)

7. C.R.Pollock; J.Lum. **35**, 65 (1986)

8. C.R.Pollock, J.F.Pinto, E.Georgiou; Appl.Phys.B **48**, 287 (1989)

9. Dye Lasers, Topics in Aplied Physics 1, (Ed. F.P.Schafer) Springer-Verlag (1973)

10.L.F.Mollenauer; Colour Centre Lasers, Quantum Electronics Part B, (Ed. T.L.Tang) Academic Press, NY (1979)

11. N.Langford, K.Smith, W.Sibbett; Opt.Lett. **12**, 903 (1987)

12. M.A.Aegerter, F.Luty; Phys.Status.Solidi.B **43**, 227 (1971)

13. I.Schneider, C.Marquardt; Opt.Lett. **5**, 214 (1980)

14. I.Schneider, C.R.Pollock; Journ.Appl.Phys. **54**, 6193 (1983)

15. J.F.Pinto, L.W.Stratton, C.R.Pollock; Opt.Lett. **10**, 384 (1985)

16. J.F.Pinto, E.Georgiou, C.R.Pollock; Opt.Lett. **11**, 519 (1986)

17. R.Beigang, K.Klameth, B.Belker, Z.Yoon, M.Welling; Opt.Commun. **65**, 383 (1988)

18. C.F.Culpepper, T.J.Carrig, J.F.Pinto, E.Georgiou, C.R.Pollock; Opt.Lett. **12**, 882 (1987)

19. E.Georgiou, J.F.Pinto, C.R.Pollock; Phys.Rev.B. **35**, 7636 (1987)

20.A.E.Seigman; Lasers; University Science Books, CA. USA (1986)

21. H.W.Kogelnik, E.P.Ippen, A.Diennes, C.V.Shank; IEEE J.Quan.Elect. **QE-12**, 123 (1972)

Chapter 3

The Generation and Measurement of Ultrashort Laser Pulses

3.1 Introduction

The generation of ultrashort optical pulses covering the visible and infrared regions of the spectrum is achievable when the technique of modelocking, in one of its forms, is applied to suitable laser gain media such as dyes, colour centres and semiconductor diode lasers [1-6]. The application of ultrashort laser pulses is of extreme importance in many areas of physics and chemistry [7-9]. For example, ultrashort optical pulses can be used to investigate the relaxation kinetics of many materials [7,10] in order to gain information on the physical properties of the material concerned and in the field of telecommunications the requirement of a suitable ultrashort laser source is of paramount importance. In this chapter the methods of generating and measuring such ultrashort laser pulses will be discussed.

3.2 An introduction to modelocking

A laser essentially consists of a gain medium, such as a colour centre crystal or a dye jet, placed within an optical resonator formed by two (or more) mirrors. When such a laser is allowed to operate continuously (CW) the photon flux within the cavity is evenly distributed and is confined in frequency to the cavity modes with sufficient gain to overcome the resonator losses and the laser output consists of a random and fluctuating series of spikes. Depending on the geometry of the resonator many transverse modes may resonate, each characterised by the transverse mode integers l and m, and each of these modes has an associated set of longitudinal modes which which have a Gaussian profile

and are characterised by the integer q. The frequency separation $\Delta\nu$ of these longitudinal modes (fig 3.1a) is given by

$$\Delta\nu = \frac{c}{2L} = \frac{1}{\tau_{cav}} \qquad (3.1)$$

where c is the speed of light and L the cavity length. It may be shown that the total resonator mode frequencies may be expressed as

$$\nu = \Delta\nu \, [\, q + r \, (l + m + 1) \,] \qquad (3.2)$$

where $\cos(r\,\pi) = (1 - \frac{L}{R})$, R being the radius of curvature of the mirrors. However, for the laser resonators operated throughout this thesis the transverse mode structure was confined to the fundamental, TEM_{00}, type by the insertion of appropriate intracavity apertures and therefore the transverse mode integers in equation (3.2) can be ignored so the number of possible oscillating modes may be found by the following

$$q = \frac{\Delta\nu_g}{\Delta\nu} \qquad (3.3)$$

where $\Delta\nu_g$ is the bandwidth of the laser gain medium. As the laser modes have a random phase relationship and oscillate independently of each other such that the temporal output of the laser varies randomly the resultant electric field due to the n^{th} oscillating mode is given by

$$E_n(t) = E_n \exp\{\, i[2\pi\nu_n (t - \frac{z}{c}) + \theta_n] \,\} + cc \qquad (3.4)$$

along the z direction. Therefore the resultant electric field E_{TOT} due to all the oscillating modes may be obtained from the summation of all the electric fields to give the following expression for the total intracavity electric field

$$E_{TOT}(t) = \exp\left\{ i\left[2\pi\nu_n\left(t - \frac{z}{c}\right)\right]\right\}\left[\sum_n E_n \exp\left\{i\left[2\pi n\Delta\nu\left(t - \frac{z}{c}\right)\right]\right\}\right] + \theta_n + cc \quad (3.5)$$

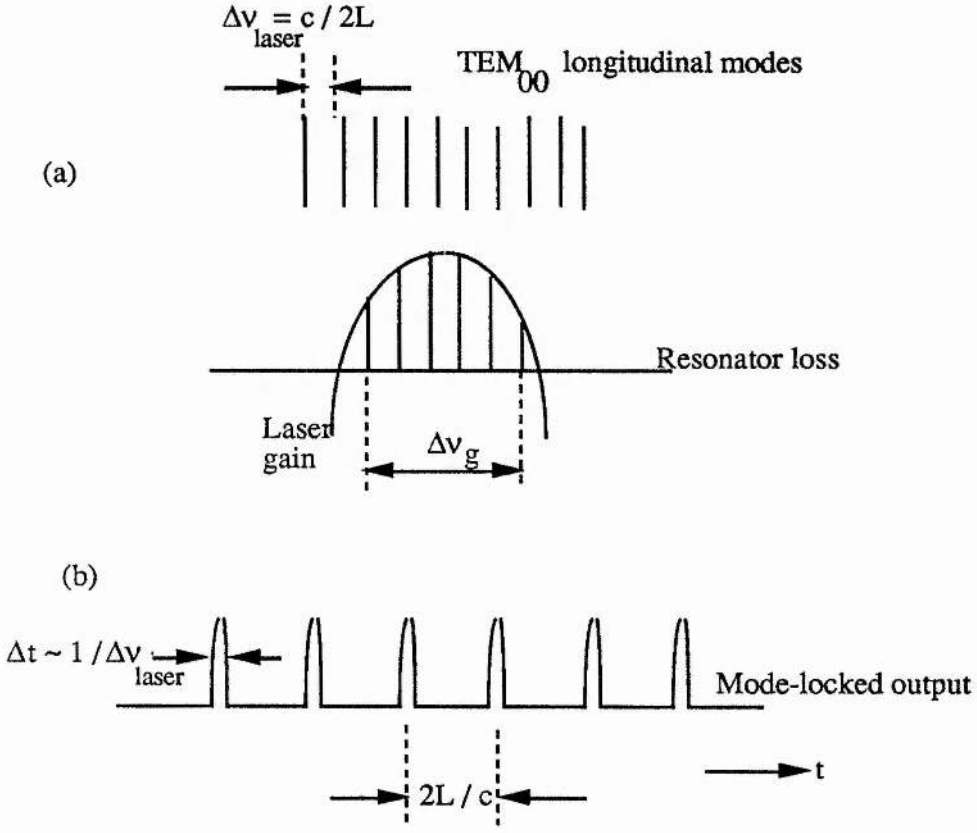

Figure 3.1 (a) The spectral output of a laser operating on TEM_{00} and (b) the temporal output of a modelocked laser

If these randomly varying modes where forced to maintain a fixed phase relationship to each other the laser is said to be phaselocked or modelocked and the temporal output of the laser consists of a train of pulses separated in time $T = \frac{2L}{c}$ (fig 3.1b) where the pulse duration is related to the laser bandwidth $\Delta\nu$ by

$$\Delta\tau\,\Delta\nu = \alpha \qquad (3.6)$$

where α is a constant whose value is determined by the profile of the pulse envelope and is given in table 3.1. Modelocking may be visualised by considering the simple vector diagram shown in figure 3.2.

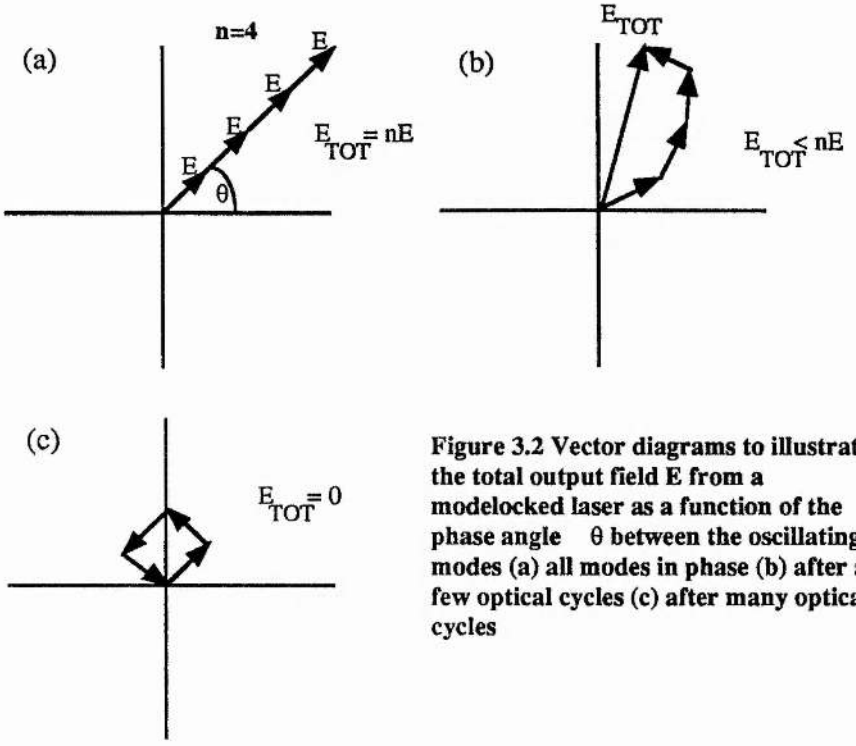

Figure 3.2 Vector diagrams to illustrate the total output field E from a modelocked laser as a function of the phase angle θ between the oscillating modes (a) all modes in phase (b) after a few optical cycles (c) after many optical cycles

Here it is assumed that the modes have equal amplitudes E and that each mode is represented by a vector which has an angular rotation frequency of $2\pi\nu_n$. At t = 0 all the vectors have the same phase and add constructively such that $E_{TOT}=nE$. After a few optical cycles they will no longer be in phase so $E_{TOT}<nE$ thus the output intensity falls and after a large number of optical cycles the vectors will add to zero thus $E_{TOT}=0$ and the optical intensity will be zero. This condition will recur when the phase difference $\Delta\theta$ between each mode is

$$\Delta\theta = \frac{2\pi}{n} \qquad (3.7)$$

therefore the total electric field $E_{TOT} = 0$ when

$$2\pi(\nu + \Delta\nu)t - 2\pi\nu t = \frac{2\pi}{n} \qquad (3.8)$$

where t is the time and may be expressed as $t = \frac{1}{n\Delta\nu}$. The vector components will be in phase again when the phase difference between each is 2π i.e.

$$2\pi(\nu + \Delta\nu)t - 2\pi\nu t = 2\pi \qquad (3.9)$$

such that $t = \frac{1}{\Delta\nu} = \frac{2L}{c} = \tau_{cav}$ which is the modulation period for the total electric field vector.

In practice a laser may be modelocked by several means which may be classified into the two distinctive categories of (i) active modelocking which involves modulating the laser gain by an externally-controlled means such as by an acousto-optic device or indeed by pumping from a modelocked source which is known as synchronous pumping or (ii) passive modelocking whereby a saturable absorber is located within the laser cavity. Both of these methods of modelocking will now be discussed in the following sections.

3.3 Active Modelocking

A laser may be modelocked by providing a dynamic loss, gain or phase to the intracavity flux by means of an acousto-optic or electro-optic device modulated at the cavity round-trip period or at a suitable harmonic such that the flux experiences periodic perturbations whose frequency coincide with the cavity mode spacing [11-13]. The active modelocking device used throughout this thesis was a Spectra physics model 3425 acousto-optic modelocker which consisted of a fused silica prism which was modulated by a piezo-electric transducer at frequencies of ≈ 41MHz which is appropriate for a cavity length ≈

1.8m. This device was mounted close to the end mirror and maintained at a temperature of $\approx 5^0$C above the ambient laboratory temperature (to an accuracy of 0.1^0C) which served to help maintain the resonant frequency of the prism. The elasto-optic properties of the medium result in a spatially periodic disturbance of the refractive index such that the intracavity flux incident on this effective "spatial array" is diffracted with the wavelength of the acoustic waves within the medium determining the grating spacing. The standing waves which are set up within the prism are given by fig 3.3

$$y_1 + y_2 = 2A \sin kx \cos \omega t \qquad (3.10)$$

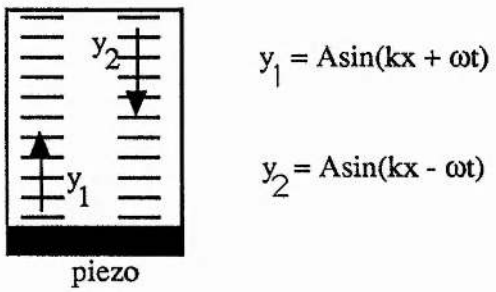

Figure 3.3 Schematic diagram of an acousto-optic cell illustrating the formation of a standing wave.

Thus if the periods are chosen as indicated in figure 3.4 it can be seen that twice per cycle the acousto-optic cell is completely transparent and therefore the resonant frequency of the cell is selected such that it is half that of the cavity round trip period τ_{cav}.

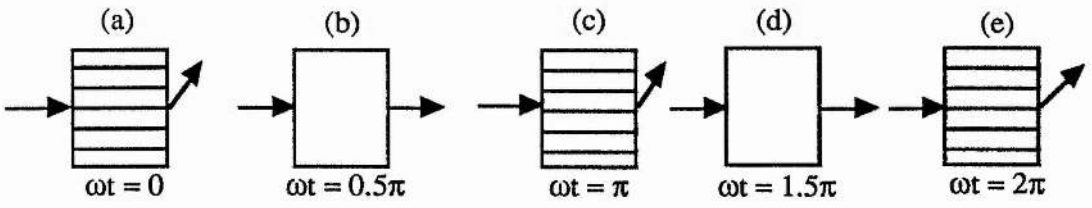

Figure 3.4 Diagram showing that the acousto-optic cell provides minimum loss twice per excited period at (b) $\omega t = 0.5\pi$ and (d) $\omega t = 1.5\pi$

Typical pulse durations produced by this method are 10-100 ps [14] with the pulse duration depending on the number of modes that can be properly phase-coupled.
A method by which shorter pulse durations can be obtained from the technique of active modelocking is that of synchronous pumping,which was first applied to dye lasers in 1971 [15]. In this approach an actively modelocked laser is used to pump a "slavelaser" whose cavity round-trip period is closely matched to or is a multiple of that of the pump laser such that the pulse train of the pump laser causes the gain of the "slavelaser" to be modulated. As the pulse evolution kinetics evolve pulse shortening occurs due to suppression of the leading and trailing edges by timing the return of the pulse to the gain medium such that the peak preferentially receives the optical gain. Experimentally it has been found that the minimum pulse durations are produced when the slave cavity is slightly longer than that of the pump and typically better than x10 compression in pulse durations may be achieved by this method [16] when for example this technique is applied to dye lasers where sub-picosecond pulse durations have been reported, where the pump-pulse duration is of the order of 100ps.

3.4 Passive Modelocking

Passive modelocking is the simplest of all the modelocking techniques and in general produces the shortest pulses. This technique involves the insertion of a saturable absorber such as an organic dye, or more recently multiple quantum wells [1,2,17,18], into the laser cavity which basically acts as an optical switch allowing only the transmission of high intensity intracavity flux.

Low level intracavity flux incident upon the saturable absorber is absorbed causing electrons to be excited to an upper state level to form an excited state population within the absorber which relaxes to the ground state with a characteristic recovery time τ_{abs}. As the flux intensity incident upon the absorber increases, the rate of excitation to the upper excited state exceeds decay by spontaneous emission to the lower ground state and thus

the absorber becomes bleached and saturates. The dye, for example, therefore becomes transparent and allows the transmission of high intensity intercavity flux. This allows a high intensity optical pulse to evolve within the laser cavity as once the high intensity pulse has passed through the absorber it quickly recovers to attenuate the low level fluctuations thus allowing the high intensity flux to receive all of the the optical gain.

This process will be discussed in detail in chapter 8 when a passively modelocked LiF:F_2^+ colour-centre laser will be presented. Initial passive modelocking experiments involved placing the saturable absorber within a thin dye cell placed close to one of the cavity mirrors [19]. However as this technique was further developed this cell was replaced by a fast flowing thin dye jet in order to reduce the number of intracavity surfaces, improve the optical quality and to ensure that efficient recycling of the dye was carried out. Passively modelocked lasers of this nature implementing a variety of organic dyes have enabled ultra-short pulses to be produced over the spectral range 490 - 950nm [1,2,20] and have led to the direct generation of 19fs pulses from a colliding pulse ring dye laser [21]. More recently the organic dye saturable absorber has been replaced by multiple quantum wells when this modelocking technique has been applied to colour-centre and diode lasers operating in the 1.3 - 1.5μm region of the spectrum where the operation of suitable dyes becomes very unstable and ineffective due to the molecular chain for such dyes being relatively long and delicate for absorption in this spectral region.

As well as absorber saturation, saturating the optical gain plays a dominant role in the production of ultrashort pulses as the loss on the leading edge of the pulse occurs due to absorber saturation whilst the loss experienced by the trailing edge is incurred by gain saturation. The interplay of these two processes was first discussed by New [19] who defined several experimental conditions that must be met in order for the technique of passive modelocking to be effective. These are (i) the resonator round trip time τ_{cav} be greater than the gain recovery time τ_{gain}.

$$\tau_{cav} > \tau_{gain}$$

and (ii) the absorber recovery time τ_{abs} should be less than that of the gain recovery time τ_{gain}.

$$\tau_{abs} < \tau_{gain}$$

By modelling the pulse evolution kinetics New showed that pulse compression occurred when the system parameters lay within a set of boundaries known as the stability region defined by the so called "S" parameter given by

$$S = k\frac{\sigma_a I_g}{\sigma_g I_a} = k\frac{\sigma_a A_g}{\sigma_g A_a} \qquad (3.11)$$

where σ_a and σ_g are the absorber and gain cross sections, I_a and I_g are the optical intensities within the absorber and gain media and A_a and A_g are the focal areas of the beamwaist within the absorber and gain media. From equation (3.11) it may be deduced that the S parameter magnitude may be made large experimentally by employing a "folded focussing" section around the gain and absorber media with the focal length of the absorber mirrors chosen such that a tighter beam waist is produced in the absorber than that of the gain. The S parameter may be increased further when a colliding pulse modelocked (CPM) travelling-wave (or ring) cavity is employed as theoretically predicted by several workers [22,23]. In a CPM cavity the saturable absorber is located at the centre of the optical cavity. Two counter-propagating pulses collide within the absorber where the pulse originates from noise fluctuations. This produces a transient grating due to the coherent interference of the two pulses. This has the effect of reducing the saturation level of the absorber and consequently the optical flux within the absorber appears higher than that of the gain which (ref.equation (3.11)) increases the S parameter.

3.5 Ultrashort Laser Pulse Duration Measurement

3.5.1 Introduction

With the advent of picosecond and femtosecond optical pulse production the convenient and standard combination of a fast photodiode and oscilloscope arrangement as a temporal diagnostic has become inadequate. This method has a temporal resolution in the order of 25ps when repetitive pulse trains are sampled using a suitable sampling head [24,25]. Instead, a higher temporal resolution of ultrashort pulses is provided by nonlinear measurement techniques such as second harmonic generation (SHG) [26,27] and two photon fluorescence [27] or by direct linear measurement using electron-optical streak cameras [28]. In the work described in this thesis all temporal measurements were carried out using second harmonic generation autocorrelation techniques and by a synchroscan streak camera [29] and it is here that that these methods will be discussed.

3.5.2 Autocorrelation by Second Harmonic Generation

An efficient technique by which ultrashort pulse durations can be measured with femtosecond resolution [27] is the nonlinear technique of autocorrelation by second harmonic generation (SHG). This technique was first demonstrated in 1967 [26] and basically involves dividing the laser pulse train into two equal intensity pulse trains which after being allowed to travel two different optical paths are recombined in a nonlinear crystal to generate the second harmonic signal. There are essentially two experimental methods by which second harmonic generation autocorrelation may be carried out these being (i) SHG of the first kind, which involves two collinear pulse trains having the same polarisation being allowed to pass through the nonlinear crystal. Thus the second harmonic signal may be generated by the presence of only one of the pulse trains (therefore a background signal is always present). The second method (ii) SHG of the

second kind is where the polarisation of the two pulse trains are made orthogonal [26,30] or the pulse trains are made to be noncollinear [31] such that it is necessary that both pulse trains need to be present in order to produce a second harmonic signal.

In the work discribed here SHG of the first kind was implemented and the experimental configuration for such an autocorrelator is illustrated in figure 3.5.

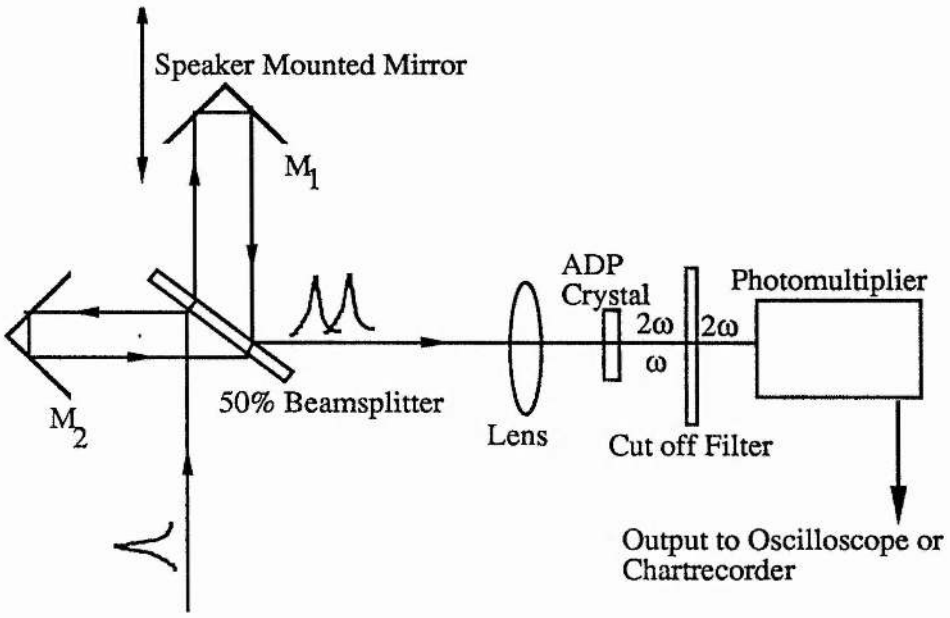

Figure 3.5 The experimental configuration for a second harmonic autocorrelator

A Michelson interferometer type of optical delay arrangement was used to provide a time calibration for the autocorrelator. To accomplish this a movement for the end mirror M_2 was provided by means of a stepper motor and micrometer arrangement. Real time pulse monitoring was also effected by vibrating mirror M_1 with a speaker arrangement driven from a waveform generator. After passing through the optical delay line the pulse trains were focused tightly with a 2cm focal length lens onto the ADP (ammonium dihydrogen phosphate) second harmonic crystal which was cut for phasematching at normal incidence for the selected laser operating bandwidth. A Schott RG 780 filter was

used to block the fundamental frequency signal and the second harmonic signal was monitored using a photomutiplier-oscilloscope combination.

The second harmonic signal produced may be expressed as

$$I_{(2\omega)}(\tau) = C[1+2G^{(2)}(\tau)+r(\tau)] \qquad (3.12)$$

where C is a constant, τ is the time delay between the pulses, $r(\tau)$ is an interference term which averages to zero for translations greater than a fundamental wavelength and $G^{(2)}$ is the second order correlation function given by

$$G^{(2)}(\tau) = \frac{\int_{-\infty}^{+\infty} I_\omega(t)I_\omega(t+\tau)dt}{\int_{-\infty}^{+\infty} I_\omega(t)I_\omega(t)dt} \qquad (3.13)$$

where $I_\omega(t)$ is the fundamental pulse envelope. For a free running laser consisting of independently oscillating modes a "spike"with a peak-to-background ratio of 3:2 is obtained as indicated in figure 3.6a with the fullwidth at half maximum (FWHM) of the spike giving the coherence time of the laser. If the laser intracavity flux consists of noise bursts or pulses consisting of incoherent modes a coherence spike is obtained upon a broad pedestal with a contrast ratio of 3:2:1 (figure 3.6b), the pedestal indicating the duration of the pulse profile. For a multipulsing laser whose output consists of N pulses an autocorelation profile consisting of 2N-1 peaks is obtained (figure 3.6c). Finally for a perfectly modelocked laser all the intracavity flux will be contained within a discrete pulse envelope and a contrast ratio of 3:1 of peak signal to background noise level is to be expected for the autocorrelation signal as illustrated in figure (figure 3.6d). Thus with the SHG of the first kind a contrast ratio is clearly displayed but it has been shown that if

only 10% of the intracavity flux is contained within the pulse envelope then a contrast ratio of 2.92:1 is still obtained [32]. The laser pulse duration Δt may be deduced from the FWHM of the autocorrelation trace $\Delta\tau$ by the following expression

$$\Delta t = \frac{2\Delta l}{k\,C} = \frac{\Delta\tau}{k} \qquad (3.14)$$

where Δl is the translation distance of mirror M_2, c is the velocity of light and k is a constant which depends on the profile of the pulse envelope (see Table 3.1).

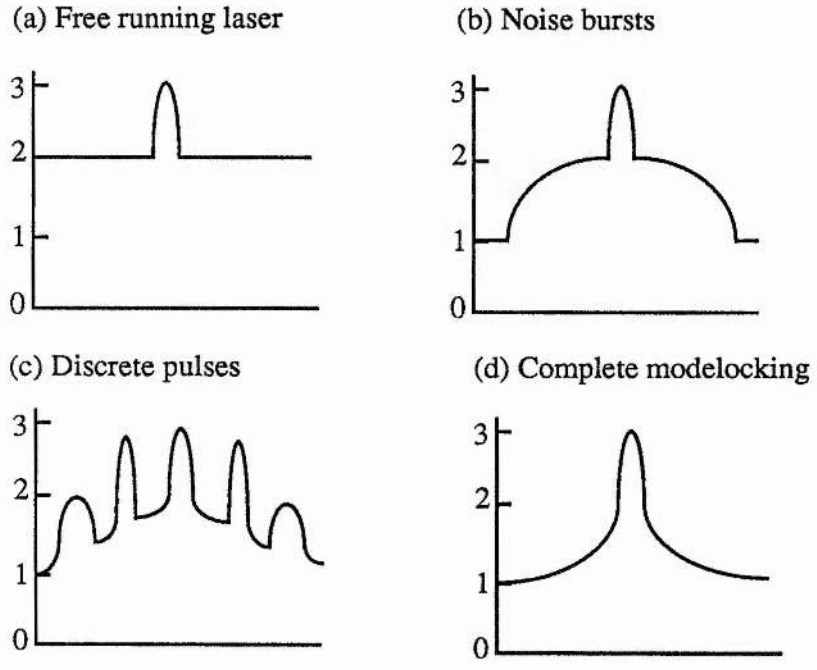

Figure 3.6 Second harmonic generation autocorelation profiles

As the correlation function is symmetric it therefore does not yield information concerning the profile of the pulse envelope and therefore the pulse profile is inferred by assuming one of a theoretically determined profile as also indicated in table 3.1. However, even this best fit approach to determining the pulse shape is unsatisfactory as the measured pulse durations are averages taken over many pulses ($\approx 3\times10^6$ with a 25Hz

window) and therefore the autocorrelation profile is not sensitive to individual pulse durations but to the distribution of pulse durations [33]. Due to the nonlinear nature of this measurement technique the autocorrelation profile is weighted towards shorter pulse durations [33,34]. Thus to determine the pulse shape, higher order [35] or cross-correlation techniques need to be employed [36]. Information can be obtained however concerning the amount of frequency chirp present within the pulse by interferometric autocorrelation and this may be achieved by slowing the stepper motor or speaker frequency within the optical delay line to such rates that the autocorrelation profile may be recorded with interferometric accuracy as shown in figure 3.7 It may be seen from this figure that for a properly modelocked laser the contrast ratio is 8:1. This is due to the fact that the autocorrelation profile is dependent on the fourth power of the electric field within the second harmonic crystal [27].

Pulse shape	Intensity profile I(t)	α	k
Square	$1(0 \leq t \leq \Delta t)$	0.866	1
Gaussian	$\exp[\frac{-(4 \ln 2)\, t^2}{\Delta t^2}]$	0.441	$\sqrt{2}$
$Sech^2$	$sech^2[\frac{1.76t}{\Delta t}]$	0.315	1.55

Table 3.1 Common pulse shapes with corresponding autocorrelation constant k and the duration bandwidth product α

The optical interference fringes or cycles may be directly counted to obtain the bandwidth of the pulse and as already mentioned the shape of the interferometric pulse envelope gives information as to the degree of frequency chirp within the pulse. For a pulse which is frequency chirped the "wings" of the interferometric profile deviate from the normal profile (figure 3.7) due to the interference resultant obtained from the frequency chirp. Interferometric autocorrelation profiles displaying frequency chirp will be presented later in chapter eight for a passively modelocked colour-centre laser.

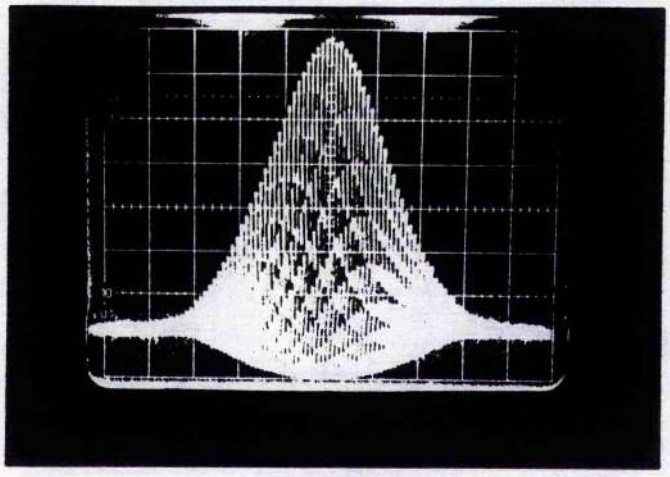

Figure 3.7 An interferometric autocorrelation profile

3.5.3 The Electron-Optical Streak Camera

The concept of electron-optical streak cameras was first reported in 1956 by Zavoisky and Franchenko [37] and its development since then has led to the production of 300 femtosecond resolution cameras in the visible to near-infrared and picosecond resolution in X-ray regions of the spectrum [38,39]. The streak camera operated throughout this work was the Photochron II [40] and its operation may be explained by referring to figure 3.8.

The optical pulse to be measured is incident upon a narrow slit which is imaged by an appropriate coupling lens onto the photocathode. Once illuminated the photoelectrons liberated from the photocathode surface are accelerated to typical energies of 15keV, by means of an appropriate potential gradient set up between the mesh and the anode, towards a phosphor screen situated at the back of the camera. The photoelectron distribution is streaked en route to the phosphor screen by means of a synchronised linear voltage ramp applied to the deflection plates thereby converting the the photelectron

temporal distribution into a spatial distribution on the phosphor screen which can then be displayed via photographic film or an optical multichannel analyser.

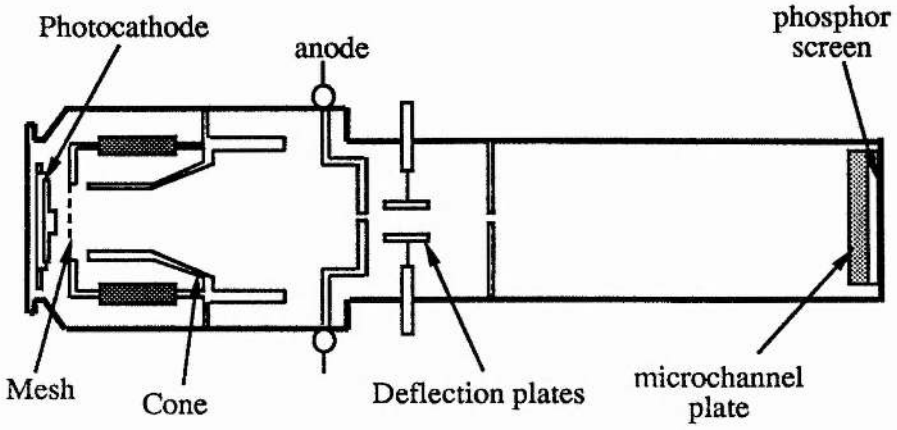

Figure 3.8 Schematic diagram of the Photochron II Streak Camera

The temporal resolution of a single-shot electron-optical streak camera is governed by two primary processes. These are firstly the photoelectron transit time dispersion Δt_d which arises due to an energy distribution of the emitted photoelectrons [37]. This limitation Δt_d may be expressed as a function of the photoelectron energy distribution by

$$\Delta t_d = \frac{(2.34 \times 10^{-8})\sqrt{\Delta\varepsilon(eV)}}{E} \qquad (3.15)$$

where $\Delta\varepsilon(eV)$ is the photelectron energy distribution which is dependent on the energy of the incident photon and the photocathode extraction field E in Vcm^{-1}. For the Photochron II a transit time dispersion of 0.74ps has been evaluated for extraction fields of $\approx$ $20kVcm^{-1}$ for an incident wavelength of 744nm [41]. The second major influence on the camera temporal resolution is the technical time resolution Δt_{tech} [37] which arises because of the finite spatial resolution of the camera. This may be expressed as

$$\Delta t_{tech} = \frac{1}{v\delta} \qquad (3.16)$$

where v is the streak velocity and δ is the dynamic spatial resolution. For the Photochron II streak velocities are $\approx 2 \times 10^8 ms^{-1}$ and dynamic spatial resolutions are of the order of 10 line pairs per mm thus giving a technical temporal resolution limit of 500fs. If Gaussian pulse intensity profiles are assumed the pulse duration Δt_p may be obtained from the recorded pulse duration Δt_r through

$$\Delta t_r^2 = \Delta t_p^2 + \Delta t_d^2 + \Delta t_{tech}^2 \qquad (3.17)$$

When using the streak camera in a single shot mode a limiting temporal resolution of 300fs has been obtained for a more recently designed Photochron IVsystem [39].

Another method of operating the streak camera which was used throughout the work described here is that of a synchronously-repeatable (or "synchroscan") mode whereby the streak voltage ramps of the camera are carefully synchronised with the pulses in a modelocked cw laser output. This allows real-time monitoring of the pulse to be performed [29]. An added advantage of this technique is that low light levels may be measured as the signal is effectively integrated at the phosphor. The experimental arrangement for operating the Photochron II in synchroscan mode is illustrated in figure 3.9. As this mode of operation has been described in detail elsewhere [42] only a brief account need be given here.

A small fraction of the modelocked pulse train is "bled off" from the main streak camera diagnostic beam and focussed onto a tunnel-photodiode with the remaining portion of the pulse train being directed to the camera slit via the Michelson delay line. The bias of the diode is adjusted such that the incident pulses produce a sinusoidal voltage in the tunnel-diode oscillator and this is frequency doubled (normally in the range 100-200MHz) and amplified to $\approx$10W before being coupled onto the camera deflection plates by means of a high Q impedence matching network. Typically a deflection voltage $\approx$3.5kVmagnitude synchronised with the laser pulse train is made available by this scheme. The large

voltage of this deflection ramp ensures linearity of the streak image over the 5cm diameter phosphor screen. Care is taken to ensure that both the delayed and undelayed pulse trains from the Michelson arrangement arrive at the camera within the linear regions of the streak voltage so that errors in the calibration are avoided. The streak images are usually monitored by a vidicon based optical microchannel analyser (OMA) arrangement which enables the laser pulses to be monitored in real time.

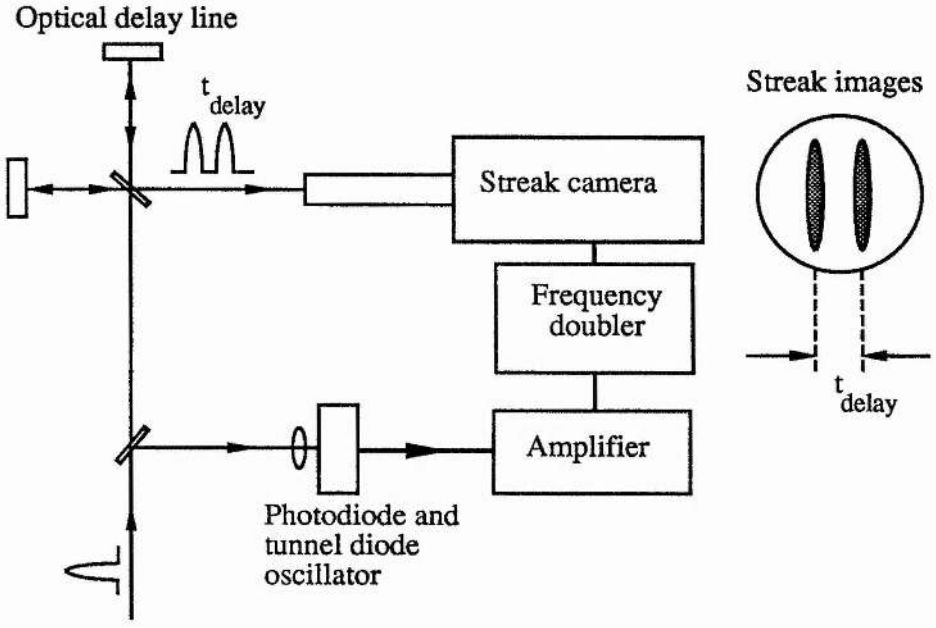

Figure 3.9 The experimental arrangement for synchroscan operation of the Photochron II streak camera

The temporal resolution of the camera operating on a synchroscan mode is longer than that of single-shot operation, normally several picoseconds [29]. This is due to the presence of phase jitter within the optical pulse train [43] which causes spatial broadening of the streak image formed upon the phosphor screen to occur as integration of the multiple streaked events takes place. The amount of phase jitter within the pulse train will depend upon the modelocked laser source and hence the temporal resolution will vary according to the source of the pulses under investigation [43]. Recently a temporal resolution of 1ps has been obtained from a Photchron II camera operating in synchroscan

mode when a stabilised passively modelocked CPM ring dye laser (≈100-200fs pulse durations) operating at 620nm was implemented [44].

3.6 Summary

Within this chapter an introduction to the techniques of producing and measuring ultrashort laser pulses has been presented. The technique of passive modelocking in general produces the shortest pulses, however the laser operational wavelength is confined to the absorption peak of the saturable absorber. Active modelocking generates slightly longer modelocked pulse durations compared to those produced from passively modelocked pulse sources, but allows tunability, across the laser gain bandwidth.

Measuring the ultrashort pulse durations can be performed using linear and non-linear techniques. The non-linear measurement technique of autocorrelation by second harmonic generation provides a high temporal resolution (10's of fs) compared to linear measuring measuring devices such as the streak camera (≈ps). The streak camera, however provides a facility to measure low intensity signals over large spectral ranges.

Chapter 3. References

1. P.M.W.French, J.R.Taylor; Appl.Phys.Lett. **50** 1708 (1987)

2. K.Smith, N.Langford, W.Sibbett, J.R.Taylor; Opt.Lett. **50** 559 (1985)

3. L.F.Mollenauer, Tunable Lasers (Ed. L.F.Mollenauer, J.L.White) Topics in Appl.Phys. **59**, 227 (1887) Springer, Berlin,Heidelberg.

4. N.Langford, K.Smith, W.Sibbett; Opt.Lett **12**, 903 (1987)

5. P.T.Ho; Appl.Phys.Lett. **33**, 241 (1978)

6. J.T.Chang, J.I.Vukusic; IEEE J.Quan.Elec.**QE-23** 1329 (1987)

7. C.V.Shank, R.L.Fork, B.I.Greens, C.Weisbuch, A.C.Gossard; Surface Science **113**,108 (1982)

8. L.F.Mollenauer, R.H.Stolen, J.P.Gorden; Phys.Rev.Lett. **45**, 1095 (1980)

9. C.V.Shank, R.L.Fork, R.F.Leheny, J.Shah; Phys.Rev.Lett. **42**, 112 (1979)

10. W.Sibbett, J.Taylor, D.Welford; IEEE J.Quan.Elec. **QE-17**, 500 (1981)

11. A.Yariv; J. Appl.Phys. **36**, 388 (1965)

12. B.C.Johnson, P.F.Moulton, A.Mooradian; Opt.Lett. **10**, 4 (1984)

13. J.P.Willson; PhD. Thesis University of London (1982)

14. A.Scaveenel; J.Appl.Phys. **36**,388 (1965)

15. P.K.Runge; Opt.Commun. **4**, 195 (1971)

16. P.G.May, W.Sibbett, K.Smith, J.R.Taylor, J.P.Willson; Opt.Commun. **24**, 285 (1982)

17. P.W.Smith, Y.Silverberg, D.A.B.Miller; J.O.S.A.(B) **2** (1985)

18. M.N.Islam, E.R.Saunderman, C.E.Soccolich, I.Bar-Joseph, N.Saver, T.Y.Chang, B.Miller; IEEE J.Quan Elect. **QE-25**, 2454 (1989)

19. G.H.C.New; Rep.Prog.Phys. **46**, 877 (1983)

20. E.P.Ippen, C.V.Shank, A.Diels; Appl.Phys.Lett. **21**, 348 (1972)

21. A.Finch, G.Chen, W.Sleat, W.Sibbett; J.Mod.Opt. **35**, 345 (1988)

22. D.Kulhke, W.Rudolph, B.Wilhelmi; IEEE J.Quan Elect. **QE-19**, 570 (1983)

23. M.S.Stix, E.Ippen; IEEE J.Quan.Elect. **QE-19**, 520 (1983)

24. S.Y.Wang, D.M.Bloom, D.M.Collins; Appl.Phys.Lett. **42**, 190 (1983)

25. W.Margulis, W.Sibbett; Appl.Phys.Lett. **42**, 975 (1983)

26. H.P.Weber; J.Appl.Phys. **38**, 2231 (1967)

27. E.P.Ippen, C.V.Shank; Ch.2 Ultrashort Light Pulses (Ed. S.L.Shapiro) Springer-Verlag, Berlin (1971)

28. D.J.Bradley, W.Sibbett; Appl.Phys.Lett. **27**, 382 (1975)

29. M.C.Adams, W.Sibbett, D.J.Bradley; Advances in Electronics and Electron Physics **52**, 265 (1979)

30. J.A.Armstrong; Appl.Phys.Lett. **10**, 16 (1967)

31. M.Maier, W.Walker, J.A.Giordmaine; Phys.Rev.Lett. **17**, 1275 (1966)

32. D.Von Der Linde; IEEE J.Quan.Elect. **QE-8**, 328 (1972)

33. E.W.Van Stryland; Opt.Commun. **31**, 93 (1971)

34. E.I.Blount, J.R.Klauder; J.Appl.Phys. **40**, 2874 (1969)

35. H.P.Weber, R.Dandliker; Phys.Lett. **28A**, 77 (1968)

36. W.Dietel, J.J.Fontaine, J.C.Diels; Opt.Lett. **8**, 4 (1983)

37. E.K.Zavoisky, S.D.Fanchnko; Sov.Phys.Doklady. **1**, 285 (1956)

38. C.F.McConaghy, L.W.Coleman; Appl.Phys.Lett. **25**, 268 (1974)

39. A.Finch, Y.Liu, H.Nui, W.Sibbett, W.Sleat, D.R.Walker, Q.L.Yang, H.Zhang; Ultrafast Phen. VI Springer Series in Chem.Phys. **48**, 159 (1988)

40. P.R.Bird, D.J.Bradley, W.Sibbett; Proc.11TH Int.Congress High Speed Photography & Photonics, 112 (1975)

41. H.Nui, W.Sibbett; Rev.Sci.Inst. **52** 1830 (1981)

42. W.Sibbett; Proc.Int.Congress High Speed Photography, San Diego (1982)

43. A.Finch, X.Zhu, P.N.Kean,W Sibbett; IEEE J.Quan.Elect. **QE-26**, 1115 (1990)

44. J.P.Willson, W.Sibbett, W.E.Sleat; Opt.Commun. **42**, 208 (1982)

Chapter 4

Electroluminescence "An Introduction"

4.1 Introduction

Since the discovery of electroluminescence in 1920 [1], which essentially involves the production of photons from a suitable host material upon the application of an appropriate electric field, its usefulness was not really utilized until the 1950`s [2,3]. Since then the research and development in this field of interest has increased dramatically with, for example, the production of commercially available light emitting diodes (LED`s) emitting over the visible and infrared regions of the spectrum, large area panel displays and more appropriately laser diodes. All of these are essentially electroluminescent devices and their use for domestic and commercial purposes is becoming increasingly widespread. In particular, since its development the laser diode has many applications because of its extreme compactness and reliability. Such laser devices are now used widely in the field of telecommunications [4] and more recently to pump, very efficiently, solid-state microlasers such as Nd:YAG [5]. Diode-array pumped microlasers have a low power budget and potentially long (years) operating lifetimes so that they are suitable for applications associated with satellite communications for example [6].

Essentially the laser diode owes its success to its ruggedness, size and to its simple and low cost electrical pumping scheme whereby minority carriers are simply injected under the influence of a low magnitude forward bias (typically a few volts) across a pn junction whereby they recombine radiatively with majority carriers. Though versatile, the operation of a colour centre laser involves the use of another laser source as a pump mechanism and so the overall efficiency of such a system compares poorly with that of a diode laser. It follows therefore, that if an electrical pumping scheme could be applied to the colour centre

laser then the operation and versatility of such a laser would be revolutionised. Notably, its running costs would be dramatically reduced, the overall size would be very substantially reduced and the efficiency of such a system would be vastly superior to that of the optically pumped counterpart. Significantly, also, it has been observed [7-10] that such an electrical pumping scheme applied to colour centre hosts such as the alkali halides actually provides a tuning range in the visible and ultraviolet (UV) regions of the spectrum.

4.2 Mechanisms of Electroluminescence

4.2.1 General Introduction

The phenomenon of electroluminescence has been observed in a wide range of materials under the application of suitable electric fields [11] .Historically Gudden and Phohl [1] were the first workers to observe this phenomenon in 1920 when they discovered that electric fields of ~ 5 $kVcm^{-1}$ applied to a zinc sulphide phosphor caused the material to give off "bursts of light". It was later in 1935 when Destriau [12] constructed a thin (~100μm) layer of zinc sulphide phosphor embedded in a dielectric mounted between two electrodes, one of which was transparent that it was shown that continuous light emission was possible from this new phenomenon. Destriau continued to work in this field and produced a useful review of his work in 1947 [12]. Electroluminescent studies on many other materials have been carried out since Destriau`s initial work particularly since 1950 when a practical use of this form of luminescence was provided in the form of an electroluminescent lamp [3].

As a consequence of Destriau`s early pioneering work with phosphors the above mentioned form of electroluminescence is generally termed as Destriau type electroluminescence and several possible excitation mechanisms have been proposed [13,14]. For a ZnS phosphor, for example, it is generally accepted that the luminescence is caused by the recombination of excess carrier pairs which have been impact ionized by hot electrons produced within a

high field region at a metal insulator interface [2]. Theoretically there are several feasible mechanisms by which luminescent solid materials may be excited by the application of an external electric field. These include (i). Injection luminescence (Losev luminescence) [15], (ii) Impact luminescence (Destriau luminescence) [16] and (iii) Field luminescence [17].

4.2.2 Impact luminescence

Impact luminescence may occur when high velocity electrons produced under high electric field conditions (eg within a potential barrier) collide inelastically with luminescence centres causing the centre to be excited or ionized. Subsequent relaxation to the ground state gives rise to the emission of a photon. To cause luminescence by this mechanism there are three prerequisites, namely; (i) a high electric field region capable of accelerating charge carriers to relatively high kinetic energies must be provided, (ii) charge carriers must be injected into this high field region where they may be accelerated to suitable impact velocities and (iii) appropriate luminescence centres must be available to absorb by inelastic collisions a significant percentage of the kinetic energy extracted from the high field region.This is illustrated in figure 4.1.

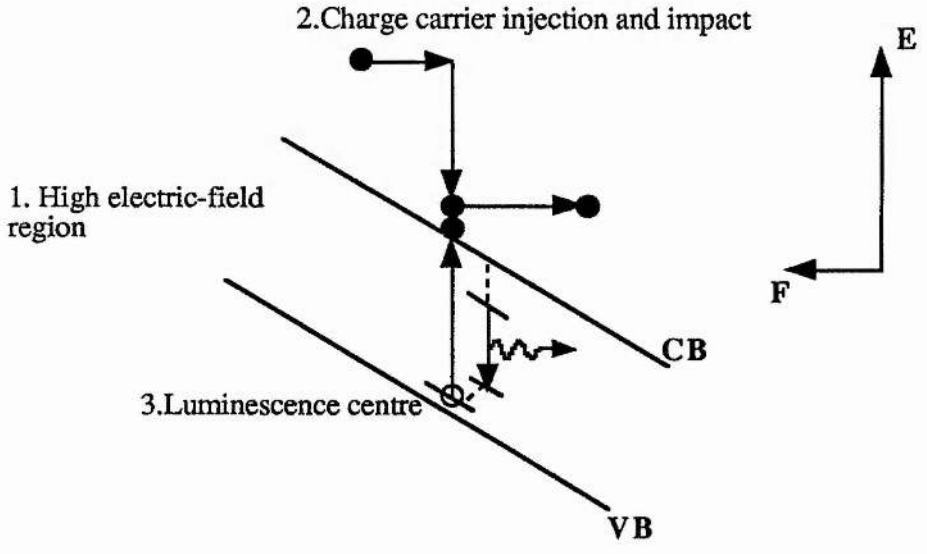

Figure 4.1 Schematic diagram showing the three prerequisites for impact luminescence.

The charge carriers produced in this process are known as hot electrons (or hot holes where appropriate) because their energy is considerably higher than that of the surrounding lattice. The lattice will of course gain energy from the applied field during collisions (Joule heating) whereby acoustical modes will be excited under low field conditions and optical modes will arise under high field conditions. Within the high field region the energetic electrons will retain some of their energy between collisions such that their average speed increases as a result of this cumulative process and so if an electron travelling with velocity v moves a distance $v\tau$ before being scattered, then the energy gained between scattering events is $eEv\tau$. Thus if on scattering the electron transfers the LO phonon energy $h\upsilon_{LO}$ to the lattice then it may be seen that if the condition

$$eEv\tau > h\upsilon_{LO} \qquad (4.1)$$

is met then electron runaway (or an avalanche effect) may occur. However, this effect is limited by acoustic scattering and band structure effects.

The electroluminescence obtained from ZnS:Cu is attributed to impact luminescence where it is assumed that the high electric field is produced in a Mott-Schottky exhaustion barrier [16] which is formed at the contact electrode and the charge carriers are provided from shallow donor states which are field excited. The electric field experienced across a high field exhaustion region is given by

$$E(x) = \frac{1}{2} A^2 (x - d) \qquad (4.2)$$

if an electron at the negative contact has a potential energy of V_0 with respect to the positive contact then

$$V(x) = -\int_{x}^{d} E(x)\, dx = \frac{1}{4} A^2 (d - x)^2 \qquad (4.3)$$

On combining equations 4.2 and 4.3 then

$$E(x) = -A\,[\,V(x)\,]^{1/2} \qquad (4.4)$$

The potential barrier width d is therefore given by

$$d = \frac{2V_o^{1/2}}{A} \qquad (4.5)$$

where $A = \left[\frac{8\pi Ne}{\varepsilon}\right]^{1/2}$, V_0 is the applied voltage, N the donor trap density and x the distance into the crystal from the contact. Thus from equation (4.5) the width of the active luminescence region below the metal contact may be calculated for a Mott-Schottky type barrier if the donor trap density is known.

4.2.3 Field Ionization

The mechanism of luminescence by field ionization is where the application of an electric field of suitable magnitude leads to the direct excitation of the luminescence centres. In this case it is possible that an electron may gain enough energy from the applied field to enable ionization to occur. Due to the large field strengths required before this process can occur it is possible that dielectric breakdown of the crystal may occur. To illustrate this, work has been carried out upon atomic hydrogen (the band energy structure of such being simple and well documented) and it has been calculated [15,17] that a field strength of 7×10^5 Vcm^{-1} is required to ionize the n=5 state which is only 0.54 eV below the ionization limit and that the necessary field strength required for ionization varies as the square of the depth of the level. Thus for the case of ZnS:Cu whose luminescence centre lies ≈ 3 eV below the conduction band the ionization field required is calculated to be 2×10^7 Vcm^{-1} which is well in excess of the breakdown field of 10^5–10^6 Vcm^{-1} for ZnS. Nevertheless, under sufficiently high field conditions when the bands become tilted it may be possible for an electron to tunnel across the band gap to states of equal energy thereby creating a possible recombination site.

Another process which may occur under high field conditions is that of avalanche breakdown, where field-ionized electrons may gain enough kinetic energy to impact-excite further electrons from impurity centres or the valence band such that the number of free electrons multiplies by successive collisions. This process continues until current saturation occurs at the contact or more drastically when the material vaporizes. The threshold energy E_{th} for such a process to occur is given by:

$$E_{th} = \frac{m_h^* + 2\, m_e^*}{m_h^* + m_e^*} E_g \qquad (4.6)$$

where E_g is the energy gap and m_e^* and m_h^* the effective masses of the electrons and holes respectively. It may be realized therefore that for a material to luminesce under direct field ionization it should have a wide bandgap with shallow donor levels. On this basis it follows that infrared emission via this process will be most probably observed.

4.3 Electroluminescence in Alkali Halides

Interest in the field of electroluminescence within alkali halides began in the early 1960`s in order that information concerning the mechanism of charge injection, charge transport and the formation of space charge within semiconductors and insulators be obtained [18,19]. This was due to the fact that it is difficult to obtain electric current measurements within such materials whereas the electroluminescence induced by injected electrons could be readily detected using high gain photomultiplier tubes. Also large size single crystals became available so that reasonable emission regions could be accessed for this purpose.

The first report of electroluminescence within this category of materials was for KI [20] at 77K under the application of a 500Hz AC field of magnitude 5 x 10^4 Vcm^{-1}. Other workers [21,22] have carried out similar work on other alkali halides where data on effects such as space charge [8], impact ionization [21,23,24] and indeed a brief report on laser

action has been published [25]. Typically, electroluminescence has been observed from these alkali halide crystals at liquid nitrogen temperatures with field strengths of 10^4-10^6 Vcm^{-1}. Electrical contact to the crystal surfaces has been made using several metals [8], notably evaporated aluminium, silver or melted indium [10] upon which a pressure contact can be made. In all the reports to date the luminescence signal was observed to be twice the frequency of the applied excitation signal and the emission spectrum observed to coincide with that of the intrinsic luminescence of the crystal concerned.

4.4 The Self Trapped Exciton

Electronic excitation within ionic crystals causes the creation of vacancies and interstitials within the lattice [26]. Within the alkali halides the self trapped exciton is the most easily excited species of luminescence centre created by an electric field [27,28] and so a brief description of the self trapped exciton within the alkali halides is included here.

Experimental studies of the luminescence of several alkali halides which were known to contain V_k centres and similar work carried out on exciton luminescence of pure alkali halide crystals show that their corresponding emission lines overlap indicating that the V_k centre upon trapping an electron forms a species of luminescence centre which has states indistinguishable from those of the exciton [29,30,31]. In KI for example these are the 297nm and 375nm lines [20,29]. This luminescence centre is known as the Self Trapped Exciton (STE). The V_k centre consists of two bound halogen anions oriented in the [110] direction and is formed when one of the halogen ions loses a valence electron because a neutral halogen ion within a normal lattice is unstable the hole forms a covalent bond with a neighbouring anion to form what is known as a V_k centre.The STE may be formed in an alkali halide lattice under the application of an externally applied electric field when a field excited electron impact ionizes a halogen ion to form a free exciton. Lattice relaxation to the V_k centre configuration may then occur with a nearest neighbour anion to form a covalent

bond along the [110] direction in a few picoseconds whilst the electron is still in its excited state with the associated emission of phonons. This lattice relaxation reduces the exciton energy and thus it becomes trapped at a single site to form the STE. Radiative recombination of the electron and hole may occur at liquid nitrogen temperatures and once in the ground state the "molecule" becomes unstable and Pauli repulsive and electrostatic forces return the halogen ions to their normal lattice sites. This process is illustrated in figure 4.2.

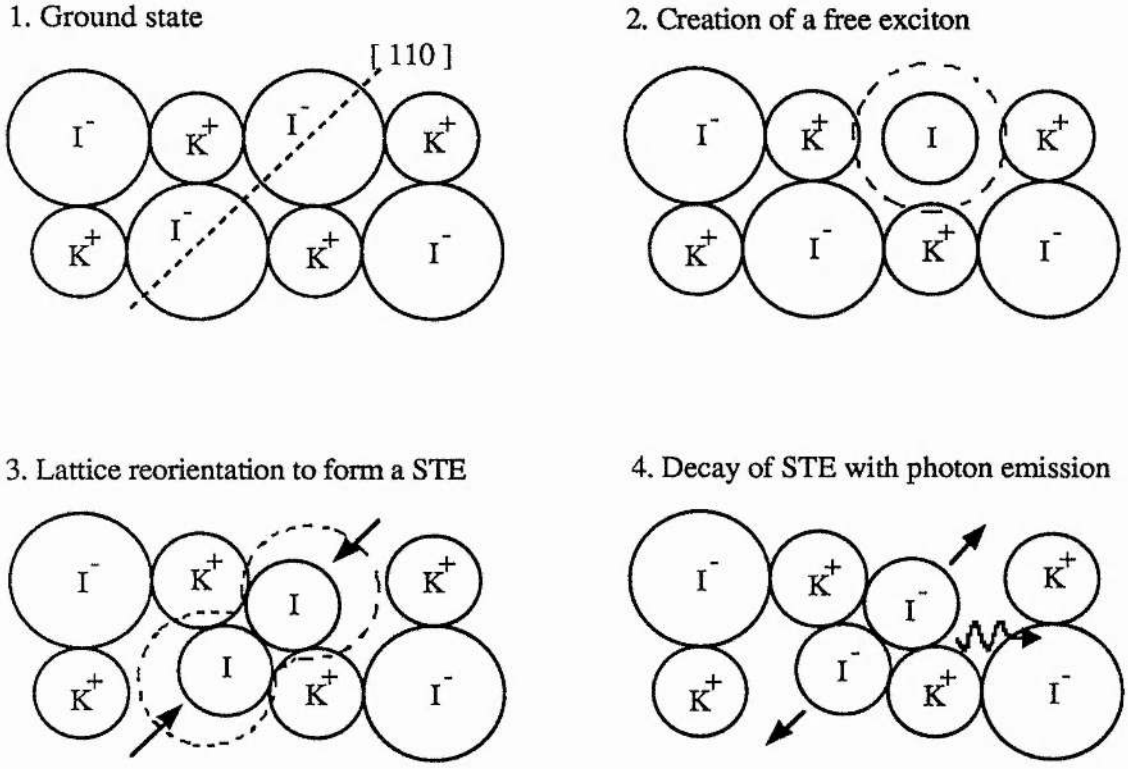

Figure 4.2 The creation and subsequent relaxation of a self trapped exciton in an alkali halide lattice.

The lattice adjustment which takes place to accommodate the creation and annihilation of the STE creates a four level process which can be represented on a configurational coordinate diagram similar to that shown earlier in figure 2.3 for the F_2^+ centre. The luminescence from a STE is emitted from the minimum of the configurational coordinate curves [26] and the large Stokes shift indicates, as expected, that a strong electron lattice coupling is

involved in the formation of the STE. The luminescence spectrum from STEs' in the alkali halides consist in many cases of two luminescence bands. The longer wavelength band which is π polarised with respect to the [110] axis is normally longer lived having lifetimes typically in the μs region. This lifetime is attributed to a triplet transition [29,32] and the shorter wavelength band which is σ polarized and has a shorter lifetime (typically of a few nsecs) is attributed to singlet states [29,32]. Table 4.1 gives the peak position of the σ and π luminescence bands from the STE in some alkali halides.

Alkali Halide	Singlet transition σ peak (eV)	Triplet transition π peak (eV)
LiF		3.5
NaF	4.27	2.7
KF	3.2	2.48
NaCl	5.47	3.47
KCl		2.54
RbCl		2.41
LiBr	5.3	3.95
NaBr		4.65
KBr	4.4	2.44
RbBr	4.13	2.36
CsBr	4.74	3.55
KI	4.13	3.31 3.3 (Na)
RbI	3.88	3.09
CsI		4.28 2.95 (Na) 3.35(K)

Table 4.1 Peak positions in eV of the luminescence bands in several alkali halides. Where shown in brackets indicates the shift in the luminescence peak due to the presence of an impurity ion. [ref 34]

The electronic energy level diagram for the STE is illustrated in figure 4.3 where the electron occupation for the lowest π luminescence state is shown for KCl.

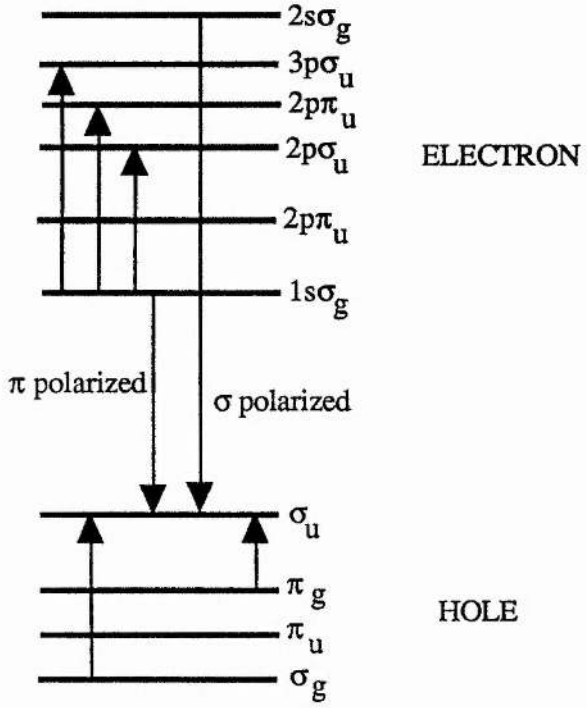

Figure 4.3 Energy level diagram for the lowest state self trapped exciton in KCl.

As with other luminescence species the STE can also relax via non-radiative processes. The rate W of the non-radiative transition from the initial state Φ_1 to a final state Φ_2 under an interaction Hamiltonian H_i as given by Huang and Rhys [33] is

$$W = \frac{2\pi}{h} Av \; |< \Phi_2 \; | H_i | \Phi_1 >|^2 \, \delta (E_1 - E_2) \qquad (4.7)$$

where E_1 and E_2 denote the total energy eigenvalues for the states Φ_1 and Φ_2 and Av denotes the taking of an average over all possible phonon occupancies. Itoh [34] considered the two types of non-radiative processes which may have large transition rates in STEs'. These are phonon induced one-electron transitions and Auger transitions, and by

dividing the transition matrix elements into an electronic component and phonon component he derived the following expression:

$$W = \frac{2\pi}{h}\Omega^2 G(\omega) \qquad (4.8)$$

Ω^2 determines how strongly the initial and final states interact with each other and $G(\omega)$ is the probability of the accepting levels taking up the electronic energy difference ΔE between the initial and final states. The factor G is known to decrease with an increase in ΔE [34]. Studies on the relaxation kinetics of the STE have indicated that it can relax by way of a precursor state to form a Frenkel pair [35]. This is an F centre and an H centre (an H centre being an interstitial halogen ion bound to a lattice halogen by a hole), as illustrated in figure 4.4.

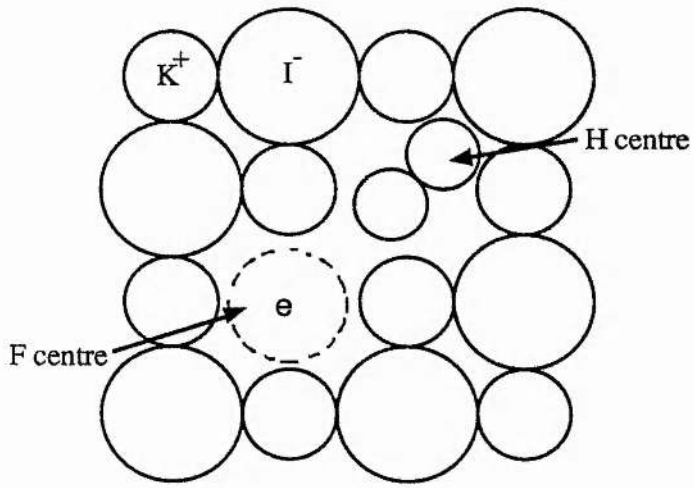

Figure 4.4 The STE may relax via a precursor state to form a Frenkel pair which consists of an F centre and an H centre.

It implies that the creation of STEs' within alkali halides can lead to lattice distortions and defect centres being created which survive after the STE has decayed.This may be an important factor when laser action is to be considered in such a disturbed lattice as these "by-product" centres could by way of further transitions to more exotic centres (the Frenkel pair being unstable in nearest neighbour sites decaying to the ground state emitting π luminescence or phonons) provide an intrinsic loss to the possible lasing process. Flynn

[36] has shown that a Frenkel pair may indeed hop to larger "stable" separation sites where the jump frequency to such a state where a potential barrier E_b exists is given by:

$$\nu = \left(\frac{3}{5}\right)^{1/2} \nu_d \exp\left(\frac{-E_b}{kT}\right) \qquad (4.9)$$

where ν_d is the Debye frequency.

As with F_A centres, studies of impurity localized STEs' show that the peak of the emission bands may be shifted by the addition of an impurity ion to the crystal lattice [27,26,34]. Ong et al [37] have discussed this topic along with the energetics of other luminescence centres that may occur in doped alkali halides. These include (i) long-distance tunnelling recombination of an electron

$$[\, M^+e \,] + V_k \rightarrow M^+ + h\nu$$

(ii) long-distance electron transfer to form a self trapped exciton intermediate

$$[\, M^+e \,] + V_k \rightarrow M^+ + [\, V_k e \,] \rightarrow M^+ + h\nu$$

(iii) capture to form an impurity localized self trapped exciton

$$[\, M^+ \; V_k \,] + e \rightarrow [\, M^+ \; V_k e \,] \rightarrow M^+ + h\nu$$

(iv) recombination capture of a free electron

$$[\, M^+ \; V_k \,] + e \rightarrow M^+ + h\nu$$

Ong and co-workers have shown that in general there is a trend for a blue shift in the luminescence for alkali halides with lighter alkali and a red shift for those doped with heavier alkali. This is confirmed experimentally in chapter 9 for work carried on CsI.

4.5 Metal-Insulator Contacts

4.5.1 Introduction

In order to obtain electroluminescence from any material an electrical contact must be constructed onto its surface (unless electron beam excitation is being used). For the alkali

halides a diverse range of contacts have been reported [10] ranging from evaporated metals onto the crystal surface, such as aluminium, silver, gold etc to saline alcohol solutions [38]. Though different in their nature, the common role of each is to inject electrons into the bulk of the crystal and thereby induce luminescence processes [8]. However, the type of electric contact formed onto a crystal surface determines the rate of carrier injection and conduction processes that occur within the crystal [39,40,41] and basically may be classified as either Ohmic or blocking. If the contact enables carriers to be injected into the insulator to form a negative space charge within the insulator below the metal-insulator interface it is said to be Ohmic [40]. Alternatively if the contact inhibits the flow of electrons from the metal contact such that a positive space charge region is set up within the insulator the contact is said to be blocking in nature [40].

For the alkali halides it has been reported that electroluminescence is only achieved for blocking contacts as this type of "barrier contact" is necessary to provide the required high field region within which electroluminescence can be sustained [29]. On the other hand it has also been reported that in order to enable laser gain within such materials threshold current densities of $\approx 19 Acm^{-2}$ are necessary [29] which implies that an Ohmic contact should be utilized. Clearly, therefore, it may be seen that an understanding of the behaviour of metal insulator contacts must be appraised so that the physical processes which occur at such an interface can be properly quantified.

4.5.2 Theory of Metal-Insulator Contacts

Generally, the physical processes which occur at metal-insulator contacts have received a rather limited coverage in the literature. Nevertheless, just as with the metal-semiconductor-metal system, the nature of the electrical contact at a metal-insulator interface is a primary consideration in respect of the determination of the current-voltage characteristics of the material [41,42]. For instance, when electrons are injected into the insulator, that is to say, the contact is Ohmic, a significant space-charge-limited current may flow through the

insulator, if not, the current flow will be insignificant [42]. In fact, as with a metal-semiconductor junction or Schottky barrier, considerable distortion of the insulator conduction band can occur at the metal-insulator interface. The main difference is that with metal-insulator junctions trapping centres are involved whereas with the metal-semiconductor junction it is donor or acceptor levels [40,41,42].

Ideally it is possible to predict the nature of a metal-insulator contact, (i.e. ,Ohmic or blocking) if the work functions of both the metal electrode and the insulating material are known [29]. For an Ohmic contact the work function of the metal ψ_m should be less than that of the insulator ψ_i, i.e.

$$\psi_m < \psi_i \quad \text{(Ohmic)}$$

and for a blocking contact the reverse condition applies

$$\psi_m > \psi_i \quad \text{(Blocking)}$$

For such contacts the effect of the energy band bending within the insulator is illustrated in figure (4.5) (surface states neglected).

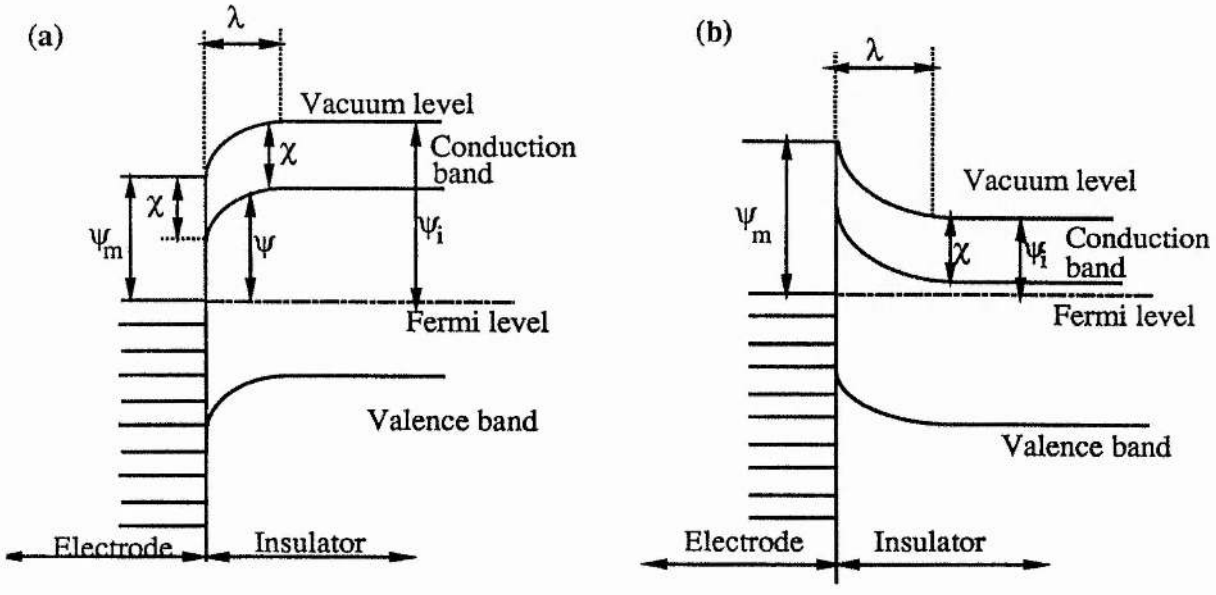

Figure 4.5 Schematic diagram to illustrate the band bending that occurs at (a) an Ohmic contact and (b) a Blocking contact

It may be seen for the case of the Ohmic contact that the Fermi levels within the metal and insulator are equalized by the injection of electrons from the electrode to the insulator which occurs initially when the two materials are brought together. This charge redistribution causes an internal space charge within the insulator to be formed causing its energy bands to become distorted due to the induced electric field which is created across the metal-insulator interface as an equal amount of positive charge is accumulated on the electrode surface. The charge exchange across the junction ceases once the two Fermi levels of each material reach a common energy. This local internal electric field varies in magnitude in accordance with the amount of injected charge and decreases with distance x away from the metal-insulator interface [40-42]. The region just within the insulator surface where the injected negative space charge is contained is known as the accumulation region whose depth is denoted by λ [41]. For an Ohmic contact if the space charge within the accumulation region is sufficiently large this negative space charge region acts as a reservoir of electrons thus allowing the unrestricted flow of current between the metal electrode and the insulator.

For the case of a blocking contact, electrons flow from the insulator to the metal in order to equalize the Fermi levels of the two materials. This produces a positive space charge region within the insulator and a negative surface layer on the metal. This leads to an opposite effect from that of the Ohmic contact to occur in that the energy bands of the insulator are bent downwards thus creating a potential barrier for electrons.

Thus far in this discussion the picture presented for the metal-insulator interface is applicable only to a perfectly pure insulator whose bandgap is devoid of traps and where the Fermi energy has been assumed to lie midway between the valence and conduction bands. In practice, an insulator abounds with traps whose occupancy states and position within the band gap determine the location of the Fermi level. The presence of traps within the insulator may determine the value of the insulator work function and hence may dictate the choice of metal required to produce the desired contact type. Some insight as to the

position of the trap levels and their density within the bandgap would therefore be desirable. Also, the width of the accumulation region λ must be considered because under certain conditions these regions may in fact overlap for a metal-insulator-metal system. This produces a space charge region within the insulator over its entire thickness and if two Ohmic contacts are used in such a system a significant space charge limited current can flow which greatly exceeds intrinsic conduction properties of the material [41-45]. For simplicity let us consider an insulator which contains a single discrete shallow and a single discrete deep trap level. In this context, a deep trap is considered to be a donor type trap which is intrinsically neutral when it contains an electron and that a shallow trap is an acceptor type. It may be shown that the Fermi level E_F may be deduced from:

$$N_{t2} \exp\left(\frac{E_{t2} - E_F}{kT}\right) + N_V \exp\left(\frac{E_V - E_F}{kT}\right) = N_{t1} \exp\left(\frac{E_F - E_{t1}}{kT}\right) + N_C \exp\left(\frac{E_F - E_C}{kT}\right)$$

$$E_F = \frac{E_{t1} - E_{t2}}{2} + \frac{kT}{2} \ln \frac{N_{t2}}{N_{t1}} \qquad (4.10)$$

E_{t1} and E_{t2} are the energy of the shallow and deep trap levels, E_C and E_V the energy levels of the bottom of the conduction band and top of the valence band and N_V and N_C the density of states of the valence and conduction bands. It may be seen from equation (4.10) that the position of the Fermi energy within the band gap E_F is determined only by the energy levels of the traps and in the absence of deep traps is given by:

$$E_F = \frac{E_V + E_{t1}}{2} + \frac{kT}{2} \ln \frac{N_V}{N_{t1}} \qquad (4.11)$$

Conversly, in the absence of shallow traps E_F may be determined from:

$$E_F = \frac{E_C - E_{t2}}{2} + \frac{kT}{2} \ln \frac{N_{t2}}{N_C} \qquad (4.12)$$

To calculate the thickness of the accumulation region an expression for λ may be derived from Poisson's equation:

$$\frac{dF}{dx} = \frac{1}{e}\frac{d^2\psi}{dx^2} = \frac{eN_t}{K\varepsilon_0}\exp\left[-\frac{(\psi - E_t)}{kT}\right] \qquad (4.13)$$

This gives

$$\lambda = \frac{\pi}{2}.\exp\left(\frac{\psi_i - \chi - E_t}{2kT}\right)\sqrt{\frac{2kTK\varepsilon_0}{e^2N_t}} \qquad (4.14)$$

where K and ε_0 are the dielectric constant and permittivity of free space, N_t the trap density within the accumulation region and χ the electron affinity of the insulator. The thickness of the accumulation region as a function of the intrinsic properties of the insulator ($\psi_i - \chi - E_t$) is illustrated in figure 4.6 for several estimated trap densities N_t.

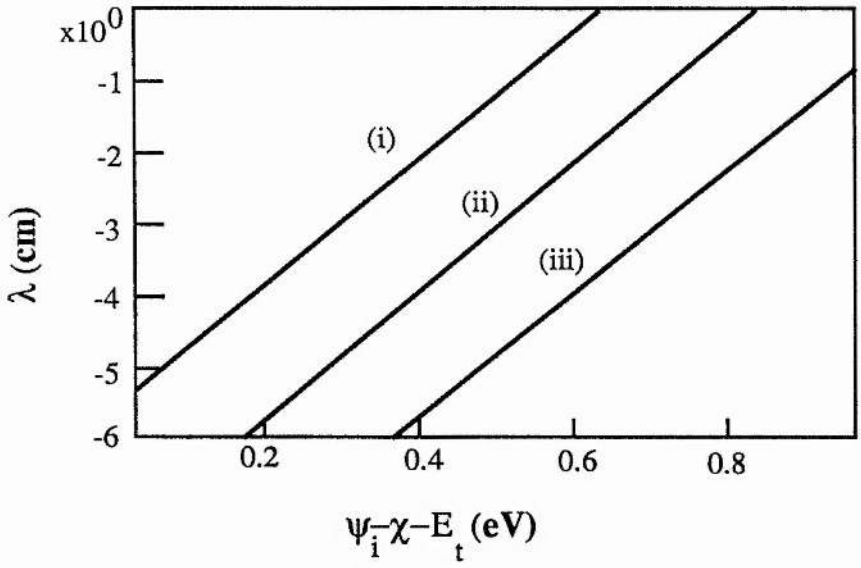

Figure 4.6 Width of the accumulation region λ verses $\psi_i - \chi - E_t$ for (i) $N_t = 10^{16}cm^{-3}$ (ii) $N_t = 10^{20}cm^{-3}$ (iii) $N_t = 10^{24}cm^{-3}$

Once an electron is injected into the insulator the current flow is heavily influenced by the presence of impurity and defect sites which lower the drift mobility of the carriers and therefore the magnitude of the space charge limited currents. Trap densities for insulating

solids of 10^{18} cm^{-3} are not unusual and may reduce space charge limited currents to unmeasurably low values. As an indication of how the presence of traps within an insulator affects the magnitude of the space charge limited current three hypothetical cases are compared here for an insulator containing (i) no traps, (ii) discrete shallow traps and (iii) traps distributed in energy.

For an insulator placed between two plane parallel electrodes the charge Q that is accommodated within the insulator below the contacts is given by $I=\frac{Q}{T}$ where T is the transient time of the charge Q. The T parameter is given as $T=\frac{d}{E\mu}=\frac{d^2}{V\mu}$ where μ is the drift mobility and the charge Q injected per cm^{-3} for a trap-free insulator is given by

$$Q=\frac{VK}{4\pi d}\times 10^{-12} \text{ Coulombs cm}^{-2} \qquad (4.15)$$

V is the applied voltage and d the separation of the contacts in centimetres. Thus the space charge limited current may be expressed as (from reference [46])

$$I= 10^{-13}\left(\frac{V^2\mu K}{d^3}\right) \text{Acm}^{-2} \qquad (4.16)$$

By way as an example consider a 150μm thick KI crystal placed between two plane parallel electrodes having an applied potential difference of say 2kV then the space charge limited current that may flow is predicted to be $35Acm^{-2}$ ($\mu=100cmV^{-1}$, K=3). This significantly exceeds the threshold current of $19Acm^{-2}$ [29]. However, if a thinner crystal is used, say 100μm, which is not impractical, the corresponding space charge limited current is increased to $120Acm^{-2}$.

For an insulator containing shallow traps, where the traps are in thermal equilibrium with electrons in the conduction band the space charge limited current is

$$I= 10^{-13}\left(\frac{V^2\mu_0\theta K}{d^3}\right) \text{amps cm}^{-2} \qquad (4.17)$$

μ_0 is the drift mobility of free carriers and θ is the fraction of free charge and is given as $\theta=\left(\frac{N_C}{N_t}\right)\exp\frac{-E}{kT}$ where N_C is the free carrier density within the conduction band and E is the energy (in eV) of the trap levels with respect to the conduction band.

Finally, for an insulator containing trapping levels which are distributed uniformly in energy the space charge limited current is obtained in the following manner [46]. The free carrier density n_C is given as

$$n_C=N_C \exp\left(\frac{-E_F}{kT}\right)\exp\left(\frac{\Delta E}{kT}\right)$$

where ΔE is the shift in position of the Fermi level from its original position after the injection of charge and is given by $\Delta E=\frac{Q}{en_td}=\frac{VC}{en_td}$ where n_t is the number of electron traps per cm^{-3} per unit range in energy and C is the capacitance of the material. Thus by substitution the free carrier density can be expressed as:

$$n_C=N_C \exp\left(\frac{-E_F}{kT}\right)\exp\left(\frac{VC}{en_tdkT}\right)$$

This may be abbreviated to $n_C=n_{C0}\exp(\alpha V)$ where n_{C0} is known as the initial thermal equilibrium concentration of free carriers and $\alpha=\frac{C}{en_tdkT}$. It can be shown that the fraction of free charge is (from reference [46])

$$\theta=\left(\frac{en_{C0}d}{VC}\right)\exp(\alpha V) \quad (4.18)$$

The space charge limited current I may then be obtained by substitution of equation (4.18) into equation (4.17):

$$I= 10^{-13}\left(\frac{V\mu_0 k}{d^2}\right)\left(\frac{en_{C0}}{C}\right)\exp(\alpha V) \text{ amps cm}^{-2} \quad (4.19)$$

Thus it may be seen from equations 4.17, 4.19 that for trap densities such as those indicated in figure 4.6 the space charge limited current may be drastically reduced. It follows therefore that suitably high current densities can only be obtained when relatively trap-free crystals are selected.

4.6 Summary

Within this chapter it has been shown that it would be very desirable to produce an "electroluminescent colour-centre laser" not only for its obvious cost-effectiveness but also as the operating bandwidth of alkali halides would be extended to cover the visible and ultraviolet regions of the spectrum due to the species of centre created by this mechanism. It has been shown for the alkali halides that the electroluminescent centre is the self-trapped exciton (STE) which is most easily produced within such materials under electrical excitation. As with colour centre media large wavelength coverage can be obtained by using several appropriate alkali halide crystals. Electroluminescence is produced from the alkali halides under the application of 10^4-$10^6 Vcm^{-1}$ fields, and injection of electrons at a Schottkey barrier and subsequent acceleration within an exhaustion region to impact energies is the most likely luminescence mechanism. Electroluminescence studies on such materials will be presented later in chapter 9.

Chapter 4. References

1. B.Gudden, R.W.Pohl; Z.Physik. **2**, 192 (1920)

2. G.F.Alfrey, J.B.Taylor; Proc.Phys.Soc.Sec.B. **68** (1955)

3. E.C.Payne, E.L.Magner, C.W.Jerome; Illum.Engr.London. **45**, 688 (1950)

4. G.P.Agrawal, N.K.Dutta; Long Wavelength Semiconductor Lasers. (Van Nostrand Reinhold Elect/Compsci.& Eng. series) (1986)

5. T.Fan, R.L.Byer; IEEE J.Quan.Elect. **24**, 895 (1988)

6. Laser Focus; p81, October (1988)

7. S.Unger, K.Teegarden; Phys.Rev.Lett. **19**, 1229 (1967)

8. C.Parrachini; Phys.Rev.B. **7**,1603 (1973)

9. N.I.Lebedeva, N.S.Nesmelov; Sov.Phys.Solid State **14**, 1406 (1972)

10. C.Parrachini; Phys.Rev.B. **4**,2342 (1971)

11. J.I.Pankove (Ed.) Electroluminescence; Tpcs in App.Phys. **17**, Springer-Verlag (1977)

12. G.Destraiu; Phil.Mag. **38**,700 (1947)

13. W.W.Piper, F.E.Williams; Phys.Rev. **98**, 1809 (1955)

14. D.R.Frankel; Phys.Rev. **111**, 1540 (1958)

15. O.Lossev; Phil.Mag. **6**,1204 (1928)

16. W.W.Piper, F.E.Williams; Phys.Rev. **87**, 151 (1954)

17. A.Fischer; Solid State Electronics, Pergamon Press (1961)

18. N.Klein, Thin Solid Films **7**, 149 (1971)

19. J.G.Simmons; J.Phys.Chem.Solids 32, 1987, 2581 (1971)

20. S.Unger, K.Teegarden; Phys.Rev.Lett. **19**, 1229 (1967)

21. C.Paracchini; Phys.Rev.B. 8, 848 (1973)

22. G.A.Vorobev, N.S.Nesmelov; Sov.Phys.Solid State **10**, 2932 (1969)

23. N.I.Lebedava; Sov.Phys.Solid State **16**, 378 (1974) Sov.Phys.Solid State **18**, 110 (1976)

24. N.S.Nesmelov; Sov.Phys.Solid State 11, 883 (1968)

25. G.A.Vorobev, S.G.Ekhanin, N.I.Lebedeva, S.N.Morev, N.S.Nesmelov; Iz.Fiz. **12,** 149 (1975)

26. B.Henderson; Defects in Crystalline Solids, Edward Arnold, London (1972)

27. C.Parracchini, G.Sshianchi; Solid State Commun. **8,** 1769 (1970)

28. A.P.Druzhinin, N.I.Lebedeva, N.S.Nesmelov; Opt.Spektrosk **47,** 917 (1979)

29. R.W.Boyd, M.S.Malcuit, K.Teegarden; IEEE J.Quan.Elect. **QE-18,** 1202 (1982)

30. G. Brunet, C.H.Leung, K.S.Song; Solid State Commun. **53,** 607 (1985)

31. R.T.Williams, M.N.Kabler; Phys.Rev.B.**9,** 1987 (1974

32. M.N.Kabler, D.A.Patterson; Phys.Rev.Lett. **19,** 652 (1967)

33. K.Huang, A.Rhys; Proc.R.Soc.A. **204,** 406 (1950)

34. N.Itoh; Adv.in Phys. **5**,491 (1982)

35. R.T.Williams, K.S.Song, W.L.Faust,C.H.Leung; Phys.Rev.B. **33,** 7232 (1986)

36. C.P.Flynn; Point Defects and Difussion (Oxford Clarendon Press) (1972)

37. C.K.Ong, K.S.Song, R.Mannier, A.M.Stoneman; J.Phys.C. **12** 4641 (1979)

38. G.A.Vorobev, I.S.Pikalova; Instrum.Expt.Tech.(USA) **Part 1** 210 (1967)

39. T.J.Lewis; Proc.1STInt.Conf. on Breakdown in Solid Dielectrics, Toulouse (1983)

40. M.A.Lampart; Rep.Prog.Phys. **27,** 329 (1964)

41. J.G.Simmons;J.Phys.Chem.Solids **32,** 1987 (1971)

42. M.A.Lampart;Phys.Rev. **103,** 1648 (1956)

43. R.W.Smith, A.Rose; Phys.Rev. **97,** 1531 (1955)

44. P.N.Murgatroyd; Solid State Electronics **16,** 287 (1973)

45. A.L.Lilly, D.A.Lowitz; J.Appl.Phys. **39,** 4360 (1968)

46. A.Rose; Phys.Rev. **97,** 1538 (1955)

Chapter 5

The LiF:F_2^+ Colour Centre Laser

5.1 Introduction

In this chapter the operation and performance of the F_2^+ colour centre within a LiF host crystal in particular will be described.

5.2 The laser cryostat

5.2.1 Introduction

F_2^+ colour centre lasers may be operated at room temperatures [3-6], but when operated under such conditions a rapid thermal bleaching and reorientation of the laser active centres is observed [3]. The mechanism of this is as yet not fully understood, but it inevitably leads to a frustration of laser action after a relatively short period, normally 10-15 minutes [7]. It is therefore desirable to operate such laser active centres at suitably low temperatures such that these degenerative effects are minimised. This may be accomplished by maintaining the host crystal at liquid nitrogen temperature (LNT) by means of a purpose designed cryostat. One design for such a cryostat to provide a facility for colour centre laser research was available at the outset of my project [6] but further refinements were sought. An upgraded version of this early cryostat design will be described, where the new and significant design feature was that all the resonator optics could be located externally from the cryostat. This is not the case with the presently available commercial colour centre lasers. Thus a much more versatile system has been developed whereby access to the resonator optics is easily facilitated. It was with this cryostat that the initial LiF:F_2^+ colour centre laser work in this thesis was carried out.

5.2.2 The Laser Cryostat

The laser cryostat may be divided into four distinct parts, namely; (i) the nitrogen reservoir, (ii) the main vacuum chamber, (iii) the cold arm assembly and (iv) the crystal chamber. A schematic illustration of this is included as figure 5.1.

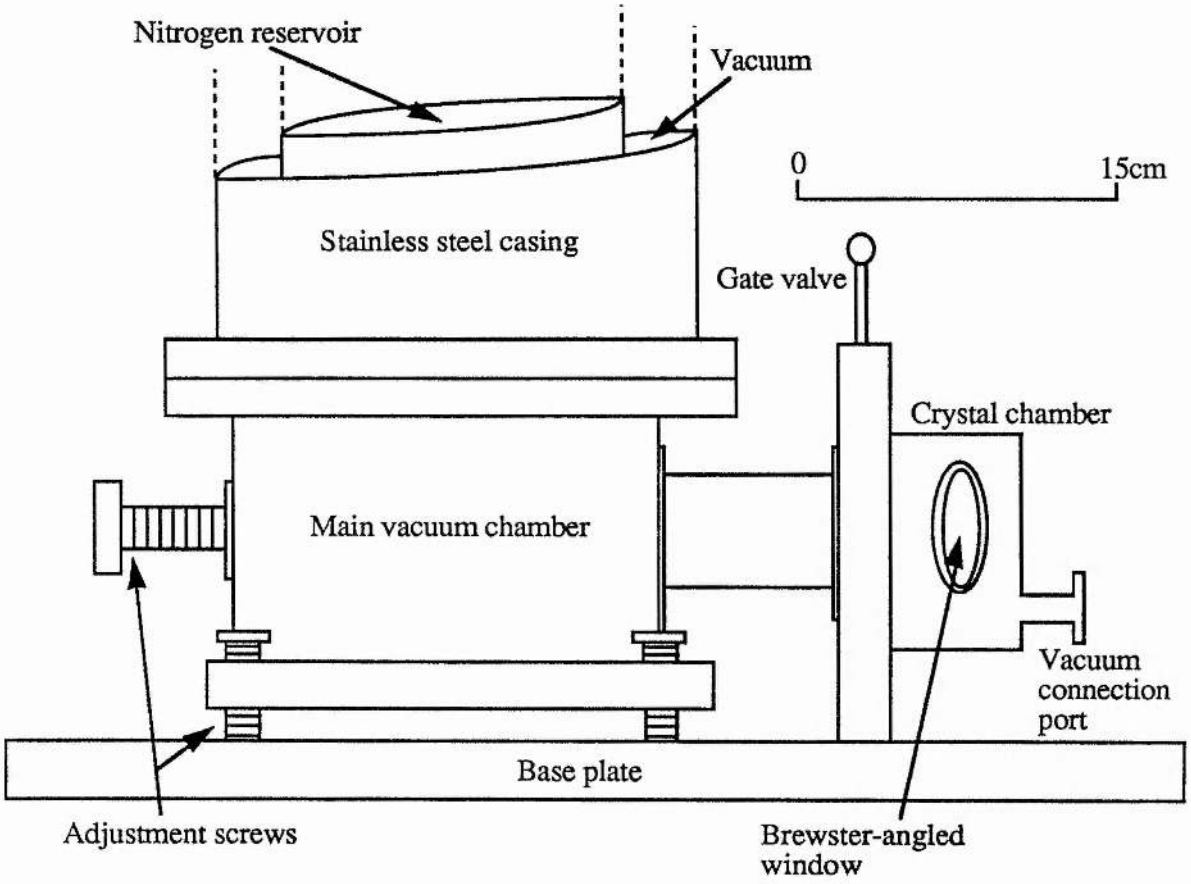

Figure 5.1 Schematic of the laser cryostat

Basically the laser cryostat maintains the LiF crystal within a suitable operating environment by means of a five litre capacity liquid nitrogen reservoir which is kept in thermal contact with the colour centre crystal.The liquid nitrogen reservoir storage time was approximately 36 hours, because thermal insulation of the reservoir from laboratory temperatures was provided by a vacuum $\approx 10^{-6}$Torr. This could be maintained for periods

of up to several months without any need for re-evacuating the chamber because three internally located adsorption pumps had been incorporated into the chamber. Once the adsorption pumps become saturated, which is indicated by the increase in boil off rate of the nitrogen reservoir, only then does the vacuum chamber need to be re-evacuated. Thus the laser may be operated for long periods without the need for any attachment of bulky vacuum pumps.

The main vacuum chamber was isolated from the crystal chamber by means of a gate valve which allowed a change of colour centre crystal to be carried out without the need to bring the entire vacuum chamber up to atmospheric pressure. This permitted a quick and relatively easy crystal replacement procedure to be developed. Thermal contact from the liquid nitrogen reservoir to the colour centre crystal is facilitated by a copper "cold arm" which is connected to the crystal mounting block via a stainless steel locking rod which enables the cold arm to be detached from the mounting block and retracted beyond the gate valve when a change of crystal was required. The crystal mounting block or "cold finger" is constructed in such a manner as to allow optical access to both sides of the crystal which is mounted at the Brewster angle, and held against the cold finger by a light spring-loaded clamp. Placed between the crystal and the cold finger is a thin sheet of indium which serves to maintain a good thermal contact between the two materials.

Optical access to the colour centre crystal is provided by way of two Brewster-angled infrasil windows. Vertical and horizontal movement of the cold finger assembly is afforded by three vertical mounting screws situated on the base of the cryostat and by a horizontal translation screw which sits to the rear of the main vacuum housing. The temperature of the colour centre crystal is monitored by a platinum resistance thermometer which is located in the cold finger.

5.2.3 Loading of the colour centre crystal

Loading of the colour centre crystal is carried out in the following manner. Firstly the cold arm is disconnected from the cold finger by unscrewing the stainless steel connecting rod and the cold finger rested upon a small table located within the crystal chamber. The cold arm is then retracted beyond the gate valve and the crystal chamber isolated from the main vacuum chamber. The colour centre crystal is then allowed to warm to room temperature. This process took several hours and was considered inconvenient and thus led to the provision of a heating element being incorporated into the cold arm assembly of an improved design of cryostat, which will be described in section 6.2. Whilst the cold finger and "spent" colour centre crystal were being removed, via an upper port window, the main vacuum chamber pressure was tested and repumped as necessary. Any moisture which may have condensed upon the cold finger and crystal chamber inner walls was dried using in a flow of nitrogen.

Once ready for use a LiF crystal, (preparation of which is described in detail elsewhere [3,6]), was removed from a cryogenic storage container and allowed to warm to room temperature. This annealing process allowed empty anion vacancies within the crystal to become mobile and become associated with solitary F centres to form laser active F_2^+ centres. Approximately three minutes after removing the LiF crystal from the storage container the protective aluminium foil jacket, within which the crystal was stored, was removed under filtered red light illumination. Removal of the protective jacket before this wait time only caused the polished crystal surface to be damaged by condensation. Once exposed, the crystal was inspected for any signs of damage and both polished surfaces were lightly buffed on a piece of soft lens tissue to remove any traces of condensation. During this procedure a distinct colouration of the crystal was observed to take place in that the interior of the transparent crystal was seen to become "green". The amount of colouring which occurred at this stage gave some indication as to the expected performance of the colour centre crystal, that is, poor colouring indicated a low concentration of centres being

formed and thus the crystal was discarded and a further crystal selected. Several LiF crystals with varying degrees of colouration are illustrated in figure 5.2. The crystal was then carefully mounted onto the soft indium pad placed against the cold finger and the clamping screws gently tightened. The coldfinger-crystal assembly was then replaced upon the resting table located within the crystal chamber and the upper port window cleaned and replaced. The crystal chamber was then re-evacuated, the gate valve opened and the cold arm reconnected to the cold finger thus recooling the crystal to 77K. The time taken from removal of the crystal from the storage container to loading onto the cold finger and subsequent recooling to 77K took approximately 10-15 minutes which is adequate time for the F_2^+ centre aggregation to occur [3,6,7].

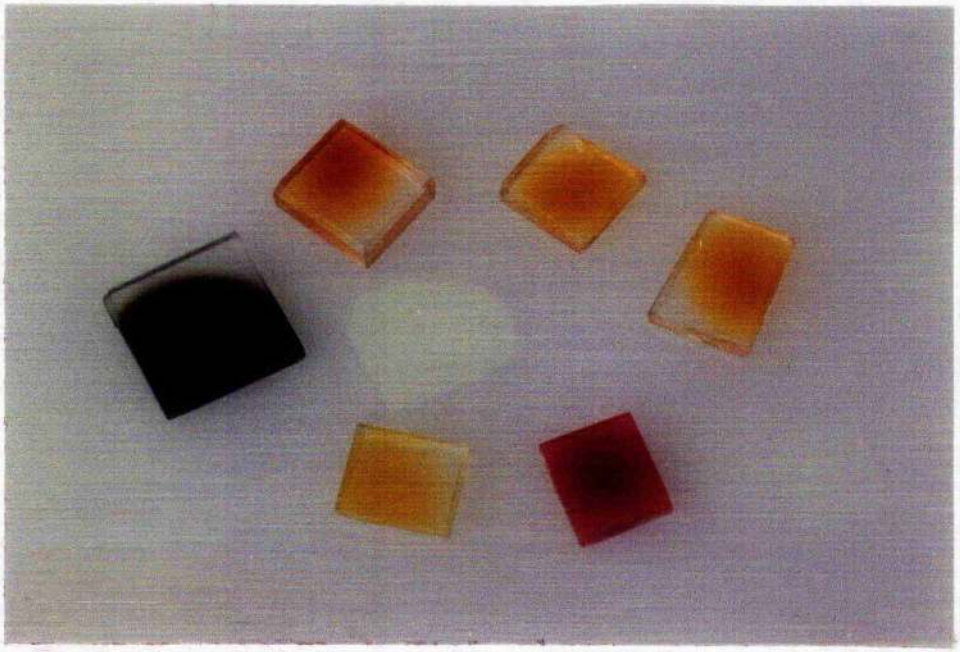

Figure 5.2 Five LiF crystals containing various colour-centre densities. The dark crystal did not produce laser action. The purple crystal is NaF for comparison.

5.3 Characterisation of the LiF:F_2^+ Colour Centre Laser

5.3.1 Introduction

This section will describe the performance characteristics of the LiF:F_2^+ colour centre laser and the exploitation of the large homogeneously broadened gain bandwidth to produce ultrashort modelocked pulse trains using the technique of synchronous modelocking [6,7].

5.3.2 The Krypton-ion pump laser

Powerful ion lasers such as Argon-ion and Krypton-ion capable of delivering output powers of up to 10W on a single line and greater than 30W on several lines simultaneously are generally used for pumping dye lasers. However the 647.1nm and 676.4nm lines from the Kr-ion laser fall within the homogeneously broadened LiF:F_2^+ absorption band which is centred around 645nm [8] thereby providing an ideal pump source for this type of laser.

The Kr-ion laser used throughout this work was a Spectra Physics model 171 which provided ≈ 4W CW output power when operated simultaneously on both the 647.1 nm and 676.4 nm lines. When acousto-optically modelocked on the single 647.1 nm line average output powers of ≈ 1W were obtained with typical pulse durations of 80-100 ps. As mentioned in section 3.3 the modelocker used here was a Spectra Physics model 3425 and the RF power at a resonant frequency of ≈41MHz was provided by a Racal model 9081synthesiser and amplifier unit. Figure 5.3a shows the spectrum of the signal applied to the modelocker by the Racal system. Once the optimum frequency of the modelocker had been determined a crystal oscillator operating at this frequency was constructed in house. The much cleaner signal obtained from this resonant device is shown in figure 5.3b.

(a)

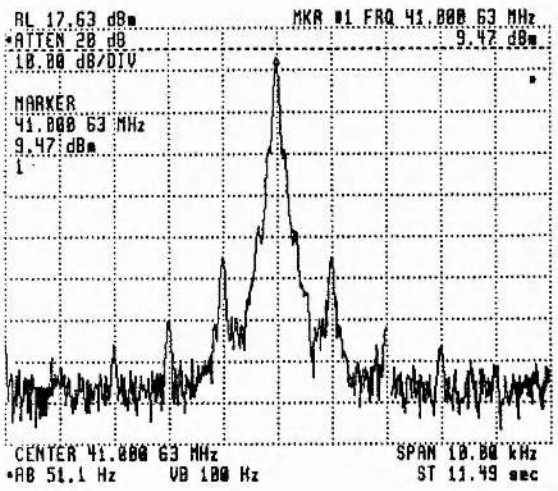

(b)

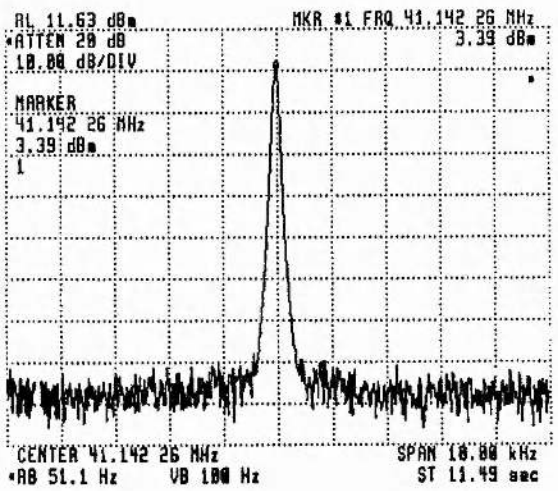

Figure 5.3 The output signal (a) from the Racal and (b) the inhouse built crystal oscillator

It was found that although little or no change in the modelocked pulse durations were observed when the much narrower band inhouse resonant frequency source was employed the phase-noise properties [9] were better with the latter. The pulse duration as a function of the acousto-optic frequency (the cavity length optimised for each case) is also presented if figure 5.4

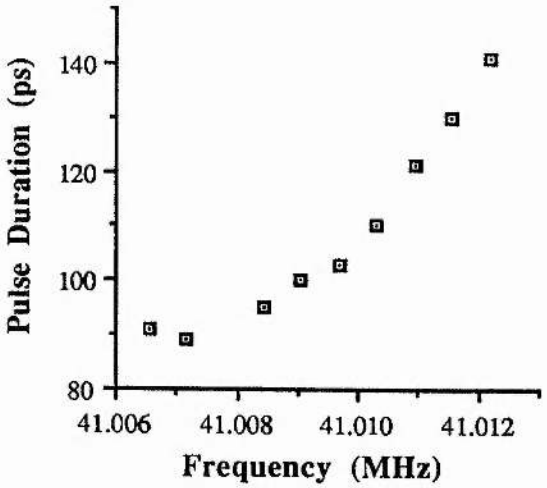

Figure 5.4 The pulse durations from the Kr-ion modelocked laser as a function of the acousto-optic modulator frequency

5.3.3 Characterisation of the Laser

Initial investigations of the characteristics of the LiF:F_2^+ Colour-centre laser were carried out using the cryostat described in section 5.2 where a basic three-mirror folded standing wave cavity (l≈0.5m) was employed (see figure 5.5).

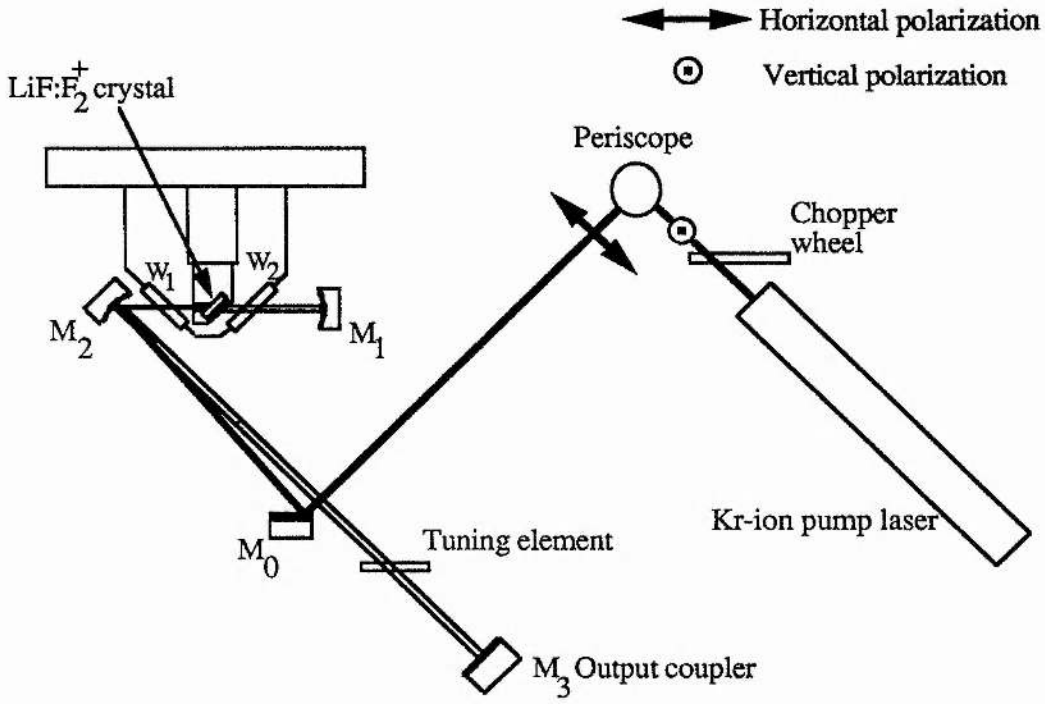

Figure 5.5 Experimental three-mirror cavity arrangement used for characterisation of the LiF:F_2^+ laser

The polarization of the vertically polarized Kr-ion pump laser was rotated to the horizontal plane, to minimise reflection losses from the windows, by a periscope arrangement which also served to correct the height of the pump beam for use within the CCL cavity.

The CW Kr-ion pump beam was non-collinearly coupled into the LiF crystal by way of the steering mirror M_0 and the 10cm radius of curvature concave mirror M_2 which focused the pump beam to a 20μm waist diameter. The multi-layer dielectric coating of mirror M_2

provided a broadband reflectivity ≈100% over the 640 - 960nm spectral range. Mirror M_1 which had a radius of curvature of 5cm acted as retroreflector and had a similar reflectivity profile to that of mirror M_2.

The plane mirror M_3 was the output coupler for the laser and the operating wavelength was selected by means of a Brewster-angled dielectric tuning wedge or a Brewster-angled prism. The tuning curve for the laser is shown in figure 5.6a for a pump power of 2W (at higher pump powers the laser tended to oscillate on one of several bands) and a 3%-transmitting output coupler. It may be seen that the laser was tunable from ≈ 815nm to 980nm and not over the entire LiF:F_2^+ tuning range of 0.8-1.0 μm. This was attributable to the reflectivity characteristics of the folded mirror M_2. Mirror M_2 also contained three low reflectivity "glitches" (a,b,c) over the laser tuning range thus preventing laser action to be established within these particularly "lossy" spectral regions. A typical laser bandwidth trace for the same experimental parameters as mentioned above is shown in figure 5.7b where the structuring of the spectra has been attributed to etalon effects due to the Brewster-angled windows within the cavity [4].

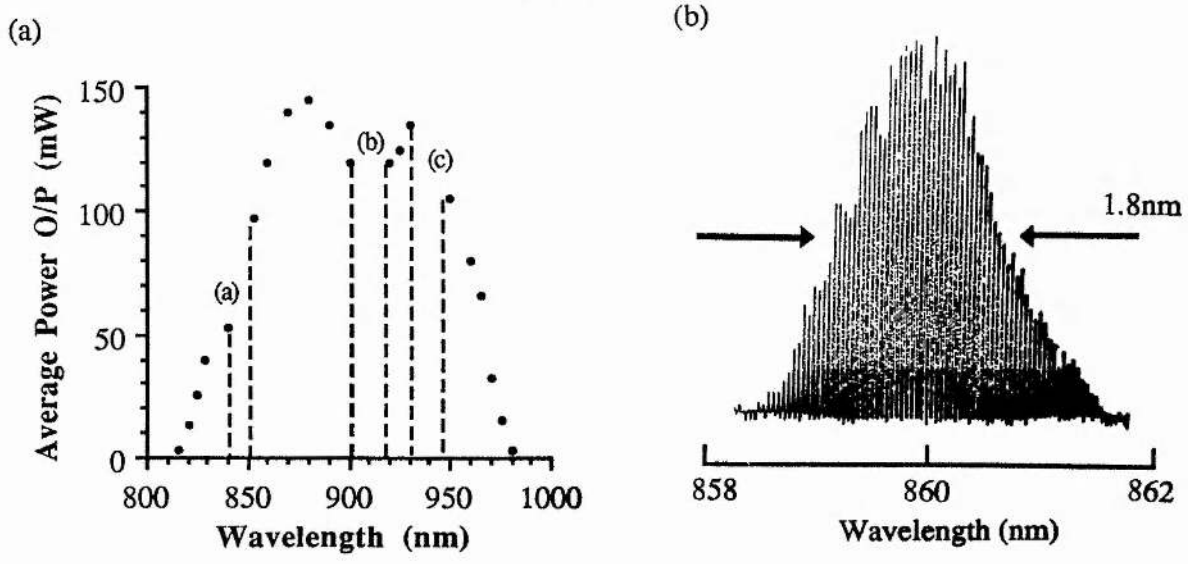

Figure 5.6 (a) The tuning curve for the laser and (b) A typical laser operating bandwidth

All spectral measurements were obtained using an S20-type photomultiplier tube (PMT) and a Monospek 1000 monochromator. The laser output power as a function of the input pump power was determined for 3% and 10% output couplers and is shown in figure (5.7). With the 3% output coupler typical pump power thresholds of ≈ 150mW were observed and this value increased to ≈ 250mW when the 10% output coupler was employed. Output efficencies of 14% and 25% were obtained for the 3% and 10% couplers respectively.

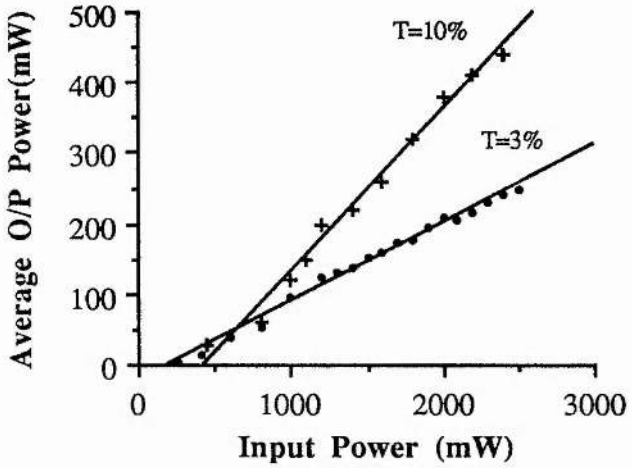

Figure 5.7 The Input-Output characteristics of the laser when employing a 3% and 10% output coupler

The laser output power P_0 was measured for a range of output couplers (T = 37%, 10%, 3%) and the data inserted into the following (obtained from ref.11)

$$P_0 = \text{const} \cdot T \left(\frac{g_0}{L_i + T} - 1\right) \qquad (5.1)$$

$$\frac{dP_0}{dT} = 0 \text{ then } T_{opt} = -L_i + \sqrt{g_0 L_i} \qquad (5.2)$$

where T is the transmission, g_0 the small signal gain and L_i the the internal cavity losses. It was thus determined that the internal losses were ≈12-13% and that the optimum output coupling was ≈ 20%. An optimum output coupler was not available during this initial phase of my work but one was subsequently purchased and the performance of the laser was assessed again at a later stage.

It should be mentioned here that the Kr-ion pump laser was chopped to give a duty cycle reduction of x10 to prevent thermal ionization and bleaching of the laser active colour centres. Under these pumping conditions stable operation from the same spot on the crystal was obtained for operational periods of approximately 200 hours before the laser threshold increased by a factor of two or three. The laser threshold was returned to its normal values for approximately 40-60 hours by altering the crystal position within the pump beam using the cold arm adjusting screw provided. This performance thus meant that the LiF:F_2^+ colour centre laser operated to give a satisfactory practical source of tunable near-infrared coherent radiation.

5.4 The Synchronously Modelocked LiF:F_2^+ Colour Centre Laser

The large homogeneously broadened gain bandwidth of the LiF:F_2^+ CCL was exploited by applying the technique of synchronous modelocking [6,7]. Initial investigations were carried out whilst employing the simple folded three mirror cavity shown in figure 5.5. The position of the end mirror M_3 was suitably adjusted such that the slave laser cavity length matched or was a multiple of the modelocked Kr-ion pump laser cavity length and was mounted onto a high precision translation stage to allow finite cavity adjustment. The Kr-ion pulse durations were monitored using a Photochron II streak camera operated in synchroscan mode and a typical synchroscan trace is presented in figure 5.8

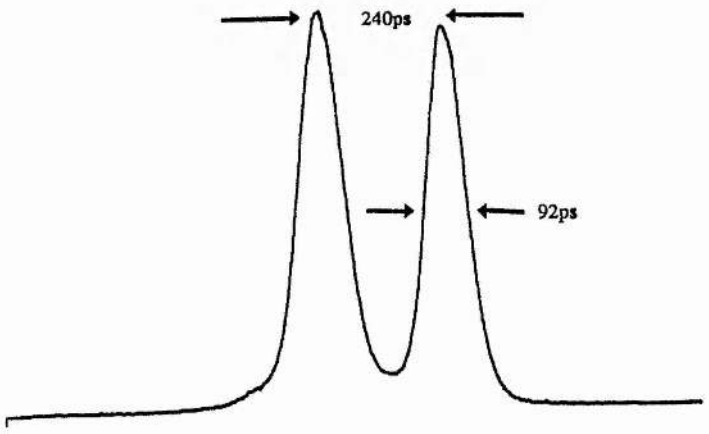

Figure 5.8 Typical streak camera trace of the modelocked Kr-ion laser pulses

The modelocked output of the colour centre laser was monitored using a Photochron II synchroscan streak camera. The experimental setup is shown in figure 5.9. Initially the CCL cavity length was set to half that of the pump laser and modelocking was achieved by monitoring the CCL output with a fast photodiode. Once a stable modelocked pulse sequence was obtained from the CCL the pulse durations were then measured using the streak-camera. Precise cavity adjustments and pulse monitoring were then carried out while both streak-camera and second harmonic autocorrelator diagnostics were used. The drive electronics for the synchroscan streak camera where triggered from the chopped colour centre laser pulse train which tended to broaden the streak images due to the presence of phase jitter which occured between successive pulse train due to the chopped pump beam. The streak camera electronics could have been synchronised directly from the pump laser but this would have reduced the pump power available to the colour-centre laser.

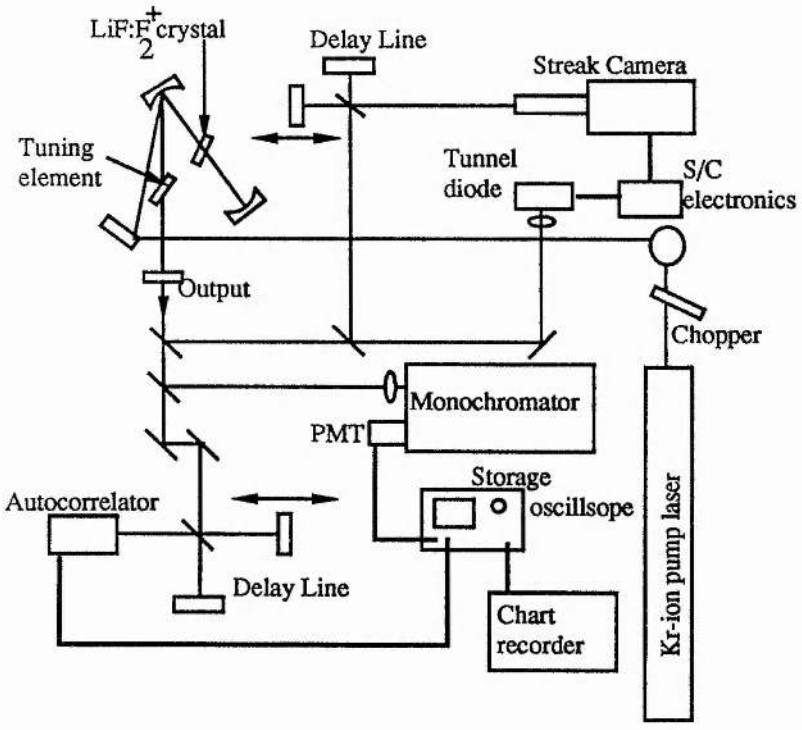

Figure 5.9 The experimental setup for the synchronously pumped standing-wave $LiF:F_2^+$ colour-centre laser

However because the streak camera was only used for preliminary modelocking of the CCL and not for monitoring absolute pulse durations the jitter that was present could be tolerated. Typical pulse durations as monitored by the autocorrelator, which where obtained over the $LiF:F_2^+$ tuning range of 820-980nm, were in the region of 2-3 ps and a typical autocorrelation trace along with the corresponding laser bandwidth is shown in figure 5.11a. If a Gausian pulse envelope is assumed, then the duration-bandwidth product of 0.5 was close to the Fourier-transform limit.The average output power of this pulse train was 30 mW (75W peak) for an output coupling of 3%.

At this stage it was decided to implement the technique of colliding-pulse modelocking (CPM) [11,12] where two counter-propagating pulses within a travelling-wave resonator are allowed to collide in the gain medium. As explained in section 3.4 this gives rise to a more efficient pulse forming process. The travelling wave cavity is shown in figure 5.10. Mirrors $M_1$and M_2 were of 10cm radius of curvature, M_3 had a high reflectivity over the 800-1000nm spectral range and M_4 was a 3% output coupler.

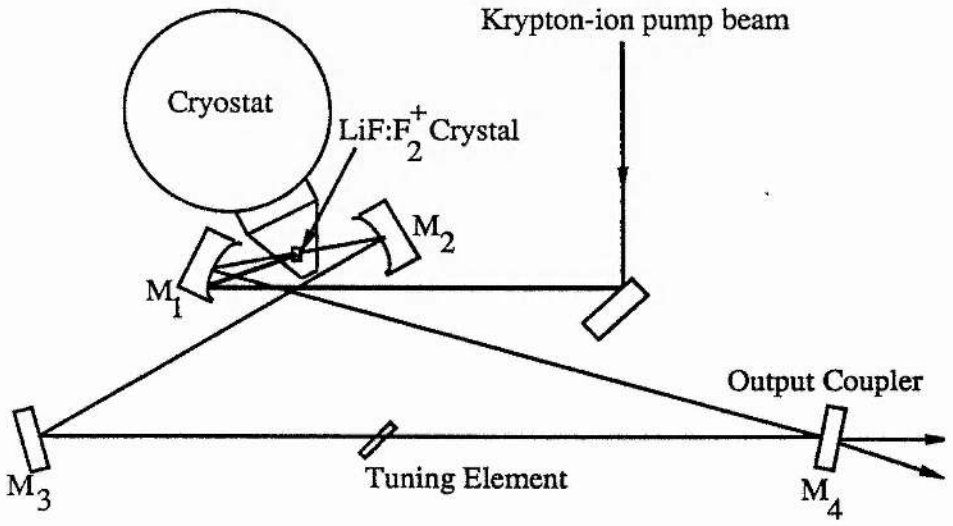

Figure 5.10 Schematic of the synchronously-pumped colliding-pulse-modelocked $LiF:F_2^+$ colour centre laser

Under CW conditions the threshold pump power for the CPM system was 300mW and the output power observed in both beams were similar to those obtained from the CW standing-wave cavity. The repetition frequency of the CPM system was ≈ 82MHz and the laser was modelocked and monitored using the same diagnostic setup as illustrated in figure 5.9. Pulse durations of 700fs (Gausian pulse profiles assumed) were obtained from the synchronously pumped CPM LiF:F_2^+ laser and an autocorrelation trace of such a pulse train and its corresponding spectrum (FWHM of 1.8nm) are indicated as figure 5.11b. The implied duration-bandwidth product 0.49 was again close to the transform limit.

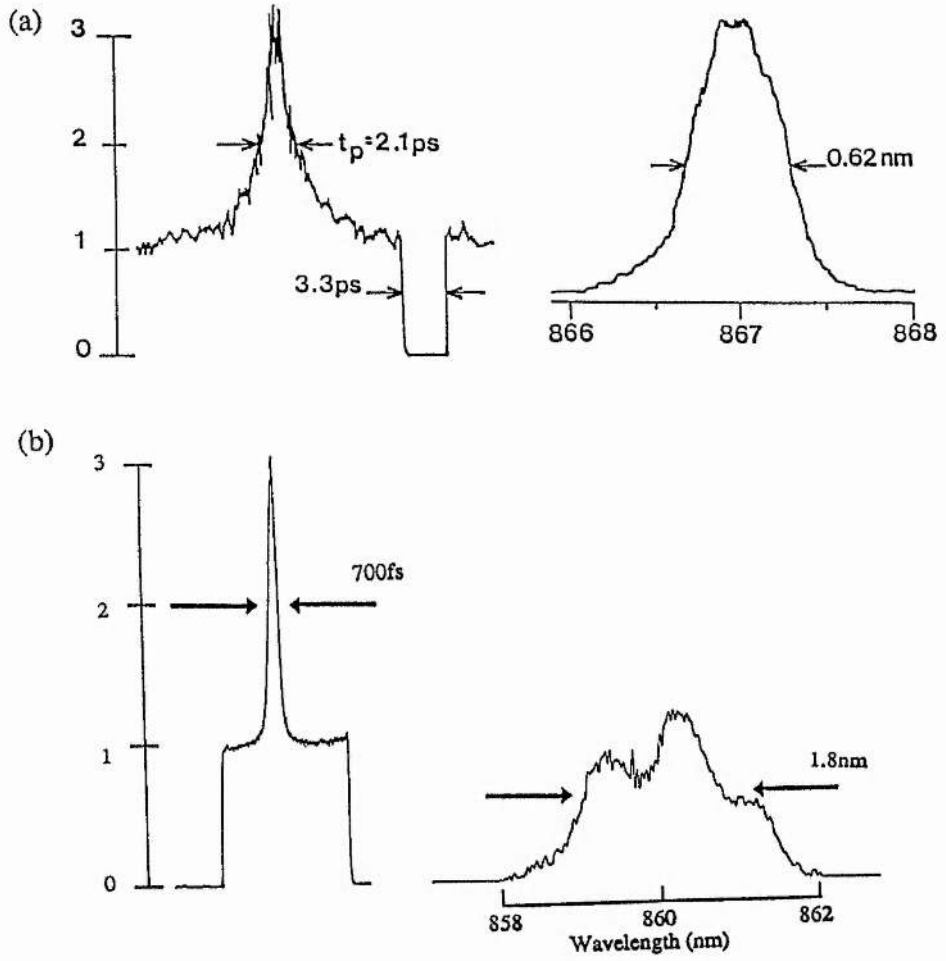

Figure 5.11 (a) Typical autocorrelation trace and the associated bandwidth for the standing-wave synchronously pumped LiF:F_2^+ colour centre laser and (b) autocorrelation trace and associated spectrum obtained from the synchronously pumped colliding pulse modelocked LiF:F_2^+ colour centre laser.

5.5 Summary

Within this chapter the performance characteristics of a non-collinear pumped LiF:F_2^+ colour centre laser has been described using a novel inhouse designed cryostat. This allowed for the easy configuration of different optical cavities to be employed and investigated as the optics were all located outside the cryostat. The laser has been shown to provide a reliable infrared source over the 820-980nm region of the spectrum and unlike dye laser counterparts operating within this region has shown to be stable over 200 hours operating time. The technique of synchronous modelocking has been demonstrated for the first time with this laser source and the pulse durations obtained have shown to be comparable to those produced directly from synchronously pumped dye lasers. By implementing for the first time to this laser the technique of colliding-pulse modelocking pulse durations of 700fs have been observed, which at this time were the shortest pulses produced from the LiF:F_2^+ colour centre laser. Shorter pulse durations were later produced when the technique of passive modelocking was applied, which will be discussed in chapter seven.

Chapter 5. References

1. L.F.Mollenauer; Methods of Experimental Physics **15** Part B, Academic Press (1979)

2. J.D.Kafka, B.H.Kolnel, T.Baer, D.M.Bloom; Opt.Lett. **9**, 505 (1984)

3.M.Leduc, G.Treel; Rev.Phys.Appl. **17**, 355 (1982)

4. K.Smith; PhD Thesis, University of London (1985)

5. N.Langford; PhD Thesis, University of London (1989)

6. P.K.Runge; Opt.Commun. **4**, 195 (1971)

7. N.Langford, K.Smith, W.Sibbett; Opt.Commun. **64**, 274 (1987)

8. J.Nahum; Phys.Rev. **174**, 1000 (1968)

9. A.Finch, X.Zhu, P.N.Kean, W.Sibbett; IEEE J.Quan.Elect. **QE-26**, 1115 (1990)

10. A.Yariv; Introduction to Optical Electronics; (Holt-Rinehart-Winston) 1976

12. D.Kulhke,W.Rudolph, B.Wilhelmi; IEEE J.Quan.Elect. **QE-19**, 570 (1983)

12. M.S.Stix, E.P.Ippen; IEEE J.Quan.Elect. **QE-19**, 520 (1983)

CHAPTER 6

The Redesigned Colour Centre Laser Cryostat

6.1 Introduction

In this chapter an upgraded laser cryostat will be described and its performance characteristics evaluated for a similar LiF:F_2^+ colour centre laser to that described in chapter 5. The major new design features of this cryostat are that both optical and electrical pumping of crystals may be facilitated. It also features an improved cold arm assembly design which allows the liquid nitrogen coolant to flow directly onto the back of the crystal mounting block, the performance of which will also be described.

6.2 The upgraded laser cryostat

Though already novel in its versatility it was decided to design and construct an upgraded version of the laser cryostat that was described in section 5.2. There were several limitations of this previous early design. One was that heat was removed from the colour centre crystal via a copper cold arm connected to the liquid nitrogen reservoir and this had the inconvenience that the temperature of the crystal could not be controlled with acceptable response times. Secondly, this cryostat could not facilitate electrical pumping schemes. To overcome these practical limitations, new design features were introduced. Firstly, the cold arm has a liquid flow system that allows the liquid nitrogen coolant to flow directly onto the back of the crystal mounting block at a rate of flow from the nitrogen reservoir that can be appropriately controlled by a needle valve. This provides a more efficient heat exchange route for the crystal and a very fast temperature control response time in that the nitrogen flow may be halted if necessary and the crystal block heated to room temperature to allow rapid crystal changeover times (typically 30 minutes).

With the new design, investigations into laser efficiency as a function of temperature, or luminescence efficiency in the case of electrical pumping can be performed. The second major new design feature of this new cryostat is that optical and electrical pumping of crystals can be performed. This has been achieved by designing two interchangeable crystal mounting chambers. The optical pumping chamber is shown in figure 6.1.

As with the previous cryostat design, optical access to the crystal chamber was provided by two Brewster-angled infrasil II windows which have a high transmission in the ultraviolet (UV) to the near-infrared (NIR) spectral regions. The optical chamber was attached to the cryostat by a NW 50 centred 'O'-ring and clamp and once evacuated it was connected to the main chamber via the vacuum port as illustrated in figure 6.1. As already described (see chapter 5) the colour centre crystal was mounted onto a Brewster-angled mounting block and this was attached to the cold arm by a spring loaded dove tail fitting which ensured good thermal contact. Horizontal positioning of the mounting block was facilitated by a micrometer screw which was pressed against the cold arm which was spring loaded by means of a flexible steel bellow. A similar capacity (5 litres) liquid nitrogen reservoir was used where this reservoir provided the necessary hydrostatic pressure to maintain a flow onto the crystal mounting block. Again the temperature of the crystal was monitored by a platinum resistance thermometer.

When the laser crystal was to be changed the needle valve was closed and the crystal mounting block warmed to room temperature by an internal heater. This entire process typically takes about 30 minutes whereas with the the earlier cryostat design up to 12 hours was needed to allow the crystal to reach room temperature. To remove the crystal from the chamber a three way isolation valve is used which enables the optical chamber to be removed from the cryostat face whilst maintaining the main cryostat at a high vacuum. Once a fresh crystal has been mounted onto the crystal mounting-block and cold-arm assembly the chamber is simply replaced, re-evacuated and reconnected via the three way

isolation valve to the main chamber for which the vacuum fidelity is maintained by means of three internal adsorption pumps.

An additional feature is that the level of the liquid nitrogen within the reservoir is monitored by a platinum resistance thermometer which adds a useful further refinement to the system. The entire cryostat assembly is mounted onto a base plate by three adjustable legs which permits fine adjustments of the colour centre crystal position within the cavity. A photograph of the redesigned cryostat is presented as figure 6.2.

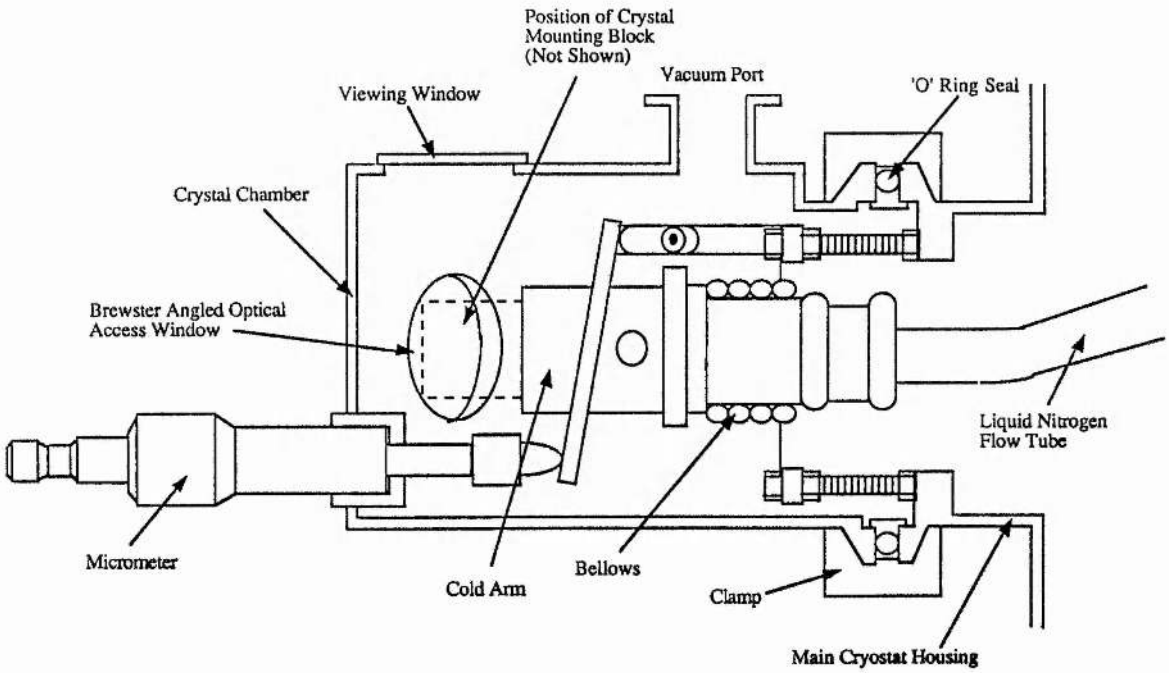

Figure 6.1 Schematic of the optical pumping chamber

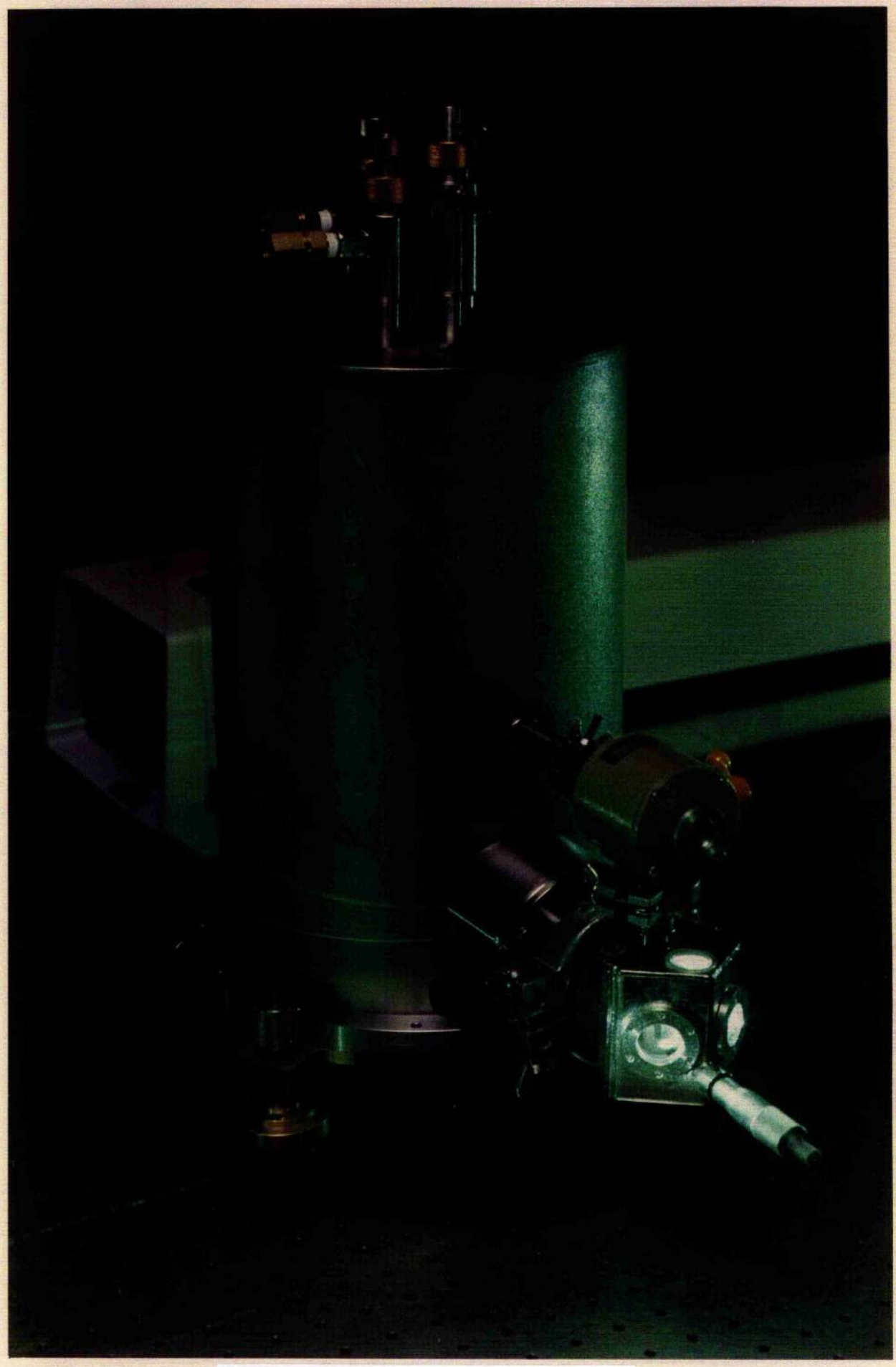

Figure 6.2 The redesigned laser cryostat

6.3 Characterisation of the Redesigned LiF:F_2^+ Colour Centre Laser

The performance characteristics of the redesigned LiF:F_2^+ colour centre laser were evaluated using a simple astigmatically-compensated three-mirror folded standing-wave cavity with a Brewster angled prism being used as the tuning element. The 2mm thick LiF crystal was mounted into the optical chamber simply by removing the optical chamber and inserting the crystal mounting block onto the cold arm assembly as described above in section 6.2. A Kr-ion laser delivering up to 4W of output power when operating CW on the 647.1nm and 676.4nm resonance lines was used to non-collinearly pump the colour centre crystal. The input-output characteristics for 3%, 10% and 20% output coupling from the laser cavity are presented in figure 6.3 and slope efficiencies of 9%, 12% and 20% respectively were obtained .

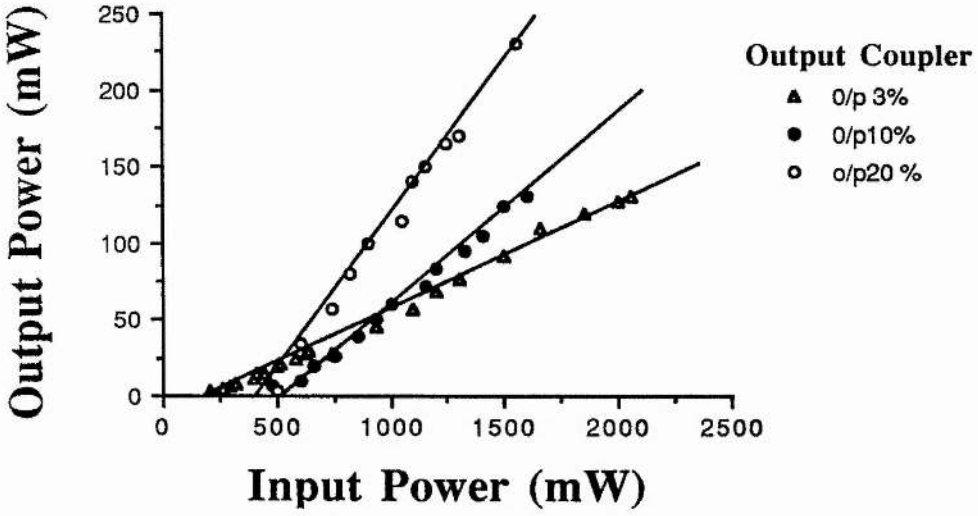

Figure (6.3) The input verses output power characteristics for the Redesigned LiF:F_2^+ Colour Centre Laser

Comparing the data presented in figure 6.4 with the data presented earlier in section 5.3 it may be seen that the efficiencies for the laser described here are somewhat lower. This is

explained by the fact that during the radiation treatment of the LiF crystals assessed in the work described in this chapter (and subsequent chapters) the electron bombardment current was 1.4 μA for the 1.5 MeV electron beam as compared to 2.6 μA for the 1.5 MeV electron beam used for the irradiation of the laser crystals described in chapter 4. Higher F_2^+ centre densities are produced at the stronger irradiation and so the laser efficiency is expected to be somewhat lower as observed here. The tuning curve for the redesigned LiF:F_2^+ colour centre is presented in figure 6.4. It can be seen that tuning is available over the entire LiF:F_2^+ tuning range due to the availability of suitable resonator mirrors.

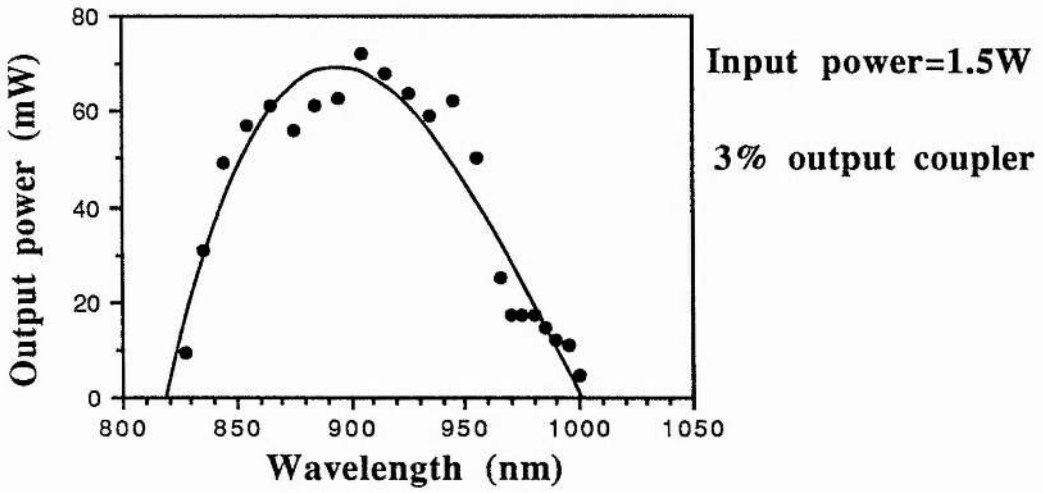

Figure (6.4) Tuning range for the LiF:F_2^+ colour-centre laser

Because the redesigned laser cryostat contained an internal heater and a needle valve which allowed the flow of liquid nitrogen to the colour-centre crystal to be controlled the laser performance was also characterised as a function of the crystal temperature. These data are presented in figure 6.5 where the crystal temperature was slowly raised whilst pumped by a chopped (x10) 2W beam.

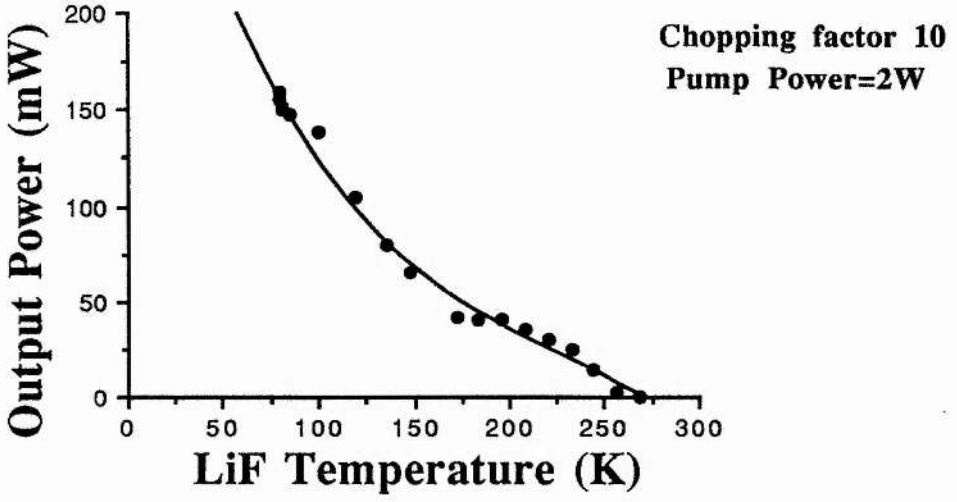

Figure (6.5) The output power as a function of temperature for the LiF:F_2^+ colour centre laser

As mentioned earlier in section 2.3 it is necessary to chop the pump beam for the LiF:F_2^+ colour centre laser in order to reduce the thermal degradation of the laser active centres. To illustrate the effect of thermal degradation of the colour centres a LiF:F_2^+ colour centre crystal was pumped cw by a 2W pump beam and the laser output power monitored as a function of the operating time (see figure 6.6)

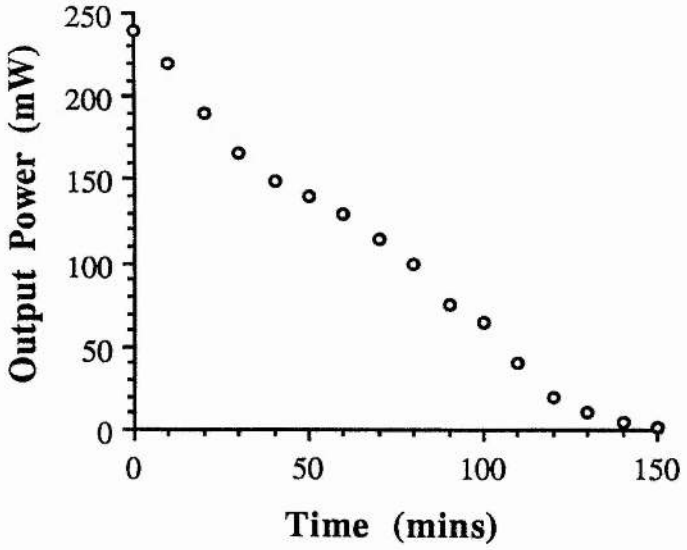

Figure (6.6) Output power as a function of time when the laser is cw pumped (crystal temp 77K)

The laser action ceases after approximately two hours of operating time under these optical pumping conditions. To illustrate the enhancement of the laser action when the pump beam is chopped, the LiF crystal temperature as a function of the input power for four chopping factors are presented in figure 6.7.

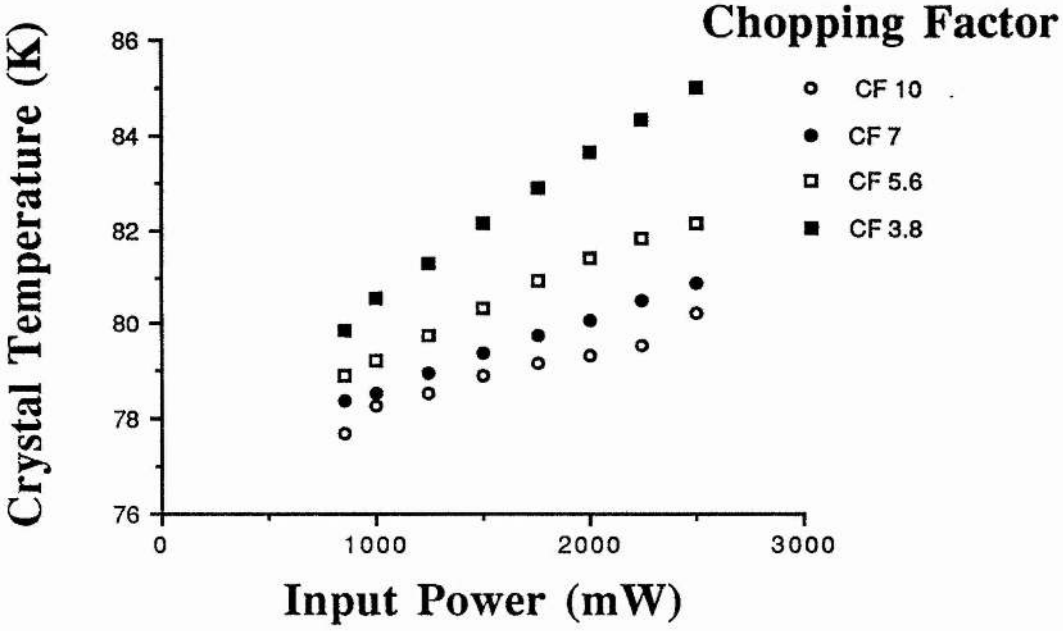

Figure (6.7) The colour centre crystal temperature as a function of pump power for four chopping factors

6.4 Summary

In this short chapter a redesigned colour-centre laser cryostat has been described. This design has proved to be superior to its predecessor in that the colour centre crystals could can be much more quickly and conveniently changed when necessary. Another advantage has been that the crystal housing chamber can be isolated from the main cryostat housing thus enabling optical and electrical pumping options for the colour centre crystals by simply interchanging the pumping chambers. This novel design of cryostat also allows the temperature of the crystal under investigation to be controlled and this has particular relevance to the electrical pumping experiments described in chapter 9.

Chapter 7

Passive Modelocking of the LiF:F_2^+ Colour-Centre Laser

7.1 Introduction

The generation of ultrashort optical pulses having picosecond and femtosecond durations is now readily achievable over the visible and near-infrared (NIR) regions of the electromagnetic spectrum when the technique of passive modelocking is applied [1,2]. This technique which was originally developed for flashlamp-pumped Nd:glass solid-state lasers [3] has now been applied to dye lasers, laser diodes [4,5,6] and titanium-sapphire lasers [7]. Within this chapter the technique of passive modelocking will be discussed for the colour-centre laser [8] .

Passive modelocking has enabled the direct generation of sub-30fs pulse durations when the combination of the laser active dye rhodamine 6G and the saturable absorber DODCI is utilized within group-velocity dispersion compensated colliding pulse modelocked (CPM) travelling-wave cavities [9]. The active-passive combination of these and other suitable dye combinations provide reliable ultrashort pulse sources over the visible and NIR spectral region 490nm-1.0μm [9-12]. However, organic dyes capable of operation within the NIR spectral region prove to be unreliable in that their working lifetimes are much reduced by thermal instabilities compared to their visible counterparts [12,13]. More recently it has been demonstrated that the technique of passive modelocking can be applied to the LiF:F_2^+ colour-centre laser [8] operating around 860nm using the saturable absorber IR140 and by selection of the further complementary saturable absorber DaQTeC, the operating range of this "solid state" ultrashort optical pulse source has been extended to 950nm [14]. In this chapter the passive modelocking of a LiF:F_2^+ colour-centre laser implemented within various cavity configurations will be described.

7.2 Group-Velocity Dispersion (GVD) and Self-Phase Modulation (SPM) within Ultrashort Pulse Laser Resonators.

Within ultrashort pulse laser cavities (typically within the femtosecond regime) the effect of dispersive elements and processes such as the presence of intracavity glass [15], off-resonance saturable absorption and gain saturation [16-19] and that of the nonlinear optical Kerr effect [15] can have detrimental effects on the evolution kinetics of the optical pulses produced during the modelocking process. Such effects have led to much theoretical [15,17,18] and experimental work [16,19] being carried out and this has led to the design of group- velocity dispersion compensated cavities using various techniques [17] whereby the intracavity dispersive processes have been compensated or exploited to optimise the modelocked pulse durations [20]. Within this section the sources of intracavity dispersion will be identified for the passively modelocked LiF:F_2^+ colour-centre laser and the technique used to compensate/optimise such dispersion, to the advantage of the pulse evolution kinetics of this laser will be discussed.

7.2.1 Sources of Intracavity Dispersion

Dispersion in temporal and frequency domains of optical pulses within laser cavities is due essentially to two optical processes, these being linear and nonlinear in nature [21]. Linear dispersion occurs as a result of group-velocity dispersion (GVD) of the optical wave packets as the pulse propagates through intracavity dispersive elements, such as a colour-centre crystal for example, as generally the refractive index n of a material is a function of the optical frequency ω. Nonlinear dispersion occurs due to self-phase modulation (SPM) of the optical pulse which arises due to the optical Kerr effect [21] or to off- resonance saturable absorption or saturable gain [21] both of which give rise to a frequency chirp across the pulse. These nonlinear processes may both occur within the cavity where the energy density of the optical beam is very high. This is the case at the beam waist within the gain and absorber media in the laser to be described here. Linear frequency chirping

mechanisms or GVD arises within the LiF:F_2^+ colour-centre laser cavity due to the presence of the two infrasil optical access windows situated around the colour centre crystal and from the LiF crystal itself.

Firstly, for linear intracavity dispersion we may consider the propagation of a Gaussian pulse through a dispersive element, assuming that such a pulse envelope is easier to work with mathematically, and that the conclusions drawn are not significantly different from those obtained when a $Sech^2$ modelocked pulse envelope is assumed. Thus a Gaussian pulse profile with a peak frequency of ω_0, with no frequency chirp, and duration τ_{in} (FWHM) may be expressed as

$$E=E_0 \exp-[(2\ln 2)\, t^2/\tau_{in}^2] \exp i\omega_0 t \qquad (7.1)$$

To obtain the output phase of the pulse after passing through a dispersive medium the propagation constant in the medium β may be expanded as a Taylor series about the centre frequency ω_0 to give

$$\beta(\omega)=\beta(\omega_0)+\dot{\beta}(\omega-\omega_0)+\frac{1}{2}\ddot{\beta}(\omega-\omega_0)^2+..... \qquad (7.2)$$

where $\beta(\omega)=n(\omega)k$, $\dot{\beta}=\frac{d\beta}{d\omega}$ and k the free space propagation constant given by $k=\frac{2\pi}{\lambda_0}$. It may be shown that [21] the dispersion has the effect of broadening the pulse duration by a factor $\frac{\tau_{out}}{\tau_{in}}$ given by

$$\frac{\tau_{out}}{\tau_{in}}=\left(1-\frac{\ddot{\beta}^2}{4\left(\frac{\tau_{in}^2}{(7\ln 2)}\right)^2}\right)^{1/2} \qquad (7.3)$$

and to create a frequency chirp across the pulse whose sign is opposite to that of $\ddot{\beta}$ and which may be expressed as

$$\ddot{\beta}=\frac{-\ell\lambda^3}{2\pi c^2}\frac{d^2n}{d\lambda^2} \qquad (7.4)$$

where ℓ is the length of the optical medium. To obtain values of the linear dispersion within the LiF:F_2^+ colour-centre laser cavity the values of $\frac{d^2n}{d\lambda^2}$ for the LiF gain crystal and the infrasil windows were obtained from the three-term Sellmeier expansion [22].

Nonlinear dispersion arises within the laser cavity due to the effects of self-phase modulation which may occur by way of three processes. These are, (i) the optical Kerr effect due to the intensity dependence of the refractive index of the dye solvent, (ii) off-resonance absorption of the saturable absorber and (iii) off-resonance saturation of the optical gain [15,21]. However, under the operating conditions of the laser used here the pulse intensity within the optical gain was much less than that observed within the saturable absorber in order to satisfy S parameter conditions [1] and for these operating conditions it has been shown that the contribution of SPM from the off-resonance gain saturation is only significant for very short optical pulses [16,23].

The main intracavity SPM contribution comes from the optical Kerr effect which as mentioned briefly above arises as a direct consequence of the intensity dependence of the refractive index of the dye solvent which may be expressed as

$$n=n_0+n_2I \qquad (7.5)$$

n is the index of refraction, n_0 the index of refraction at an arbitrary low intensity, n_2 is the Kerr coefficient or the nonlinear index (for ethylene glycol $n_2=3\times10^{-16}cm^2W^{-1}$). This nonlinear effect may be considered as instantaneous as it arises due to the polarisation of the electric field in the medium and thus being electronic in nature has time scales in the order of 10^{-15}s [21,24]. Again, as in the case of linear dispersion, if we consider the propagation of a Gaussian pulse through a dispersive medium, say for example, the ethylene glycol solvent of the saturable absorber dye jet it may be seen that different points

of the pulse envelope will experience a different refractive index due to the variation of the flux intensity I across the pulse and thus a phase change $\Delta\phi$ will be experienced across the pulse. This is given by

$$\Delta\phi = -\frac{2\pi}{\lambda} \ell n_2 I \qquad (7.6)$$

where ℓ is the path length of the medium. The instantaneous frequency change $\Delta\omega$ which occurs across the pulse envelope as a function of time is given as

$$\Delta\omega = -\frac{d(\Delta\phi)}{dt} = -\frac{2\pi}{\lambda} \ell n_2 \frac{d(I)}{dt} \qquad (7.7)$$

Thus it may be seen that as the pulse propagates through the medium the intensity dependence of the refractive index leads to a red-shift in the leading part of the pulse and a blue shift on the trailing edge of the pulse. This is illustrated in figure 7.1.

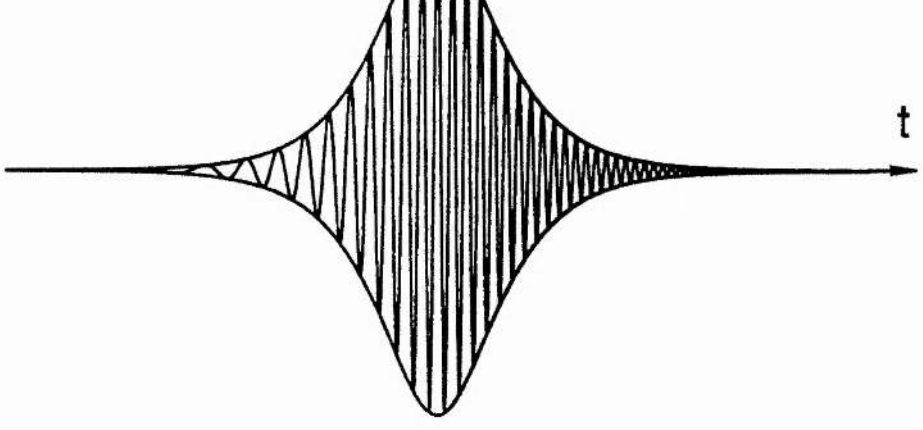

Figure 7.1 Computer generated temporal and spectral envelopes for a pulse illustrating the frequency sweep resulting from a nonlinear Kerr effect

The second major source of SPM that may arise within the laser cavity may arise from off-resonance absorption by the saturable absorber [15,21,23]. The sign of the frequency chirp produced by this effect depends upon the duration and energy of the optical pulse and also upon which side of the absorption peak the laser is operating [15,23]. For absorption occurring on the short wavelength side of the absorption peak the chirp obtained across the pulse has been shown to be generally positive in sign (or up-chirped), for small ratios of pulse energy to saturation energy. For the same pulse parameters but with the laser operating on the long wavelength side of the absorption profile a negative chirp is experienced across the centre of the pulse [15,23]. Alternatively for large ratios of pulse energy to absorber saturation energy a large positive chirp is manifest only on the leading "foot" of the pulse [15,23]. It may be seen therefore that the sign and amplitude of the nett frequency chirp experienced by the pulse will depend upon a convolution of processes and operational parameters and will be the combination of the Kerr effect occurring within the dye solvent and the chirp experienced due to off-resonance absorber saturation. This has been modelled quite effectively by Miranda et al [23] who have treated the propagation of a Gaussian pulse through a saturable absorber and solvent. The absorber is assumed to have a Lorentzian line shape given as:

$$g(\omega)=2\pi\left[\Delta\omega\left(1+\frac{4(\omega_0-\omega)^2}{\Delta\omega^2}\right)\right]^{-1} \qquad (7.8)$$

where ω_0 is the centre frequency of the absorption profile and $\Delta\omega$ is the halfwidth of the spectral line. The refractive index of the saturable absorber is given as:

$$n_r=\frac{\pi}{2}(\omega_0-\omega)\frac{c}{\omega_0}\alpha g(\omega) \qquad (7.9)$$

where n_r is the refractive index at the resonance peak of the saturable absorber and α the absorption coefficient given by:

$$\alpha=\alpha_0 \exp\left(\frac{-a\int_{-\infty}^{t} I\,dt}{E_{sat}}\right) \qquad (7.10)$$

α_0 is the absorption coefficient at the peak of the absorption profile, a the cross-sectional area at the beam waist and E_{sat} the saturation energy of the absorber. Hence an expression may be obtained giving the total phase delay $\Delta\phi_{TOT}$ across the pulse resulting from the nonlinear Kerr effect in the solvent plus the chirp arising from the off-resonance absorption as:

$$\Delta\phi_{TOT}= -\frac{2\pi}{\lambda} \ell n_2 I - G(\omega)\frac{2\pi}{\lambda} \ell \alpha(t) \qquad (7.11)$$

where
$$G(\omega)= \frac{\pi}{2} (\omega_0-\omega)\frac{c}{\omega_0} g(\omega) \qquad (7.12)$$

and thus the total frequency chirp $\Delta\omega_{TOT}$ induced by both nonlinear processes may be obtained from the differentiation of the total phase delay as:

$$\Delta\omega_{TOT} = \frac{d(\Delta\phi_{TOT})}{dt} = -\frac{2\pi}{\lambda}\left(\ell n_2 \frac{dI}{dt} + G(\omega)\, \ell \frac{d\alpha}{dt}\right) \qquad (7.13)$$

Lastly, it should also be mentioned that a linear frequency chirp may also be brought about within ultra-short pulse laser cavities by dispersion arising from the optical mirrors and the theory of such has been detailed elsewhere [20,25].With the large tuning ranges available from dye and colour-centre lasers the cavity mirrors usually have broadband characteristics and it is with these type of mirrors that dispersion can arise [26]. The manner in which the dielectric layer sequences for the mirrors are deposited is known to play an important role in determining the degree of dispersion expected and several workers have in fact reported optimisation of pulse durations by careful construction of their resonator optics [26]. However, the precise details of the dielectric layer sequences for the mirrors used in the laser cavities to be described here are unknown and thus a quantitative knowledge of the

dispersion introduced by these is not available. However, because dispersive effects arising from dielectric stacks is really only significant for sub-100fs pulse durations these mirrors with unspecified deposition detail were used.

7.2.2 Group Velocity Dispersion (GVD) Compensation of laser cavities.

Optimisation of pulse durations within ultrashort modelocked laser cavities may be achieved by balancing the group velocity dispersion (GVD) and self phase modulation (SPM) by introducing to the cavity suitable compensatory amounts of negative or positive GVD. This may be achieved by insertion into the cavity of a prism delay line which was first suggested and demonstrated by Fork et al [27] or a pair of Gires-Tournois interferometers [18,28]. For GVD compensation within the laser cavities described throughout this chapter a prism delay line was implemented. (For the pulse durations observed in this work it was not necessary for Gires-Tournois interferometers to be implemented as this device is mainly used to compensate for third order nonlinear dispersion effects which is only significant for hypershort pulses (<50fs) [29]).

The use of a prism sequence is a very effective technique by which both positive and negative group velocity dispersion may be introduced to an optical cavity in the absence of any negative material dispersion [27,30]. Such a device is superior to say that of a diffraction grating pair to produce negative dispersion in that it has very low loss and also does not produce any transverse displacement of the laser beam [27]. A prism sequence used within the travelling-wave ring cavities of CPM dye lasers is illustrated in figure 7.2. For standing-wave cavities only two prisms need be used because this sequence consists of a mirror-imaged pair of prisms along the axis M M'. The prisms were constructed such that the angle of minimum deviation of the beam was also Brewster's angle for the laser operating wavelength and the operation of the sequence is as follows. Prism I serves to positively disperse the pulse over an angle β and the control of the negative GVD is provided by the separation x of the prisms. The second prism recollimates the beam whilst

the prisms III and IV mirror image the first set of prisms and produce an exit beam along the original beam path.

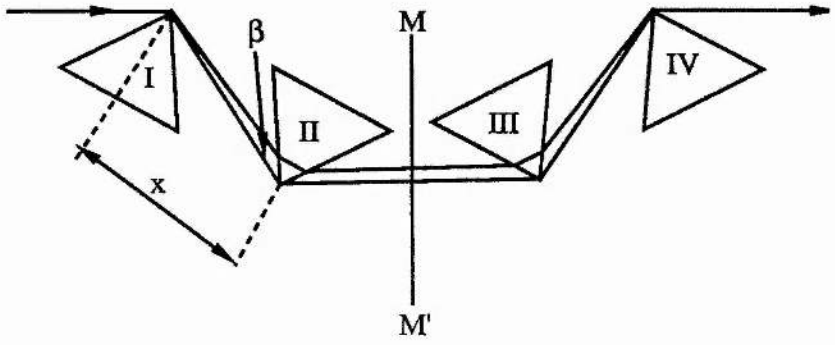

Figure 7.2 Layout of the prism sequence that enables the group velocity dispersion to be controlled in the laser cavity

From a geometrical consideration it may be shown that the total optical path length P that contributes to dispersion is given as

$$P=2x\cos\beta \qquad (7.14)$$

and that the dispersion constant D by

$$D=\frac{\lambda}{cx}\frac{d^2P}{d\lambda^2} \qquad (7.15)$$

where
$$\frac{d^2P}{d\lambda^2}=4x\left[\left(\frac{d^2n}{d\lambda^2}+\left(2n-\frac{1}{n^3}\right)\left(\frac{dn}{d\lambda}\right)^2\right)\sin\beta-2\left(\frac{dn}{d\lambda}\right)^2\cos\beta\right] \qquad (7.16)$$

To calculate $\frac{d^2P}{d\lambda^2}$ the values of $\frac{dn}{d\lambda}$ and $\frac{d^2n}{d\lambda^2}$ may be obtained from a three-term Sellmeier expansion [22]. For the LiF:F_2^+ colour-centre laser cavity used here the minimum separation of the prisms x was calculated such that the positive dispersion contribution introduced by the cryostat windows and the colour-centre crystal were compensated.

Additional adjustment of the amount of intracavity dispersion was facilitated by mounting one of the prisms (no.II) onto a translation stage which permitted the amount of intracavity glass to be adjusted as necessary.

7.3 The Passive Modelocking of the LiF:F_2^+ colour centre laser around 860nm

The saturable absorber chosen for the initial investigation of a passively modelocked colour-centre laser was the dye 5, 5'-dichloro-11-diphenylamino-3, 3'-diethyl-10, 12-ethylenethiatricarbocyanine perchlorate (IR140 Eastman-Kodak) which has a peak absorption crosection $\sigma=6x10^{-16}cm^2$ at 810nm and whose absorption profile is shown in figure 7.3. Photoisomerisation of this dye is well known [31] and the radiative decay time has been measured as ≈1ns [32]. Initially, as passive modelocking of such a laser gain medium had not been investigated before, a simple-standing wave cavity was employed with no GVD compensation elements present as illustrated in figure 7.4.

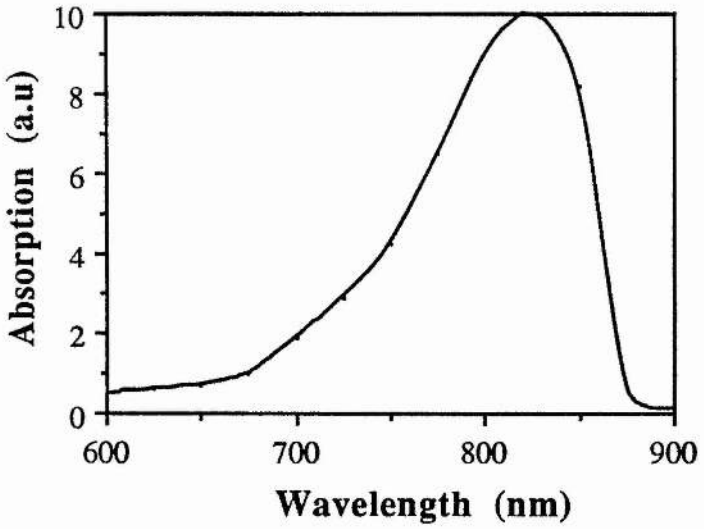

Figure 7.3 The absorption profile of the saturable absorber dye IR140

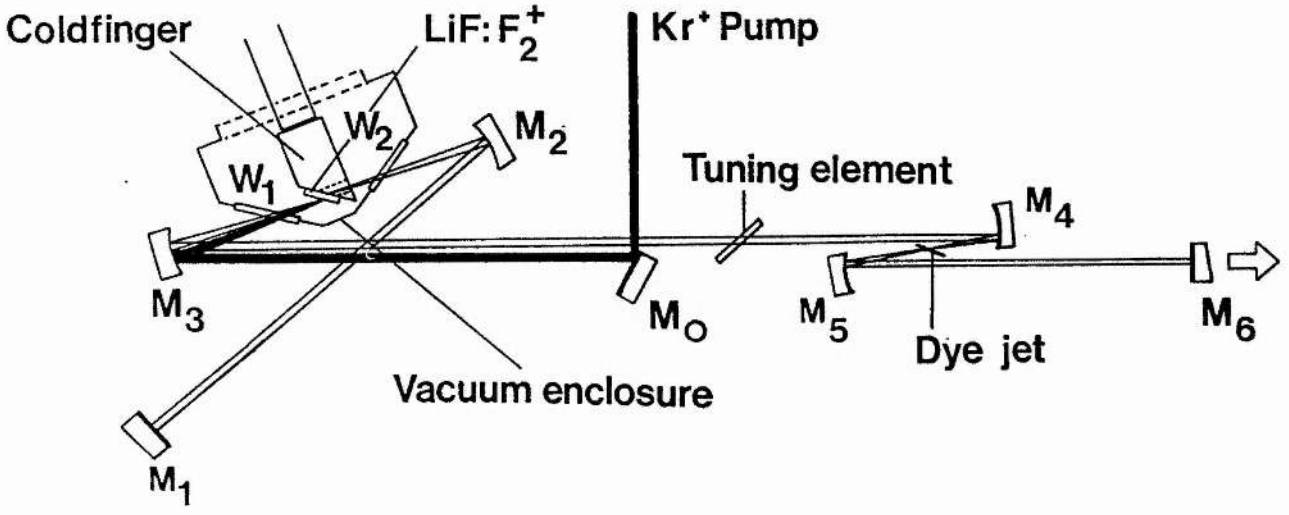

Figure 7.4 The simple standing-wave resonator implemented for preliminary investigations of the passively modelocked LiF:F_2^+ colour-centre laser

This resonator arrangement is very convenient as it can be readily modified to form a colliding-pulse-modelocked (CPM) travelling wave ring cavity by suitable reorientation of the the mirrors M_1 and M_2. Mirrors M_1, which was a plane retroreflector, to M_5 have 100% reflectivity over the LiF:F_2^+ colour centre tuning range (800-1000nm) and the output coupler M_6 was either 3, 10, 20% transmitting over this spectral range. The focussing mirrors around the gain crystal M_2 and M_3 were of 10cm radius of curvature which provide ≈20μm beam waist within the gain medium. Mirror M_3 was a double-stack mirror because it also served as a focussing mirror for the Kr-ion pump laser beam. The infrared reflecting stack was deposited above the pump beam reflecting sequence in order that phase distortion within the pulses be minimised [25]. The focussing mirrors M_4 and M_5 around the saturable absorber dye jet were of 5cm radius of curvature which ensured that the so-called "S parameter" is made appropriately high in order that stable passive modelocking conditions could be achieved for this laser [1]. Tuning of the laser was carried out using a dielectric tuning wedge or a Brewster-angled prism as shown and the cavity round-trip period was 13ns.

The laser cryostat used throughout this experiment has been described in chapter 6. With an initial absorber dye concentration of $0.9 \times 10^{-4} ML^{-1}$ stable modelocked pulse trains were obtained with typical durations of 1-2psec, assuming $sech^2$ pulse profiles. The modelocked laser pulse train was monitored using a Telefunken BPW28 photodiode and a Tektronix 7834 oscilloscope arrangement and the pulse durations were determined using a second harmonic generation autocorrelator. Oscillograms from the chopped output pulse trains for this laser are shown in figure 7.5 and a typical intensity autocorrelation trace and associated spectrum presented in figure 7.6. The duration bandwidth product $\Delta\tau\Delta\nu=0.9$ which is far in excess for a Fourier transform limited $sech^2$ pulse profile of 0.315 indicates the presence of large intracavity dispersion. For the standing-wave cavity highly stable modelocked pulse trains were obtained over a tuning range of 870-880nm for pump powers of 200-400mW above the laser threshold pump power level of approximately 2W.

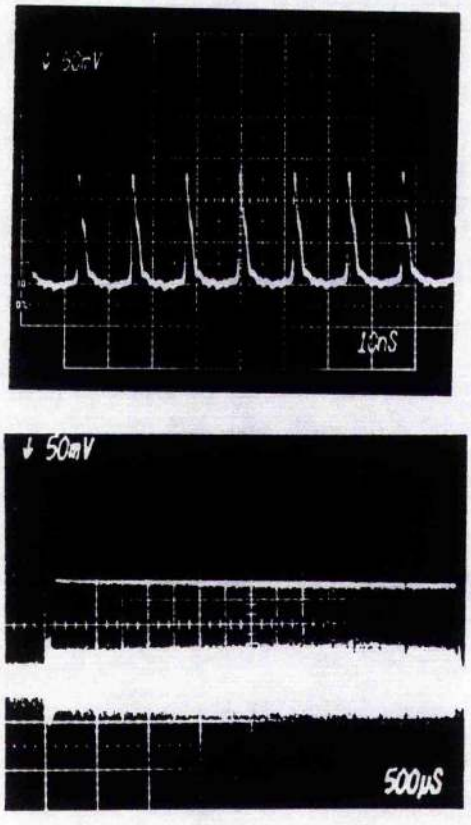

Figure 7.5 The output chopped pulse train from the passively modelocked LiF:F_2^+ colour-centre laser

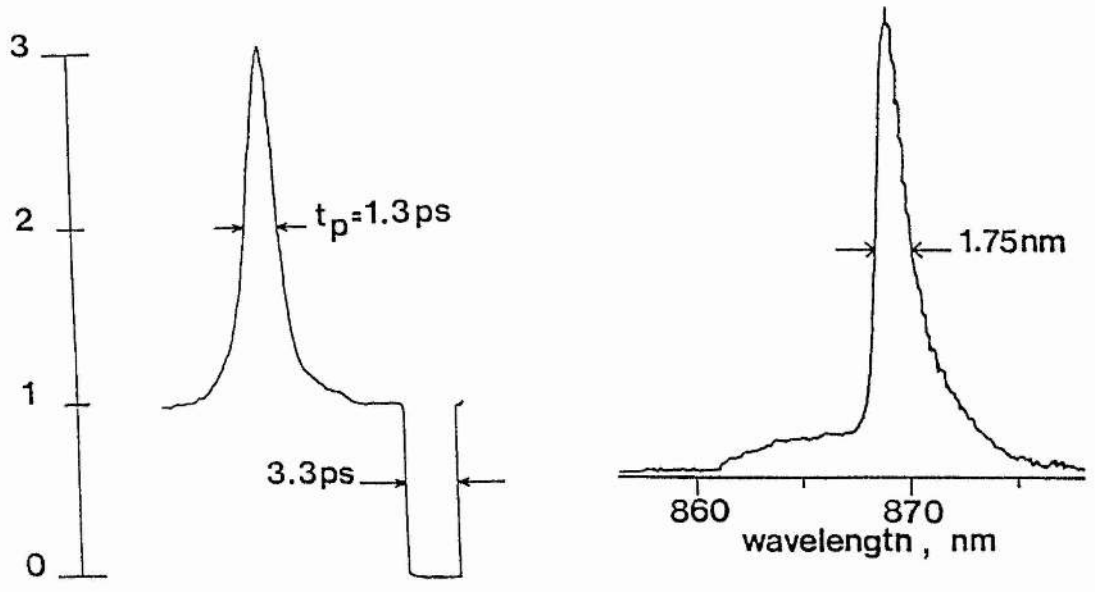

Figure 7.6 Intensity autocorrelation and corresponding spectrum for typical pulses produced by the standing-wave cavity passively modelocked LiF:F_2^+ colour-centre laser

Once the passive modelocking of the LiF:F_2^+ colour-centre laser had been demonstrated it was decided to investigate the improvement, if any, that could be made upon reducing the pulse durations by implementation of the technique of colliding-pulse-modelocking.This was achieved by suitably reorienting mirrors M_1 and M_2 to form a CPM ring travelling-wave cavity which has been shown to be a more efficient pulse shaping and shortening process whereby the two counter propagating pulses collide within the saturable absorber [33,34]. The cavity round-trip time of the travelling-wave ring laser was approximately 15ns and the temporal separation of the gain crystal and saturable absorber jet was made one quarter of the round-trip period to allow for sufficient gain recovery to occur between each successive counter-propagating pulse. For similar saturable absorber dye concentrations used within the travelling-wave cavity pulse durations having somewhat shorter durations of 0.8psec were obtained. By increasing the absorber concentration in

$1.0x10^{-5}$mol/l increments a plot of pulse duration versus absorber concentration was obtained and is presented in figure 7.7.

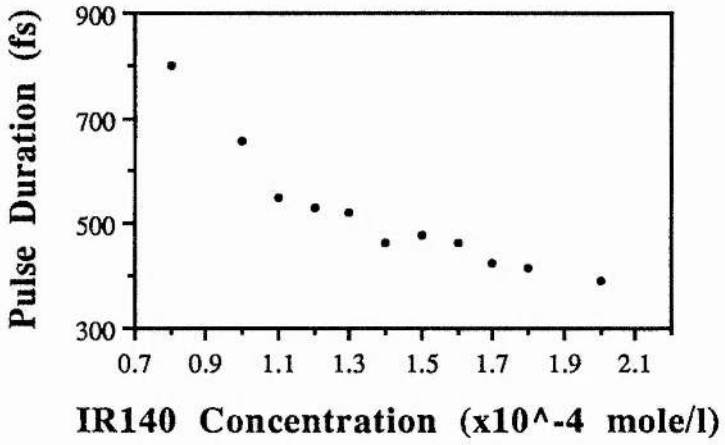

Figure 7.7 Pulse duration as a function of the saturable absorber concentration for the CPM ring passively modelocked LiF:F_2^+ colour-centre laser (Pump power=2.4W)

An intensity autocorrelation trace of the shortest pulse durations, which were obtained for an absorber concentration of $2.0x10^{-4}$mole/l are presented in figure 7.8. These had durations of 390fsec, assuming $sech^2$ pulse profiles, and the corresponding time-bandwidth product $\Delta\tau\Delta\nu$=0.6 again indicating the presence of some excess dispersion. An interesting feature to point out here is that the slope of the laser spectrum displays a sharper edge on the short wavelength side. This has been observed by other workers [17] and is also mentioned later in this chapter and it has been shown to be indicative of too much positive dispersion within the laser cavity. The modelocked pulse trains were obtained for an input power range of ≈2.1-2.4W and approximately 6mW average power was obtained in each output beam. The peak power of the shortest pulses (390fs) was 200W. At the optimum absorber dye concentration ($2x10^{-4}$mole/l) the pulse durations were also investigated as a function of the Kr-ion pump power and these data are presented in figure 7.9. From this figure it can be seen that stable modelocked operation was lost at powers below a threshold level of 2.1W and for powers above 2.5W. This may be explained when the pulse forming processes within a passively modelocked laser are considered.

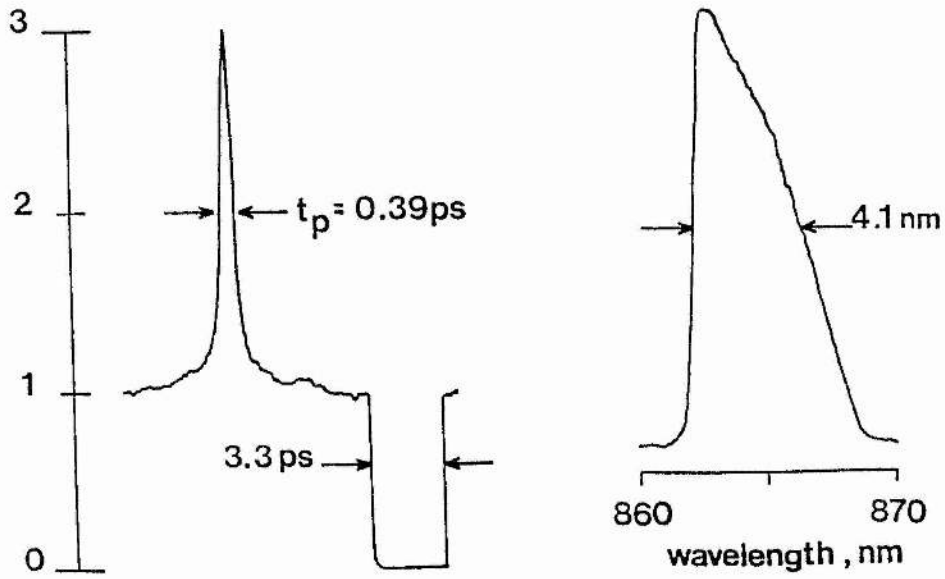

Figure 7.8 Intensity autocorrelation trace and corresponding spectrum of the shortest pulses obtained from the CPM LiF:F_2^+ colour-centre laser

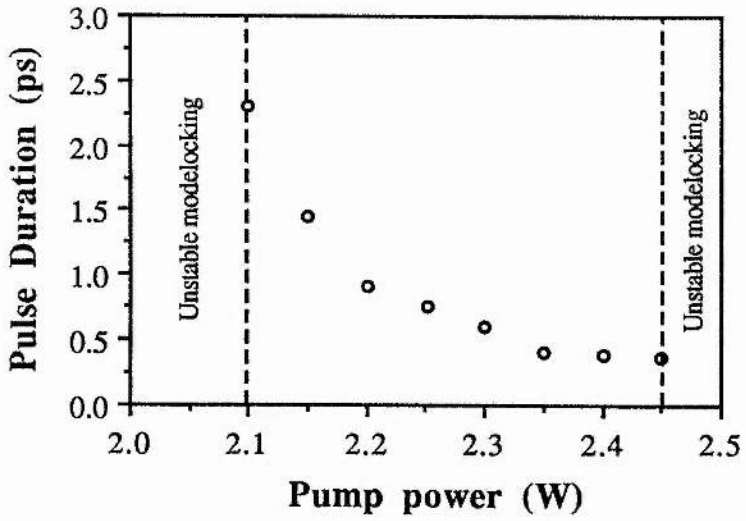

Figure 7.9 Pulse duration as a function of the input pump power

As mentioned in section 3.4 it is the role of gain and absorber saturation which contribute to the initial pulse forming and shaping processes within a passively modelocked laser. Saturation of the optical gain by the leading edge of the propagating pulse produces a gain deficit for the trailing edge whilst it is saturation of the absorber that produces a loss for the leading edge of the pulse and thus these two processes acting together contribute to the initial pulse formation and shaping. Therefore, with reference to data produced in figure 7.9 the loss of stable modelocked operation below a pump powers of 2.1W and above 2.45W may be explained. At low intensity pump powers the intracavity flux intensity may not be sufficient to saturate the optical gain, therefore the trailing edge of the pulse will receive amplification and thus the pulse shortening process is restricted. Conversly at large pump powers where the intensity of the intracavity flux may be such that the leading foot of the pulse alone may be of sufficient intensity to bleach the saturable absorber the leading edge of the pulse receives no loss and hence again the pulse shortening mechanism is inhibited.

As already mentioned the duration-bandwidth product $\Delta\tau\Delta\nu$ for the modelocked pulses produced within both the standing-wave and travelling-wave cavities for the passively modelocked LiF:F_2^+ colour-centre laser operating at 860nm were seen to be in excess of the Fourier transform limit of 0.315 for $sech^2$ pulse profiles. This suggests the presence of some frequency chirping within the laser cavities and so it was decided to construct similar cavities but with GVD compensated resonators using the prism sequences as described earlier such that optimisation of the pulse durations could be studied.

7.3.1 GVD Compensation of the passively modelocked LiF:F_2^+ colour-centre laser operating at 865nm

Investigations of GVD compensation of the passively modelocked LiF:F_2^+ colour-centre laser operating at 865nm was carried out for standing-wave and travelling-wave ring cavities in order that improvements in the pulse durations, if any, could be directly

compared for their uncompensated-GVD counterparts.The GVD-compensated standing-wave resonator is shown in figure 7.10. A prism separation of approximately 65cm was calculated to compensate for the GVD due to the LiF crystal and cryostat windows at the operating wavelength of 870nm. As before, the cavity round-trip period was 13ns and the concentration of the IR140 was $9x10^{-5}$mole/l such that direct comparison of the pulse durations produced from uncompensated and compensated resonators could be made.

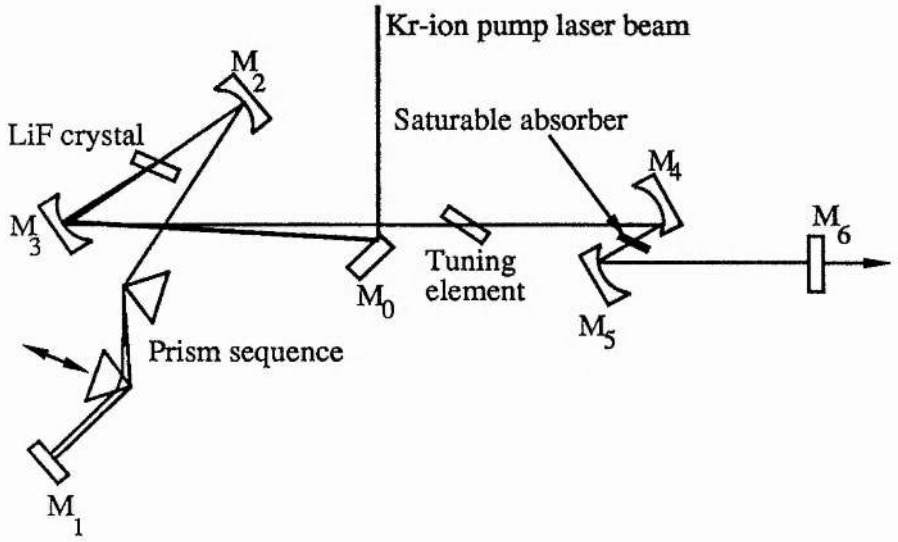

Figure 7.10 The GVD-compensated standing-wave passively modelocked LiF:F_2^+ colour-centre laser

The laser operating wavelength was tuned using a dielectric tuning wedge and the magnitude of the intracavity GVD was adjusted by moving one of the prisms through the beam path with a translation stage. Under these operating conditions the shortest pulse durations obtained where ≈ 250fs for pump powers of 2.8W and the time averaged output was 16mW (x10 chopping factor). An intensity autocorrelation trace and associated spectrum are reproduced in figure 7.11. The duration-band width product $\Delta\tau\Delta\nu$ was 0.5. For a direct comparison of this laser performance with that for a travelling-wave cavity the mirrors M_1 and M_6 were suitably adjusted to form the GVD compensated CPM colour-centre laser as illustrated in figure 7.12.

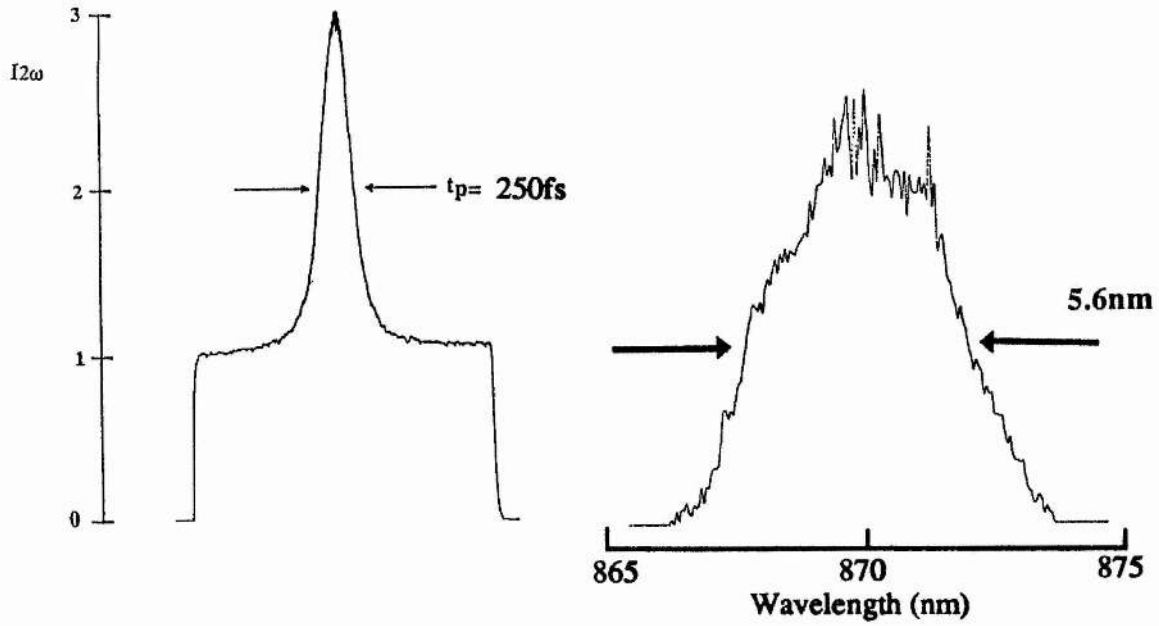

Figure 7.11 Intensity autocorrelation trace and associated spectrum for the GVD-compensated standing-wave passively modelocked LiF:F_2^+ colour-centre laser

The cavity round-trip period for the CPM laser cavity was 15ns and wavelength selection was carried out using a spatial filter which was traversed through the dispersed beam where indicated. The saturable absorber dye concentration was slowly increased until the shortest pulses were obtained and this occurred for concentrations of $3x10^{-5}$mole/l.

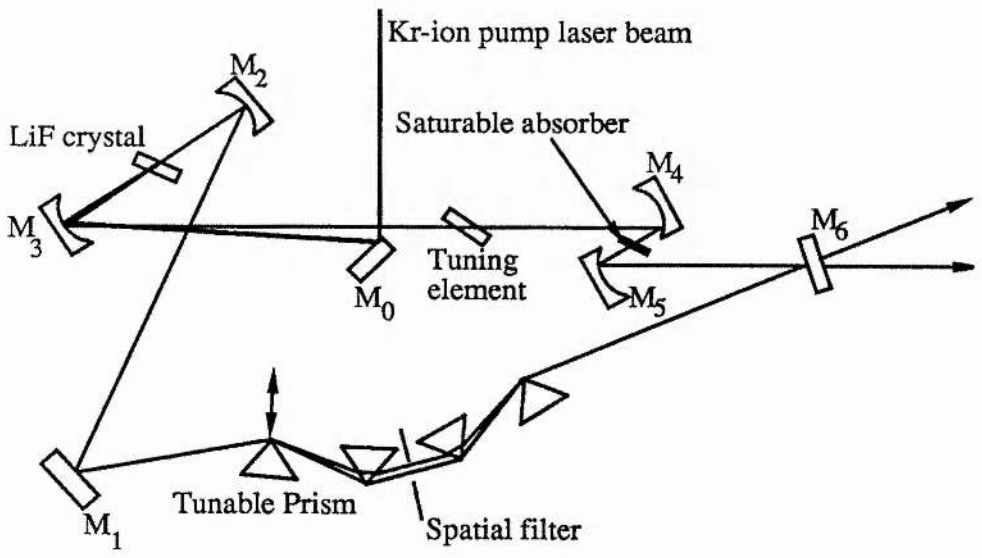

Figure 7.12 The GVD-compensated CPM LiF:F_2^+ colour-centre laser

This was slightly higher than that required for the standing-wave cavity as expected because two optical pulses collide within the saturable absorber. As each pulse only travels through each optical component once in the ring cavity the prism spacing was calculated to be 55cm to provide the required negative dispersion. Optimisation of the pulse durations was carried out by traversing one of the prisms through the beam path to adjust the intracavity dispersion and the shortest pulses obtained had durations of 180fs with a corresponding bandwidth of 4.2nm, figure 7.13, which gave a duration-bandwidth product of $\Delta\tau\Delta\nu$=0.317. This confirmed that successful GVD compensation had been achieved. The pump power required to produce these pulses was approximately 5W and the time-averaged output power in each arm was 15mW corresponding to pulse peak powers of 2kW.

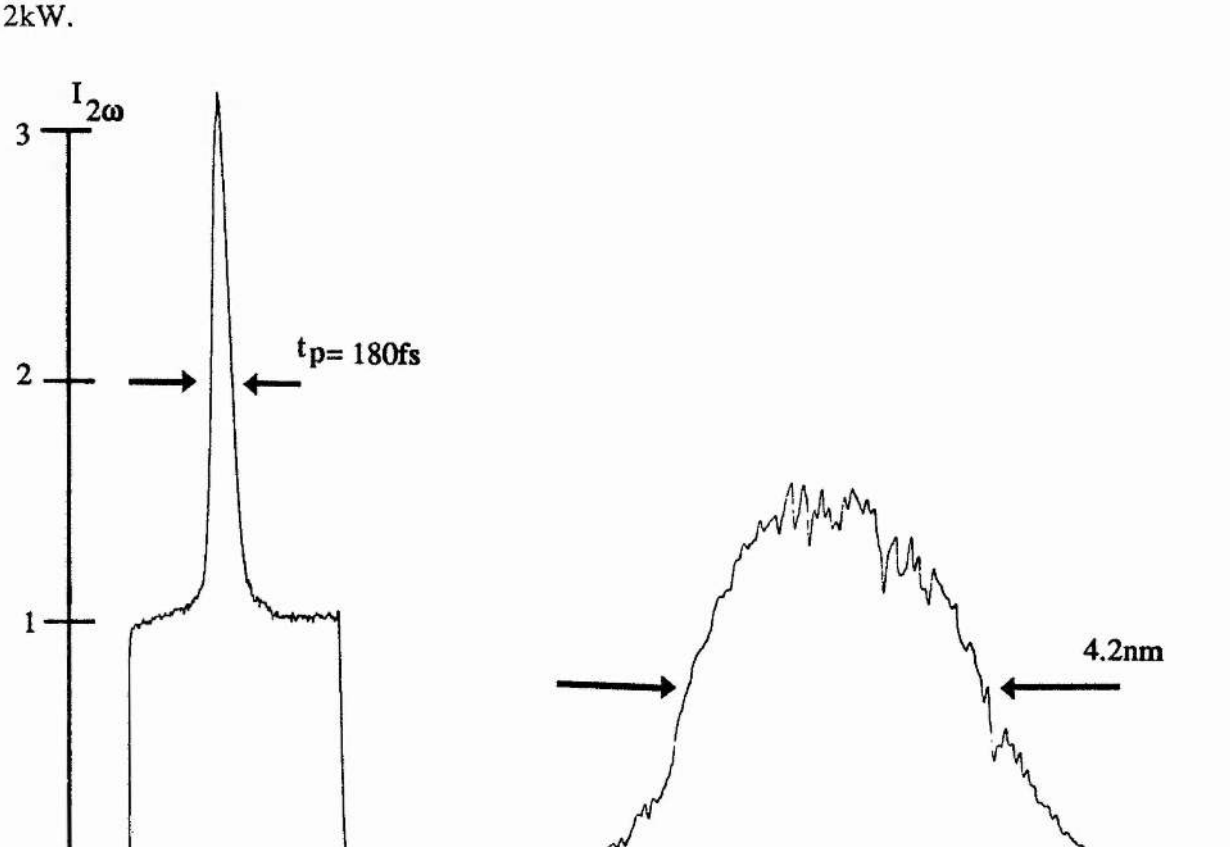

Figure 7.13 Intensity autocorrelation trace and associated spectrum for the shortest pulses obtained from the GVD compensated CPM LiF:F_2^+ colour-centre laser

7.4 Passive modelocking of the LiF:F_2^+ colour centre laser operating in the 900-950nm region

In the previous section the successful operation of a passively modelocked colour-centre laser was described for operation around 860nm using the saturable absorber IR140. In subsequent work, the operation of a similar passively modelocked colour centre laser was investigated for the 900-950nm spectral region. The photosensitive dye 1-diethyl-2, 13-acetoxy-1, 2 quinotetracarbocyanine perchlorate (DaQTeC) was used and this has been used (in iodide form) by other workers to produce ~ 230fs pulse durations by hybrid modelocking of dye lasers near 975nm [13]. In addition, the potential applicability of the coupled-cavity modelocking scheme [35] to enhance the pulse evolution kinetics at the spectral extremes of the saturable absorber dye absorption or where the effectiveness of the saturable dye decreases (through ageing for example) will also be described. Throughout this experiment the upgraded laser cryostat was implemented and a description of this along with the output characteristics of the LiF:F_2^+ crystal used have been presented in chapter six. The saturable absorber (DaQTeC) has a peak absorption cross-section α_0=3x10^{-16}cm^2 at 930nm and its absorption profile is presented in figure 7.14.

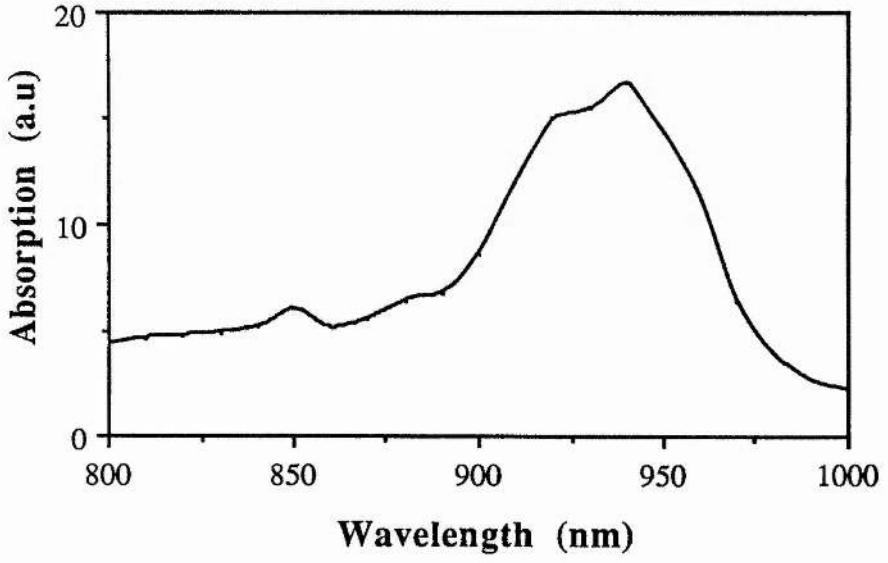

Figure 7.14 Absorption profile of the saturable absorber DaQTeC

As before, a standing-wave resonator was initially implemented with a cavity round-trip period of 12ns (figure 7.15) for which the optics here are described in the previous section. Tuning was facilitated using a Brewster-angled prism and stable modelocked pulse trains were obtained with threshold pump powers of 2.0W over the tuning range of 924nm to 946nm.

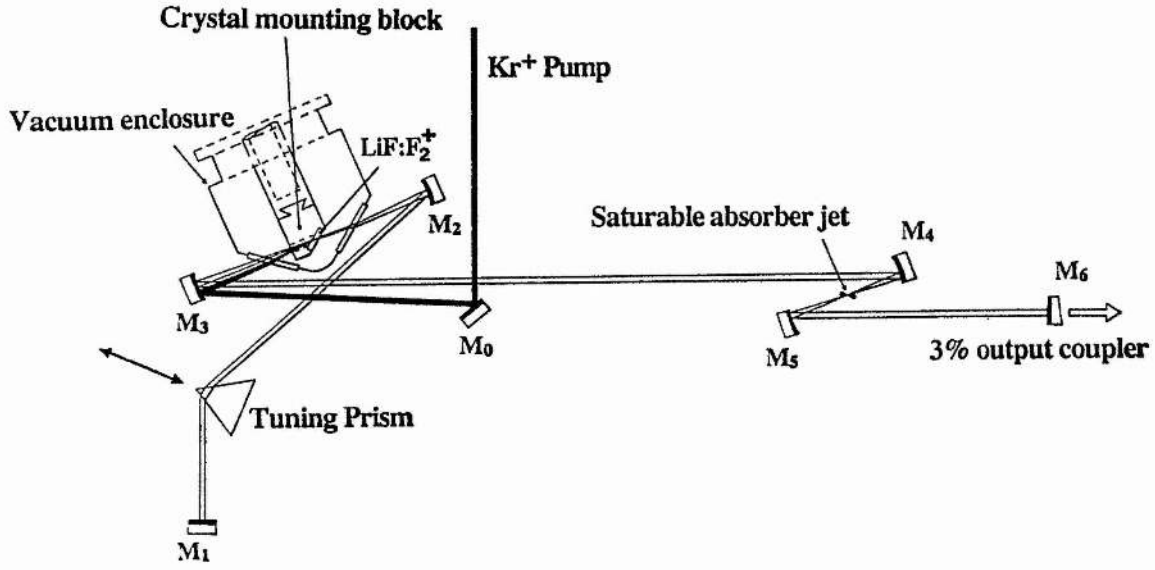

Figure 7.15 The standing-wave cavity $LiF:F_2^+$ colour-centre laser operating at 930nm

The dependence of the pulse durations on the operating wavelength for several saturable absorber concentrations is presented in figure 7.16. The shortest pulse durations measured where obtained for a saturable absorber concentration of 9.6×10^{-5}mole/l for pump powers of 2.3W and had durations of 170fs, assuming sech^2 pulse profiles. Varying the pump power had the same effect as described earlier in section 7.2 for the other passively modelocked colour-centre laser (see figure 7.9). A reproduction of the intensity autocorrelation trace for the shortest pulse trains obtained within the standing-wave

resonator is presented in figure 7.17 along with the corresponding laser spectrum for which $\Delta\lambda$=6.25nm.

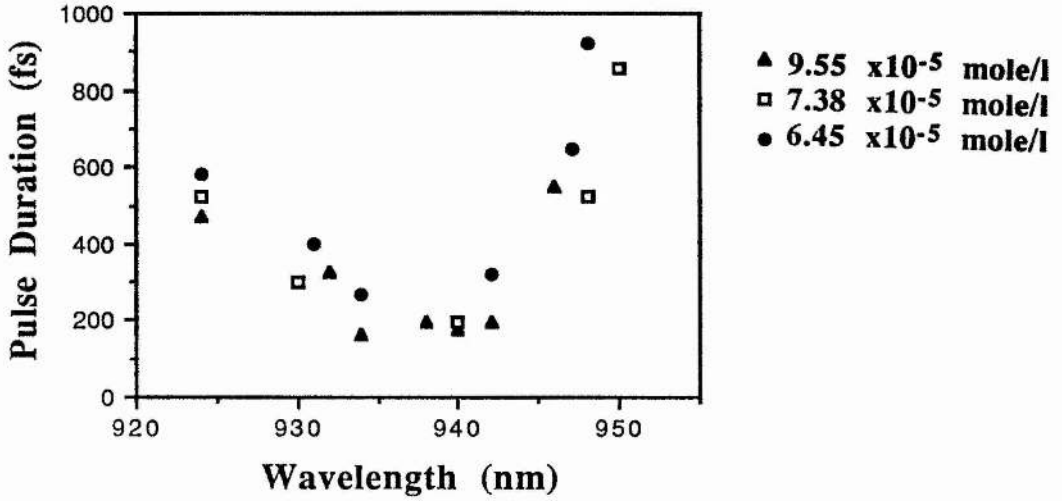

Figure 7.16 The pulse duration as a function of wavelength for several saturable absorber dye concentrations

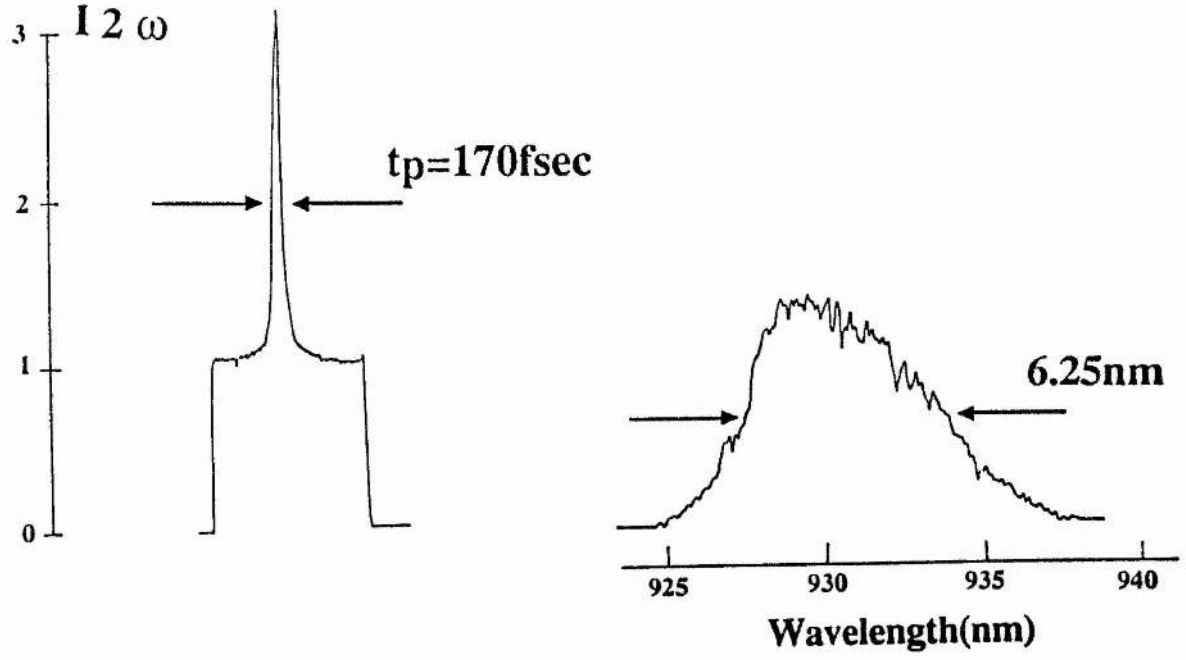

Figure 7.17 Intensity autocorrelation profile of the shortest pulse durations and associated spectrum obtained from the standing-wave passively modelocked LiF:F_2^+ colour centre laser operating at 930nm

The duration-bandwidth product $\Delta\tau\Delta\nu$ was 0.37 indicating the presence of only a small amount of excess bandwidth for the operating conditions of the laser. The duty chopping cycle was ten and the time-averaged output power was 10mW.

Again, it was decided to construct a CPM travelling-wave ring cavity with the aim of improving upon the standing-wave cavity pulse durations. This was achieved by suitably adjusting the positions of mirrors M_1 and M_6 to produce a ring cavity with a round-trip period of 13ns. At this stage the useful working lifetime of the saturable absorber had elapsed which was typically a few days and as the dye was being replaced the pulse duration as a function of the saturable absorber concentration was obtained, figure 7.18.

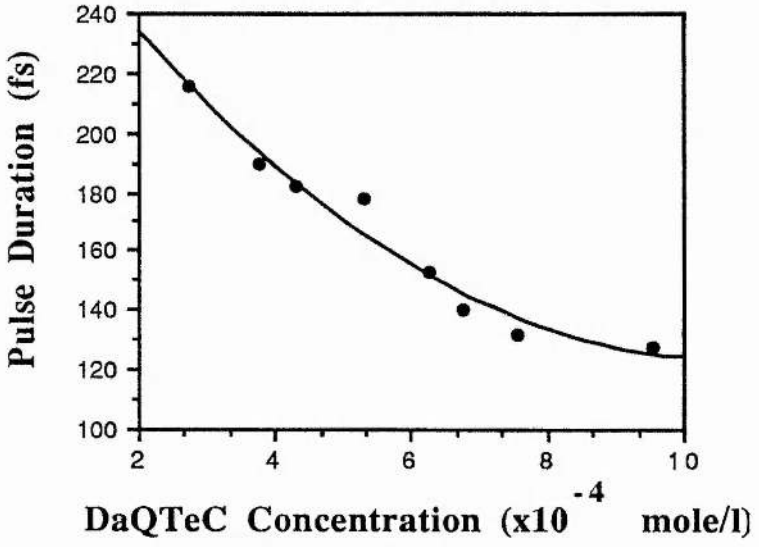

Figure 7.18 Pulse duration as a function of the DaQTeC saturable absorber concentration for the CPM travelling-wave ring cavity.

Stable modelocked pulse trains were obtained over dye concentrations ranging from $1.0\text{x}10^{-5}$mole/l to approximately $1.0\text{x}10^{-4}$mole/l and the shortest pulse durations of 128fs were obtained at a concentration of $1.0\text{x}10^{-4}$mole/l. The intensity autocorrelation trace and corresponding spectrum for such pulses are presented in figure 7.19 and the duration bandwidth product $\Delta\tau\Delta\nu$ of 0.34 again implies that little or no nett frequency chirp existed within the cavity for the operating parameters and conditions of the laser described here.

The optimum pump power necessary for the shortest pulses was 2.3W and a time averaged output power of 6mW from each arm was obtained with a duty chopping cycle of ten.

Although the duration-bandwidth products obtained for the modelocked pulses were close to the Fourier transform limit of 0.315 for $sech^2$ pulse profiles it was decided to insert an intracavity prism sequence into the CPM ring cavity in order to investigate the effects of varying the amount of GVD within the laser (See figure 7.12). As previously, the prism spacing was chosen such that the dispersion arising due to the cryostat windows and laser crystal was compensated and adjustments were made by traversing one of the prisms perpendicularly through the beam. However, once inserted the prism sequence served merely to retain the stability of the pulse train and had little or no effect upon the pulse durations.

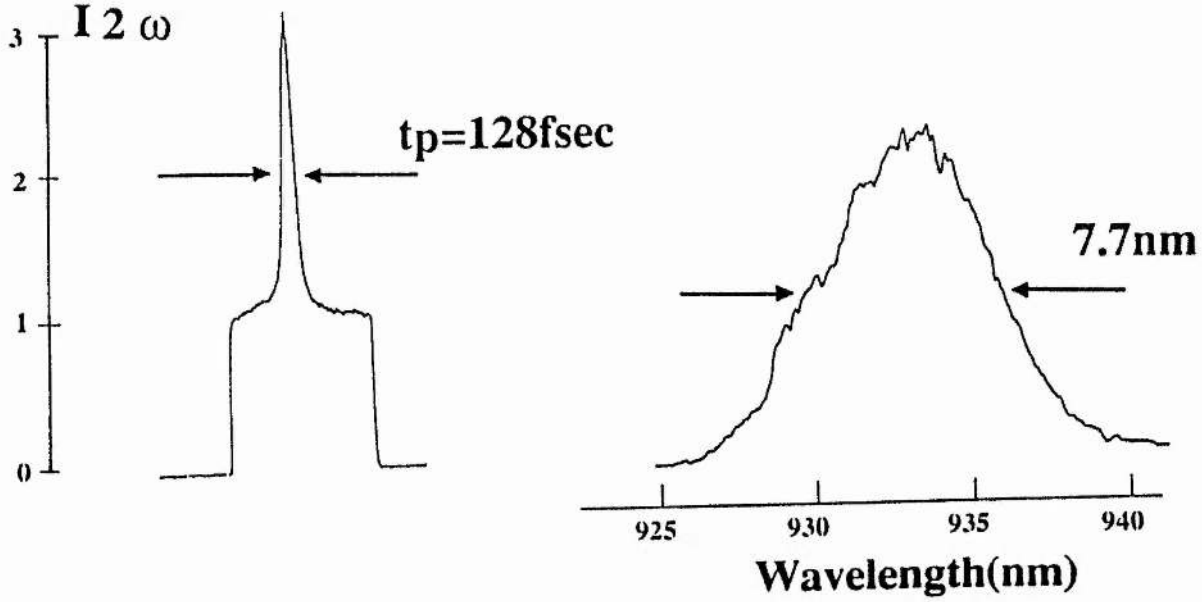

Figure 7.19 Intensity autocorrelation trace and associated spectrum for the shortest pulses obtained from the CPM-ring passively modelocked LiF:F_2^+ colour-centre laser operating at 930nm

The effect of varying the amount of intracavity glass was investigated and it was observed that for less glass within the the cavity necessary for the optimum pulse durations that the spectrum profile became asymmetric with the long wavelength side having a steep edge.

Conversely when additional intracavity glass than that required for the optimum pulse durations was inserted into the cavity the effect upon the pulse spectrum is mirror imaged with a sharp slope appearing on the short wavelength side. For optimum conditions the pulse spectra were found to be symmetrical. This is illustrated in figure 7.20 for the three conditions described together with the corresponding intensity and interferometric autocorrelation traces. The intensity autocorrelation data do not provide any indication of frequency chirp but some indication as to the degree of chirp present may be gleaned from the interferometric autocorrelation profiles [17]. For the latter, the presence of intracavity frequency chirp which effects the visibility of the interference fringes in the wings is not as dramatic as those presented elsewhere [36]. However, some information regarding the presence of chirp may be resolved if the wings and shape of the interferometric autocorrelations are inspected for operational parameters incorporating too much and too little intracavity glass. This can be contrasted to the previously reported passive modelocking of the LiF:F_2^+ colour-centre laser operating around 850nm using the saturable absorber IR140 in this chapter and elsewhere [36].

As already mentioned the useful working lifetime of the DaQTeC saturable absorber dye solution was of the order of days as is typically the case with other dyes operating within this wavelength regime [13]. Beyond this short and therefore limited operating period the durations of the modelocked pulses were observed to increase substantially and the operating wavelength of the laser tended towards the peak of the LiF:F_2^+ colour-centre gain profile around 900nm. Under such operating conditions when the laser was tuned to operate around 930nm where the shortest pulses were normally obtained, temporally broadened pulses were produced along with, in most cases, evidence of sub-pulsing occuring behind the main pulse. At this point it was decided to implement the the technique of coupled-cavity modelocking [35] to the passively modelocked LiF:F_2^+ colour centre laser whereby the laser cavity is coupled to a second cavity containing a dispersive nonlinear element. This may be achieved by a suitable length of optical fibre displaying either positive

or negative dispersion or a semiconductor diode [37]. The operation and theory of such coupled cavity modelocking schemes is described in detail by other workers [35,38].

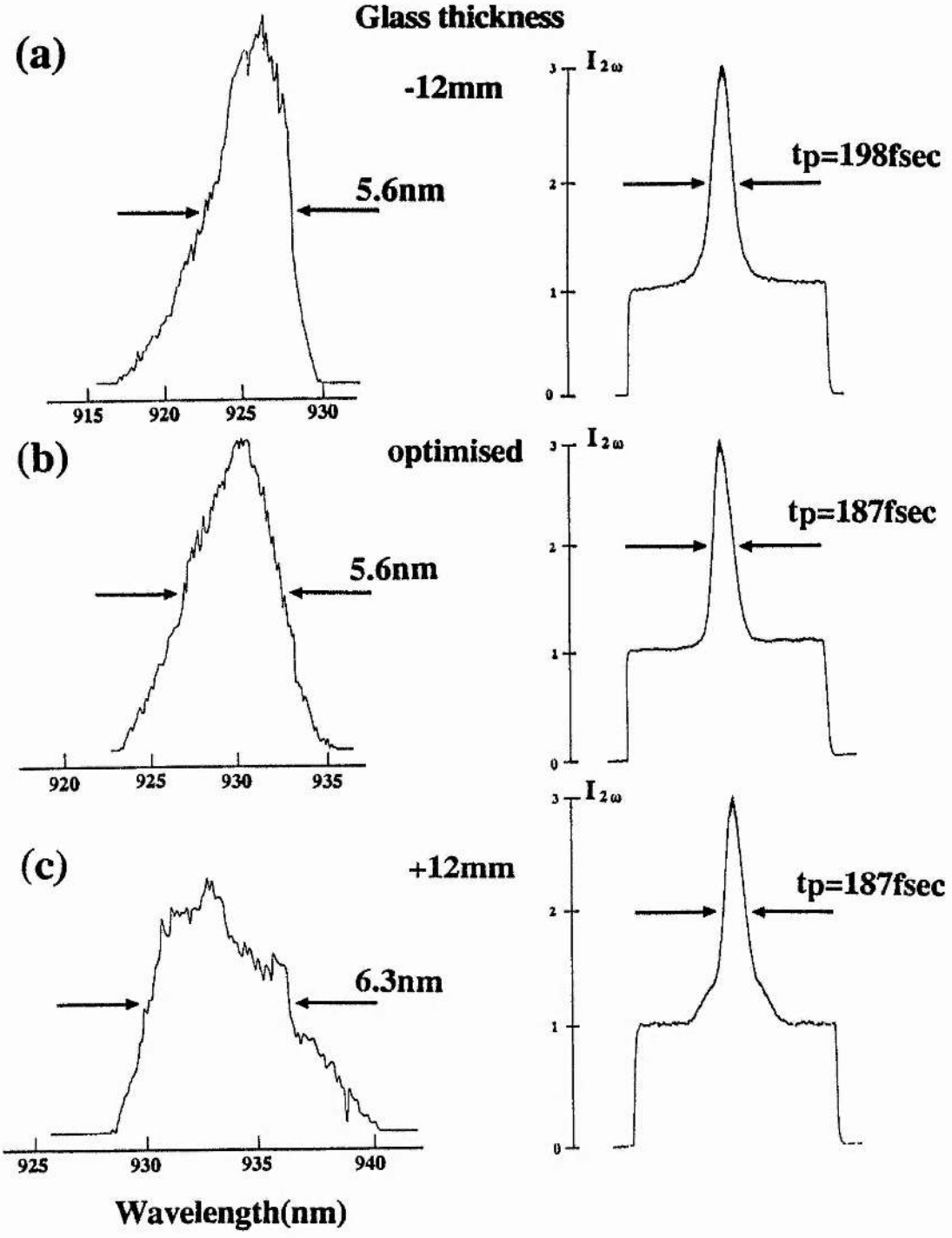

Figure 7.20(a) The effect upon the pulse spectrum for (i) less than optimum GVD compensation, (ii) optimum GVD compensation and (iii) more than optimum GVD compensation. Intensity autocorrelation profiles are also presented.

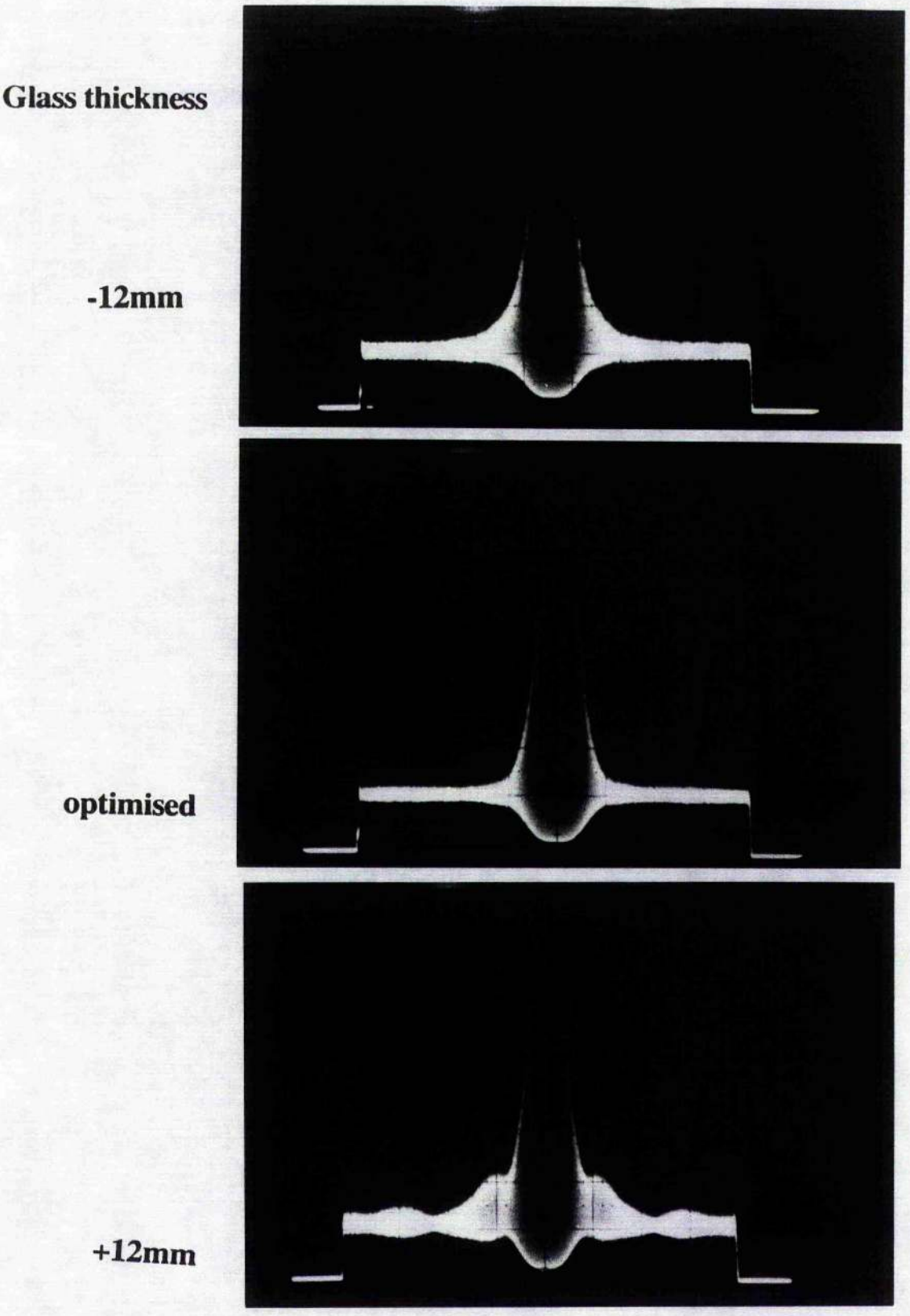

Figure 7.20(b) Interferometric autocorrelation profiles corresponding to the spectra presented in figure 7.20(a) illustrating that an indication as to the presence of frequency chirping across the pulse may be obtained from examination of the wings of the interferometric autocorrelation profiles

Basically this enhanced modelocking technique operates due to spectral broadening occuring within the nonlinear element and suitably returning the spectrally broadened pulse to the main cavity such that desirable interferometric interaction occurs between the two pulses. This leads to the enhanced phase-locking of further longitudinal modes and the production of shorter duration modelocked pulses [35,37].

This technique was applied to the laser described here under the operating conditions beyond the useful working lifetime of the saturable absorber such that the coupled-cavity modelocking (CCM) process contributed to the pulse shapening and shortening kinetics. (If successful this "hybrid" modelocking scheme would therefore be beneficial when the saturable absorber becomes less efficient either through aging or when operated at the spectral extremes of the absorption profile). This "hybrid" scheme was assessed by modifying a standing-wave cavity by suitably reorienting the mirrors M_1 and M_6. The intracavity prism sequence was removed and the 3% output coupler replaced by a 10% output coupler. A normal dispersion optical fibre was used (Andrew Corporation-type) in the control cavity which was polarization preserving having an elliptical core with dimensions 1.25μmx2.5μm and the core cladding Δn=0.034. The passively modelocked coupled-cavity scheme is illustrated in figure 7.21.

Coupling into the optical fibre was achieved using suitable objective lenses which were index matched to the freshly cleaved fibre ends to reduce retroreflections back to the main cavity. Mirror M_8 was a 100% plane reflector mounted upon a translation stage to allow cavity length adjustments to be made. Initially a 68cm long piece of fibre was mounted within the external cavity (also known as the control cavity) and the round-trip period period was half that of the main or master cavity. Under these conditions no enhancement of the modelocked pulse durations was observed when the laser was tuned over the DaQTeC absorption spectrum. Consequently a longer length (4.3m) of fibre was inserted into the control cavity and the control cavity round-trip period extended to twice that of the master cavity. With this configuration significant enhancement of the much degraded

modelocked pulse durations was obtained over the much extended tuning range of 900-950nm.

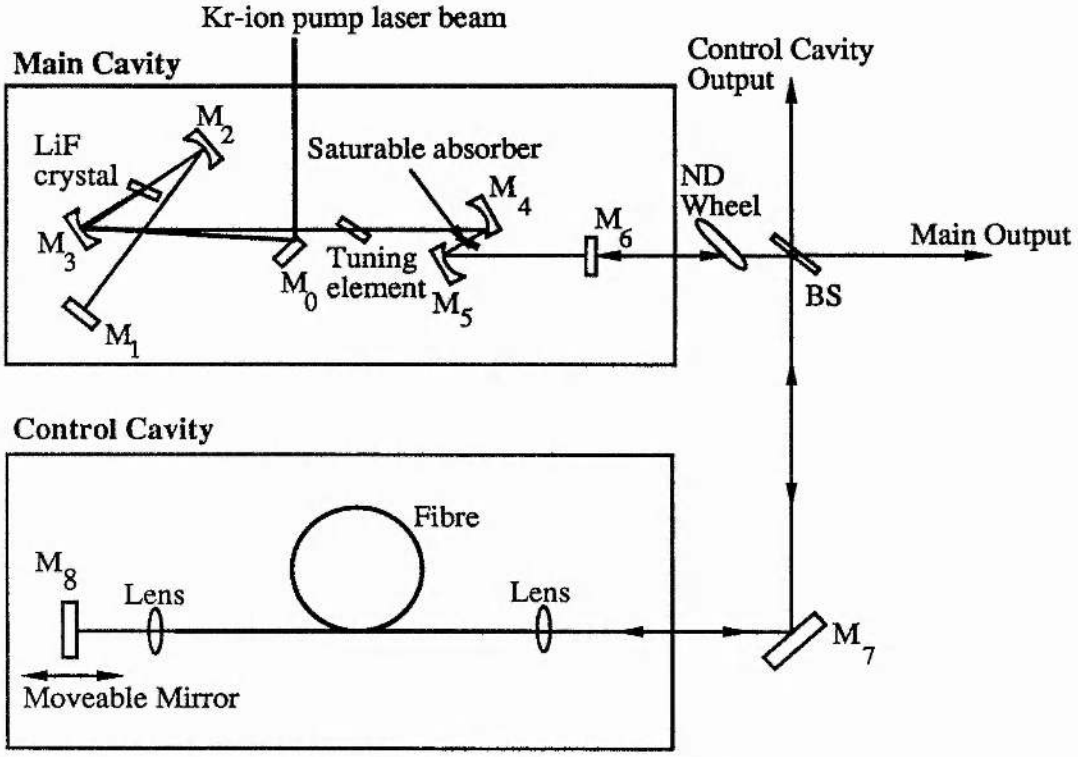

Figure 7.21 The "Hybrid" passively modelocked coupled-cavity modelocking scheme.

Intensity autocorrelation traces for pulses produced from the LiF:F_2^+ colour centre laser cavity alone with a much degraded saturable absorber dye are reproduced in figure (7.22a) operating at a much extended operating wavelength of 904nm and also in figure (7.22c) operating at the normal wavelength of 932nm which shows evidence of the subpulsing mentioned earlier within this section. With the control cavity unblocked we see that in both cases significant shortening of the modelocked pulses is achieved, figures (7.22b) and (7.22d). For both cases the Kr-ion pump power was 2.2W and the power launched into the fibre was approximately 20mW time averaged, the chopped duty cycle of ten being retained.

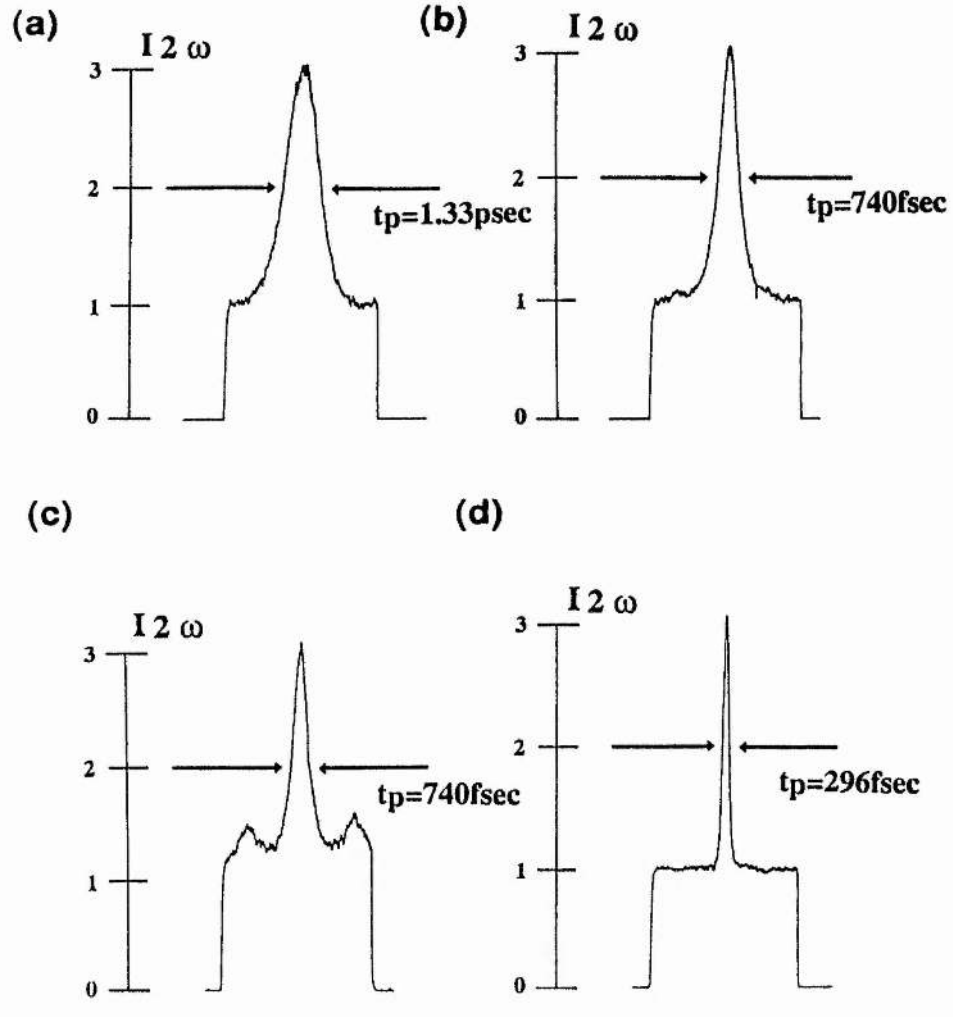

Figure 7.22 Intensity autocorrelation profiles obtained from the "Hybrid" passively modelocked LiF:F_2^+ colour centre laser for (a) operating at 904nm, coupled cavity blocked, (b) operating at 904nm, coupled cavity opened, (c) operating at 932nm, coupled cavity blocked and (d) operating at 932nm, coupled cavity opened

7.5 Summary

In this chapter the successful passive modelocking of a LiF:F_2^+ colour centre laser has been discribed. By implementation of the saturable absorber dyes IR140 and DaQTeC stable modelocked pulse trains have been obtained around 860nm and 930nm. It is interesting to note that only two of the three operational constraints required for stable passive modelocking with a slow saturable absorber [1] have been met here. These operational constraints are (i) the relaxation time of the gain medium must be of the order of the cavity round trip period, (ii) the saturable absorber relaxation time must be less than that of the

gain media, and (iii) the "S parameter" must be large (normally >2). The second and third constraints were both readily fulfiled with the saturable absorber relaxation time being of the order of 1ns compared to the 29ns recovery time of the gain media and by the formation of a tighter beam waist within the saturable absorber than in the gain media so that the S parameter was made suitably large. It may be seen that the first operational constraint has not been met . This may be explained if the role of gain saturation, the magnitude of the small signal gain and the laser loss is considered [1,22]. Under the operational parameters of the laser discussed here the return of the modelocked pulse to the gain medium after approximately 12ns appears to be of sufficient time whereby the laser gain has sufficiently recovered to suitable level above that of the loss.

It has also been shown for both lasers that operation within CPM travelling wave ring cavities proved to be a more efficient pulse forming process as has been shown elsewhere both experimentally and theoretically for dye lasers. Group-velocity-dispersion-compensated cavities have been demonstrated for the first time for a passively modelocked colour-centre laser producing until quite recently the shortest pulses reported from a passively modelocked colour-centre laser. Shorter pulse durations from a passively modelocked colour-centre laser operating at 1.6μm have been reported using a multiple quantum well as a saturable absorber [39].

Pulse durations obtained when operating with the saturable absorber DaQTeC around 930nm were considerably shorter than those obtained with the IR140 saturable absorber operating at 865nm .The amount of GVD present whilst operating at 930nm was also less than that of the shorter wavelength operating conditions.

Finally it has been shown that by the implementation of a "hybrid" coupled-cavity modelocking scheme for the passively modelocked LiF:F_2^+ colour-centre laser the useful operating tuning range and working lifetime of the saturable absorber may be substantially increased. This "hybrid" modelocking scheme should also prove to be useful when

implemented, for example, to dye lasers and indeed any passively modelocked laser. In particular this could prove to be a useful technique for extending the narrow (several nm) operating range of passively modelocked lasers utilizing multiple quantum wells as the saturable absorbers.

Chapter 7. References

1. G.H.C.New; Rep.Prog.Phys. **46**, 877 (1983)

2. C.V.Shank, R.L.Fork, R.Yen, R.H.Stolen, W.S.Tomlinson; Appl.Phys.Lett. **41**, 223 (1982)

3. A.J.De Mara, D.A.Stetser, H.Heyman; Appl.Phys.Lett. **8**, 174 (1966)

4. W.Schmidt, F.P.Schafer; Phys.Lett.A. **26**, 558 (1968)

5. P.Georges, F.Stalin, A.Brown; Opt.Lett. **14**, 940 (1989)

6. P.W.Smith, Y.Silverberg, D.A.B.Miller; JOSA.B. **2** (1985)

7. D.E.Spence, W.Sibbett; Opt.Lett.Jan 1991 (To be published)

8. N.Langford, K.Smith, W,Sibbett; Opt.Lett. **12**, 903 (1987)

9. J.A.Valdamis, R.L.Fork, J.P.Gordon; Opt.Lett. **10**, 131 (1985)

10. P.M.W.French, J.R.Taylor; Appl.Phys.Lett. **50**, 1708 (1987)

11. E.P.Ippen, C.V.Shank, A.Diennes; Appl.Phys.Lett. 21, 348 (1972)

12. K.Smith, N.Langford, W.Sibbett, J.R.Taylor; Appl.Phys.Lett. **50**, 1708 (1987)

13. M.D.Dawson, T.F.Boggess, A.L.Smirl; Opt.Lett. **12**, 590 (1987)

14. C.I.Johnston, D.E.Spence, R.S.Grant, W.Sibbett; Opt.Commun. **73**, 370 (1987)

15. S.De Silvestri, P.Laporta, O.Svelto; IEEE. J.Quan.Elect.**QE-20**, 533 (1984)

16. J.A.Valdamis, R.L.Fork; IEEE. **QE-22**, 112 (1986)

17. J.C.M.Diels, J.J.Fontaine, I.C.McMichael, F.Simoni; App.Opt. **24**, 1270 (1985)

18. O.E.Martinez, R.L.Fork, J.P.Gordon; Opt.Lett. **9**, 156 (1984)

19. J.J.Fontaine, W.Dietel, J.C.Diels; IEEE. J.Quan.Elect. **QE-19**, 1467 (1983)

20. R.L.Fork, C.V.Shank; IEEE. J.Quan.Elect. **QE-19**, 500 (1983)

21. A.E.Seigman; Lasers; University Science Books, CA. USA (1986)

22. D.Marcuse; Appl.Opt. **19**, 1653 (1980)

23. R.S.Miranda, G.R.Jacobovitz, C.H.Britocruz, M.A.F.Scarparo; Opt.Lett. **11**, 224 (1986)

24. R.R.Alfono, L.L.Hope, S.L.Shapiro; Phys.Rev.A. **6**, 433 (1972)

25. P.Laporta, V.Magni; Appl.Opt. **24**, 2014 (1985)

26. P.M.W.French, J.R.Taylor; Opt.Commun. **61**, 224 (1987)

27. R.L.Fork, O.E.Martinez, J.P.Gordon; Opt.Lett. **9**, 150 (1984)

28. J.Kuhl, J.Heppner; IEEE. J.Quan.Elect. **QE-22**, 182 (1986)

29. A.Finch; PhD. Thesis University of St.Andrews (1989)

30. O.G.Martinez, J.P.Gordon, R.L.Fork; J.Opt.Soc.Am.A. **10**, 1003 (1984)

31. J.P.Fouassier, D.J.Lougnot, J.Faure; Opt.Commun. **23**, 393 (1977)

32. J.P.Fouassier, D.J.Lougnot, J.Faure; Opt.Commun. **18**, 293 (1978)

33. M.S.Stix, E.P.Ippen; IEEE. J.Quan.Elect. **QE-19**, 520 (1983)

34. D.Kuhlke, W.Rudolph, B.Wilhelmi; IEEE. J.Quan.Elect. **QE-19**, 526 (1983)

35. L.F.Mollenauer, R.H.Stolen; Opt.Lett. **9**, 13 (1984)

36. N.Langford, R.S.Grant, C.I.Johnston, K.Smith, W.Sibbett; Opt.Lett. **14**, 45 (1989)

37. P.N.Kean, X.Zhu, D.Crust, R.S.Grant, D.Burns, W.Sibbett; Opt.Lett. **14**, 39 (1989)

38. R.L.Lang, A.Yariv, IEEE. J.Quan.Elect. **QE-24**, 66 (1988)

39. G.E.Soccolich, M.N.Islam, M.G.Young, B.I.Miller; Appl.Phys.Lett. **56**, 2177 (1990)

Chapter 8

The NaCl:OH^- Colour-Centre Laser

8.1 Introduction

The NaCl:OH^- colour centre laser is an important type of stabilized laser based upon the F_2^+ centre. Such a laser is capable of delivering up to 3W CW output power when pumped by a CW 10W Nd:YAG laser [1]. Stabilization of the normally degenerate F_2^+ centre is provided by spatially trapping it to an oxygen ion which also acts as an electron trap. Known as the $F_2^+:O^{2-}$ centre this class of highly stable colour centre was first reported in 1985 [2] and offers a tuning range covering the 1.4-1.8μm spectral region. Within this chapter the production of a home-built NaCl:OH^- colour-centre laser and its output performance will be described.

8.2 The preparation of laser active $F_2^+:O^{2-}$ colour centres within a NaCl host crystal

A brief introduction to the stabilized F_2^+ colour centre within a NaCl host has already been given in chapter 2. The preparation of such centres within this laboratory will now be described.

A crystal boule of NaCl doped with $\approx 5 \times 10^{-7}$ mol% of NaOH was obtained from the University of Utah [3]. The NaCl boule which measured 7cm tall and 3cm diameter was cleaved, using a sharpened wood chisel and hammer, into 5-6mm slices. From each of the slices eight 2mmx8mmx9mm crystal slabs were obtained using a sharp scalpel blade. This particular size of crystal was chosen because it conveniently fitted the cold finger of the redesigned cryostat and also that astigmatically compensated folded cavities had already been designed for 2mm thickness LiF crystals.

As already stated in chapter 2 it is necessary to additively colour the NaCl crystal within a Na vapour and this together with some "additional treatment" leads to the production of stabilized $F_2^+:O^{2-}$ colour centres. Other workers [4] have carried out colouration of their NaCl crystals within a controlled Na vapour environment using a specially designed heat pipe and the output characteristics of these has been described elsewhere [2,4]. This type of apparatus was not available for use in this work so a stainless-steel "heat bomb" was constructed from Varian vacuum flanges, see figure 8.1.

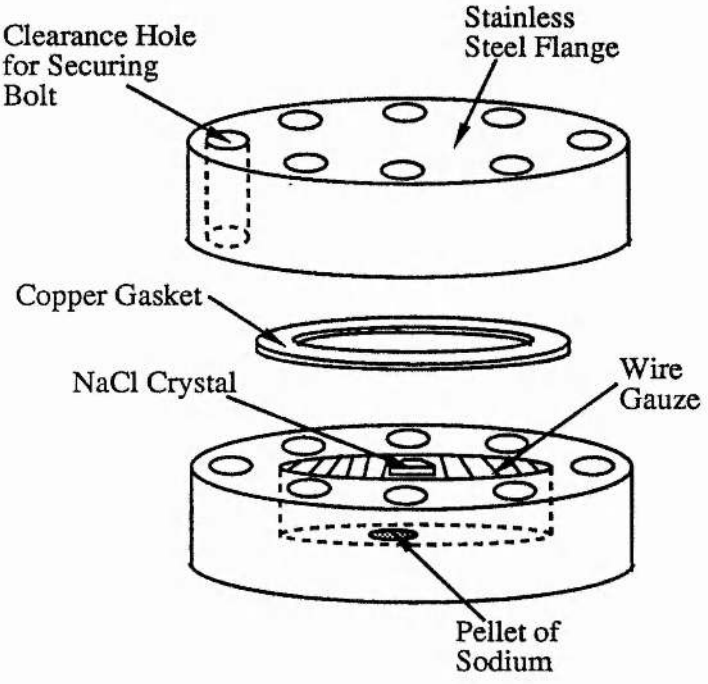

Figure 8.1 The stainless-steel "heat bomb" within which the NaCl crystals where coloured within a sodium vapour environment

Within this apparatus approximately 0.1g of Na was placed into the bottom flange and the NaCl crystal to be coloured rested upon a fine wire gauze located above the Na metal. At this stage the NaCl crystal had been polished to optical quality so that after the colouration treatment the crystal was ready to be placed within the laser cavity. The heat bomb was sealed by tightly bolting the flanges together against a soft copper gasket. The retaining bolts were lubricated with a carbon solution (Aquadag) in order that they could be undone after the heating process. Once tightened, fine adjustment of the bolts was made by

checking the flange separation at each bolt with a feeler gauge such that the flange separation was less than 0.2mm at each bolt. It was found experimentally that for flange separations greater than this then an insufficient sodium vapour pressure was produced and also there was a high probability of water leakage into the crystal chamber whilst rapidly cooling the heat bomb.

Once adequately prepared the heat bomb was placed into an oven at 700^0C for approximately 90 minutes during which the NaCl was additively coloured within the sodium vapour. This colouring process produces F, F_2 and F_3 colour centres and causes dissociation of the OH^- ions into H^-, O^- and O^{2-} to take place which occupy anion sites within the crystal lattice. Of these species it is the O^{2-} ion which produces the stabilization for the F_2^+ colour centre (see figure 2.7) when it is subsequently produced during further post-colouration treatment. The baking time mentioned here differs from that reported elsewhere [4] and this is most probably due to the additional time required to bring the heat bomb up to the necessary temperature. Following this baking procedure the heat bomb was removed from the oven and cooled as quickly as possible. Ideally the crystal should be quenched at this stage to restrict the migration of the centres but due to the physical constraints on the heat bomb it was only possible to cool the crystal to room temperature in the order of 5-10 minutes. This was achieved by submerging the bomb first in cold water, and then when adequately cooled, in liquid nitrogen. The bomb was rapidly disassembled and the crystal inspected and a successful baking status was inferred if the crystal was dark blue. Crystals produced during early stages of this work which appeared otherwise (mainly light green in colour) failed to produce the necessary absorption spectrum indicative of a crystal suitable for laser action after the necessary further optical processing treatment had been performed. Crystals not appearing dark blue in colour indicate an insufficient Na vapour pressure within the bomb and this was most likely due to inadequate flange-gasket compression by the retaining bolts.

Once treatment of the crystal was undertaken it only needed to be exposed under ambient light conditions for short periods to avoid degradation of the centres and thus inspection of the crystal was swiftly carried out. The blue crystal was then carefully wrapped within a protective layer of copper foil and returned to the oven at 700^0C for approximately $3\frac{1}{2}$ minutes. This second bake time was carried out in order that the crystal colour be changed to a dark olive green. The crystal should have this appearance after the first bake period but with the system used here insufficient quenching leads to the blue appearance mentioned above. Returning the coloured crystal to the oven for this further period leads to a reorientation of the necessary "preliminary" colour centres to occur and these can be trapped in situ because the small copper containment-package could be rapidly quenched in liquid nitrogen.

When the additive colouration phase has been satisfactorily completed the NaCl crystal was ready for optical processing. Before this the crystal surfaces were inspected for condensation under low-level filtered red light conditions and the surfaces given a gentle repolish if necessary. The crystal was then mounted into a suitable cryostat and the following processes carried out. Firstly the crystal was exposed to F-band light (at 452nm using a suitably filtered 200W mercury arc lamp with Corning filters 5-56, 1-75) for approximately one hour at room temperature. This process caused the formation of an absorption band around 1.05μm to occur and also caused the F-band absorption located around 650nm to decrease in strength which is consistent with the formation of F_2^+ colour centres within the crystal [4]. To produce stabilized F_2^+:O^{2-} colour centres the crystal was then cooled to 77K and illuminated with the same filtered UV light for approximately 10 minutes. This gave rise to a slight long wavelength shift and broadening of the F_2^+ colour-centre absorption band and also a shift in the fluorescence emission in NaCl from 1.47μm to the F_2^+:O^{2-} peak of 1.55μm [4]. In order to monitor the various processes occurring within the crystal an absorption spectrum was obtained after each treatment and relevant data are presented in figure 8.2. With reference to figure 8.2 curve (i) represents the absorption spectrum obtained after the additive colouration process only and may be

compared to that reported by other workers [4]. In the crystal processed here it may be seen that there is a slight absorption peak due to existing F_2^+ colour centres. After illumination with F-band light at room temperature it may be seen that the F_2^+ absorption peak grows at the expense of the F_2 absorption band (curve(ii)) and when this process is repeated at 77K the absorption profile of the stabilized $F_2^+:O^{2-}$ colour centre becomes that presented as curve (iii).

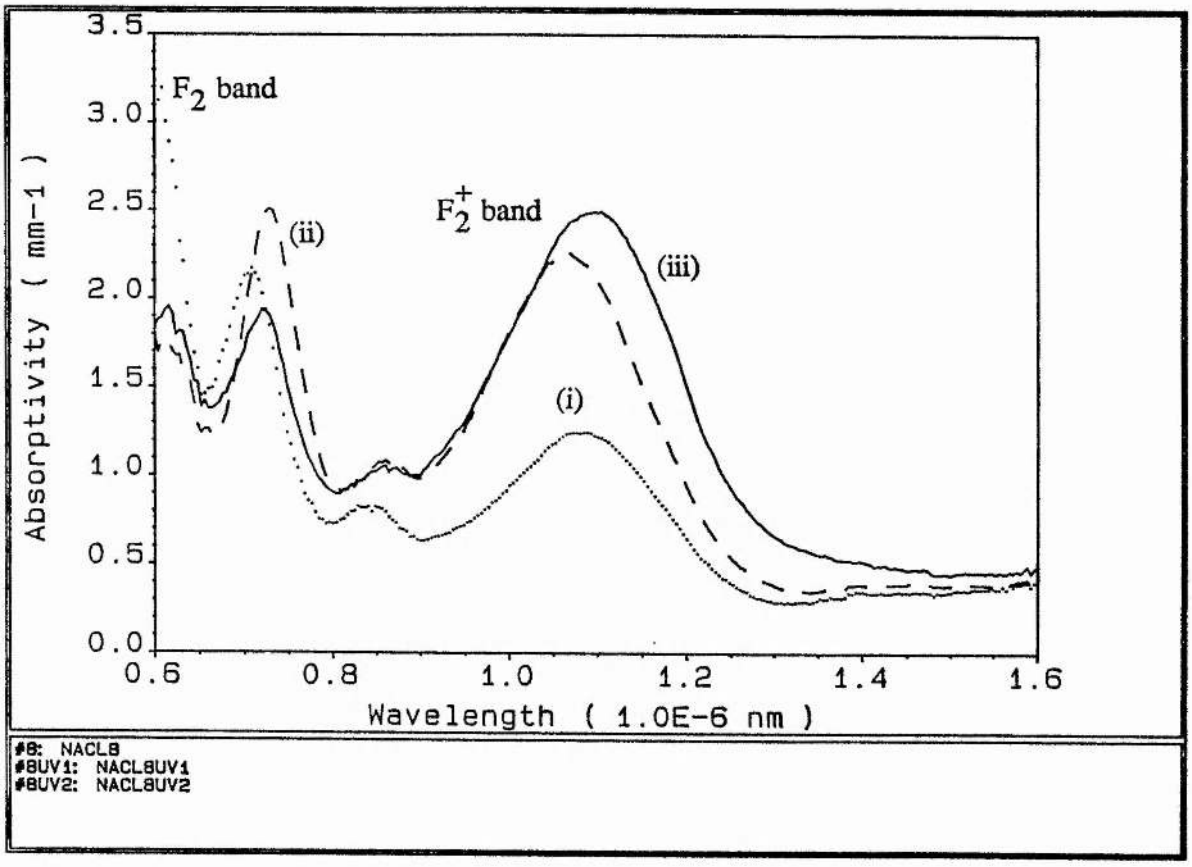

Figure 8.2 Absorption profiles of a home produced laser active NaCl:OH^- crystal after (i) Additive colouration, (ii) illumination with F-band light at room temperature and (iii) as for (ii) but at 77K

The laser output characteristics of this particular crystal are presented later within this chapter. During the development stage of our crystal processing technique the absorption profile of a known laser active crystal which was obtained from another research group [4] was used as a "bench mark". For comparative purposes the absorption profiles of this crystal and those of two crystals produced in this work are presented in figure 8.3.

Prepared crystals which were stored for long periods (months) in the dark at 77K showed no deterioration in output performance when removed from storage conditions and located within the laser cryostat.

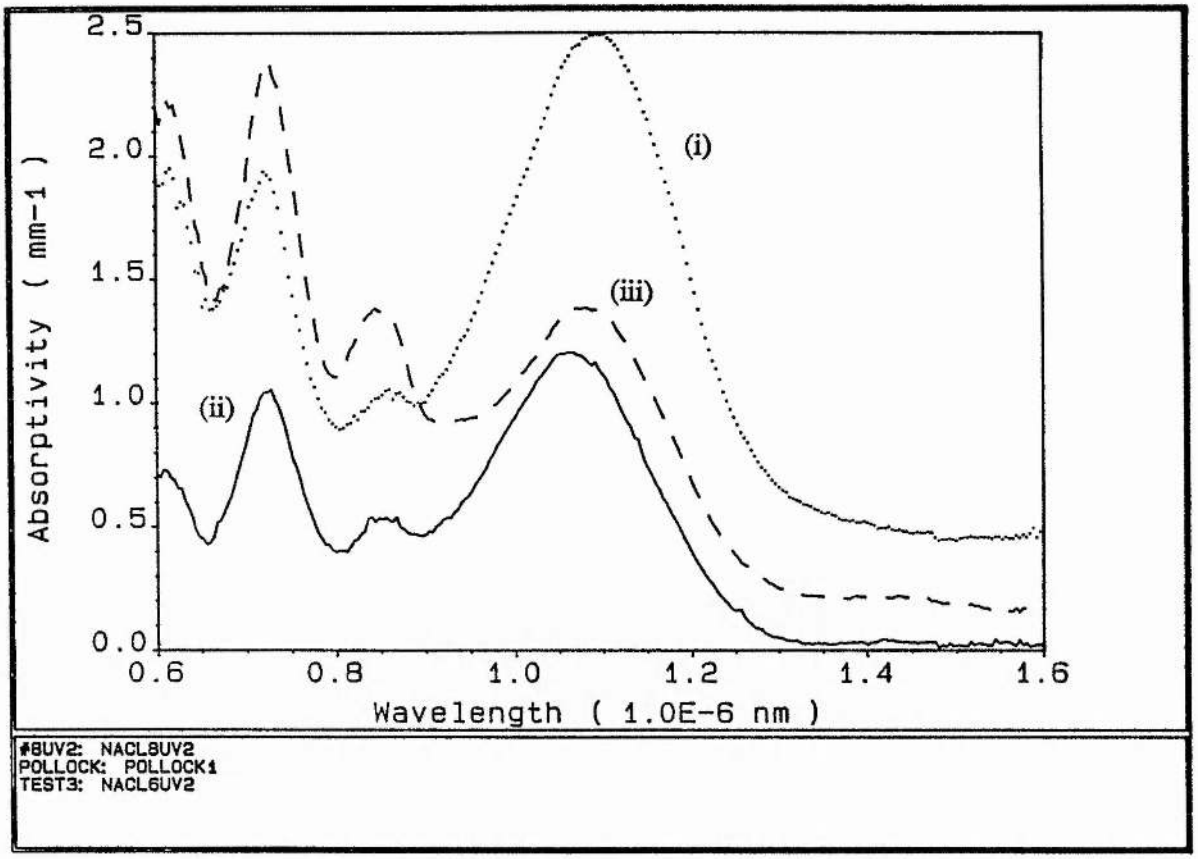

Figure 8.3 Absorption profiles of three NaCl:OH⁻ crystals (i) Home produced (Laser action observed), (ii) Home produced (Laser action not observed), Laser crystal obtained from reference 4.

It was not necessary to store coloured crystals at cryogenic temperatures because storage in the dark is adequate for indefinite periods [4-6]. Crystals were in fact stored under cryogenic conditions as such a facility was conveniently at hand within which all other colour-centre crystals used within this laboratory were stored. Storage of the coloured crystals at room temperature under non-darkened conditions leads to degradation of the laser active centres within several days [4] and this is indicated by a change of colour in the crystal from olive green to dark blue. For this reason loading of the coloured crystal into the laser cryostat was carried out under filtered red light conditions.

8.3 Characterisation of the NaCl:OH^- colour-centre laser

To obtain the best performance from the stabilised NaCl:OH^- colour-centre laser it is important that reorientation of laser active centres to states orthogonal to the pump beam polarisation be minimised [2,6,7]. This reorientation arises mainly from excited-state absorption effects. The mechanism by which this process occurs has not as yet been fully confirmed. It is thought that excitation of the centres by an intense optical pump beam can lead to two-photon absorption from the $2p\sigma_u \rightarrow 3d\pi_g$ states to occur. On subsequent relaxation back to the $2p\sigma_u$ state it is believed that some reorientation of the centres takes place (see figure 2.8). It is also thought [4] that a contribution to centre reorientation arises by way of the radiationless transition $2p\pi_u \rightarrow 2p\sigma_u$. In general, however, if the ionic nature of the host crystals are considered it may then be perceived that reorientation of colour-centres may occur due to lattice "breathing" which occurs as a direct consequence of the four level process that takes place during the optical pumping cycle. Also, as mentioned earlier in chapter 2, there are six possible axes along which the F_2^+ colour centre can be located within the crystal lattice (see figure 2.6) and therefore it is possible that upon relaxation to the ground state that one of these orientations may be occupied.

These two detrimental processes may be overcome by pumping the NaCl:OH^- crystal with circularly polarised pump light together with a secondary auxiliary light source [2,6-8]. The vertical and horizontal components of the circular polarised pump source maintains a dynamic equilibrium between the two orthogonally polarised centres and therefore leads to constant output level being maintained. The role of the auxiliary illumination is to pump the misaligned centres to the $2p\pi_u$ level, or higher, whereupon a nonradiative decay to the $2p\pi_u$ level occurs without reorientation of the centres. Throughout the work described here the auxiliary illumination was obtained by frequency-doubling a portion of the Nd:YAG pump laser beam (1060nm→532nm) which caused excitation from the $2p\sigma_u \rightarrow 3d\sigma_g$ transition to occur and this had the practical convenience that a secondary independent light source was not required.

The experimental set-up for the NaCl:OH^- laser is illustrated in figure 8.4. As with the LiF:F_2^+ colour centre laser, described in chapter 4, the 2mm thick NaCl:OH^- crystal was mounted at Brewster's angle within the redesigned cryostat described in chapter 6. A simple (3 mirror) folded astigmatically-compensated standing-wave cavity was constructed using readily available optics designed for a KCl:Tl colour-centre laser for which the tuning range (≈1.4-1.56μm) is incorporated by that of the NaCl:OH^- colour-centre laser (≈1.4-1.8μm). Mirror M_1, which was ≈100% reflecting over the 1.4-1.65μm spectral range and whose radius of curvature was 5cm, and mirror M_2, whose reflectivity profile was similar to that of M_1, 10cm radius of curvature, provided the necessary pump power density within the gain medium.

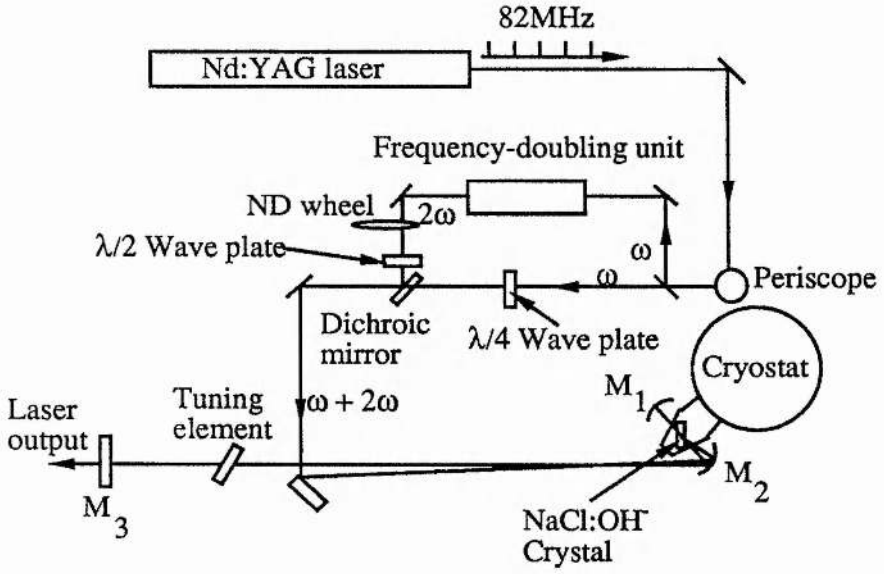

Figure 8.4 The experimental set-up for the NaCl:OH^- colour-centre laser

M_2 also acted as a focussing mirror for the 1.06μm Nd:YAG pump laser beam, this being achieved by the deposition of a double-stack dielectric sequence with the colour-centre laser reflecting stack being deposited on top. The output coupler M_3 was either a 12% or 22% transmitting mirror with similar reflectivity profiles to that of mirrors M_1 and M_2.

As already mentioned, the homogeneously broadened absorption band of the NaCl:OH^- colour-centre crystal may be pumped by a Nd:YAG laser and in this work a series 500 Nd:YAG Control laser was used. To obtain the peak powers required to achieve suitable auxiliary light intensities from the KTP frequency doubling crystal it was necessary to acousto-optically modelock the pump laser. Pump pulse durations were typically ≈100-120ps and had repetition rates of ≈ 82MHz. The maximum (average) output power delivered from the pump laser was ≈9W of which 30% was directed to the doubling crystal using a suitable beamsplitter. The cavity length of the colour-centre was deliberately mismatcthed with that of the pump laser in order to avoid synchronous modelocking conditions occurring such that the cw output characteristics of the laser could be retained. The relatively long lived upper state life time of the NaCl:OH^- laser (≈150ns) ensured that a cw output was obtained under these pumping conditions.

To ensure the most favourable operating conditions the auxiliary and pump beam polarisations, together with the type of auxiliary illumination used, were characterised and the data relevant are summarised in Table 8.1. In each case the Nd:YAG pump power was 3W and the output coupling was 12%. It can be seen from the data in Table 8.1 that a 250mW output was obtained when the combination of circular pump polarisation and the UV output of a 100W mercury arc lamp was used. This was due to the high auxiliary power incident upon the colour-centre crystal because the output power of the NaCl:OH^- is actually dependent upon the power of the auxiliary illumination. There is an associated saturation behaviour as may be seen in figure 8.5 for circularly polarised Nd:YAG laser pump and horizontally polarised and frequency-doubled Nd:YAG laser illuminations. The best operating conditions were therefore observed when the Nd:YAG pump beam polarisation was circular and the auxiliary polarisation (frequency-doubled Nd:YAG) was horizontal. This scheme where 80mW of 532nm illumination was available was as effective as that involving the UV illumination from the 100W mercury arc lamp. In addition the use of such a high output power UV source was considered to be hazardous and inconvenient

in the laboratory and thus the frequency-doubled source of auxiliary illumination was preferred and employed.

Nd:YAG pump polarisation	Auxiliary illumination	$NaCl:OH^{2-}$ laser output
Horizontal	80mW of 532nm	Initially 200mW but faded after several minutes
Circular	80mW of 532nm	200mW constant output
Horizontal	≈100W mercury arc lamp	Initially 250mW but faded after several minutes
Circular	≈100W mercury arc lamp	250mW constant output
Horizontal	none	100mW but quickly faded
Circular	none	200mW but quickly faded

Table 8.1 Characterisation of the pump polarisation and auxiliary illumination

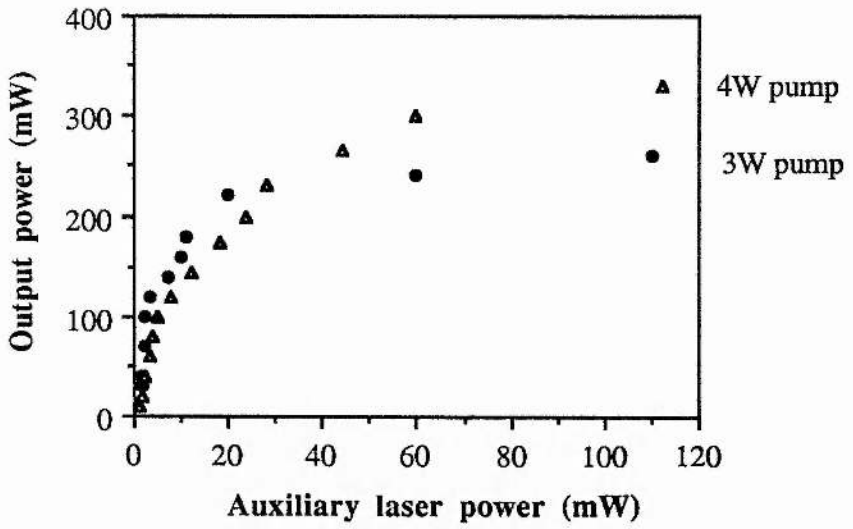

Figure 8.5 The $NaCl:OH^-$ colour-centre output power characteristics as a function of the auxiliary input laser power.(22% output coupling)

The tuning power curve for the laser which was obtained with prism-tuning is presented in figure 8.6.

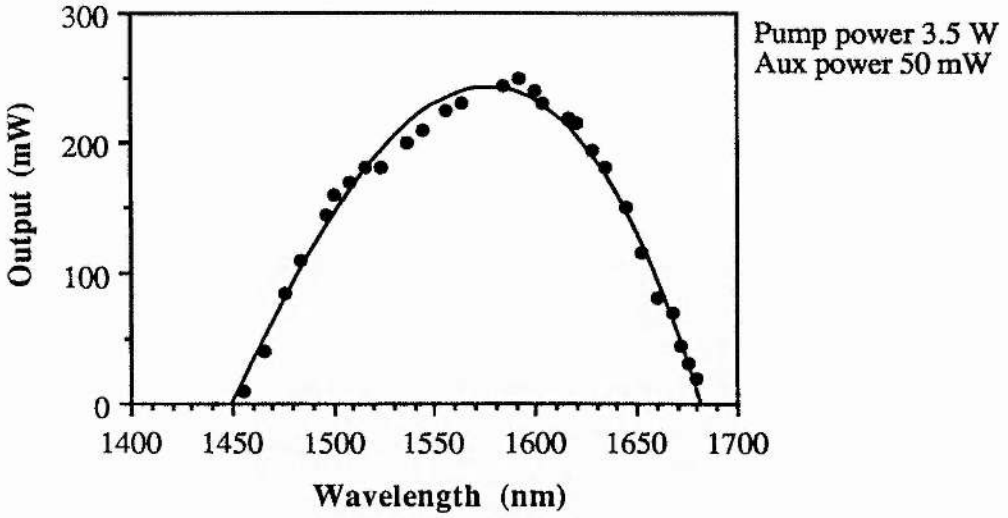

Figure 8.6 The power tuning curve for the NaCl:OH⁻ colour-centre laser

It can be seen from this figure that the long wavelength operation ceases at approximately 1.68μm and not at 1.75μm as reported elsewhere [7]. This is due to the non availability of the necessary broadband reflecting dielectric mirror sequences required for this laser. The input-output power relationship for the NaCl:OH⁻ colour-centre laser was obtained for 12% and 22% output coupling and slope efficiencies of 7% and 12% were obtained respectively (figure 8.7) and which compare favourably with data presented elsewhere [9].

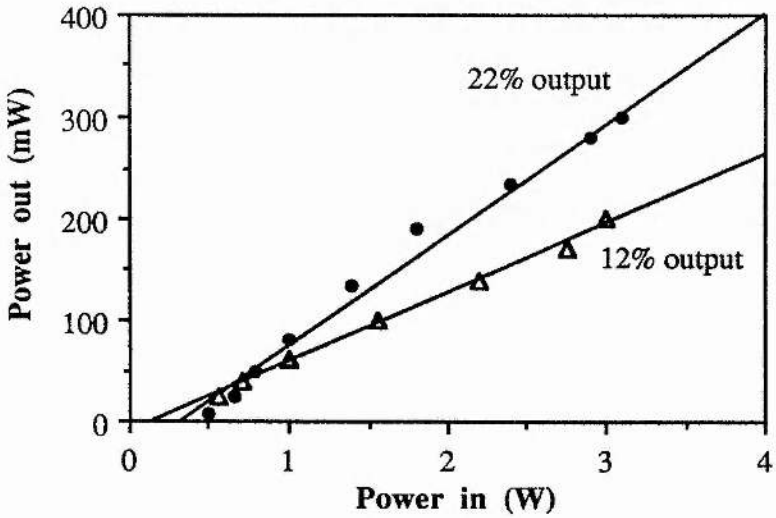

Figure 8.7 The input power versus output power characteristics for the NaCl:OH⁻ colour centre laser

8.4 Summary

Within this chapter it has been confirmed that stable NaCl:OH^- colour-centre gain media can be reliably produced within this laboratory. The extended tuning range of this media over the KCl:Tl colour centre-laser combined with the high stability of the F_2^+:O^{2-} centre, which enable much higher output powers to be achieved, make this a preferred source of infrared radiation covering the important 1.4-1.8μm region of the spectrum.

Chapter 8. References

1. C.R.Pollock, J.F.Pinto, E.Georgiou; Appl.Phys.B. **48**, 287 (1989)

2. J.F.Pinto, L.W.Stratton, C.R.Pollock; Opt.Lett. **10**, 384 (1985)

3. Nacl crystal boule doped with $\approx 5 \times 10^{-4}$ NaOH obtained from Professor Rosenberger, Dept. of Physics, University of Utah

4. E.Georgiou, J.F.Pinto, C.R.Pollock; Phys.Rev.B. **35**, 7636 (1986)

5. C.R.Pollock; J.Lum. **35**, 65 (1986)

6. K.R.German, C.R.Pollock; Opt.Lett.**12**, 474 (1987)

7. R.Beigang, K.Klameth, B.Becker, Z.Yoon, H.Welling; Opt.Commun. 65, 383 (1988)

8. J.F.Pinto, E.Georgiou, C.R.Pollock; Opt.Lett. **11**, 519 (1986)

9. G.Phillips, P.Hinske, W.Demtroder, K.Mollmann, R.Beigang; Appl.Phys.B. **47**, 127 (1988)

CHAPTER 9

Electroluminescence Studies of Alkali Halide Crystals

9.1 Introduction

Since the demonstration of the first optically pumped colour-centre laser in 1965 [1] which took the form of a flashlamp pumped rod containing F_A(II) centres, the diversity of laser active colour centres and the magnitude of the tuning range available from such lasers has increased enormously [2]. More recently it has been shown that the large tuning range which extends from 0.8 - 4.0 μm when such centres are hosted within the alkali halides, can in fact be extended into the ultraviolet region of the spectrum when such colour-centre host materials are directly excited by electrical means [3,4]. In this chapter the aim is to present a study of electroluminescence from some alkali halide crystals.

9.2 Sample Preparation

The alkali halide crystal samples used throughout this part of the project were obtained from the British Drug House [5]. Samples for electroluminescence studies were prepared from large 10 x 10 x 250 mm crystals of KI, KCl, NaCl, CsI, CsI(Na), CsI(Tl). Electroluminescence is observed from the alkali halides under the application of a transient electric field where the required magnitude is of the order of 10^4-10^5 Vcm^{-1}. To achieve these large electric fields without having to use very high voltage sources thin crystal samples with thicknesses ≈ 100-150μm were therefore prepared. This also had the advantage that Paschen ionization effects were reduced. To prepare an alkali halide crystal sample for electroluminescence studies the following sequence of procedures was undertaken.

The freshly obtained 10x10x250 mm crystal was placed upon a clean metallic surface and a clean sharp blade aligned along the appropriate cleavage plane, in this case this was perpendicular to the crystal length axis. It is found that the crystals cleave easily and cleanly when cleaved in halves. Cleaving is carried out by simply tapping a metal blade firmly with a suitable weight or hammer and the cleaving by halves process was continued until thin 0.5 - 1.0 mm crystal slices are obtained as illustrated in figure 9.1. A freshly cleaved crystal is then mounted onto a polishing die, (see figure 9.1), using a suitable adhesive (Crystal Bond 509). The crystal was then ground on a flat glass plate to a thickness of approximately 200-300μm using a coarse grained 600 grade SiC abrasive powder mixed with oil to constitute a smooth slurry. The oil used was Engis polishing fluid.

When this thickness was reached the crystal was removed from the polishing die and its surfaces thoroughly cleaned using acetone (Crystal Bond 509 dissolves in acetone). The crystal was then replaced upon the polishing die, which was also thoroughly cleaned of 600 grade SiC powder to avoid the formation of "potholes" in the crystal surfaces when polishing was resumed with finer grades of powder. Further thinning and fine polishing was carried out to obtain thicknesses of approximately 100 - 150μm using a fine 1200 grade SiC oil slurry mixture which began to produce a mild sheen on the crystal surface. The crystal was then removed from the polishing die and cleaned as before. Final polishing of the surface is carried out by hand using a 3μm diamond polishing paste or a fine TiO powder with ethanol on a soft cloth stretched over a flat glass plate. The crystal was then cleaned with ethanol and its thickness measured and surfaces inspected using a microscope equipped with a suitably calibrated graticule. Once a satisfactory thickness and surface finish was achieved the edges of the crystal were then inspected and cleaved while viewed under the microscope. This ensures that good optical quality crystal edges were available so that optical feedback could be introduced to the crystal. It was necessary to cleave the crystal edges for this purpose because they tend to become tapered and damaged during the polishing process.

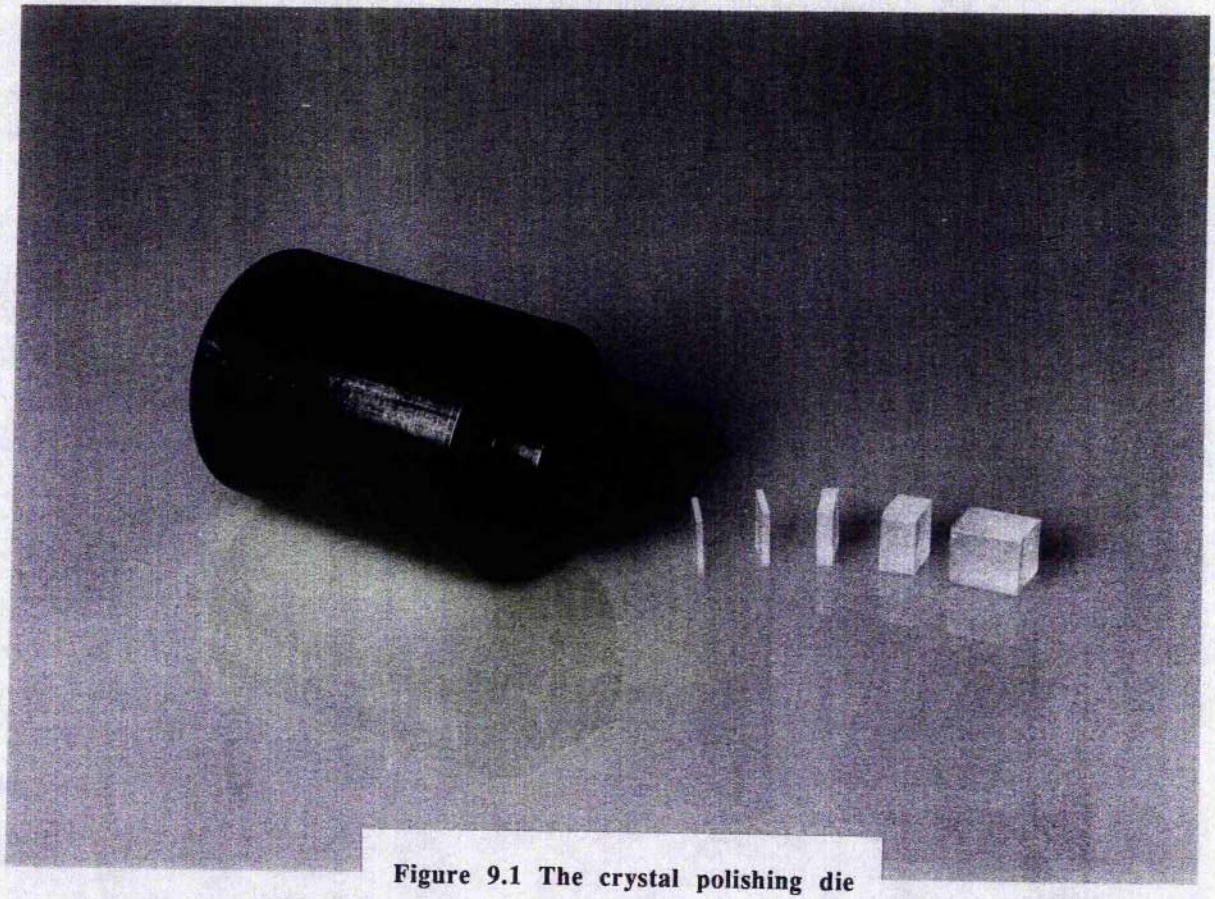

Figure 9.1 The crystal polishing die

9.3 Contact Schemes and Characterisation

Several types of electrical contacting schemes onto the alkali halide samples have been produced and their performance characteristics obtained in order to assess the most favourable and reliable metal-insulator contact. The aim was to reach the target current density of $\approx 19 Acm^{-2}$ in the quest to obtain laser action by this novel pumping mechanism within these crystals [4]. In all, five types of electrical contacting schemes were assessed and relevant details for each will be presented and discussed.

It was decided that an Ohmic contact should be produced on the alkali halide crystal surface because this offered the most favourable chance of achieving the necessarily high threshold current density. Accordingly materials for such a contact were chosen with relatively low work functions. The first contact that was constructed and assessed was a simple spring loaded stainless steel point contact made directly onto the sample under test. The experimental arrangement to obtain current voltage relationships consisted of a dc high voltage power supply (Brandenburg, model Alpha series II) and a Keithley 615 digital electrometer as illustrated below in figure 9.2. The sample under test was mounted within a purpose-built test cell inside which was placed within an inhouse-designed cryostat cold finger arrangement (see section 9.4.2 for details).

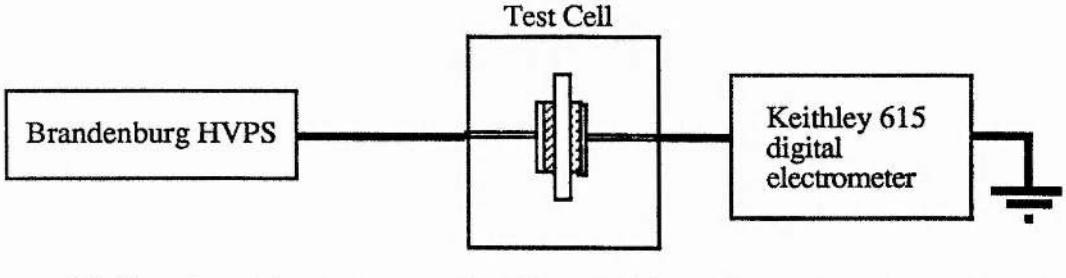

Figure 9.2 Experimental arrangement for characterising the metal-insulator contacts

The current-voltage curve for this simple contact is presented in figure 9.3a. It may be seen from these data that for a potential difference of approximately 2kV supplied to the sample

via this contact that a current of just 90nA was obtained. The data obtained for the other contacting schemes upon KI were also obtained using the experimental arrangement mentioned above are also presented in figure 9.3a and schematic representations of these schemes are shown in figure 9.4.

The second type of contact tested was constructed by melting a small bead of indium onto the crystal surface within a dry nitrogen environment. The surface of the indium was freshly scraped with a clean scalpel blade to remove any oxide layer that may have formed and the indium bead plus a small clean weight, which ensured that it the indium adhered to the crystal surface when molten, were placed upon the crystal surface Once prepared the sample was mounted within the test cell and the electric field supplied via the indium contacts by way of spring loaded copper contacts. From the current-voltage curve for this contact, which is also presented in figure 9.3a, for a KI crystal it may be seen that that its characteristics are very similar to that produced for the direct contact. However, it was found that the indium bead tended not to adhere securely to the crystal surface and that during the construction process it was difficult to shape the contact.

The third metal-insulator contacting scheme as illustrated in figure 9.4c was made by evaporating a 6mm diameter film of aluminium onto the surfaces of the sample and again the applied voltage was supplied to the contact via a spring loaded copper contact. It may be seen from the current-voltage characteristic curve for this contact (presented in figure 9.3a) that for a potential difference of 2kV a current of $\approx$ 120nA flows through the alkali halide (KI) sample. A similar contact was also constructed where the voltage was fed to the aluminium film by a thin wire held permanently onto the contact by silver-loaded epoxy covered with a protective layer of araldite adhesive. As expected it was found that the I-V characteristic for this permanent contact did not differ from that of the aluminium film and pressure contact. However, in some cases it was desirable to construct a permanent contact such as this because it constituted a more durable and robust contact than that of the rather fragile pressure contact.

From scientific data tables it may be found that the work function ψ_m for aluminium is 4.2eV and for indium ψ_m is 4.12eV and thus it was assumed that these metals would produce Ohmic contacts onto a KI crystal which has a work function of 7.3eV (assuming a relatively low trap density [4,6]). Significantly, however, the I-V characterisation curves presented in this section imply that space charge limited currents are not in evidence and thus it can be assumed that the contacts constructed are of the blocking type. These observations were also made by Boyd et al [4] but they found that contacts of this nature could be converted to Ohmic types by first applying a large electrical pulse onto the contact. In an effort to duplicate this finding a high voltage pulse generator was connected to the crystal samples and a 7kV pulse of 100ns duration applied. Following this treatment reinvestigation of the I-V characteristics for such contacting schemes showed that no significant change in the I-V characteristics had been produced.

It was then decided to construct a very low work function metal contact onto a crystal sample in an attempt to obtain an improvement in the characteristics hitherto observed. Such a scheme is illustrated in figure 9.4e and consisted of a sodium-potassium amalgum being constructed on the sample surface (ψ_m(Na)=2.75eV, ψ_m(K)=2.3eV). The contact was constructed by glueing a 4mm internal diameter glass tube onto the surface of the crystal into which the amalgam was injected with a syringe. This was done as rapidly as possible because an oxide layer tended to form quickly upon the surface of this amalgum. The amalgum was prepared on a hot plate and a contact wire was inserted into the Na-K mixture before the tube was sealed with an epoxy glue. Once prepared the contact current-voltage characteristic was investigated and the data are reproduced in figure 9.3a. As may be seen from these data, which represent the best set of data obtained for several similar contacts on a range of crystal samples, the I-V curves show no improvement on previously described characteristics. In fact they are not as good as those obtained for aluminium contacts. The relatively poor performance of the NaK amalgum contacts is thought to be attributable to the unavoidable formation of an oxide layer between the crystal surface and the amalgum layer.

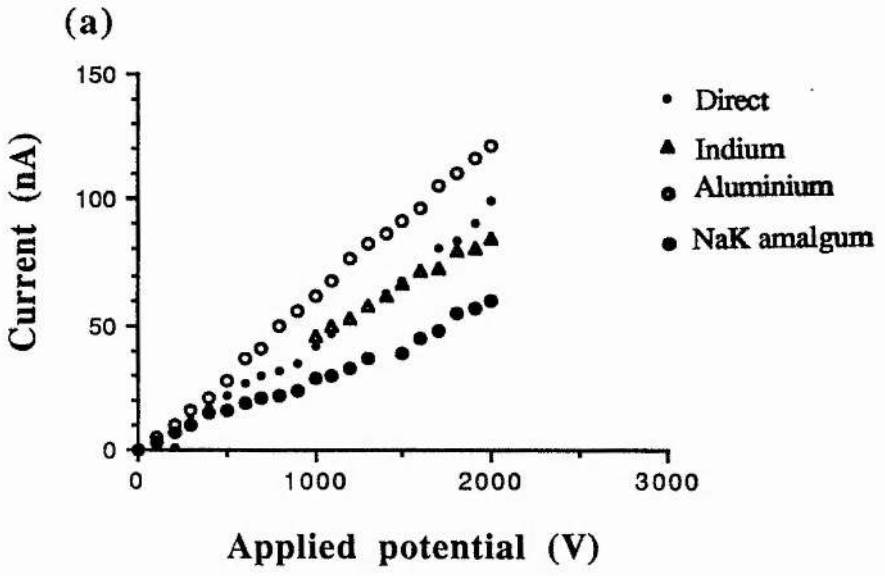

Figure 9.3a Current-voltage characteristics for several contacting schemes for KI crystal samples

Similar metal-insulator contacts to those described here were formed on NaCl and CsI samples and were found to be markedly less efficient in injecting current into the insulator. Data are presented in figure 9.3b for an evaporated aluminium contact only on NaCl and CsI samples and this scheme was again found to produce the best current injection characteristics.

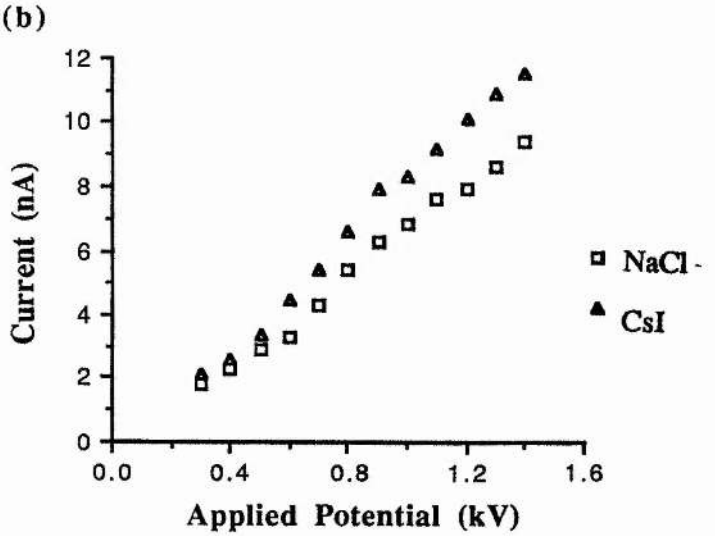

Figure 9.3b Current-voltage characteristics for CsI and NaCl crystals with evaporated aluminium contacts

Due to the slightly more favourable performance characteristics and also due to its relative robustness and comparative ease for construction it was decided to use evaporated aluminium contacts. Some studies were also carried out using the alternative contact schemes for the purposes of comparison.

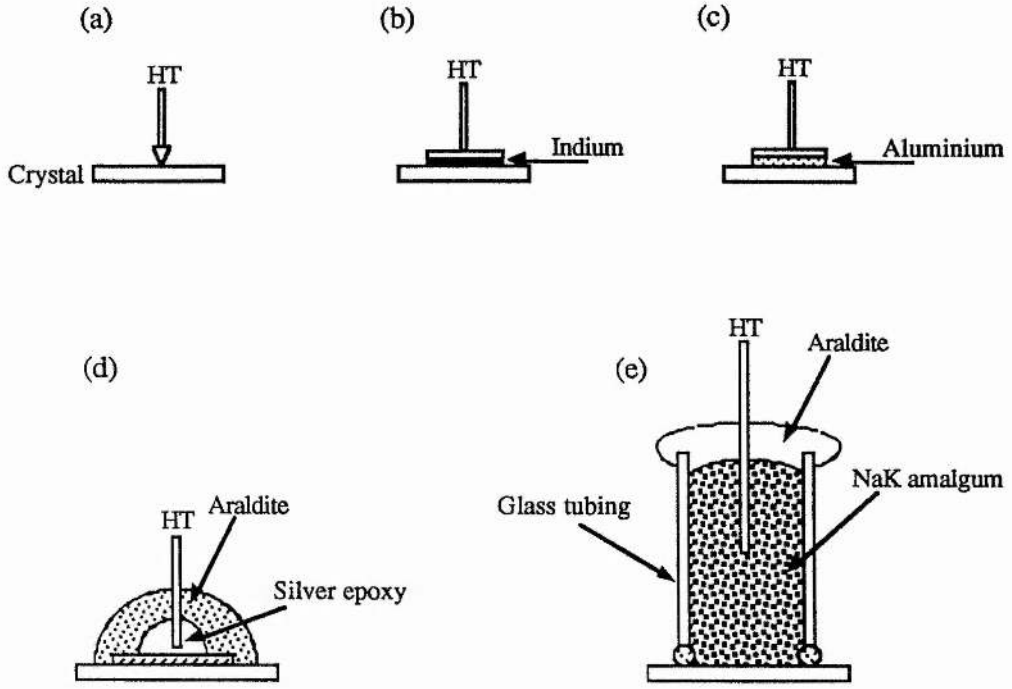

Figure 9.4 Schematic diagrams to illustrate the contact schemes that were carried out for the crystal samples; (a) direct stainless steel point (b) copper pressure contact onto indium (c) copper pressure contact on aluminium (d) permanent aluminium contact (e) Na-K amalgam

9.4 Electroluminescence from Alkali Halides

9.4.1 Introduction

Within this section experimental observations of electroluminescence from alkali halide crystals will be presented and discussed. Initial observations were obtained from a simple purpose-built cryostat which was constructed at the Royal Armaments Research and Defence Establishment (RARDE) and is referred to here as the RARDE cryostat. The luminescence signal was detected on an axis perpendicular to the applied electric field using a calibrated EMI 10-stage (linear focussed) fast response bialkali photomultiplier tube (PMT) having a spectral response ranging from 200-650nm. Each crystal contacting scheme was assessed using the RARDE cryostat and the crystal type and contacting scheme

which produced the most efficient electroluminescence was selected for further investigations. Also a simple standing-wave resonator cavity was designed which incorporated an electrical pumping chamber which could be attached onto the purpose-built laser cryostat described in chapter 6.

9.4.2 Experimental observations of Electroluminescence

All experimental observations of electroluminescence from the alkali halide crystals studied were carried out with the crystal sample housed within a suitably designed vacuum cryostat. This permitted electroluminescence to be observed at 77K where the luminescence efficiency of the self-trapped exciton within these materials is high [7,8]. Initial investigations were carried out using the RARDE cryostat which is illustrated in figure 9.5 together with the crystal cold finger and mounting jig. There are three observation ports on this cryostat each having a suprasil II window which allows transmission over the ultraviolet region of interest studied here and electrical access to the crystal was facilitated by means of a hermetically sealed high voltage BNC connector. The cold finger was mounted directly onto the base of the liquid nitrogen reservoir and the crystal temperature monitored by a platinum resistance thermometer. The cold finger, constructed from copper, comprised two parts, a base plate which is directly mounted onto the stainless cryostat with good thermal contact being ensured by a thin layer of cryocon grease, and the crystal mounting block which was allowed to rotate within the base plate for positioning of the crystal and be removed entirely if necessary for cleaning purposes. The cryostat and the cold finger were both electrically earthed and complete the electrical circuit for the crystal sample. The crystal mounting block dimensions were chosen such that it fits into the crystal polishing die to enable the contacting surface to be polished clean and flat as this prevented damage to the crystal surface and also ensured a good electrical contact. The upper contact to the crystal was housed within a stable cradle constructed from nylon or P.T.F.E which was mounted onto cold finger base plate and allows a versatile range of contacting schemes to be investigated.

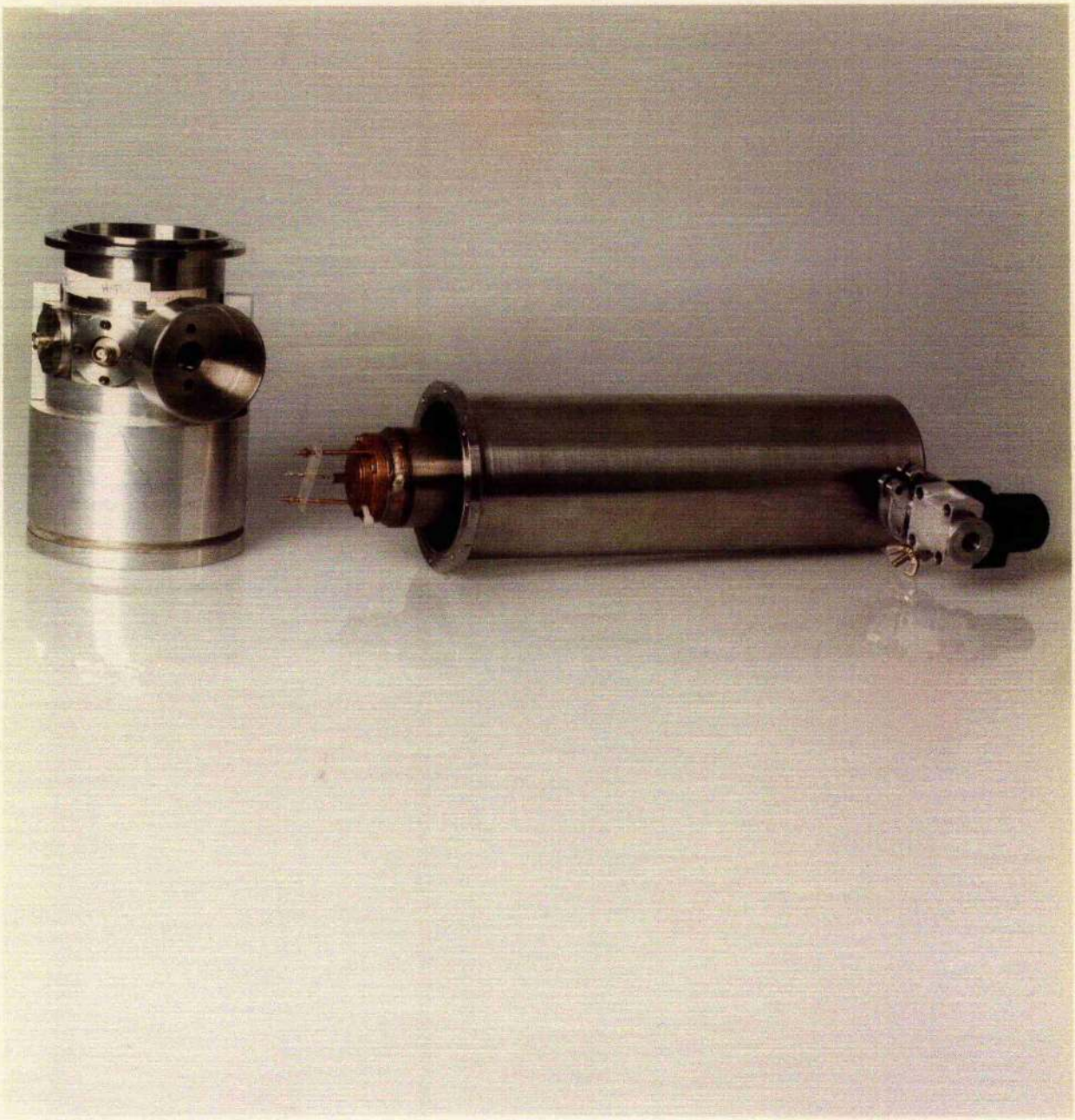

Figure 9.5 The RARDE Cryostat

Electrical contacts onto the crystal samples were initially made by evaporating a thin 6mm diameter film of aluminium onto each of the 10mm square crystal surfaces which ensured that no electrical arcing occurred between each contact along the crystal edges. Once prepared a crystal was placed within the RARDE cryostat and cooled to 77K in a vacuum enclosure at a pressure of 10^{-6} Torr. The typical crystal mounting arrangement is illustrated in figure 9.6.

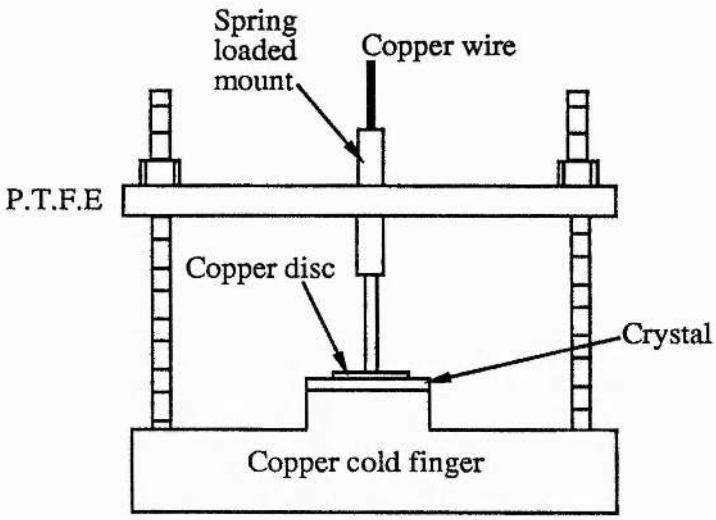

Figure 9.6 Schematic diagram illustrating the crystal mounting scheme used for the majority of electroluminescence observations.

The excitation signal was provided from a signal generator whose 16V output was transformed up to a maximum output of 5kV by a series of transformers and the voltage waveform monitored using a Tektronix P6015 high voltage probe. Thus the output brightness waveform and voltage profiles could be directly compared. All emission spectra were obtained using a Photophysics F/3.4 grating monochromator and the output signal from the PMT was detected by a lock-in amplifier (EG&G 5209) having a reference signal provided by the signal generator. In most cases one side of the crystal (cold finger side) was insulated from the second contact by a thin sheet of mylar. This prevented the high voltage taking a low resistance path to ground in the event of the crystal cracking due to electrical breakdown. Under high field conditions this was a relatively common occurrence

after several hours of operating time and was attributed to weakening of the crystal lattice along dislocation lines and other imperfections [9]. As will be described later within this chapter, electrons were injected into the sample from one contact only and typical electroluminescence output intensity profiles obtained at 77K for this type of contact scheme are presented in figure 9.7. It is clearly evident from each of these profiles that the luminescence signal leads the excitation signal and that the intensity associated with the negative-and positive-gradient voltages were different. For the CsI samples this effect was more pronounced than that observed from KI samples where the intensity of each are similar in magnitude.

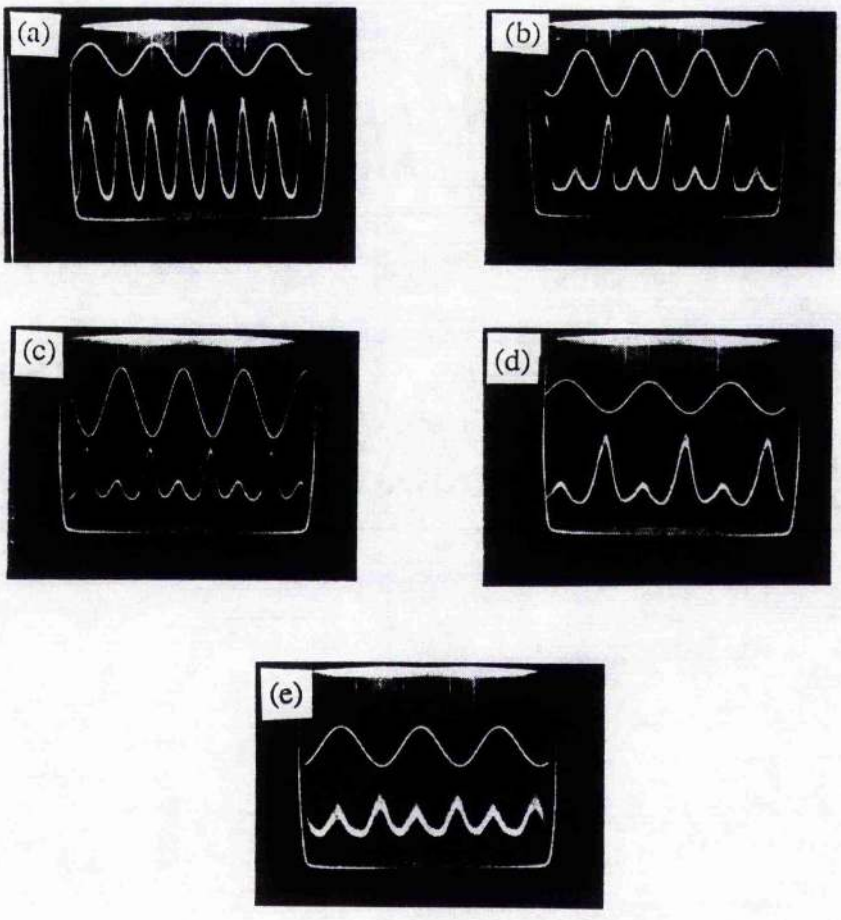

Figure 9.7 Output electroluminescence profiles for (a) KI (b) CsI (c) CsI:Na (d)CsI:Tl (e) NaCl

The intensity of the output luminescence as a function of the externally applied field E for the samples mentioned are presented in figure 9.8. In each case an exponential curve has been fitted to the data points. The KI crystal produced the most intense light output for an equivalent electric field strength (E) and this was deemed to be the most efficient material of all the those tested. Reports from other workers are consistent with this conclusion [4,8]. On this basis therefore, it was decided to concentrate most of the further electroluminescence studies upon this material, although data for other materials will be presented and compared where appropriate.

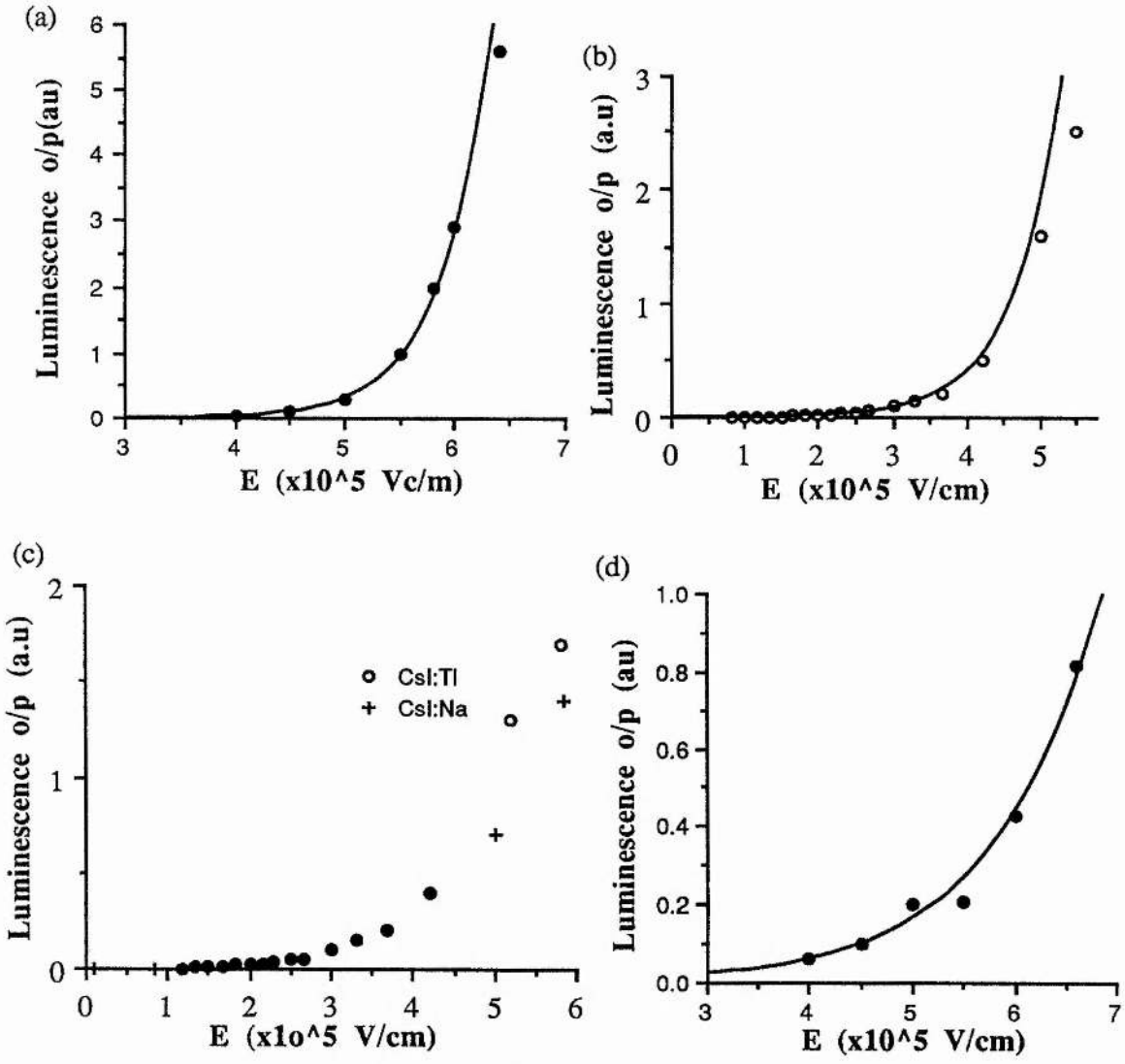

Figure 9.8 Luminescence output intensity as a function of the externally applied field E for (a) KI, (b) CsI, (c) CsI:Tl and CsI:Na, (d) NaCl

The electroluminescent spectra for the samples mentioned are reproduced in figure 9.9 and may be compared with those obtained by other workers [3,7,8].

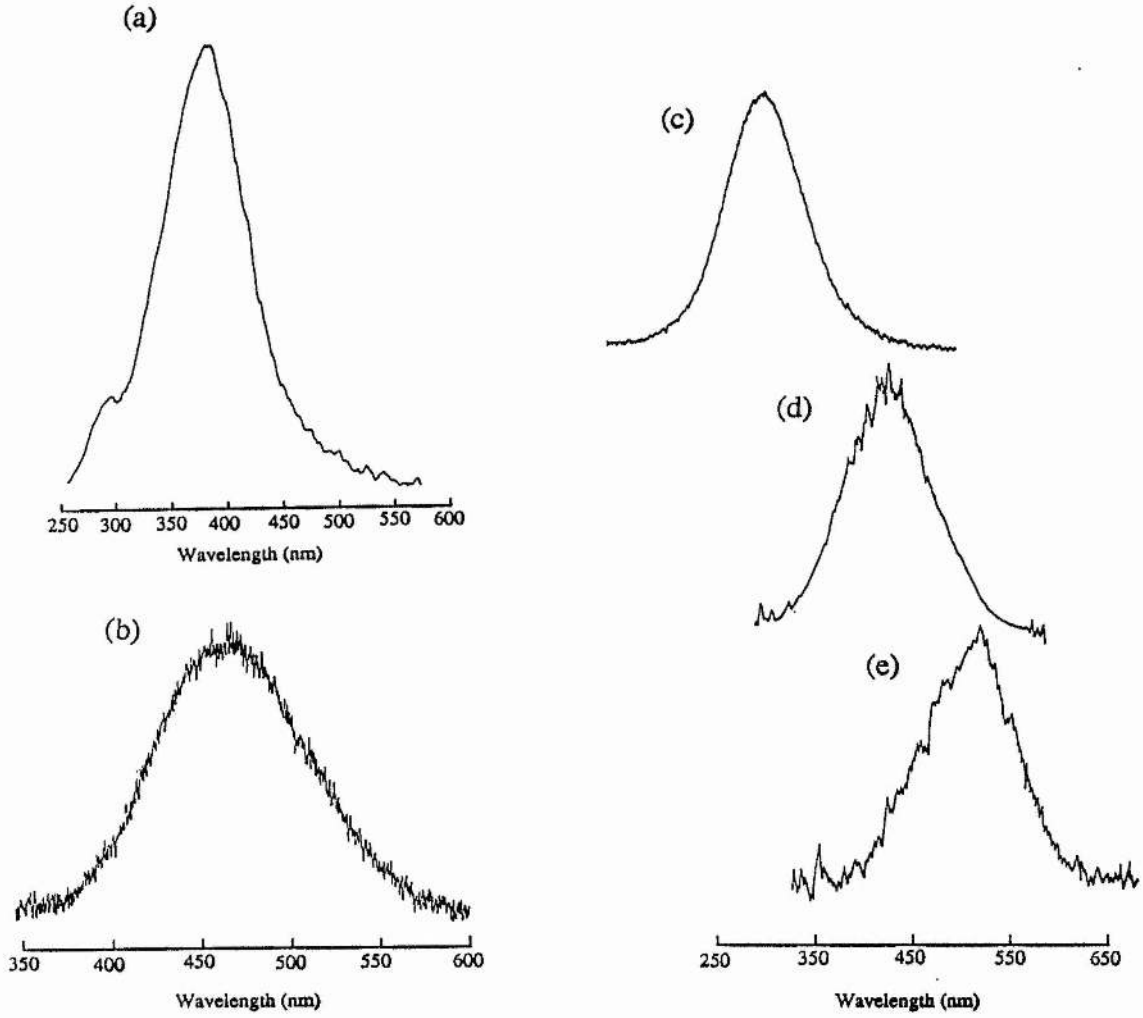

Figure 9.9 Electroluminescence spectra for (a) KI (b) NaCl (c) CsI (d) CsI:Na (e) CsI:Tl

The spectrum obtained for each sample investigated here is attributable to that of the self-trapped exciton. Two peaks are evident from the KI spectrum and they are associated with a longer lived (μs) triplet band centred at 375nm and a shorter lived (ns) band centred at 297nm [4,8,10]. It may also be observed from the spectral data that the presence of dopants within the alkali halide lattice produces a shift on the emission peak towards the red end of the spectrum which increases with increasing size of impurity ion.

The electroluminesence output intensity was also investigated as a function of the excitation frequency and it was observed that the build up of space charge within the crystal lattice plays a dominant role in determining the output intensities.To study the intensity-frequency relationship a square wave high voltage source was used in order that any effect related with the variation of $\frac{dV}{dt}$ be avoided. Such a high voltage excitation source was constructed using a thyristor switch gated by a square wave signal generator which produced up to 2kV pulses over a frequency range from 1Hz-40kHz. The circuit diagram is shown in figure 9.10. An RC network on the output of the thyristor circuit enabled the risetime of the square wave pulses to be varied from several nanoseconds to microseconds which enabled the luminescence output also to be examined as function of the excitation pulse risetime. As before, the crystal with aluminium contacts formed on both surfaces was mounted within the RARDE cryostat and in this case both contacts were connected to the supply source.

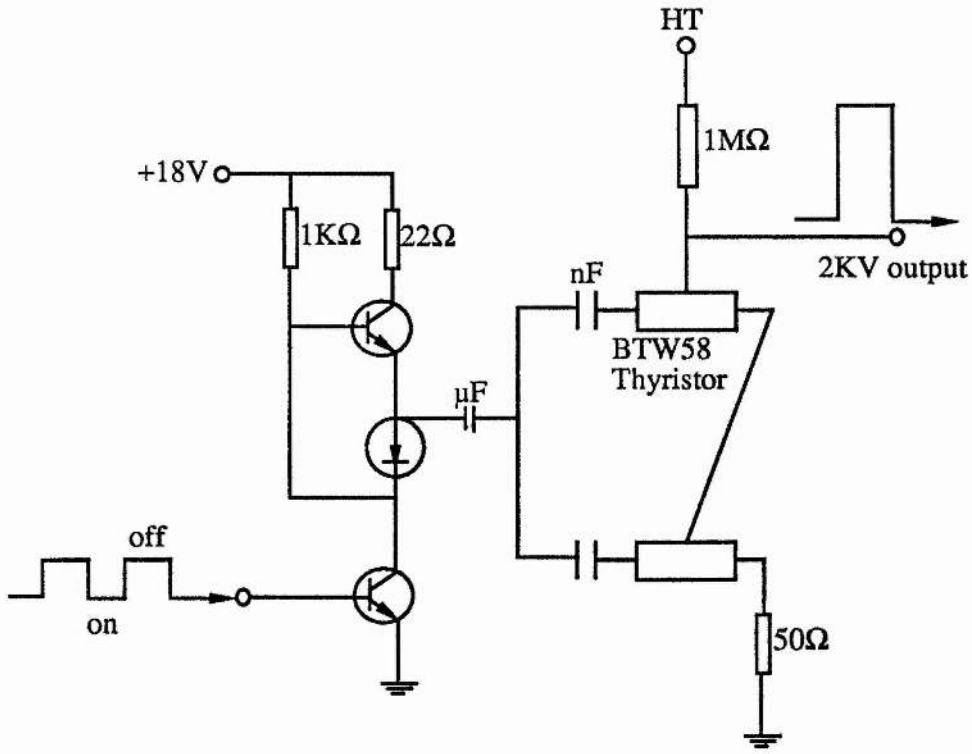

Figure 9.10 High voltage pulsed circuit designed for investigation of dV/dt upon the luminescence signal

Four oscillograms illustrating the variation of the electroluminescence intensity with $\frac{dV}{dt}$ are included as figure 9.11 and this is also presented graphically in figure 9.12.

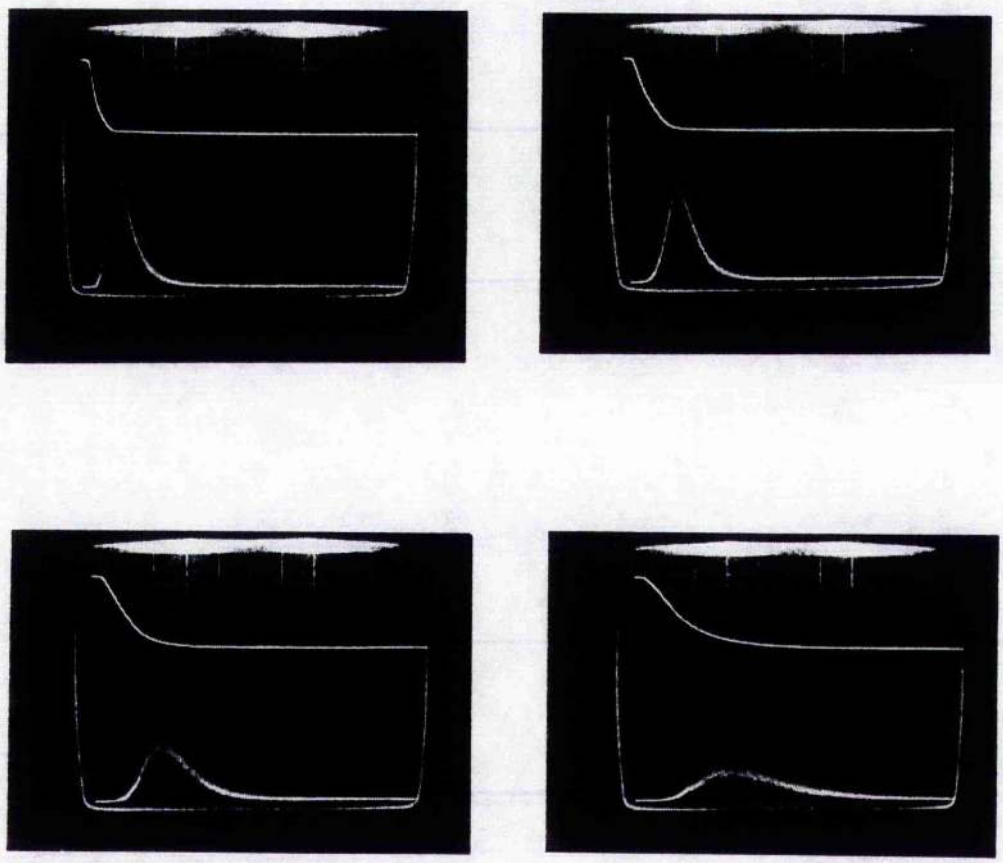

Figure 9.11 Output electroluminescence (lower trace) from a CsI crystal (150μm thick) as a function of the excitation field risetime (upper trace). (All photographs; Timescale 2μs/div, Potential difference 500V/div)

The sample used for this experiment was a CsI crystal polished to a thickness of 150μm. Data were obtained by exciting the sample for only a few seconds at each data acquisition time in order to avoid the build up of space charge within the crystal. (The effect of such a building up of space charge is discussed later within this section.)

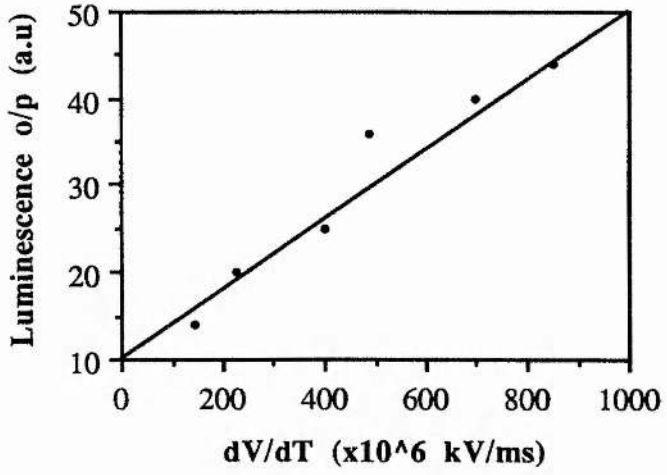

Figure 9.12 Luminescence intensity as a function of the excitation signal risetime. (Square excitation pulse)

The output luminescence intensity as a function of excitation frequency was obtained for a 100μm thick KI sample having evaporated aluminium electrodes. 1.5kV square wave pulses were applied over the 300Hz-30.5kHz the frequency range and the results are reproduced graphically in figure 9.13a.

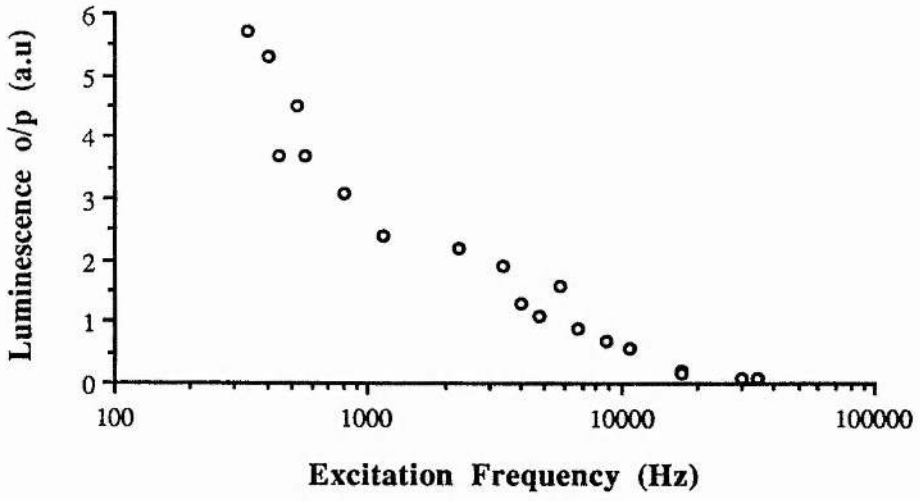

Figure 9.13(a) Luminescence output intensity as a function of the excitation frequency using square wave voltage pulses

It can be seen that the electroluminescence intensity falls rapidly with increasing excitation frequency and this is due to the fact that the rate at which carriers form the internal space

charge increases with frequency.This implies that the electroluminescence intensity will be inversely proportional to the excitation frequency. For interest, data for the output intensity as a function of excitation frequency were also obtained using a sinusoidal voltage waveform which gives a convolution of increasing $\frac{dV}{dt}$ and of a build up of the space charge. The result shown in figure 9.13b for a 150μm CsI sample shows the interesting feature that an optimum excitation frequency is obtained at around 300Hz.

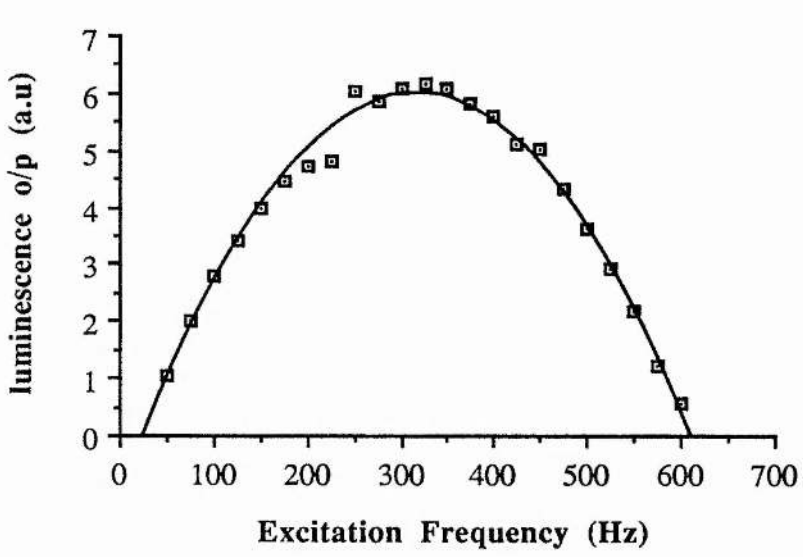

Figure 9.13(b) Luminescence intensity as a function of excitation frequency for a sinusoidal voltage waveform

The electroluminescence outputs from the alkali halide samples were also investigated as a function of the crystal temperature. A sample was cooled to 77K with liquid nitrogen and the nitrogen allowed to slowly boil off thus enabling the crystal temperature to rise progressively. The crystal temperature was monitored with a calibrated platinum resistance thermometer and the output electroluminescence intensity level was recorded at suitable intervals when a 300Hz sinusoidal waveform of 3kV magnitude was applied. Continuous excitation of the crystal results in a much more rapid depletion of the luminescence signal with time to be obtained due to the more dominant space charge effects. The data obtained from this experiment are presented in figure 9.14a. Electroluminescence was observed up

to crystal temperatures of approximately 160K under these operating conditions when space charge build up within the crystal was minimised. However, when the same experiment was repeated with the excitation signal run continuously it was found that a long tail feature was observed on the temperature curve which extended the operating temperature range to room temperatures (see figure 9.14b). This is caused by the thermally-activated release of trapped electrons from the space charge which accumulate during the continuous pumping.

Under non-space-charge-conditions it is expected that as the crystal temperature rises above 77K the efficiency of the luminescence of the self-trapped exciton begins to fall and that the number of centres relaxing to the ground state by way of phonon emission should increase with a concomitant decrease in the luminescence intensity. However, for a crystal containing a large population of trapped electrons it may be seen that as the crystal temperature rises the trapped electrons are thermally released from the trapping sites back to the conduction band thereby increasing the number of available electrons within the insulator which may then be excited to impact ionization energies. As a result higher populations of self-trapped excitons are produced. Though the majority of these decay by phonon emission, the number of centres which relax by optical transitions also increases to levels which may be observed and this accounts for the long tail observed in the luminescence-temperature characteristic of figure 9.14b.

The presence of a space charge within the alkali halides clearly plays an important role in determining the output characteristics of the electroluminescence and as a consequence further investigations into the space charge phenomena were carried out. The intensity of the luminescence was investigated as a function of time by continuously pumping a 100μm thickness KI sample at 77K with a 6kV sinusoidal voltage at a frequency of 500Hz for several hours and monitoring the output intensity.The recorded data are presented graphically in figure 9.15.

(a)

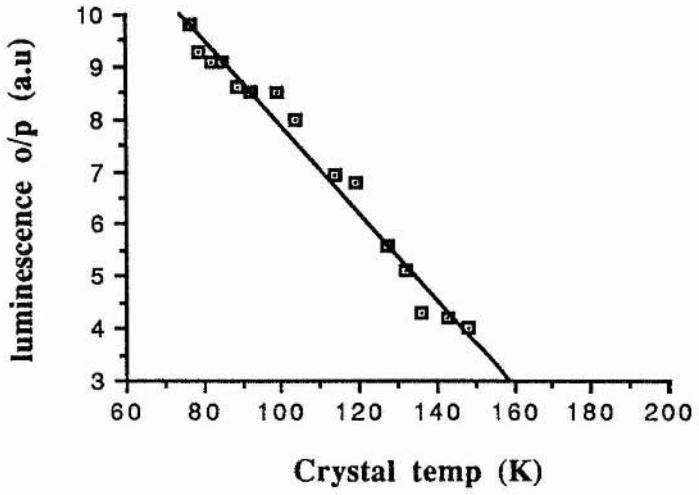

(b)

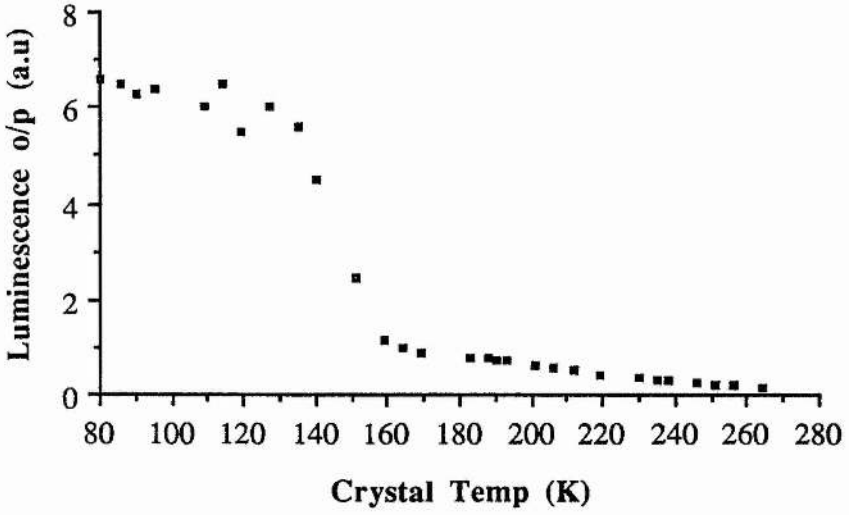

Figure 9.14 Output luminescence intensity (a.u) as a function of crystal temperature (K) for (a) intermittent excitation and (b) for a cw pumped crystal.

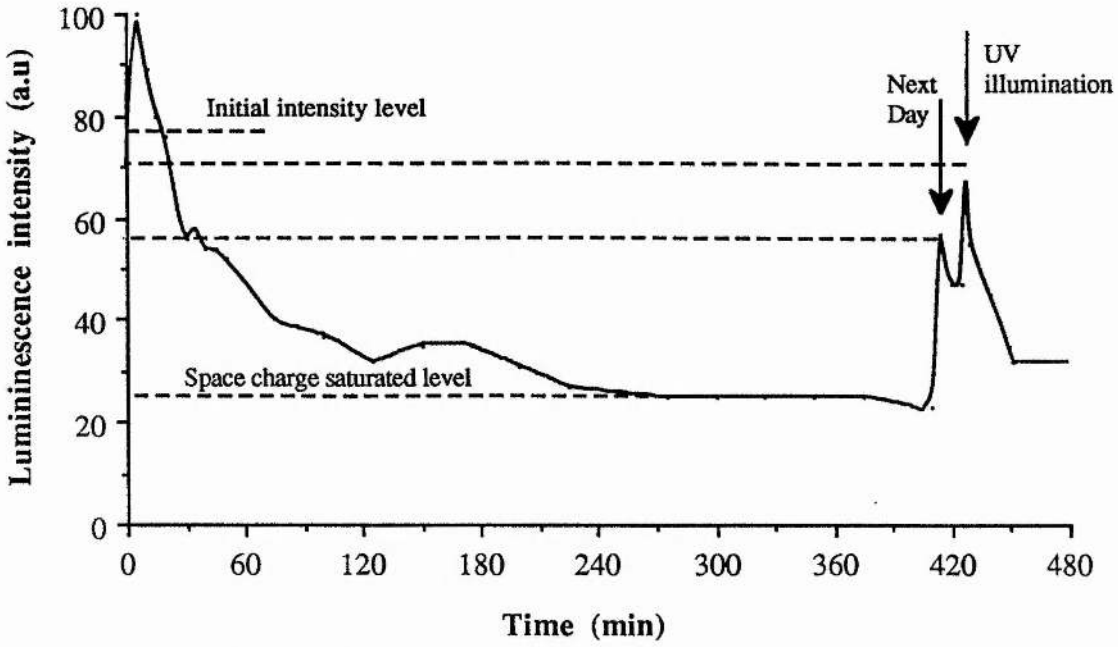

Figure 9.15 The luminescence intensity as a function of time for cw pumping conditions for a 100μm thick KI sample at 77K. The frequency of the excitation signal was 500Hz and the applied voltage 6kV

It can be seen that the output intensity increases during the initial 5-10 minutes of excitation before decreasing to a steady state saturation level (approximately one quarter of the peak value) after approximately three hours of pumping time.This initial increase in signal was observed with all samples and may be attributed to a change in the characteristics of the metal-insulator contact [4] as mentioned earlier in section 9.3. The steady-state level of the output was attributed to the filling of all of the trapping levels and hence to a saturation of the space charge. The pumping was continued after the space charge saturation level had been established for a further several hours before the excitation signal was switched off and the crystal left to stand overnight in darkness at 77K. On resuming the pumping the following day it was found that the signal had recovered to almost half of the peak value and upon illumination with a 200W mercury arc lamp for ten minutes the signal was further restored and then, as before, the signal dropped to a steady-state value. Oscillograms illustrating the variation of the intensity from the positive and negative peaks relative to each other over the period of this experiment are shown in figure 9.16.

To explain the steady depletion of the electroluminescence ouput intensity with time the formation of a space charge forming within two different trapping sites T_1 and T_2 may be considered where the capture cross-section for T_1 is greater than that for T_2. When a single-contact scheme is considered then we may distinguish between the negative and positive luminescence events during each excitation cycle. When the excitation field is first applied to the crystal the initial injected electrons find two species of trapping sites free to accept them but are preferentially trapped at T_1 sites. (See figure 9.17). With a field reversal the T_1 sites are field ionized and the electrons accelerated back towards the accumulation region where luminescence is again excited (fig 9.17 ii). When electrons are injected into the crystal again on the following negative phase (fig 9.17 iii) the presence of electrons trapped at the T_2 sites from the previous cycle reduces the magnitude of the injecting field and so the luminescence intensity is thereby reduced. This sequence of events occurs with a characteristic reduction of the luminescence intensity as the space charge trapped at the T_2 trapping sites accumulates until all are filled and the luminescence intensity stabilizes (as indicated in figure 9.15) after approximately 3-4 hours cw excitation. The electrons trapped at the T_2 sites may be released by illumination from a suitable ultraviolet lamp (figure 9.15, or by appropriately raising the crystal temperature to thermal ionization energies, as indicated in figure 9.14b whereby some of the optical signal may be recovered.

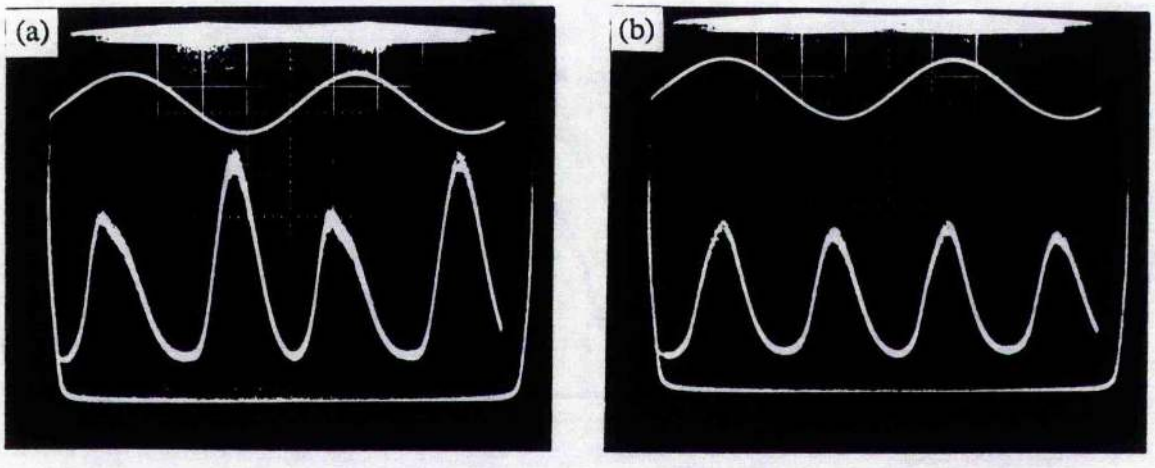

Figure 9.16 Output luminescence (lower traces) from KI after (a) 30 mins excitation. (lower trace 50mV/div, upper trace 2kV/div, 1ms/div) and (b) 240 mins excitation (lower trace 20mV/div, upper trace 2kV/div, 1ms/div) (ref fig.9.15).

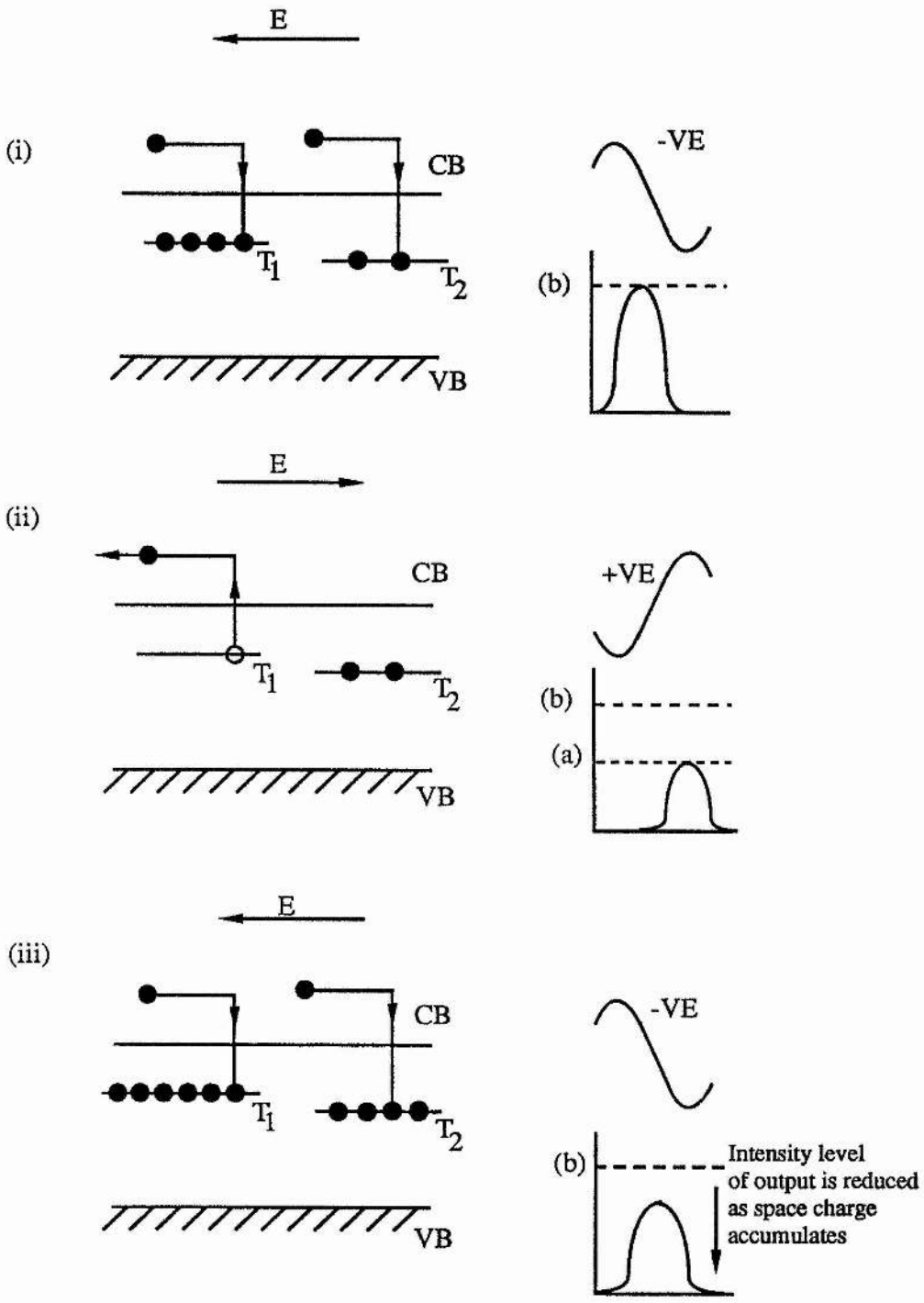

Figure 9.17 Schematic diagram illustrating the build up of space charge within an alkali halide crystal.

To illustrate the effect of releasing electrons from the trapping sites and the potentially large electroluminescence signals that can be generated by this process another experiment was carried out. Unlike the luminescence output versus temperature curve (figure 9.14b), which was obtained from a crystal whose trapping centres were far from saturated, a crystal was pumped continuously for several hours until the output signal was seen to stabilize thus indicating the saturation of the trapping sites. This was performed at 77K after which the sample was allowed to slowly warm whilst still undergoing electrical pumping. The output electroluminescence intensity data obtained as the crystal temperature increased are presented in figure 9.18. It may be seen that an enormous signal was obtained at approximately 130K whose intensity was measured to be 2-3 times greater than the original starting point when the crystal was space charge free. This large signal was maintained for several minutes as the space charge was released.

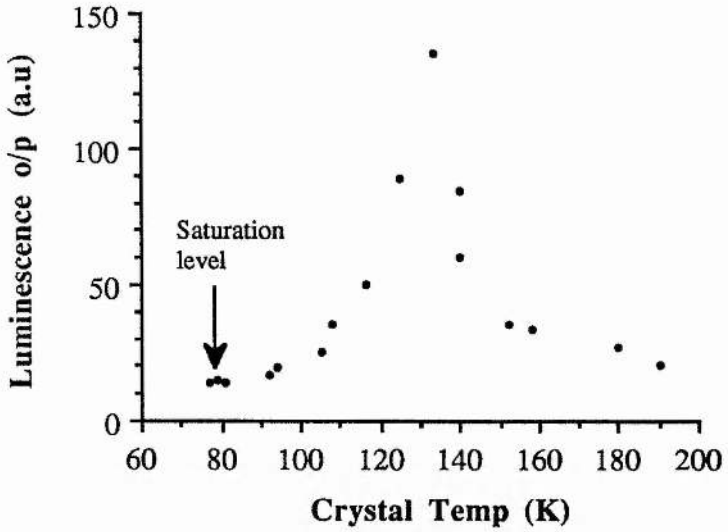

Figure 9.18 The output electroluminescence intensity of a space charge saturated crystal as the crystal is allowed to warm.

In a similar experiment where again a sample was pumped continuously such that the space charge conditions prevailed it was observed that by reducing the excitation frequency to the crystal the intensity level could be marginally retrieved because a lower excitation frequency means that the carrier injection rate is reduced.This is shown in figure 9.19 for a

KI crystal sample pumped continuously for several hours at 260Hz using a single contact configuration. It can be seen that the negative peak has been reduced to levels equivalent to those of the positive peak and that the intensity level of this peak is recovered by reducing the frequency for several minutes before exciting the crystal again at 260 Hz. Thus it has been shown that the build up of a large space charge within the crystal, which normally is considered an inconvenience, can be used to create potentially large output signals if the space charge population can be released by suitable modulation of the crystal temperature. Similar but smaller effects can also be obtained by modulating the excitation frequency or by providing suitable illumination to the crystal.

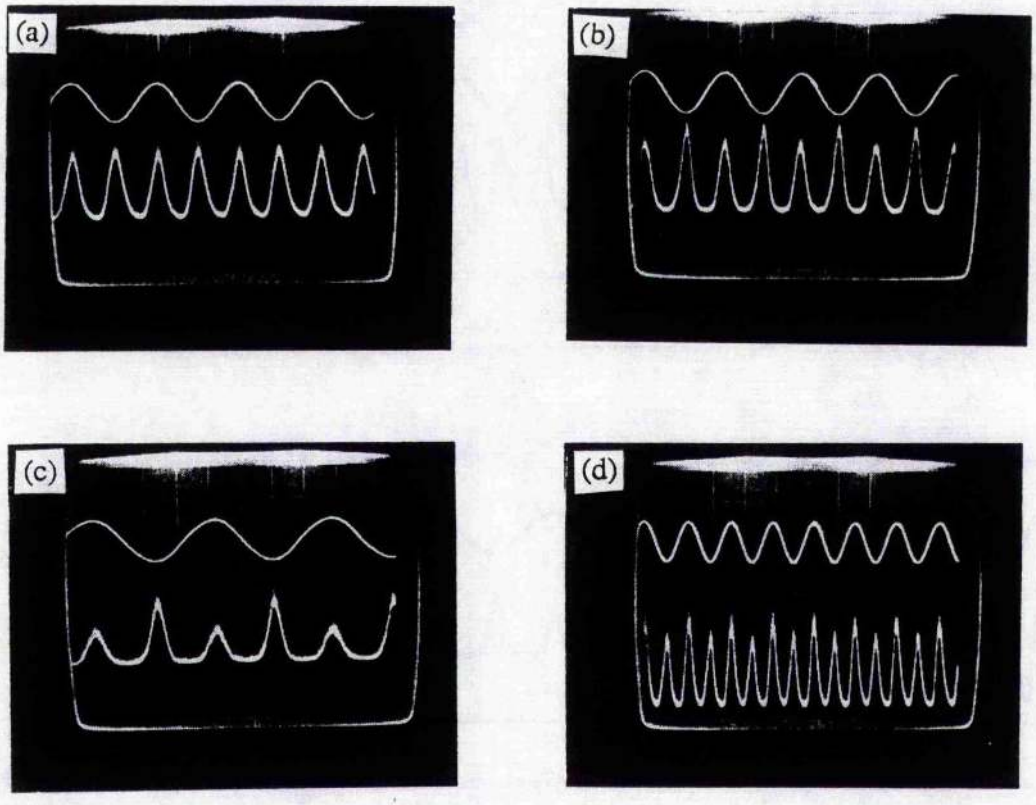

Figure 9.19 Oscillograms of output luminescence (lower trace) for a KI crystal excited at a frequency of (a) 260 Hz, (b) 150Hz, (c) 100Hz and (d) finally back to 260 Hz

9.4.3 Mechanism of Electroluminescence from Alkali Halides.

The emission spectrum obtained for all observations within the alkali halides confirm that the luminescence is attributed to the recombination of self-trapped excitons (STE). These are basically V_k type centres (self-trapped holes) which recombine with a free electron [8,11,12], and this species of luminescence centre is the most easily excited within alkali halides with an applied electric field [13,14]. Essentially two mechanisms for the production of luminescence in these materials have been proposed [3,8], namely; (i) double injection of holes and electrons and (ii) single carrier injection from the electrode causing impact ionization.

Mechanism (i) requires that injected holes are rapidly captured to form V_k centres and that the injected electrons recombine radiatively with these centres. In mechanism (ii) the injected electrons are accelerated by the applied electric fields to reach impact ionization energies. In order to ascertain the correct mechanism responsible for electroluminescence within alkali halides Paracchini [7] examined the intensity of the luminescence at different temperatures within the 20-77K range where the efficiency of the luminescence remains essentially constant. He concluded that the single carrier (because the hole mobility in alkali halides is low [7]) injection model is the most possible mechanism responsible for the luminescence. Paracchini also observed that the intensity of the luminescence increased by a factor of three at lower temperatures and concluded that if the double injection mechanism had been the mechanism responsible for luminescence then the luminescence intensity should not have increased at lower temperatures. He therefore favoured mechanism (ii) and attributed this observation to a charge multiplication process where the impact ionization rate decreases at higher temperatures due to an increased electron phonon interaction [15].

Evidence for the single injection model may be obtained by observing the output luminescence under double and single contacting schemes onto the crystal [15]. The single contact scheme is where one of the contacts is insulated from the crystal by means of a thin

mylar sheet thus enabling the positive and negative phases of the luminescence to be individually resolved. When both contacts are insulated in this way no luminescence is observed thus eliminating the luminescence process due to a field ionization mechanism [8]. A typical luminescence output obtained under sinusoidal excitation is reproduced in figure 9.20a when a double contacting scheme is employed.

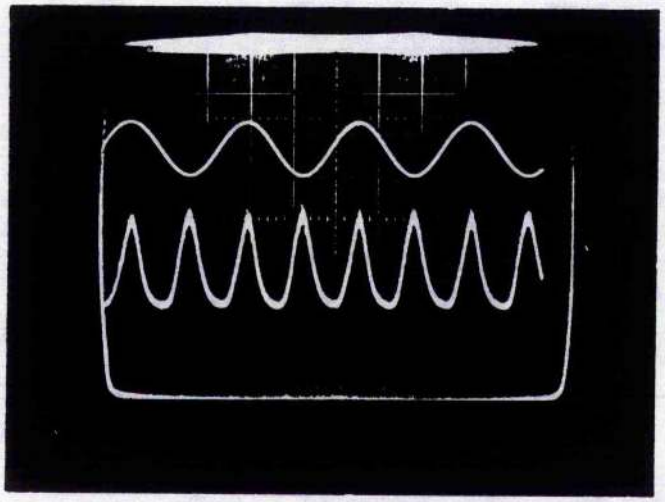

Figure 9.20(a) Typical luminescence (lower trace) obtained from an alkali halide crystal when a double contacting scheme is employed

It may be seen that the successive luminescence events are equal in intensity, however when the single contact scheme is employed it may that the successive luminescence events are not equal in intensity (see figure 9.20b).

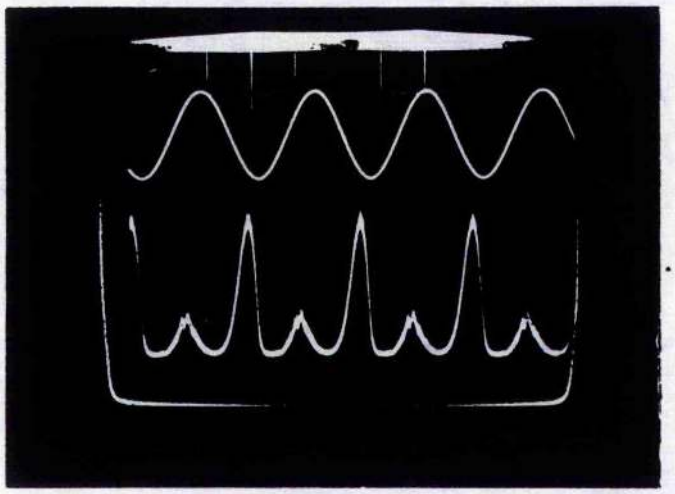

Figure 9.20(b) Typical luminescence obtained (lower trace) from an alkali halide crystal when a single contacting scheme is employed

In fact the luminescence produced by the positive going voltage ramp has a lower intensity than that associated with the negative going voltage ramp. It is also evident that the luminescence events are out of phase with and in fact lead the excitation field and that under both contacting schemes it may be seen that the frequency of the luminescence events is twice that of the excitation. These observations give evidence for the impact ionization model which is considered in the following discussion.

The observations mentioned above can be discussed in terms of both of the proposed mechanisms. Firstly if the double injection mechanism is responsible for the observed luminescence then luminescence events of twice the excitation frequency would be expected only for the double contact conditions. This is because under this scheme electrons and holes would be injected from opposite sides of the crystal simultaneously during each half cycle. However, when one of the contacts is insulated from the crystal, thereby inhibiting injection from this contact, the frequency of the luminescent events remain twice that of the excitation and not as expected. If the proposed mechanism was correct, then only during

the negative going phases of the excitation would luminescence be expected when electrons are injected into the crystal to recombine with the V_k centres created during the previous positive cycle. This observation along with Paracchini's temperature related studies [7] rule out this mechanism as being responsible. Further reinforcement to this claim is that the double injection mechanism also cannot explain (i) the phase shift between the luminescent events and the applied field and (ii) the intensity difference between the "negative going" and "positive going" events. In contrast if we consider that the luminescence mechanism is due to impact ionization by single carrier injection then it may be seen that the experimental observations may be explained by such a mechanism. For clarity a single electrode scheme will be assumed which allows the "negative" and "positive" luminescence events to be resolved.

Impact luminescence requires a suitable electric field by which the injected electrons can be accelerated to impact ionizing energies to be available. It has been shown that this can be achieved, under suitable conditions, within the alkali halides by means of a potential barrier formed just below the metal insulator junction. Direct visual observation of luminescence for such conditions confirms the formation of this barrier as the light output is only obtained from this region of the crystal. Experimental evidence obtained from thermoluminescence glow curves [3] suggests that the barrier type is likely to be exponential in nature and known as a Rose-type barrier [15]. Thus knowing that suitable high field regions can be produced within the alkali halides the following sequence of events is suggested. When the bias of the excitation field is negative with respect to the contact electrons are injected from the metal-insulator contact into the high field region of the potential barrier where they are accelerated to impact ionization energies and collide inelastically with valence electrons to produce electron hole pairs in the form of self trapped excitons which decay radiatively at 77K in a few picoseconds [4]. This process accounts for the induced "negative-bias" luminescence event. Once beyond the high field region of the barrier the injected electrons reach a low field region where they are decelerated and become trapped to build up a negative space charge within the bulk of the crystal. The

magnitude of this space charge increases with the injection of electrons until the external electric field E is quenched by this space charge and luminescence ceases. The variation of the space charge q with time is given by

$$q = q_0 \left[1 - \exp\left(\frac{-t}{\tau}\right)\right] \qquad (9.1)$$

where τ is a time constant which may be obtained from the phase difference between the luminescence peak and the peak of the excitation. Thus the internal field F leads the external field E rather like that of a charging capacitor and hence explains the phase difference between the luminescence and the externally applied field E. After a time t' from the beginning of the excitation the internal field F may be given as

$$F(t') = \int_0^t \frac{dE(t)}{dt} \exp\left[\frac{-t-t'}{\tau}\right] dt \qquad (9.2)$$

If E increases linearly with time then (9.2) becomes

$$F(t') \sim \beta \left(1-\exp\left[\frac{-t'}{\tau}\right]\right) = E\left[\frac{t}{t'}\right]\left(1-\exp\left[\frac{-t}{\tau}\right]\right) \qquad (9.3)$$

where $\beta = E/t$.

Upon field reversal, that is when the excitation field is positive, the trapped electrons are field ionized, assisted by the internal space charge, from the shallow levels and once again accelerated to ionizing energies. In this instance, the accelerated electrons are drawn towards the high field region to create electron hole pairs on recombining with V_k centres which may have survived from the previous half cycle. The radiative decay thus gives rise to the characteristic "positive peak" luminescence. The noisy nature of this luminescence event is attributed to field emission from the shallow traps and its lower intensity levels

may be attributed to the the fact that this excitation process is not as efficient as the negative counterpart because not all of the trapped electrons may be liberated by field emission.

9.5 Feasibility of achieving laser action from an electrically-pumped alkali halide crystal

9.5.1 Introduction

This section is concerned with the assessment procedures of the parameters and conditions required for obtaining laser action from an electrically-pumped alkali halide material. To date, a considerable amount of research has been carried out on the electroluminescence from these materials [3-8] with one group of workers reporting laser action from such a novel pumping mechanism within a NaCl host in 1975 [16]. As yet no further reports of such laser action has been published, either by the above mentioned workers or other groups working within the same field of interest [3-8,17]. It is relevant therefore that the conditions for obtaining laser action from such materials should be reassessed in the present context.

9.5.2 Conditions for laser action from an electrically-pumped alkali halide material

The proposal for an ultraviolet exciton laser was first presented in 1963 by E.L.Fink and G.N.Ellison [18] for an optically pumped KI crystal operating on the self-trapped exciton 375nm line. Ultraviolet laser emission from an alkali halide gain media was reported by these workers two years later for an optically pumped KBr crystal maintained at 77K with a peak operating wavelength of 315nm [19].

By drawing conclusions from experimental observations obtained in this chapter and from information obtained from a search of relevant literature [3-8 and refs. therein] the conditions for laser action will be presented here for KI only in that this material is selected as the most likely laser candidate. If the conclusions drawn by Fink et al [18] (1963) and Boyd et al [4] (1983), are considered, each group based their calculations for laser action from the self-trapped exciton operating on different spectral lines, Boyd et al favoured the 297nm singlet transition and Fink et al the 375nm triplet transition. Fink and coworkers probably based their assumptions on the longer lived triplet line due to the fact that at this period (1963) many laser physisists tended to favour longer lived upper laser level as much pioneering research was being carried out upon the dye laser at this time. In this present consideration the singlet line is favoured but for comparison the threshold population inversion required for laser action will be presented for both lines. The crystal geometry envisaged here is a crystal that is 100μm thick with a length of 4mm along the resonator axis with 2mm diameter contacts on both surfaces.

The population inversion required for threshold Δn_{th} within a potential laser gain media can be expressed as:

$$\Delta n_{th} = \frac{8\pi\nu^2}{c^3} \frac{\tau_{sp}}{\tau_{photon}} \Delta\nu \qquad (9.4)$$

where ν is the centre frequency of the line shape function $g(\nu)$ assumed here to be Lorenzian, τ_{sp} is the upperstate lifetime of the of the radiative transition, τ_{photon} is the average lifetime of a photon within a cavity before it is transmitted by the output coupler and $\Delta\nu$ is the full width at half maximum of the line shape function $g(\nu)$. τ_{photon} may be expressed as

$$\tau_{photon} = \frac{2l}{c(2\gamma l - \ln R_1 R_2)} \qquad (9.5)$$

where l is the length of the population inversion region within the gain medium and γ is the loss per distance due to scattering and absorption within the active medium and R_1 and R_2 the reflectivities of the cavity mirrors.Thus if we assume γ=0.2 and l=2mm and the product R_1R_2=0.98 we arrive at a value of τ_{photon} = 0.63ns.Now if this value is substituted into equation (9.4) to calculate the threshold population inversion, firstly for the singlet 297nm line which has a centre frequency $\nu=1.01\times10^{15}$Hz, $\Delta\nu=6\times10^{13}$Hz and an upper state lifetime τ_{sp}=5ns, a value of $\Delta n_{th}=4.52\times10^{14}cm^{-3}$ is obtained and similarly for the triplet 375nm line where $\nu=8.0\times10^{14}$Hz, $\Delta\nu=1.0\times10^{14}$Hz and an upper state lifetime τ_{sp}=0.9μs, a value of $\Delta n_{th}=8.5\times10^{16}cm^{-3}$ obtained which as may be seen is two orders of magnitude greater than that required for the singlet transition. Boyd et al have obtained an expression for the threshold electrical input power needed to be delivered to the crystal as

$$P_{in}=\frac{4\pi^2n^2\Omega h\nu\alpha\Delta\nu}{l\lambda^2\eta_{el}} \qquad (9.6)$$

where n is the refractive index (n=1.83 at 297nm for KI) Ω the volume of the active medium, α the small gain coefficient, η_{el} the electrical efficiency and the other symbols have their usual meanings. From equation (9.6) the threshold current density per centimetre squared may be deduced to be:

$$J=\frac{4\pi^2n^2Dh\nu\alpha\Delta\nu}{l\lambda^2\eta_{el}V} \qquad (9.7)$$

where D is the thickness of the crystal in cm and V the applied potential across the electrodes. A threshold current density of $\approx20Acm^{-2}$ was calculated for the 297nm transition for crystal geometries already mentioned.

9.5.3 Design of a simple standing-wave resonator

The design of a simple standing-wave resonator for the KI crystal was undertaken incorporating the newly redesigned laser cryostat and electrical pumping head. As the

crystal samples where of the order of 100μm in thickness it was decided to incorporate into the cavity two internal focussing lenses to couple light back into the crystal facets. Two planoconvex lenses where chosen each of 25mm focal length and were antireflection coated for the luminescence spectra (275-430nm) of KI. Two flat mirrors each having a reflectivity profile of 99% over the same spectral range where also selected. The electrical pumping chamber head was designed accordingly to accept the two objective lenses where the position of each lens could be adjusted whilst still maintaining the vacuum within the cryostat. The alkali halide crystal was mounted on a removable "cassette" which was accommodated in the electrical chamber and located onto the cold finger by means of a similar adapter to that used in the optically-pumped counterpart. This ensured good thermal contact between the two components. The electrical pumping crystal cassette is illustrated in figure 9.21.

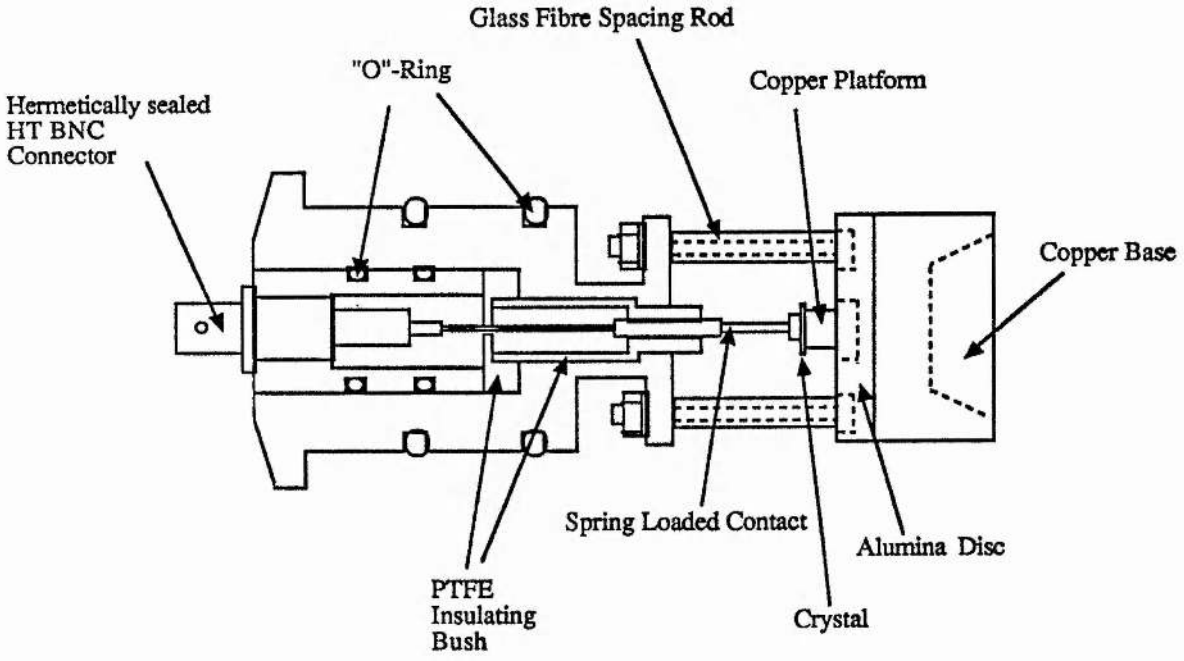

Figure 9.21 The electrical-pumping crystal cassette

With reference to figure 9.21 it may be seen that the crystal is held in position by a spring loaded pressure contact which locates the crystal tightly against a copper platform which is kept in thermal contact with the cold finger. This copper platform also acts as the second

electrical contact for the crystal and thus completes the electrical circuit whereby a return wire from the copper platform exits the cassette by a small vacuum maintaining plug (not shown in diagram). The cassette is electrically insulated from the main cryostat by an alumina disc which has excellent electrical insulation properties whilst also having excellent thermal conduction properties. Three glass fibre spacing rods inside which locating screws are housed hold and maintain the pressure contact in place upon the crystal. The electrical signal to the crystal is provided by a high tension voltage source which is connected to the pressure contact via a connecting cable from a hermetically-sealed BNC fitting. To avoid the chamber from becoming electrically live the pressure contact is electrically insulated from the cassette by a PTFE bush. The chamber vacuum is maintained by way of two O-ring seals with the spring loaded cold arm being compressed by atmospheric pressure which thus ensures a good thermal contact between the cassette and cold arm assembly.

The simple standing wave resonator design is depicted in figure 9.22 and a photograph of the electrical pumping chamber given as figure 9.23.

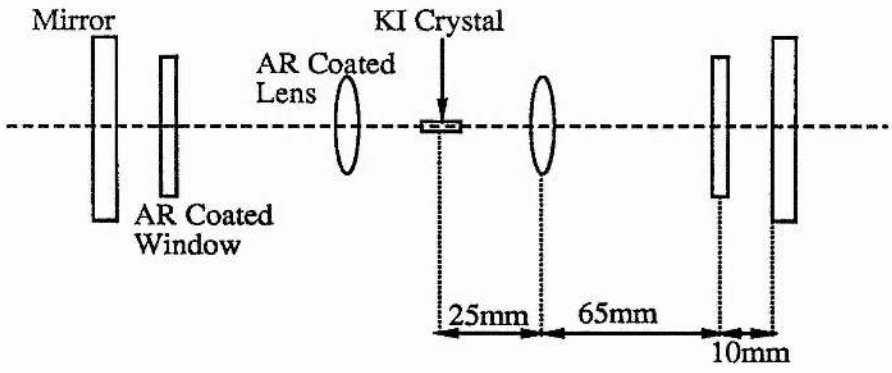

Figure 9.22 The simple resonator constructed for the electrically pumped KI crystal

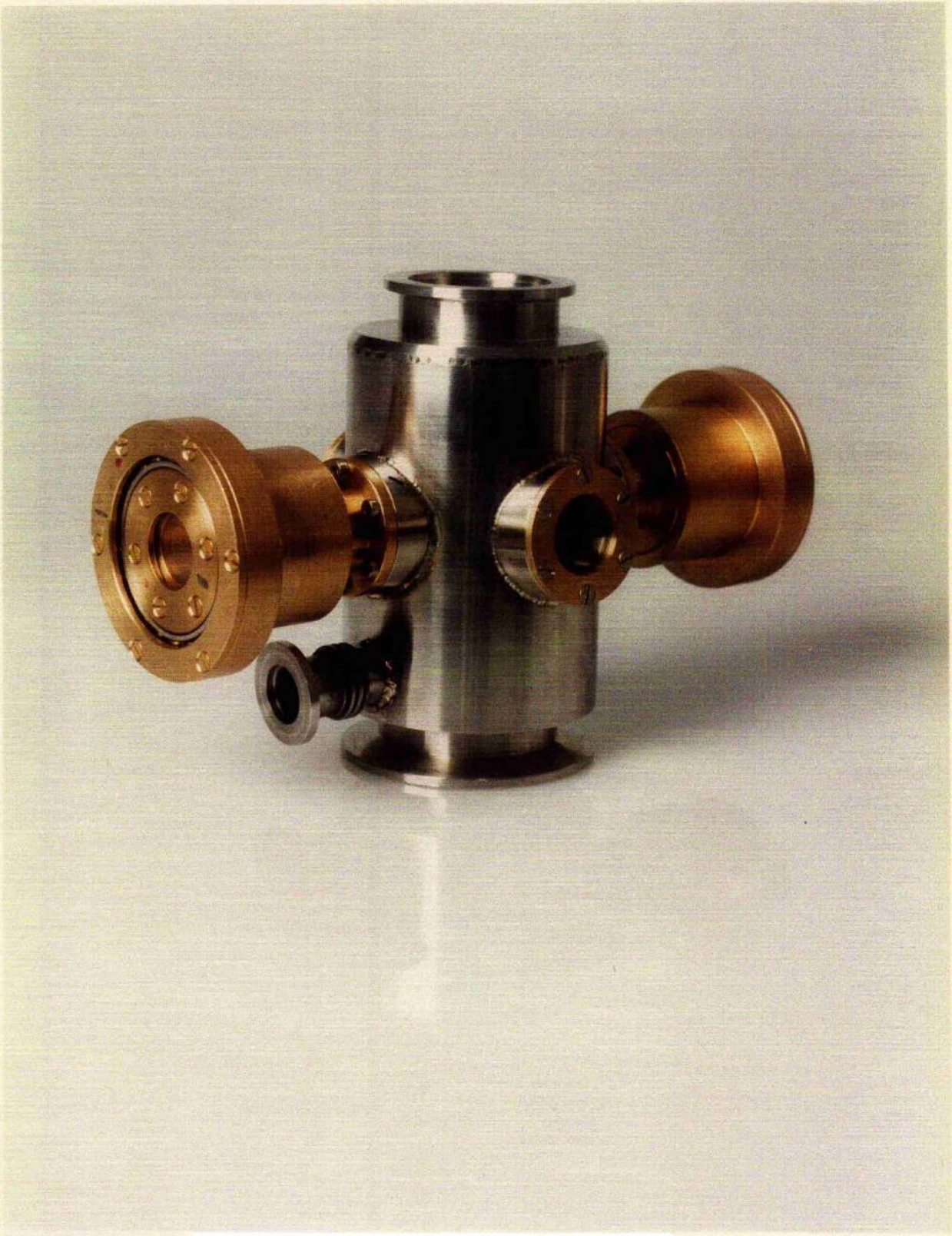

Figure 9.23 The electrical pumping chamber

The beam profile within the KI crystal was obtained using the following expressions:

$$w_o = \frac{f\lambda}{\pi\omega_1} \qquad (9.8)$$

and

$$w_{(Z)} = w_o\left[1+\left(\frac{\lambda Z}{\pi w_o^2}\right)^2\right]^{1/2} \qquad (9.9)$$

where w_o is the beam waist at the focal length f of the lens and w_1 is the beam spot size incident upon the lens and $w_{(Z)}$ is the beam waist along the resonator axis Z. The beam waist parameters are shown in figure 9.24. Once a crystal was inserted into the cavity the mirrors and lens positions were approximately prealigned using a He-Ne laser with optical feed back through the crystal from the He-Ne being monitored with a lock-in amplifier arrangement. Several KI samples were tested within this resonator to investigate temporal and spectral narrowing upon the luminescence output profiles. As before ~100μm thickness samples were used and the geometry of the cavity was as described above.

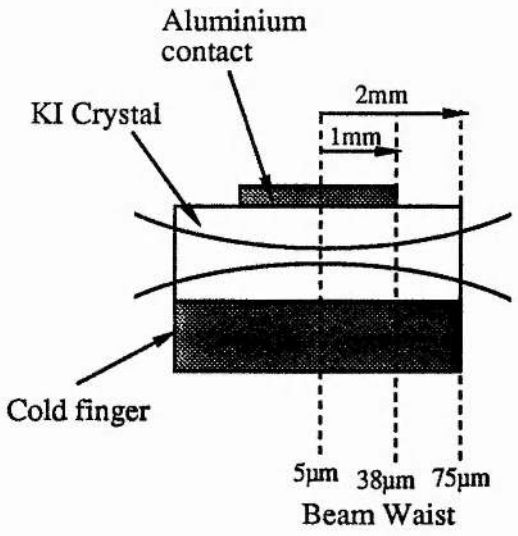

Figure 9.24 Beam waist parameters through the 100μmx4mmx4mm KI crystal

Unfortunately no optical feedback has been obtained with this resonator but one crystal sample has displayed optical feed back off its own facets and temporal narrowing has been observed along with significant intensity enhancement. The signal obtained from this particular KI sample is presented in figure 9.25. A double-contact scheme was implemented and thus consecutive luminescence signals correspond to the output luminescence from opposite contacts. The luminescence events should therefore ideally be of the same intensity but it can be seen from the photograph that the intensity profiles for each contact differ in intensity. This implies that the electron injection efficiency of each contact is unequal and is probably due to differences in the physical nature of the contacts formed. Due to the very large signal obtained with the PMT detection system it may be seen that the intensity of the luminescence in fact saturates the detector. This is very noticeable for the signal associated with the voltage trough (negative phase of the signal) and suggests that these events are of much higher intensity than the double peaked events occurring at the opposite contact.

Examination of the double-peaked events shows that they are repeatable. They exhibit constant intensity and phase characteristics and occur where a luminescence event is expected relative to the applied signal and this thus rules out this event being the result of an insulator breakdown.The onset of crystal breakdown is shown in figure 9.25c and it may be seen that light is given out anywhere in relation to the excitation voltage as indicated at 0.4ms before and after the centre line of this oscillogram. Soon after this photograph was taken the light output became more random in phase and in intensity and finally the excitation voltage trace became erratic as the insulation breakdown led to overloading of the current supply. The double-peak event could be attributed to spiking of the gain whereby the optical feedback depletes the gain which is then repumped thus allowing the second spike to be emitted before the phase of the exciting pump waveform changes. Unfortunately no spectra was obtained for these high intensity events and so conclusive evidence of stimulated emission is not available.

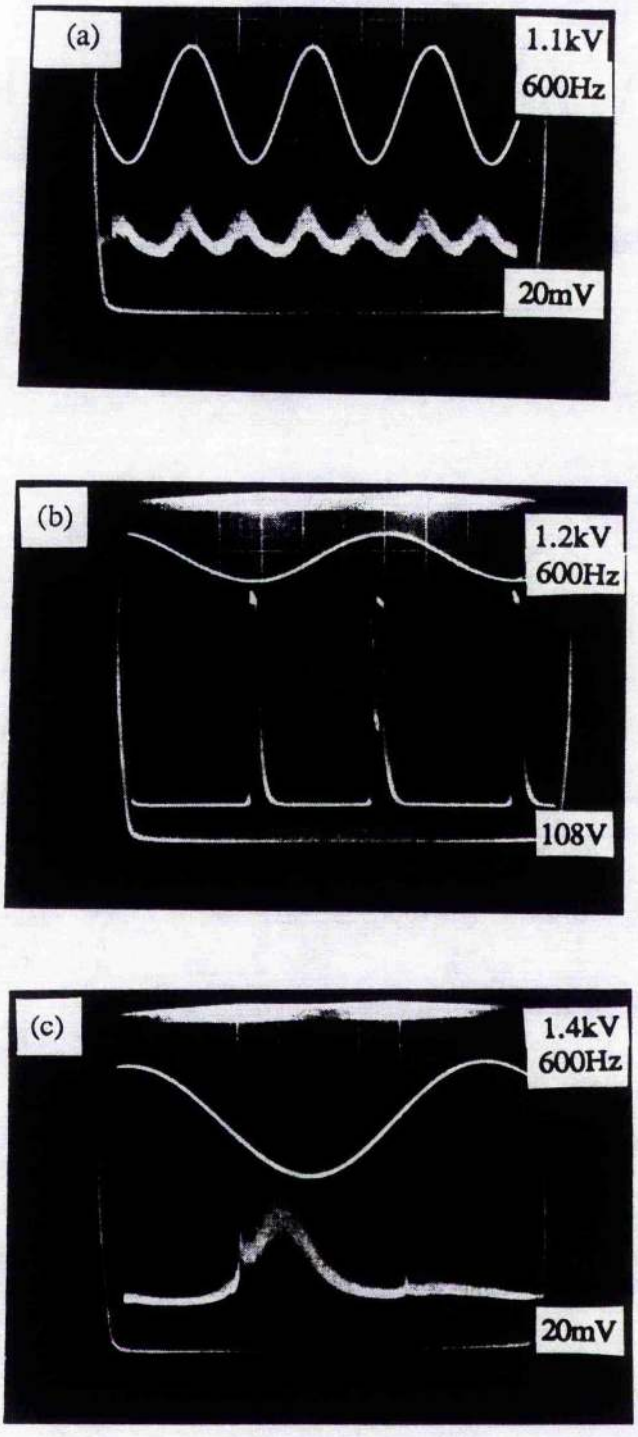

Figure 9.25 Oscillograms of (a) excitation waveform (uppertrace) and output luminescence without optical feedback and (b) with optical feedback and (c) subsequent breakdown of the crystal

From figure 9.25a it may be seen that for a voltage of 1.1kV that the output electroluminescence signal magnitude is of the order of 20mV and the FWHM is 0.5ms. When the voltage was increased slightly to 1.2kV the output signal magnitude dramatically increased to 110V and the FWHM decreased to 0.1ms (figure 9.25b) which gives an increased intensity level of $5.5x10^3$ and temporal narrowing by a factor of five. The output luminescence as a function of applied voltage for this sample is presented in figure 9.26 and showed a dramatic change in the output characteristic occuring around 1.1kV.

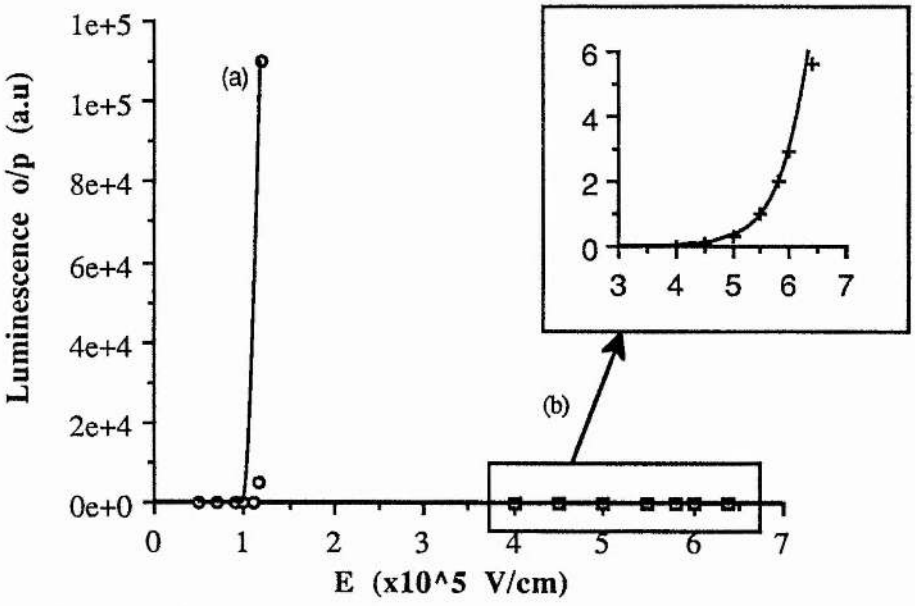

9.26 Output luminescence from a KI crystal (a) with and (b) without optical feedback.

9.6 Summary

Electroluminescence from alkali halides has been investigated with a view to assess the feasibility of obtaining laser action from these materials using the electrical pumping scheme as an excitation mechansism. The subject of constructing suitable current-injection contacts onto the crystal samples has been addressed and several schemes experimentally evaluated. It is within this area that the major hurdle of obtaining laser action from such a

pumping mechanism lies because to date construction of suitable contacts able to supply the necessary current densities have not been properly achieved. A probable solution to this problem is to produce ultra thin crystals (0.5-1.0μm) such as those used when laser action was reported because the breakdown field strength for thin crystals of this nature is known to increase as the thickness is reduced [20]. Therefore larger electric fields can be applied to the crystal without electrical break down occurring and thus the threshold current density for laser action could be obtained.

It was found that the formation of a space charge within the crystal caused the output luminescence intensity to reduce with continuous excitation to a steady state value which is approximately one quarter that of the initial intensity level. However by heating such space charge filled crystals to suitable temperatures it was found that relatively large signals could be obtained whilst the release of the space charge took place.

Temporal narrowing of the luminescence signal has in fact been demonstrated from a KI crystal with reflection occuring from the crystal facets.This thus demonstrates that if the necessary threshold current densities for laser action could be accomplished then laser action could probably be unambiguously demonstrated.

Chapter 9. References

1. B.Fritz, E.Menke; Solid State Commun. **3**, 61 (1965)

2.L.F.Mollenauer; Colour Centre Lasers in Quantum Electronics Part B (Ed.C.L.Tang)(Academic Press, NY 1979)

3. C.Parrachini; Phys.Rev.B. **7**, 1603 (1973)

4. R.W.Boyd, M.S.Malcut, K.Teegarden; IEEE J.Quan.Elect. **QE-18**, 1202 (1982)

5. BDH Limited, Broom Road, Poole, Dorset, BH12 4NN

6. J.G.Simmons;J.Phys.Chem.Solids **32**, 1987 (1971)

7. C.Parrachini; Phys.Rev.B. **8**, 848 (1973)

8. S.Unger, K.Teegarden; Phys.Rev.Lett. **19**, 1229 (1967)

9. B.Henderson; Defects in Crystalline Solids, Edward Arnold, London (1972)

10. M.N.Kabler, D.A.Patterson; Phys.Rev.Lett. **19**, 652 (1967)

11.R.B.Murrey, J.F.Keller; Phys.Rev. **137** A942 (1965)

12.R.B.Murrey, J.F.Keller; Phys.Rev. **153** 993 (1966)

13. C.Parracchini, G.Sshianchi; Solid State Commun. **8**, 1769 (1970)

14. A.P.Druzhinin, N.I.Lebedeva, N.S.Nesmelov; Opt.Spektrosk **47**, 917 (1979)

15. C.Parracchini; Phys.Rev.B. **4**, 2342 (1971)

16. G.A.Vorobev, S.G.Ekhanin, N.I.Lebedeva, I.N.Morev, N.S.Nesmelov; Iz.Fizika **12**, 149 (1975)

17. N.I.Lebedeva, N.S.Nesmelov; Sov.Phys.Solid State **14**, 1106 (1972)

18. E.L.Fink, G.N.Ellison; Proc. IEEE **51**, (1963)

19. E.L.Fink, Appl.Phys.Lett. **7**, 103 (1965)

20. N.I.Lebedeva; Sov.Phys.Solid State **16**, 378 (1974)

Chapter 10

General Conclusions and Future work

Modelocking of the LiF:F_2^+ colour-centre laser was successfully demonstrated for the first time within this laboratory and has proved to be an efficient source of frequency tuneable near-infrared (NIR) ultrashort optical pulses when modelocked both by active and passive means [1-3]. As with other modelocked systems, such as dye lasers the technique of passive modelocking was found to produce shorter pulse durations from the LiF:F_2^+ colour-centre laser than from a similar system when actively modelocked.

The actively modelocked system enabled modelocked pulses to be obtained over the entire LiF:F_2^+ tuning range (0.8μm-1.0μm) whilst the passive system limited the tuning range of the laser to a narrow spectral region centred around the absorption peak of the saturable absorber. An effective way of improving the tuning range of such a passive system was successfully carried out by coupling the laser output with that of an external cavity containing a nonlinear element, in this case an optical fibre was implemented, in a process known as coupled-cavity-modelocking [4]. This coupled-cavity scheme enabled the tuning range of the passive system to be extended to the extremes of the saturable absorber absorption profile whilst retaining the inherent ultrashort pulse durations typical of a passively modelocked device.

The poor stability of the F_2^+ colour-centre within a LiF host lattice was such that chopping of the pump beam was required to avoid thermal degradation of this laser active centre. When operated under chopped pump conditions the operating lifetime of the laser crystal was typically 200 hours. A "stabilised" NaCl:OH^- colour-centre laser, incorporating the F_2^+:O^{2-} colour-centre, which operates over the 1.4-1.8μm spectral region was constructed and such a system proved to be a very reliable device in that no fading of the laser output was observed over long operating periods (6-8 months), and also, that the F_2^+:O^{2-} colour-

centre could be pumped under non-chopped conditions. The NaCl:OH^- colour-centre laser constructed here has proven to produce (this work not mentioned within this thesis) stable modelocked pulses having durations within the 150-200fs regime when a coupled-cavity-modelocked scheme is employed. At present this laser is being operated within this laboratory as a diagnostic tool and as a modelocked source for studying the propagation of ultrashort pulses within optical fibres and other waveguiding devices.

Within the NIR spectral region there are several laser types which operate, and in particular it is the semiconductor diode laser and rare-earth doped optical fibre lasers which directly compete with colour-centre lasers. For example the Er-fibre laser which is broadly tunable from 1.5-1.6μm is very efficient and is capable of delivering relatively high output powers due to the large gain lengths that can be achieved. Semiconductor diode lasers also offer broad tuning from 1.1-1.6μm and modelocking techniques have enabled pulse durations of 3-4ps to be achieved. The applications of these two solid-state miniature laser sources to the field of telecommunications, for example, is clearly obvious due to their compact size, ruggedness and long operating lifetimes.

However, although bulky and cumbersome in nature due to the requirement for cryogenic cooling, colour-centre lasers provide an extremely versatile facility. Properties such as the ability to produce tuneable subpicosecond pulses encompass those of other lasers operating within this spectral region. They are therefore useful as experimental laser sources where, for example, the propagation of optical pulses within optical fibres may be investigated at higher peak powers and/or operating wavelengths than is presently available from semiconductor diode lasers. For similar reasons they remain as the dominant laser source in the field of time-domain and high-resolution spectroscopy over the NIR spectral region.

Electroluminescence was was shown to be readily obtained from alkali halide crystals under the application of 10^4-10^5 Vcm^{-1} electric fields and output wavelengths were observed to lie within the ultraviolet (UV) spectral region. Experiments carried out to

assess the feasibility of producing an electrically excited UV alkali halide laser concluded that ideally current injecting (Ohmic) contacts should be constructed onto the crystal surfaces in order to obtain a sufficient population of luminescence centres. However, only blocking type contacts were achieved here. Significantly though, it was noted that even with such a contact scheme large luminescence signals were obtained and the output intensity was observed to increase exponentially with the applied electric field. This was attributed to an avalanche process occuring within a high field region located close to (several microns) the metal-insulator interface known as an accumulation region. From these observations it was deamed feasible that a threshold population of luminescence centres may be achieved with either injection or blocking type contacts providing that suitably large electric fields are available for the latter contacting scheme. Such an avalanche process was observed from a KI crystal with applied electric fields of magnitude 10^5-10^6 Vcm^{-1} and evidence of stimulated emission was observed before crystal breakdown unfortunately occured.

With these findings future work in this area should be carried out upon perfecting the technique of constructing injection contacts upon the crystal surfaces and thus obtaining threshold luminescence centre populations under moderate electric fields. If however, only blocking contacts are obtained, preparation of much thinner crystals ($\approx 5\mu m$) could be carried out in order to create the necessary luminescence centre population density by an avalanche process, as the breakdown field threshold increases inversely with crystal thickness [5] . This second option would lead to crystal samples having dimensions similar to those of laser diode active regions and such ultra-thin alkali halide crystal dimensions have been constructed by soviet workers [6]. This was acheived by using a technique involving two opposing hypodermic needles, these being used as effective "drill bits" through which alcohol-alkali halide solutions were injected to bore to the required operating thickness.

Though not involving an electrical pumping scheme, UV laser emission has in fact been obtained from an alkali halide crystal (KBr) when excitons have been pumped by a flashlamp [7]. The budget of this pumping mechanism is comparative to that of the electrical pumping scheme, as an expensive ion pump laser is not required, and therefore this approach could be considered as an alternative to the difficult task of achieving laser action by electrical excitation.

Chapter 10. References

1. N.Langford, K.Smith, W.Sibbett; Opt.Lett. **10**, 817 (1987)

2. N.Langford, K.Smith, W.Sibbett; Opt.Lett. **12**, 903 (1987)

3. C.I.Johnston, D.E.Spence, R.S.Grant, W.Sibbett; Opt.Commun. **73**, 370 (1989)

4. L.F.Mollenauer, R.H.Stolen; Opt.Lett. **9**, 13 (1984)

5. N.I.Lebedeva, Sov.Phys.Solid.State. **16**, 378 (1974)

6. G.A.Vorob'ev, I.S.Pikazova; Instrum. Exper. Tech. (USA), **1**, 210 (1967)

7. E.L.Fink; Appl.Phys.Lett. **7**, 103 (1965)

Publications

Group-velocity-dispersion compensation of a passively modelocked ring LiF:F_2^+ colour-centre laser

N.Langford, R.S.Grant, C.I.Johnston, K.Smith, W.Sibbett

Optics Letters **14**, 45 (1989)

Femtosecond pulse generation in the 900-950nm region from a passively modelocked LiF:F_2^+ colour-centre laser

C.I.Johnston, D.E.Spence, R.S.Grant, W.Sibbett

Optics Communications **73**, 370 (1989)

Nonlinear refraction and absorption of an InGaAs single quantum well in an InGaAsP waveguide

D.J.Goodwill, J.E.Ehrlich, D.T.Neilson, A.C.Walker, C.I.Johnston, W.Sibbett

Accepted for publication in J.Mod.Opt.

High speed synchronously pumped Raman fibre amplification

K.C.Byron, D.Burns, R.S.Grant, G.T.Kennedy, C.I.Johnston, W.Sibbett

Accepted for publication in march 1991 edition of Elect. Letts.

Acknowledgements

I would like to thank my supervisor Professor Wilson Sibbett for his thoughtful guidance and extreme patience maintained throughout the duration of this project. I would also like to thank Mr.R.H.Mitchell for his expertise involving the cryogenic equipment used here and for designing the highly versitile colour-centre laser cryostats. Thanks must also go to Mr.Jimmy Lindsey and Mr.George Radley of the departmental workshops for swiftly "turning out" so many a fine component. Within the early stages of this project I had the pleasure of working alongside Nigel Langford, Robert Grant and David Spence and acknowledgement of their assistance in passively modelocking the LiF:F_2^+ colour-centre laser is deserved. I would like to thank Peter Kean for his help in processing the NaCl crystals. For help involving anything electronic I gratefully acknowledge the unrivalled expertise of Bill Sleat. David Crust, a big thankyou for showing me what a computer can really do. Thanks must also go to the "boys" of the "W" squad for their guiding and meaningfull discussions on life (as they see it!) and for their unsurpassed sense of humour. Thankyou Margaret and Babs for keeping my lab tidy. Lastly but not least I would like to thank Miss Carrie Simpson for providing many a gourmet masterpiece and to the members of the SGC and B.O.B. for their stabilizing influences.

Financial support from the Department of Education of Northern Ireland and also the Royal Armaments Research and Defence Establishment is gratefully acknowledged.